Master's thesis

NTNU
Norwegian University of Science and Technology
Faculty of Engineering
Department of Geoscience and Petroleum

Kristin Blilie

An evaluation of tectonostratigraphy and hydrocarbon potential of the Ellingråsa Graben, Halten Terrace offshore Mid-Norway

Master's thesis in Petroleum Geosciences and Engineering
Supervisor: Kenneth Duffaut, Halvor Bunkholt
July 2019

NTNU
Norwegian University of
Science and Technology

Kristin Blilie

An evaluation of tectonostratigraphy and hydrocarbon potential of the Ellingråsa Graben, Halten Terrace offshore Mid-Norway

Master's thesis in Petroleum Geosciences and Engineering
Supervisor: Kenneth Duffaut, Halvor Bunkholt
July 2019

Norwegian University of Science and Technology
Faculty of Engineering
Department of Geoscience and Petroleum

NTNU
Norwegian University of
Science and Technology

Abstract

The Ellingråsa Graben, situated in the immediate hanging wall of the Bremstein Fault Complex (BFC) at 65°N on the Halten Terrace, is a sparsely described structure in public literature, home to the very first wells drilled on the mid-Norwegian shelf. An overview of the tectonostratigraphy and hydrocarbon potential of this structure is provided herein. An interplay between Jurassic faulting along the BFC and Triassic evaporites is observed, with listric faults detaching in the salt interval, hanging wall rollover and gentle salt pillowing as the main features. Variations in throw, syn-rift wedge thickness, erosion of footwall and strike-direction supports a division of the BFC into 4 segments. A model for formation of the closure on which the very first well in the Norwegian sea, well 6507/12-1, was drilled is proposed. It is suggested to have formed in an area of varying strike direction of the graben-bounding listric faults, resulting in hanging wall rollover towards the master faults in multiple directions, creating a combined anticline-horst closure. Significant erosion of the graben flanks as well as locally within the graben is suggested to have occurred during the Callovian. The base Cretaceous unconformity is also erosive over footwall scarps in the study area. Rift climax occurred from the Callovian until the earliest Cretaceous, however there are signs of syn-rift deposition in the Early Cretaceous as well. Re-activation of major faults is observed in the Paleogene strata. The dry wells in the study area are attributed to immature source rocks and a lack of long-distance migration routes into the drilled closures. A closer look at erosion and syn-rift strata in the study area reveals possible syn-rift sandstones in the immediate hanging wall of the BFC. These are mainly expected to be deposited in a deep-marine environment, with a local area of possible shallow-marine syn-rift deposits on the dipslope of an eroded intra-graben fault synthetic to the BFC to the south in the study area. If hydrocarbons have entered the graben at this level, these sandstones could form a migration pathway effectively bypassing the drilled, dry prospects or constitute reservoirs partially or completely enclosed in shale in such a way that stratigraphic traps are present. However, due to a general lack of signs of hydrocarbons in the form of shallow soft bright spots or seabed pockmarks, the likelihood of significant charge having entered the Ellingråsa Graben is considered low, and the graben is proposed to be situated in a migration shadow.

Sammendrag

Ellingråsa Graben er en grabenstruktur lokalisert i den umiddelbare hengblokken til Bremstein Forkastningskompleks (BFC), i Norskehavet, 65°N. De første letebrønnene i Norskehavet ble boret og funnet tørre på denne strukturen, som siden har vært en lite beskrevet struktur i offentlig tilgjengelige publikasjoner. Denne oppgaven gir en oversikt over tektonostratigrafien og hydrokarbonpotensialet i Ellingråsa Graben. Et samspill mellom forkastningsaktivitet langs BFC i Jura og en evaporittenhet i Trias er observert, hvor listriske forkastninger som såler ut i saltintervallet, dannelse av assosiert hengblokkantiklinal og putedannelse i saltlaget er hovedtrekkene. Variasjon i sprang langs forkastningsstrøket, tykkelse på syn-rift sediment i hengblokken, erosjon av liggblokken og variasjon i strøkretning støtter en inndeling av BFC inn i 4 segmenter. En modell for dannelse av lukningen hvor brønn 6507/12-1 befinner seg er foreslått i denne opppgaven. Lukningen er foreslått å ha formet i et området med varierende strøkretning langs begge forkasntningene som avgrenser grabenen. Dette har fasilitert rollover av sedimenter i hengblokken mot hovedforkastningene i flere retninger, som har ført til dannelse av en kombinert antiklinal-horst struktur. Signifikant erosjon langs flankene av grabenen foregikk i Callovium. Inkonformiteten ved bunn Kritt er også erosiv over forkastningsskrenter. Selv om rift klimaks var fra Callovium til tidligst i Kritt, er det også tegn til syn-rift avsetninger i Tidlig Kritt. Reaktivering av forkastninger er også observert i Paleogen strata. De tørre brønnene i studieområdet kommer av umodne kildebergarter i området og mangel på langdistanse migrasjonsveier inn til de borede lukningene. Nærmere observasjon av erosjon og syn-rift sedimentasjon i studieområdet avslører mulige syn-rift sandsteiner i den ummidelbare hengblokken til BFC. Disse er forventet å være avsatt i et dypmarint miljø, men med et lokalt område av mulige grunnmarine syn-rift avsetninger ved en erodert intra-graben forkastning som er syntetisk til BFC, lokalisert sør i området. Dersom hydrokarboner har kommet inn i grabenen på dette dypet, kan disse sandsteinene utgjøre en migrasjonsrute som forbipasserer de borede, tørre prospektene. Slike syn-rift sandsteiner kan også representere reservoarer der de er helt eller delvis innkapslede i den omkringliggende skiferen slik at stratigrafiske feller blir dannet. Likevel er det en generell mangel på tegn til hydrokarboner i studieområdet, som sannsynliggjør at Ellingråsa Graben er plassert i en migrasjonsskygge.

Preface

This thesis has been carried out at the Department of Geosceince and Petroleum at the Norwegian University of Science and Technology (NTNU). The thesis is completed as the final part of a specialization in Petroleum Geology in the 5 year masters program *Petroleum Geosciences and Engineering*.

I would like to extend my utmost gratitude to my two outstanding supervisors, Associate Professor Kenneth Duffaut and Halvor Bunkholt for guiding me through this final year of my studies. The many discussions and thorough feedback throughout the work of this thesis has both been extremely motivational and helped me become a better geologist and geophysicist. I would also like to thank Dicky Harishidayat for all the help gathering and managing data, along with Diskos National Repository and Norwegian Petroleum Directorate for providing the seismic and well data.

I am also extremely thankful for the warm and friendly community among the students here at NTNU, always having each others backs and providing support whenever needed and laughs every day.

Finally, I am grateful to my parents for always answering the phone, giving me some much appreciated ventilation about my at times long, tedious and frustrating days in the computer lab. You are my favourite people.

Contents

Acronyms

$V_{clay,min}$ Minimum clay volume. 30

AI Acoustic impedance. 2, 21, 37, 69, 72

BCenU Base Cenozoic unconformity. 3, 4, 12, 24, 60, 62–64, 74–76, 110, 112, 113

BCU Base Cretaceous unconformity. 1, 2, 4, 5, 12, 24–26, 34, 36, 42, 43, 49–52, 54, 56, 61, 62, 73, 85, 91, 92, 102, 105, 106, 110, 112, 113, 116, 120

BFC Bremstein Fault Complex. 1–3, 5, 6, 8, 9, 11, 12, 16, 17, 22, 34, 36, 41–44, 46–53, 55, 56, 58–63, 73, 101–103, 106, 108, 109, 112–114, 120, 121

EWFZ Ellingråsa west fault zone. 2, 9, 34, 36, 42, 43, 46–48, 53, 54, 102, 108, 120

IMU Intra Melke unconformity. 11, 18, 53, 54, 56, 59, 61, 73, 85, 108, 113, 114, 120

KFC Klakk Fault Complex. 1, 8, 9, 11

MMU Middle Miocene unconformity. 13, 20, 76

MPU Middle Permian unconformity. 11

MTFC Møre-Trøndelag Fault Complex. 9

NCS Norwegian Continental Shelf. 6, 9, 12, 79, 85

NPD Norwegian Petroleum Directorate. 3, 22, 67, 114

RFC Revfallet Fault Complex. 11, 12

TOC Total Organic Content. 31, 73, 90, 91, 109

URU Upper Regional unconformity. 13, 19

VFC Vingleia Fault Complex. 1, 8, 9, 11, 12

YFZ Ytreholmen Fault Zone. 1, 8, 11

List of Figures

Chapter 1

Introduction

1.1 Study area

The Ellingråsa Graben structure was first formally defined by Blystad et al. (1995) as a sub-element of the Bremstein Fault Complex (BFC). Located at 65°N in the Norwegian Sea, it is an elongated graben structure delimited by mainly N-S striking faults and fault zones. Location of the study area on the Norwegian Continental Shelf (NCS) is seen in figure 1.1. Though the structure was not formally named until 1995, it is actually home to the first exploration wells drilled on the Mid-Norwegian shelf, dating all the way back to 1980.

1.2 Exploration history

On the first of July 1980 the Byfjord Dolphin rig, on mission for Saga Petroleum, marked the beginning of the exploration adventure in the Norwegian Sea by spudding the first exploration well drilled on the mid-Norwegian shelf, namely well `6507/12-1`, located on a large domal structure in the middle of the Ellingråsa Graben. Its main objective was to test the stratigraphic sequence and its primary target was an intra-Jurassic reflector at 2575 m. The well was dry, without indications of hydrocarbons (Saga Petroleum AS 1980). The second exploration well offshore Mid-Norway, well `6507/12-2` spudded in June 1981, was located on the eastern flank of the Ellingråsa Graben. Its goal was to test the possibility of having Triassic and Permian reservoirs and was to be drilled to 5000 meters or basement, whichever came first (Saga Petroleum AS 1981). This well was also dry with the exception of minor hydrocarbon traces in upper Triassic sandstone. The third and last well to be drilled in block 6507/12 to this day is well `6507/12-3` located on the edge of the Trøndelag Platform in the southeastern part of the block, close to the Midgard field. This well was also dry, but with gas peaks recorded from 474 - 804 m (Saga Petroleum AS 1985b). Another two dry exploration wells are drilled on the horst structure just west of the graben, namely 6507/11-2 (1982) and 6507/11-10 (2010). The Ellingråsa Graben has been abandoned from exploration activity since the initial exploration campaign in the 80s. Due to lack of discoveries or exploration activity in the area the last 30 years, it is a very sparsely described structure in publicly available literature. The licence comprising the Ellingråsa Graben is today held by Suncor Energy (60%) and OMV (40%) (NPD Fact Pages).

1.3 Aim of this thesis

After drilling 3 wildcat wells on block 6507/12 with disappointing results, the petroleum potential of the Ellingråsa Graben was deemed poor or non-existant, and the structure was abandoned from further exploration. Due to the lack of publications from the area there is an abundance of unanswered questions and interesting issues to focus on. This thesis will first give an overview of the regional geological framework in which the Ellingråsa Graben is found, based on previously published material. Through seismic interpretation on a 3D dataset and using information from the existing exploration wells, the geology of the graben will be outlined with its main structures, stratigraphic intervals and tectonostratigrpahic development through time. Emphasis throughout this work will be on intervals of Triassic and Jurassic age and the tectonic activity related to this strata. Special attention will be given to the Triassic evaporite unit present in the study area, and how this unit has affected the style of faulting and structural configuration within the graben. Finally, by analyzing the petroleum system elements in the area and taking a closer look at the dry wells, the thesis will attempt to answer the million dollar question: Could there be overlooked hydrocarbon potential in the Ellingråsa Graben, and if so, why have the previous exploration efforts ended in failure?

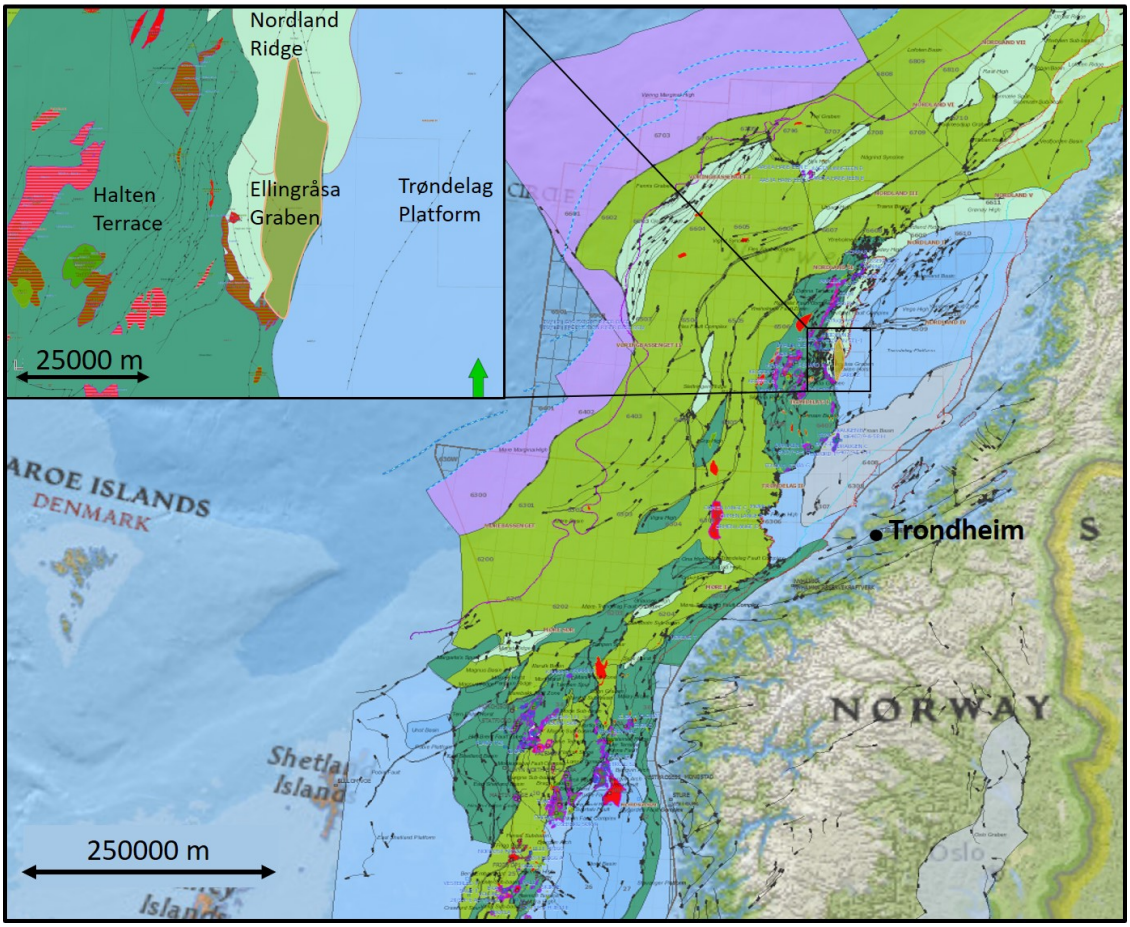

Figure 1.1: Overview of the location of the study area on the mid-Norwegian shelf

Chapter 2

Geological background

Herein the relevant literature creating the background for this thesis is briefly reviewed, outlining the geological history of the shallow water Norwegian Sea as it is understood today. This review will focus on the Halten Terrace area and geological events of pronounced petroleum geological significance. The reader is encouraged to consult the referenced literature for further elaboration. Chapter 4 is concerned with the geology of the Ellingråsa Graben specifically, as well as how this fits into the regional understanding of the Halten Terrace as outlined in this chapter.

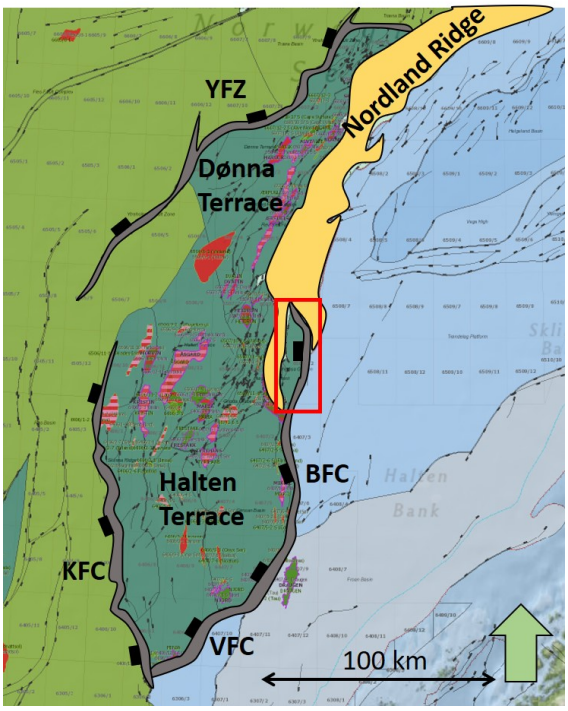

Figure 2.1: Overview of the Halten Terrace area and its bounding lineaments. BFC denotes the Bremstein Fault Complex, YFZ is the Ytreholmen Fault Zone, KFC is the Klakk Fault Complex and VFC denotes the Vingleia Fault Complex. Study area of this thesis outlined in red.

2.1 Regional tectonic setting

The Norwegian Sea, ranging from approximately 62-69°N is one of three main provinces on the Norwegian Continental Shelf (NCS). It is situated between the North Sea to the south and the Barents Sea to the north. The three provinces were part of a large epiocontinental sea before rifting leading to continental break-up and onset of seafloor spreading in Early Eocene (Bjørlykke et al. 2010). Its conjugate margin is found offshore Greenland, on the other side of the Atlantic spreading ridge. The continental margin outside middle Norway consists of a deep-water region with the deep Cretaceous Vøring, Møre and Rås basins to the west, flanked by terraces and platforms in shallower water to the east (Blystad et al. 1995). The Halten Terrace, where the Ellingråsa Graben is situated, is found in shallow to intermediate waters (Marsh et al. 2010). It is separated from the Trøndelag Platform to the east by the Bremstein Fault Complex (BFC) and from the Møre Basin to the west by the Klakk Fault Complex (KFC) (figure 2.1). In the north it is bounded by the Nordland Ridge and to the south by Frøya High (Vingleia Fault Complex (VFC). Its bounding lineaments trending N-S and NE-SW gives the terrace a rhomboidal shape. The Ellingråsa Graben which is found in the direct hanging wall of the BFC is an approximately N-S elongated graben structure located east of the southern tip of the Nordland Ridge. It is bound to the west by an antithetic fault zone, hereby termed the Ellingråsa West Fault Zone (EWFZ) .

2.2 Tectonostratigraphic development

The geological development of the mid-Norwegian shelf can be divided into three main phases, ending with today's passive margin setting (Blystad et al. 1995):

- A Late Silurian to Early Devonian compressional phase ending in the closing of the Iapetus Ocean during the Caledonian Orogeny.
- A Late Devonian to Paleocene period of several distinct rift episodes, finally ending with the break-up of Pangaea and onset of seafloor spreading in earliest Eocene.
- An Early Eocene to present day epoch of continent drift and active seafloor spreading between Eurasia and Greenland.

2.2.1 Late Silurian to Early Devonian compressional epoch

During this epoch sediments of Cambrian to Silurian age deposited in the Iapetus Ocean became thrusted onto the Baltican plate as the ocean was closing and the Caledonian Orogen was growing, creating nappe-stacks and deep thrust faults like the Møre-Trøndelag Fault Complex (MTFC) (Blystad et al. 1995). These weakness zones are important for the configuration of the mid-Norwegian shelf today because many of them were exploited to accommodate extension during the following rift episodes (Fossen 2010).

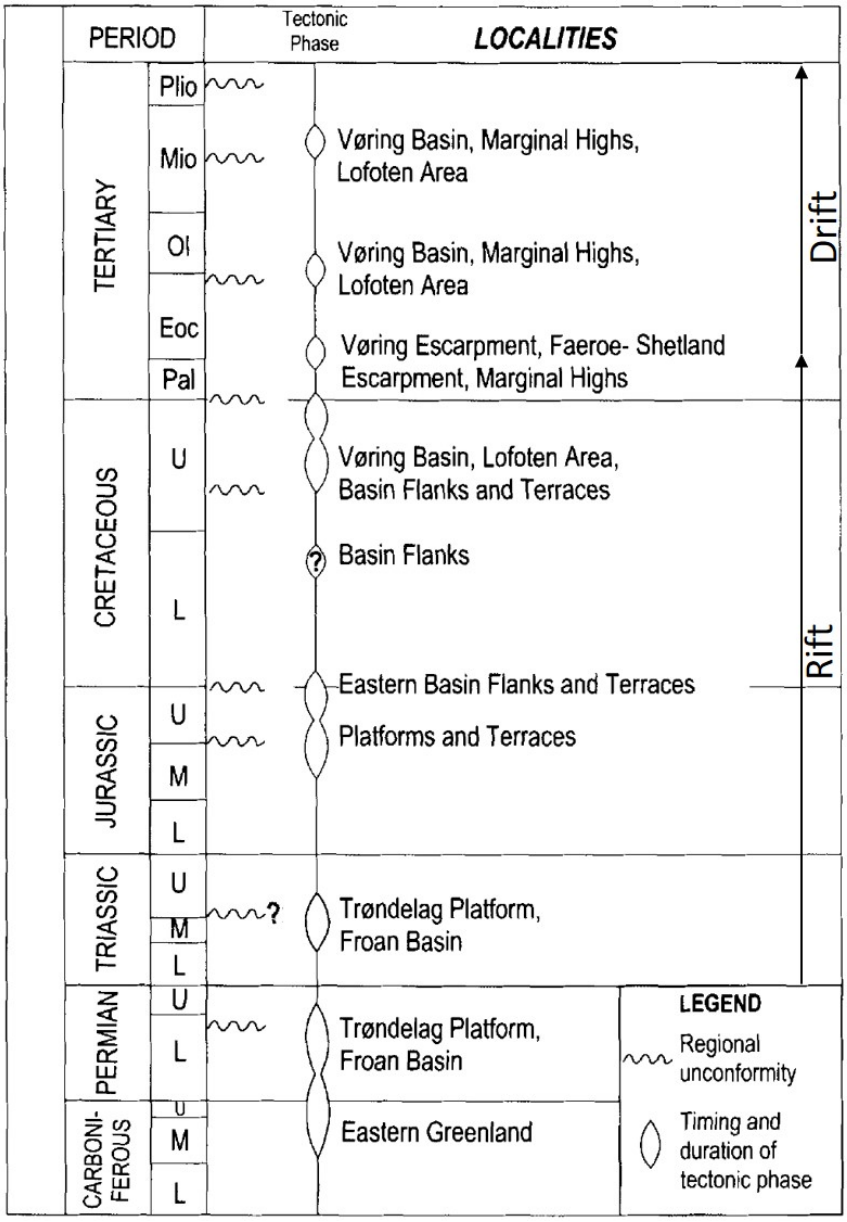

Figure 2.2: Tectonic history of the Norwegian Sea continental margin. From Brekke (2000).

2.2.2 Late Devonian to Paleocene extensional epoch

This period consisted of several distinct episodes of rifting starting at the collapse of the Caledonian Orogen and culminating with the break-up of Pangaea in earliest Eocene. Figure 2.2 shows an overview of the main tectonic history of the Norwegian Sea continental shelf from Carboniferous until Pliocene. Continental rifting during Late Devonian to Early Carboniferous created large intra-montane basins with sediments reaching great stratigraphic thicknesses. Examples are the Hornelen basin found onshore western Norway and the Bjugn Basin onshore mid-Norway (Blystad et al. 1995).

Late Carboniferous to Early Permian was a time of intense extensional block faulting and

syn-rift sedimentation in eastern Greenland (Surlyk 1990). Large half-graben basins of this time are on seismic observed deep on the Trøndelag Platform. Uplift of the late Devonian to early Permian sediments followed, causing erosion and ultimately creating a vast peneplain termed the Middle Permian Unconformity (MPU) (Brekke 2000; Bunkholt et al. submitted). This unconformity marks a change in tectonic style, from being governed mainly by crustal extension to thermal contraction becoming the primary mechanism of subsidence (Surlyk 1990). In the shallow-water region of the Norwegian Sea, the MPU separates Late Permian strata from old Caledonian thrust nappes or any Late Devonian-Carboniferous sediments which might be present (Bunkholt et al. submitted). A Middle Permian tectonic event caused transgression and a shift to generally deeper depositional environments, with marine muds deposited in half-grabens and carbonates developing on shallow-water structural highs like observed in well `6609/7-1` on the Nordland Ridge.

During Early to Middle Triassic, two episodes of rifting are identified. The first had its main syn-rift phase in Induan to Olenekian, followed by a less tectonically active phase in the Anisian and a new rift event in Ladinian. During the Induan the rift basins were still mainly in marine conditions with deposition of submarine fans and deep-marine sediments. These were subsequently overlain by more terrestrial, mainly lacustrine, deposits in the Olenekian (Bunkholt et al. submitted). The second Triassic rift phase in Ladinian led to flooding and deposition of two evaporite units present across most of the Halten Terrace (Wilson et al. 2015). Though the rifting was only moderate, this event has had a large impact on the configuration of the Halten Terrace today because the regionally extensive evaporite sequence provides an important rheological boundary in the upper crust which can act as a detachment surface, cause decoupling of faults and may thus to a large degree control geometry and configuration of structural elements (Blystad et al. 1995; Marsh et al. 2010; Wilson et al. 2015). As the Norwegian mainland was uplifted, it became an important source of sediments and an extensive fluvio-lacustrine flood basin developed in the study area. Meanwhile, the climate also gradually changed from arid to humid as the Jurassic was approached (Müller et al. 2005).

The Early to Middle Jurassic period was less tectonically active than both the Triassic rifting previously described and the next large rift episode during late Middle Jurassic to earliest Cretaceous. Over the Early to Middle Jurassic time period, the Norwegian-Greenland Sea rift evolved to a narrow shelfal strait connecting the Boreal Sea in the north to the Tethys Sea in the south. The Halten Terrace, Dønna Terrace and Trøndelag Platform were at this time combined to form a wide platform area along the eastern margin of the rift (Ravnås et al. 2014). Many of the significant reservoir units on the mid-Norwegian shelf were deposited during this time (elaboration on this in section 5.1.1).

Another period of increased tectonic activity occurred from middle Late Jurassic until Early Cretaceous resulting in significant fault block development. Faulting along the main lineaments, BFC, KFC, YFZ, RFC and VFC, began the separation of the Halten and Dønna terraces from the Trøndelag Platform. Wilson et al. (2015) shows that along the BFC the supra-salt restricted faults have an approximately N-S strike, while NE-SW striking structures appear to have a greater importance below the evaporite units. This tectonic event along with beneficial sea-level fluctuation facilitated deposition of deep-marine shales with high organic content (Dalland et al. 1988; Bunkholt et al. submitted). The Callovian intra-Melke unconformity (IMU) represents the deepest erosion in the Jurassic interval, and

thick syn-rift wedges related to this time period are often observed on seismic in hanging wall stratigraphy. At footwalls where the erosion was strong enough to penetrate into Middle Jurassic sandstones, erosion products could be re-deposited as submarine fans or shallow marine sands in the adjacent down-dip areas. The most famous feature in the subsurface of the NCS is the Base Cretaceous unconformity (BCU). This is due to both its strong soft amplitude set up by the large acoustic impedance constrast between the calcareous and soft, organic rich strata (see section 2.3) at this boundary, and because it represents the top of the petroleum geologically important Jurassic interval. Syn-rift sandstones related to the erosional period forming the BCU are also found deposited in shallow marine conditions on the dip-slope (Rogn Formation, see section 2.3) or as submarine fans in the hanging wall where the BCU erodes into Middle Jurassic sand over footwall scarps.

The Early Cretaceous was mainly a period of low tectonic activity and marine post-rift infilling of tectonic topography giving large thickness variations in this mainly shaly strata. In Late Albian to Coniacian a gradual uplift of the basin highs and margins started. With displacement increasing northward, local areas like the Nordland Ridge became exposed to subaerial erosion resulting in deposition of sandy fans on the adjacent basin floor. At the same time, the Frøya High further south remained a sediment starved area (Martinsen et al. 2005; Bunkholt et al. submitted). Because Early Cretaceous sedimentation rates were lower than the rate of thermal subsidence, the topography was not leveled out until the Santonian (Færseth and Lien 2002). At this time, the different local depocenters of the Early Cretaceous were connected into one large depocenter. Although literature describes the Cretaceous in the Norwegian Sea as a period of tectonic quiescence (Færseth and Lien 2002), as chapter 4 illustrates, there is also some evidence for active faulting during the Cretaceous in the Ellingråsa Graben.

The Norwegian Sea experienced another extensional tetonic episode from the latest Cretaceous to earliest Eocene (Doré et al. 1999). The Base Cenozoic unconformity (BCenU) represents a regional hiatus recorded in most of the wells in the Norwegian Sea (Bunkholt et al. submitted). During this time, the final separation of the Halten and Dønna terraces from the Trøndelag Platform also took place along the VFC, BFC and RFC. Westward migration of the rift axis led to major subsidence of the Halten Terrace and open marine sedimentation. The resulting flooding surface defines the base Eocene horizon (Bunkholt et al. submitted).

2.2.3 Early Eocene to present continent drift epoch

Following the Early Eocene break-up a change in the stress regime occurred, from NW-SE extension to mild SE directed compression (Doré et al. 1999). This resulted in post-rift inversion structures like the Ormen Lange Dome southwest of the Halten Terrace. In the final stages of the continental separation, lava deposition and sill intrusion took place along the Vøre and Møre margins, west of the study area (Henriksen et al. 1996). Igneous uplift happened in the west while in the east the Norwegian mainland was uplifted giving an increase of clastic input. Formations of this age observed in the study area are influenced by the igneous activity, like the Paleocene to Eocene tuffaceous Tare formation and the overlying smectite-rich Brygge formation (see section 2.3).

The last major tectonic phase was regional uplift during Neogene. Flexural doming and inversion of older depocenters during the Miocene was caused by strong compressional

events (Henriksen et al. 1996; Løseth et al. 2011). A mid-Miocene unconformity (MMU) is associated with this compression. The MMU eroded across the Nordland Ridge and on the flanks of the platform areas (Bunkholt et al. submitted). While the initial uplift was tectonic in nature, the most severe uplift occurred as a consequence of de-glaciation over the last 2.5 Ma causing major isostatic rebound (Doré et al. 1999). This also led to deposition of the massive, westward prograding Naust Formation consisting of glacial and glaciomarine sediments (Henriksen et al. 1996). During the Quarternary, the youngest unconformity seen on the mid-Norwegian shelf was formed, namely the Upper Regional unconformity (URU) (Rise et al. 2005). This Neogene period of uplift has had a large impact on the petroleum system on the mid-Norwegian margin, both through source rock maturation, reservoir quality and possibly also for seal integrity and tertiary migration.

2.3 Lithostratigraphic framework

This section gives an overview of the groups and formations defined on the mid-Norwegian shelf as they are described in literature, starting from the evaporite units in the Triassic and with emphasis on the intervals of greatest petroleum geological significance. Depositional environment and sedimentary architecture is included for key Jurassic intervals. A schematic lithostratigraphic chart of the Norwegian Sea is found in figure 2.3.

2.3.1 Triassic

The Triassic strata are informally grouped into two units, red beds and grey beds, where the grey beds are deposited in a more arid environment than the younger Red beds (Dalland et al. 1988). The Triassic rocks consist of mudstones, sandstones and evaporites, where the evaporites are divided into two intervals of approximately 400 meters each, separated by a mudstone interval of about 500 metres (Müller et al. 2005). These are penetrated by well 6507/12-2 in the study area (figure 4.3). The lower salt unit shows large thickness variations related to Ladinian syn-rift deposition, while the upper salt unit is more uniform in thickness (Bunkholt et al. submitted). There are also lateral facies variations, from halite dominated in well 6507/12-2 to more mudstone dominated with some anhydrite and carbonate in well 6507/6-1 (Wilson et al. 2015). The evaporites are overlain by a thick succession of continental clastic Red beds which are in turn overlain by Grey beds. The thickness of the entire Triassic package reaches over 3400 meters on the Nordland Ridge.

2.3.2 Båt Group

The Rhaetian-Aalenian (Dalland et al. 1988) Båt Group consisting of the Åre, Tilje, Ror and Tofte formations is the lowermost group in the Jurassic. It is present in most parts of the shallow-water Norwegian Sea region, though severly truncated towards the crest of the Norldand Ridge and locally totally missing at the apex (Bunkholt et al. submitted). It is the lower of the two principal hydrocarbon bearing groups on the mid-Norwegian shelf, with reservoir properties ranging from tight to high porosity and permeability.

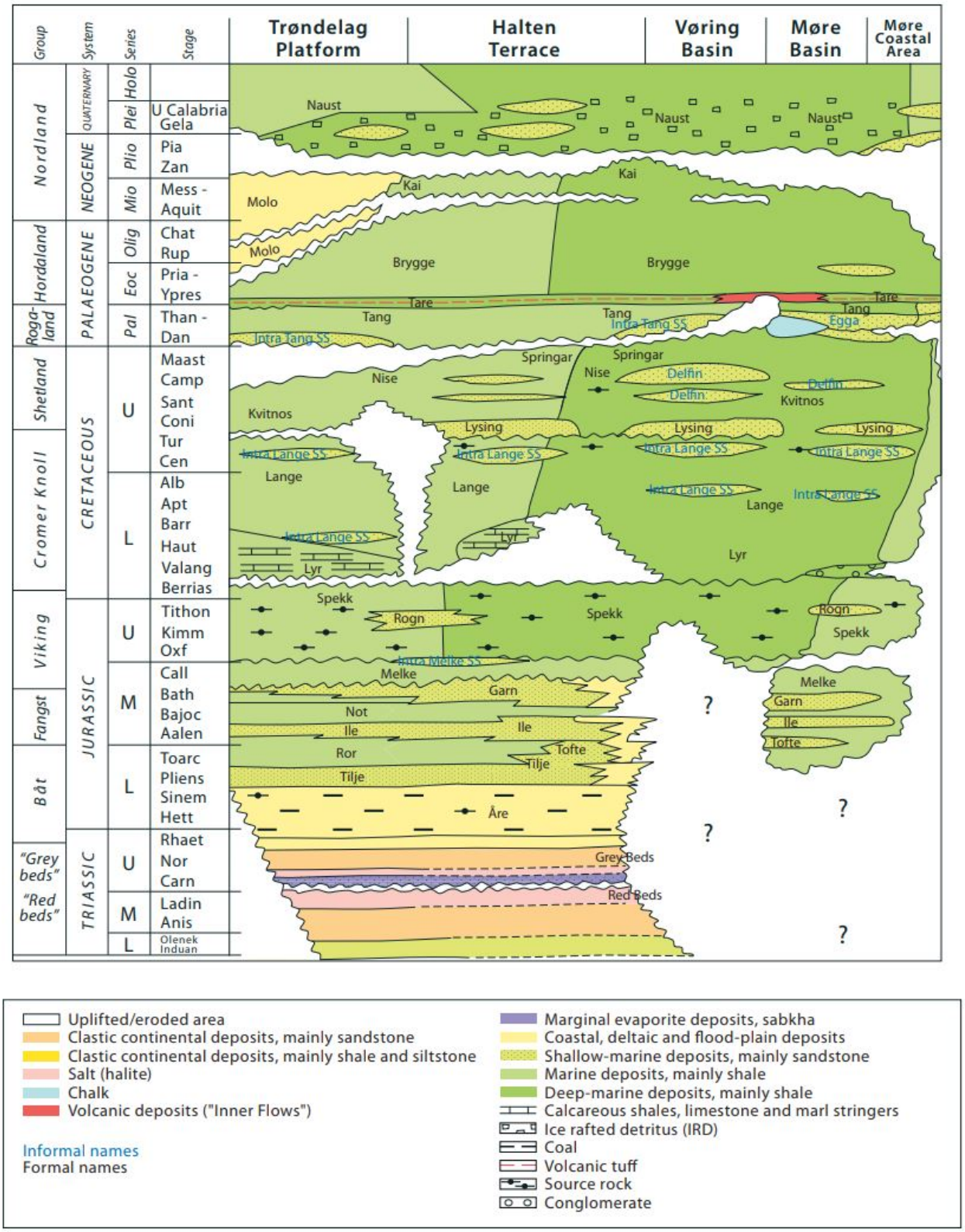

Figure 2.3: Lithostratigraphic chart of the Norwegian Sea. From NPD Fact Pages.

Åre Formation

This Formation is generally around 300-500 meters thick and of Rhaetian to early Pliensbachian age according to Dalland et al. (1988). However, its age is suggested to be Hettangian to Sinemurian in the more recent work of Martinius et al. (2001) and Thrana et al. (2014). The formation comprises coastal plain to delta plain sandstones, mudstones and coals and is thus clearly influenced by the humid climate building up in Late Triassic (Thrana et al. 2014). Traditionally, the formation has been divided into two members, the boundary between which has been defined as the top of the youngest coal-bearing strata (Dalland et al. 1988). Thrana et al. (2014) however has divided the formation into 7 zones in an overall transgressive trend reflecting the graudal tectonic development of the Halten Terrace. The oldest part of the Åre Formation consists of fluvial channel sandstones, swamp coals and floodplain mudstones deposited in a wet coastal plain environment, before a gradual transition into a lower delta plain setting occurs in the middle part of the formation. Towards the upper part of the formation a progressive transition into more open marine conditions is seen, related to the opening of a marine seaway between the Boreal Sea in the north and the Tethys Sea in the south (Ravnås et al. 2014; Thrana et al. 2014). Provenance studies for the formation suggests that the main source area shifted between and eastern Greenland source and a Norwegian margin source from the lower to upper part of the formation (Martinius et al. 2001; Morton et al. 2009).

Tilje Formation

The Early Jurassic Tilje formation of Sinemurian to Pliensbachian age overlies the Åre Formation and was deposited in a gradually forming narrow seaway between the Tethys and Boreal Sea (Martinius et al. 2001; Thrana et al. 2014). On the Halten Terrace it shows an overall tabular geometry and is generally between 100 and 150 meters thick, thinning over the Trøndelag Platform (Dalland et al. 1988). The Tilje Formation documents a transition from an embayment to a fully marine strait setting in the overlying formations (Bunkholt et al. submitted). It was deposited by strongly tide-dominated deltaic and estuarine systems with significant river influence, yielding a severely heterolithic formation (Ichaso et al. 2016). The heterogeneity of the formation is displayed at several scales, from laminae and beds to several meters thick packages (Martinius et al. 2001). An overall transgressive trend related to a late Pliensbachian to Toarcian sea-level rise is observed, from the fluvial dominated lower Åre Formation, to the various coastal tide-dominated facies of the Tilje Formation and finally into an open marine setting in the shaly Ror Formation overlying the Tilje Formation (Martinius et al. 2001; Ravnås et al. 2014; Ichaso et al. 2016). This rising sea-level was caused by a combination of local tectonic activity as well as by eustatic sea level rise (Kjærefjord 1991; Thrana et al. 2014). The main sediment source is suggested to be the mainland to the east of the Halten Terrace (Dalland et al. 1988), however a study from the Smørbukk field by Ichaso and Dalrymple (2014) suggests a northern sediment source.

Ror Formation

Overlying the sandstones of the Tilje Formation are the Pliensbachian to Toarcian mudstones of the Ror Formation, acting as a seal for the reservoir units below it. It is generally

between 70-170 meters thick on the Halten Terrace (NPD Fact Pages). It is the result of a rift induced transgression amplified by a global sea level high stand in the Early Toarcian (Bunkholt et al. submitted) and is dominated by dark grey mudstones interbedded with silty and sandy coarsening upwards sequences. These become more frequent towards the top of the formation, giving the unit an overall coarsening upwards trend on the Halten Terrace (Dalland et al. 1988).

In the western part of the Halten Terrace, the Ror Formation interfingers with the Tofte Formation (see figure 2.3) and in the northwestern corner (well 6506/12-1) the lower part of the Ror Formation is missing. Here, the Tofte Formation rests directly upon the sandstones of the Tilje Formation and the mudstones overlying the Tofte Formation represents the upper part of the Ror Formation (Dalland et al. 1988).

Tofte Formation

Tectonic activity in Late Pliensbachian and Toarcian generated uplift in both the western and eastern sediment source areas as well as locally within the study area (Bunkholt et al. submitted). Erosion from this resulted in deposition of coarse-grained, poorly to moderately sorted and texturally immature sandstone called the Tofte Formation on the Halten Terrace. The formation is deposited on the west side of the Halten Terrace as eastward prograding alluvial deltas reflecting the uplifted source area to the west. It is 65 meters in the type well, but rapidly decreasing in thickness towards east and south as it interfingers with the shales of the Ror Formation (Dalland et al. 1988). Bunkholt et al. (submitted) states that during Late Toarcian, fine-grained wave- and tide-influenced deltas also prograded from the east onto the Halten Terrace across the BFC while the rest of the shallow-water Norwegian Sea region experienced flooding and deposition of the upper part of the Ror Formation. This westward delta progradation gave way to deposition of the Tofte Formation on the eastern side of the Halten Terrace as well as to the west. This version of the Tofte Formations is younger than its western equivalent and is typically found in the area around the Mikkel Field (Bunkholt, *pers. comm.*).

2.3.3 Fangst Group

The Fangst Group of Aalenian to Bathonian age (Dalland et al. 1988) is the main hydrocarbon bearing interval in the Norwegian Sea. It overlies the Båt Group and is divided into the Ile, Not and Garn formations. In well 6507/12-1 located in the middle of the Ellingråsa Graben, the group is 119 meters thick, and northward thinning of the group approaching the Nordland ridge is reported (NPD 2019; Bunkholt et al. submitted). The thickest Fangst Group package of 378 meters is found to the south in well 6305/12-1. The group is present in most of the shallow-water Norwegian Sea region, however locally eroded over structural highs.

Ile Formation

The Ile Formation of Aalenian age is a sand-rich but highly heterogenous formation, deposited in a low-gradient tide-influenced delta setting (Martinius et al. 2005). It is described

by Dalland et al. (1988) as a mainly fine to medium grained, locally coarse grained, sandstone of variable sorting, interbedded with thinly laminated shales. On the Halten Terrace it is generally between 50-100 meters thick, thickening towards west and thinning towards northeast. Deposition occurred by two deltaic systems prograding from both west and east into the marine strait formed during the Toarcian transgression, merging on the central Halten Terrace (Bunkholt et al. submitted). Tidally influenced channel deposits and sandy tidal flat deposits are common. Provenance signatures along the BFC indicate that this part of the Ile Formation was deposited from the eastern delta system prograding westward across the Trøndelag Platform (Bunkholt et al. submitted).

The upper Ile Formation consists of deposits from an environment of lagoons and sheltered bays, as a result of a Middle Aalenian eustatic transgression (Bunkholt et al. submitted). This upper part of the Ile Formation is highly variable across the Halten Terrace from being dominated by tide-influenced deltaics and shoreline deposits in the southeast to a more eustarine setting in the southwest (Ravnås et al. 2014). The overall transgression continued into Late Aalenian culminating with the deposition of the open marine Not Formation.

Not Formation

The Not Formation of Aalenian to Bajocian age is recognized over the entire Halten Terrace where not eroded, and is generally less than 50 meters thick. Its thickest part is in the southwestern corner of the Halten Terrace and it thins gradually towards the Trøndelag Platform in the east. It consists of a coarsening upwards sequence from claystones with pyrite to carbonate cemented, bioturbated fine-grained sandstones (Dalland et al. 1988). With its basal low porosity and permeability the formation functions as a sealing unit between the Ile and Garn sandstones.

Garn Formation

The regressive pattern of upward coarsening seen in the Not formation continues into the Bajocian to Bathonian aged Garn Formation. The formation consists of braidplain and fluvial strata fronted to the southwest by mixed tide- and wave-influenced braidplain deltas and intervening wave-dominated shorelines and sandy estauries (Ravnås et al. 2014; Corfield et al. 2001). The lower part of the formation represents a regional regressive trend and a fluviodeltaic and marginal marine facies, followed by an aggradational stack of mixed wave-influenced, tide-influenced and river-influenced sandstones in the middle part of the formation (Ravnås et al. 2014). This is followed by a transgressive upper Garn member with high lateral variablility in infill pattern and sedimentary architecture (Corfield et al. 2001). According to a study by Morton et al. (2009) the regression at the base of the Garn Formation was accompanied by a switch in provenance from Norwegian sourced sediments to Greenland derived material. This reservoir sandstone unit may be over 100 meters thick on the Halten Terrace, but may also be completely eroded over structural highs. It is generally medium to coarse-grained, moderately to well-sorted with occasional mica-rich zones present (Dalland et al. 1988).

2.3.4 Viking Group

This group, divided into the Melke, Rogn and Spekk formations, is present over most of the Halten Terrace but thins toward and is locally absent over the Nordland Ridge.

Melke Formation

In late Bajocian to Bathonian a gradual transgression from northwest and southeast occurred, resulting in deposition of the Melke Formation mudstones that are of Bajocian to Oxfordian age, in part time-equivalent with the upper Garn Formation (Corfield et al. 2001; Bunkholt et al. submitted). Together with the overlying Spekk Formation, the open marine Melke Formation forms a regional seal for the reservoir units below, but can also be considered a potential source rock in the study area. As explained in section 2.2.2, uplift of rift shoulders led to deep erosion in the Callovian, development of the IMU and thick syn-rift deposits. Associated with this erosion are intra-Melke sandstones deposited in both the hanging wall as submarine fans (found in wells `6407/10-1` and `6407/10-2`) and on the dip-slope of the footwall as shallow marine deposits (well `6407/12-3`). The formation is 116 meters thick in the type well and 44 meters thick in the reference well, but can reach thicknesses of several hundred meters in local hanging walls (Dalland et al. 1988).

Spekk Formation

Deposition of the very organic rich marine Spekk Formation happened during the culmination of the major tectonic rift phase in Late Jurassic to earliest Cretaceous. This formation is of Oxfordian to Ryazanian age (Dalland et al. 1988) and constitutes the main source rock unit on the mid-Norwegian shelf. The formation is present in most of the Halten Terrace area, though absent either due to erosion or non-deposition locally at strucural highs such as the Nordland Ridge (Dalland et al. 1988). In wells it is commonly between 20-50 meters thick but since these are often drilled on structurally elevated locations somewhat greater thicknesses should be expected in structural low areas. Like for the older Melke Formation, erosion of sandstone during this time gave sandy sediments deposited as deep marine fans or shallow marine sand in hanging walls and on footwall dip-slopes. Though these sand bodies could be considered intra-Spekk sandstones, the latter is defined as the shallow marine Rogn Formation.

Rogn Formation

This formation is of Oxfordian to Kimmeridgian age and is commonly found intra-Spekk as a shallow marine sandstone, often with excellent reservoir quality. It is mainly present in the Draugen field area and down-dip on the Frøya High footwall, both locations far south of the study area in this thesis. In the type well it has a thickness of 49 meters.

2.3.5 Cromer Knoll Group

This group consists of calcareous and non-calcareous mudstones interbedded with marls and stringers of carbonate or sandstone. It is of Valanginian to Coniacian age (Dalland

et al. 1988) and is of very varying thickness, infilling the topography created by the latest rift episode (Færseth and Lien 2002). On the Halten Terrace it is generally hundreds of meters in thickness which indicates creation of accommodation space through both thermal and tectonic subsidence throughout the Early Cretaceous (Bunkholt et al. submitted). The Lysing and Lange formations are sandstones of the Cromer Knoll Group mainly deposited in a deep marine environment as submarine fans, and occasionally in a shallow marine environment.

2.3.6 Shetland Group

This group is approximately 900 meters thick in representative wells in the Norwegian Sea, though it is usually thin across the Trøndelag Platform, Frøya High and over the Norland Ridge according to Dalland et al. (1988). It consists of calcareous claystones with stringers of carbonate or sandstone. These mudstones are often highly overpressured. It is of Santonian to Maastrichtian age.

2.3.7 Rogaland Group

The Rogaland Group is of Paleocene to Early Eocene age (Dalland et al. 1988) and represent the last deposited strata before the continental break-up in Early Eocene. It consists mainly of claystones with minor silt deposited in a deep marine environment, in addition to locally developed sandstones due to uplift and erosion of the Norwegian mainland. Tuff is common in the upper part of the group due to the volcanic activity associated with the continental break-up happening in the west at the time. The group is 134 meters thick in well `6407/6-1` (Dalland et al. 1988).

2.3.8 Hordaland Group

This group consists of the Brygge Formation smectite-rich mudstones with abundant polygonal faulting. Local stringers of sandstone with glauconite, pyrite and shell fragments are observed (Dalland et al. 1988). The group is present throughout the Halten Terrace, but thins towards the Norwegian mainland before it is eventually eroded by the URU. It is of Early Eocene to Early Miocene age, has a thickness of 450 meters in the type well and was deposited in a deep marine environment (Dalland et al. 1988).

2.3.9 Nordland Group

Above the Brygge Formation the Kai Formation is found on the Halten Terrace, deposited in a marine environment with varying water depth (Dalland et al. 1988). It consists mainly of alternating claystone, siltstone and sandstone with limestone stringers. Minerals like glauconite and pyrite are common, and shell fragments are often found. It is generally of Early Miocene to Pliocene age (Dalland et al. 1988). The Molo Formation of the Nordland Group is not present in the study area, but is considered a shallow-marine time equivalent to the Kai Formation by Eidvin et al. (2007), suggested to be deposited by coastal progradation as a result of regional onshore uplift. There is however some debate about the age of the

Molo Formation. Løseth et al. (2017) concludes that the Molo Formation is younger (mainly Pliocene) than the Kai Formation (dated here to Middle and Late Miocene). According to this model, relative base level fall of several hundred meters is recorded at the onset of the Middle Miocene compression phase, simultaneous with development of the MMU and deposition of the Kai Formation to the west. This work suggests that upon termination of the Miocene compression phase a cumulative base level rise in the order of 500 meters occurred and that deposition of the Molo Formation is related to this transgression. Finally, the characteristic westward prograding Naust Formation was deposited as a thick, several hundreds of meters, wedge of glacial and glaciomarine sediments over the study area in Pliocene and Pleistocene (Henriksen et al. 1996). A thorough review of this formation is found in Ottesen et al. (1999). The rapid deposition of this formation is proposed to have caused disequilibrium compaction and overpressure build-up of underlying low-permeability strata, as well as a temporary altering of heat flow (section 5.1.3).

Chapter 3

Dataset and methodology

3.1 Dataset

3.1.1 Seismic data

The HT07 3D-seismic cube supported by the available well data (see section 3.1.2), forms the basis for the geophysical evaluations in this thesis, mainly in the form of interpretations and attribute analyses. The survey covers an area of approximately 830 km^2 and the overall quality of the seismic cube is good. The 3D interpretations are supported by regional lines from the 2D survery GMNR−94 of moderate quality. See figure 3.2 for position of seismic survey and wells used. The polarity convention of the seismic is set to reverse SEG polarity, meaning that an increase in acoustic impedance (AI) is represented by a trough (blue) (figure 3.1).

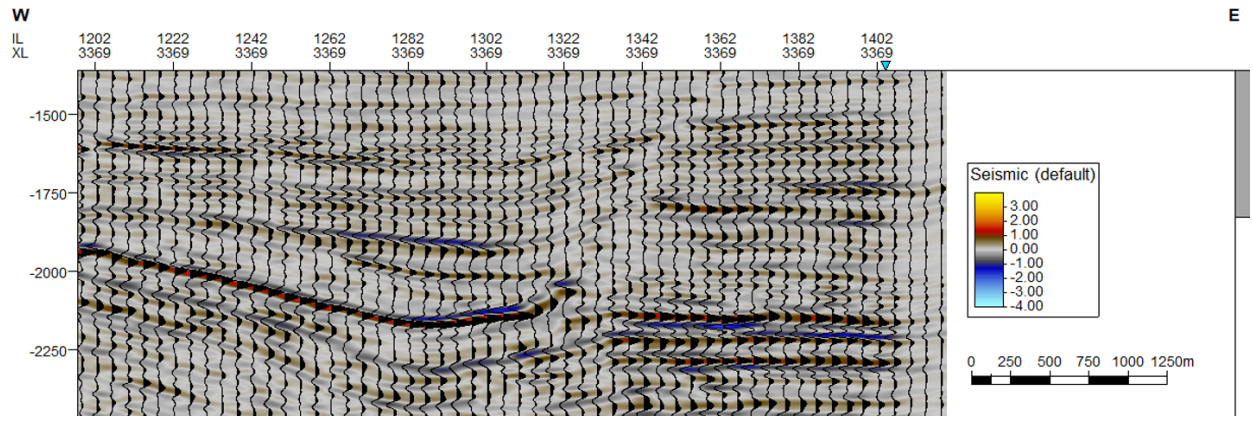

Figure 3.1: Seismic section from the HT07 survey illustrating reversed SEG polarity convention. Depth in TWT

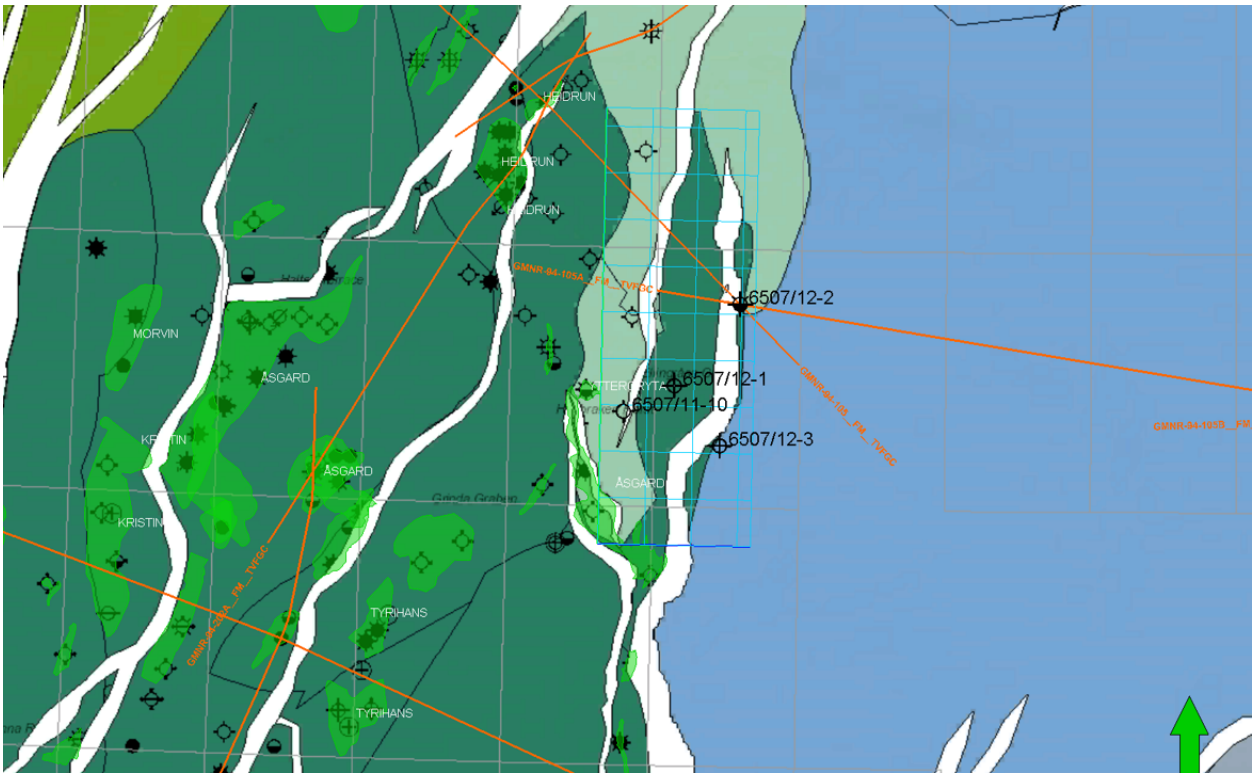

Figure 3.2: Overview of the seismic and wells used in this thesis and their location. GMNR-94 lines in orange, HT07 seismic survey in blue. Fields and discoveries on the Halten Terrace in bright green.

3.1.2 Well database

Information from 3 exploration wells drilled within the survey area in the 1980s is used in this work. The first to be drilled, `6507/12-1`, is situated in the middle of the graben on a structural anticline, and was dry without shows. This well was actually the first exploration drilled on the mid-Norwegian shelf. The second exploration well drilled in the Norwegian Sea was well `6507/12-2`, situated on the footwall of the BFC. This well was also dry, except for some traces of hydrocarbons in Triassic level minor sandstones. The last well used in the project is the `6507/12-3` well, drilled on the south-east flank of the Ellingråsa Graben, close to the Midgard field (see figure 3.2). This well was also dry, except for some gas peaks recorded at shallow levels. On the western flank of the graben, well `6507/11-2` was drilled in 1982. This well is not tied to the seismic and reports and studies from this well have not been available in this project. FInally, it should be noted that another well drilled on the western flank of the graben as recent as 2010, namely well `6507/11-10` situated just north-east of the Midgard field. While most of the information from this well is not yet publicly available, the stratigraphy reported on NPD is used for orientation and to quality check the depth conversion. This well was water bearing without shows. For a summary of key well information, see table 3.1.

Table 3.1: Well database for this project. Key information from NPD fact pages. Well 6507/11-10 is in grey due to the limited information available.

Well	Year Drilled	TD (MD)	Oldest Formation penetrated	Water depth (m)	Content
6507/12-1	1980	3720	Triassic red beds	225	Dry
6507/12-2	1981	5008	Triassic evaporites	261	Shows
6507/12-3	1985	2600	Early Jurassic Åre Formation	240	Dry
6507/11-2	1982	2905	Triassic grey beds	243	Dry
6507/11-10	2010	2319	Early Jurassic Tilje Formation	269	Dry

In addition to the reports and analyses available on NPD fact pages, several well studies of biostratigraphy, sedimentology, petrography and maturation are downloaded from the Diskos database and is used to aid and support interpretations and model. There are abundant reports available from the 6507/12-1 and 6507/12-2 wells, but limited studies conducted on the 6507/12-3 well. Core photos are also reviewed where relevant.

3.1.3 Software

This thesis has used Petrel 2018 for well-tie, well correlation, seismic interpretation and depth conversion. MATLAB was used to create an algorithm for net exhumation estimation. PetroMod 2014 was used to create a 1D model for burial in the location of well 6507/12-1.

3.2 Method

3.2.1 Seismic interpretation

Well tie

Wells 6507/12-1, 6507/12-2 and 6507/12-3 all contain good quality checkshot data. These are therefore tied to the seismic in order to create a reliable time-depth relation to aid interpretation. Especially well 6507/12-2 is considered important due to penetration of strata down to evaporite levels in the Triassic. The well-tie for 6507/12-2 is seen in figure 3.3.

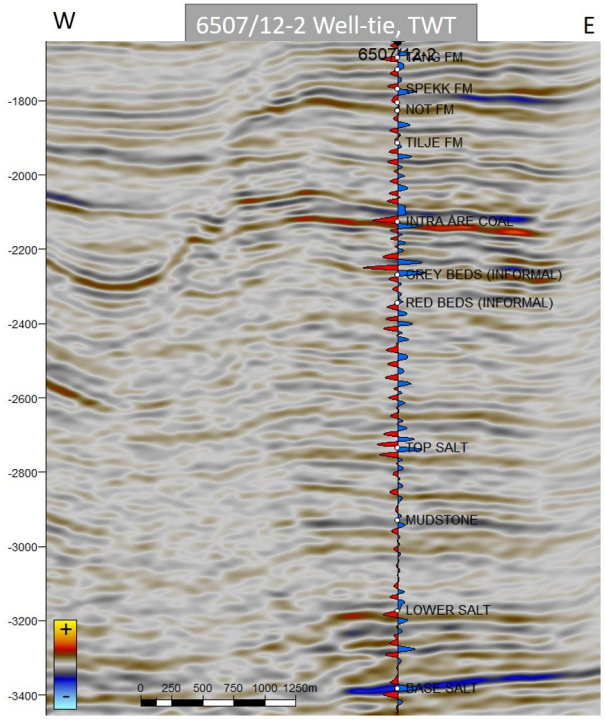

Figure 3.3: Well-tie seen on a line going through well `6507/12-2`.

Mapping

The following horizons are mapped and surfaces created:

- Top Naust
- Top Kai
- BCenU (Top Springar)
- Top Albian/Aptian reflector
- BCU
- Top Fangst
- Top Tilje
- Intra Åre Coal marker
- Top Triassic intra-Salt unit mudstone
- Top lower salt
- Base lower salt

Figure 3.4 illustrates the seismic characteristics of each of the horizons mapped. In addition, top Ile Formation, top Åre Formation, top Ror Formation and the top of the salt unit are interpreted on certain relevant lines. The choice of horizons to map is made to fit the aim of the thesis, with focus being on the Jurassic horizons. The choice of mapping top Fangst Group and top Tilje Formation is made because these horizons represent the boundary between underlying permeable zones and overlying sealing units (Viking Group and Ror Formation, respecitvely), making these horizons important considering migration and accumulation of hydrocarbons. A lot of attention is also given to the horizons within the Triassic salt unit, due to their importance for the structural configuration of the graben.

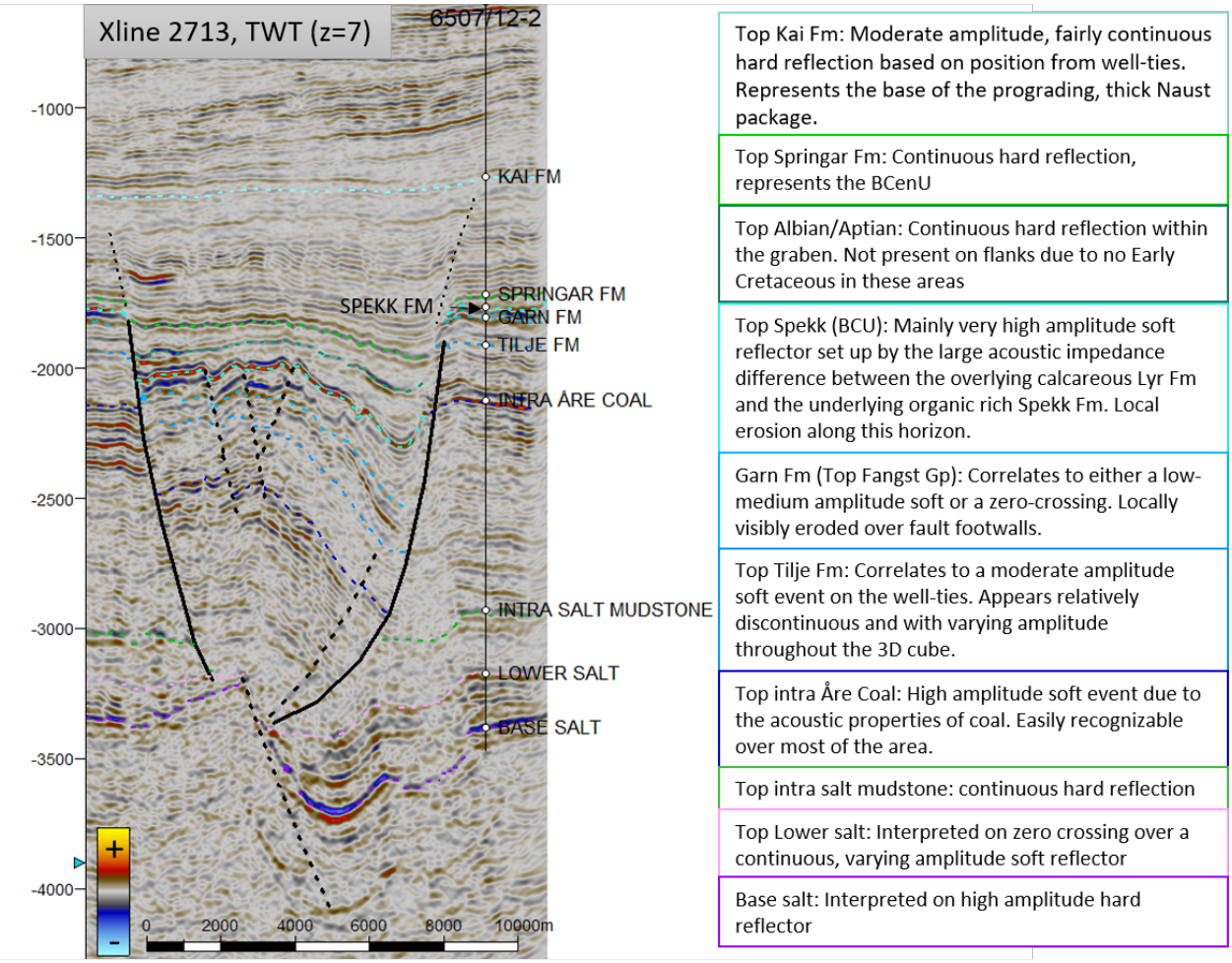

Figure 3.4: Xline 2713 illustrating and explaining the characteristics of the mapped horizons. The basis for choice of reflectors to map is, naturally, the well-ties.

Horizons are interpreted at every 16th inline or xline, with less spacing in areas close to faults or in structurally complex areas. 3D Autotracking was used where viable, such as for relatively continuous, unfaulted horizons like Top Naust and Top Kai. 3D autotracking was also applied in certain areas of the more structurally complex horizons. The structure map for the BCU surface was, after its creation, used to create arbitrary lines following relay

ramps etcetera in an attempt to find more or less continuous strata aiding interpretation in uncertain areas. Confidence polygons are created for all mapped surfaces (see chapter 6). A typical grid of interpreted lines is seen in figure 3.5

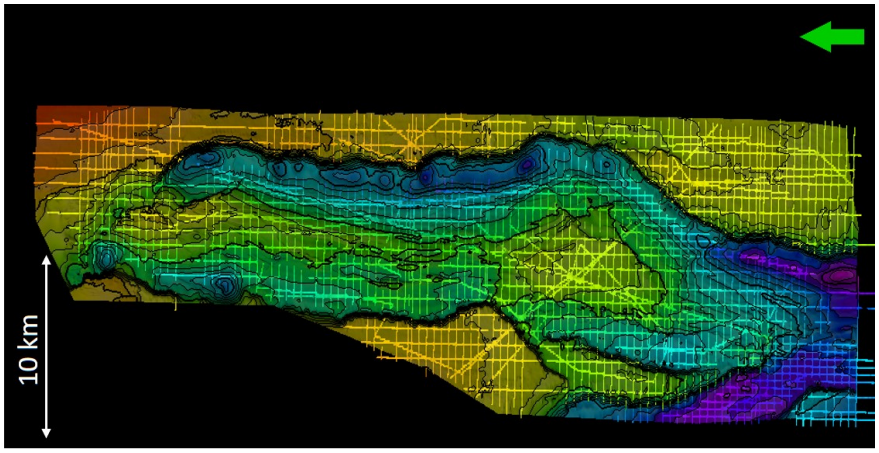

Figure 3.5: The typical mapping process. A 2D grid is created with some additional arbitrary lines through expected continuous strata to aid interpretation in low-confidence areas. 3D autotracking applied where appropriate.

Fault interpretation

Faults are interpreted on every 16 xline, or on random lines perpendicular to the strike of the fault for segments not having N-S strike. To aid interpretation of faults, a variance cube is used as input with RMS-amplitude extraction on the BCU surface. The resulting surface seen in figure 3.6 nicely outlines the major discontinuities making fault interpretation easier. Because the focus of this thesis is on strata of Triassic and younger age, faults below the salt unit are generally not considered.

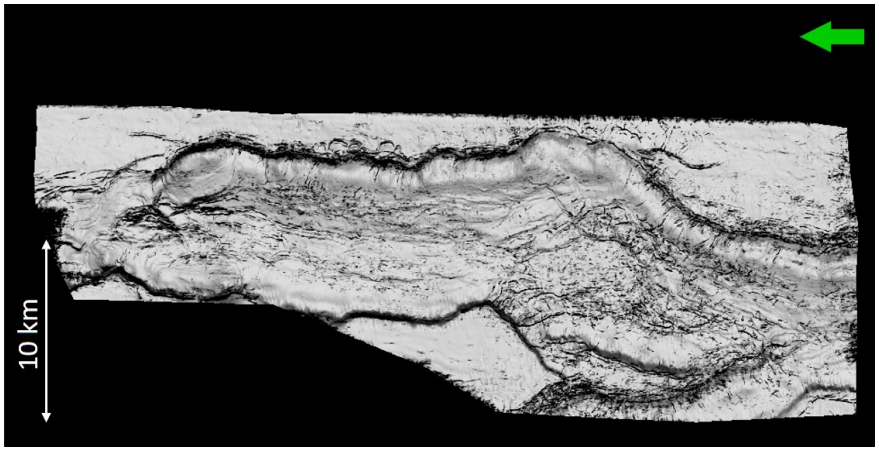

Figure 3.6: Mapping faults was aided by RMS-amplitude extraction on a variance cube in a window around the BCU surface.

3.2.2 Depth conversion and maturity maps

This section step-wise illustrates the process of converting the surfaces from the time domain to the depth domain, following the recommendations from the Petrel Geophysics handbook by Schlumberger:

1. Define velocity intervals
2. Define velocity functions for each interval
3. Quality control
4. Perform domain conversion

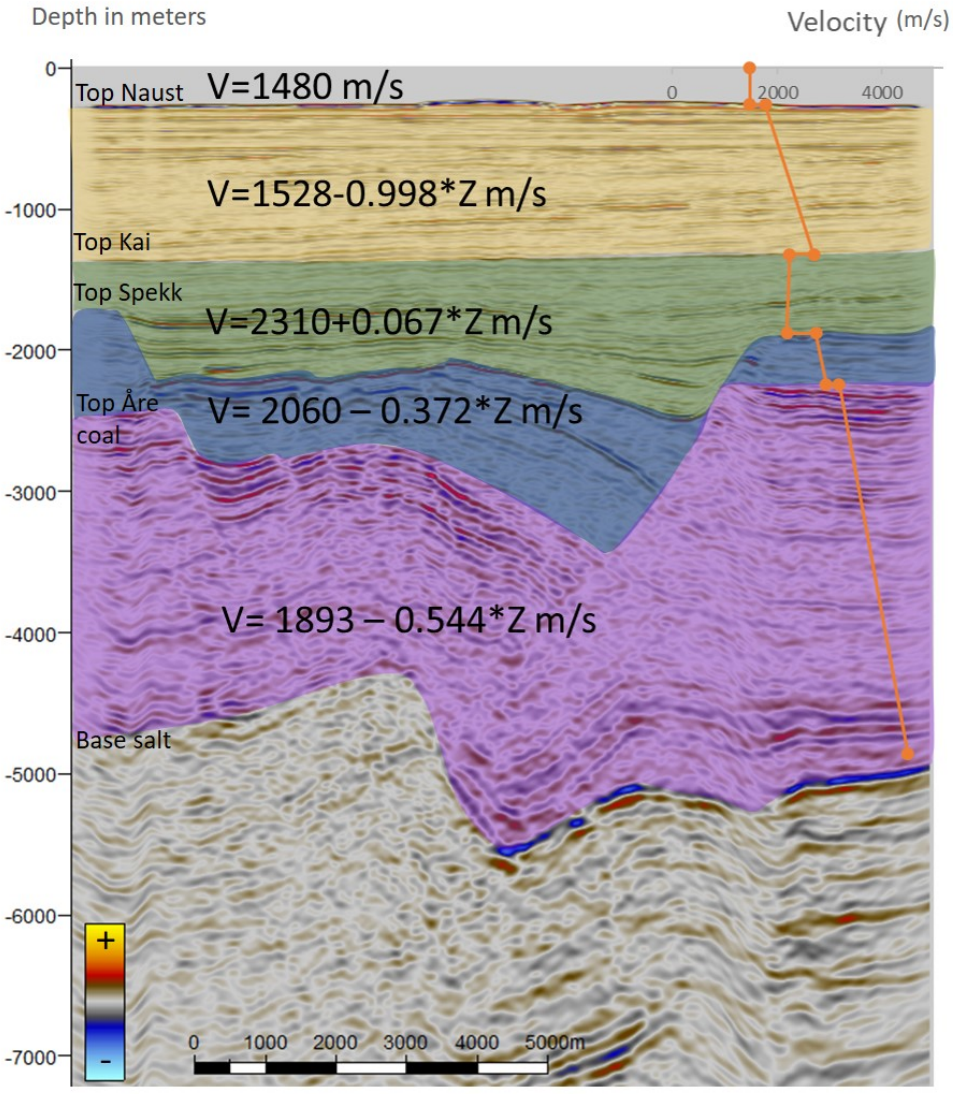

Figure 3.7: Velocity intervals with associated velocity functions (Z is negative). The resulting velocity function with depth is included in orange to the right in the figure.

First, the checkshot data is quality checked and found to be good for all wells on block 6507/12. Next, 5 velocity intervals with associated velocity functions dervied from the quality checked checkshot data are defined, as follows (figure 3.7):

- Sea level to top Naust Formation
- Top Naust Formation to top Kai Formation
- Top Kai Formation to BCU
- BCU to top Intra Åre Formation coal
- Top Intra Åre formation coal to base salt

The resulting velocity function with depth is also seen in figure 3.7, and shows that the general trends reported by Storvoll et al. (2005) hold for the Ellingråsa Graben area, with rapidly increasing velocities in the Naust Formation and a slightly inverted velocity trend in the Paleogene and Cretaceous strata. After quality checking the output data, depth conversion is conducted for the desired surfaces and seismic.

To make simple temperature maturity maps, a temperature-depth relation has to be established. Here, this relation is provided by the 6507/12-1 completion report, where bottom hole temperatures have been measured and corrected (Saga Petroleum AS 1980). The mean temperature gradient was found to be 36°C/km. The surface-water interface temprature is set to 5°C. This is found by inputting the geographical location to PetroMod. Thus, the temperature-depth relation becomes

$$T(Z) = 5°C + \frac{36°C}{1000m}Z$$

Where Z is depth in meters and T is temperature in Celcius. This relation is used to make depth windows for oil and wet gas generation based on theoretical temperature maturation windows (Allen and Allen 2013), as seen in table 3.2 below. By calculating the distance from seabed to the desired source rock interval and rendering the color table such that it is governed by these temperature intervals, simple temperature maps can be generated showing which temperature window the different parts of a surface lies within (see figure 5.11 for resulting maps).

Table 3.2: Temperature-Depth relation for theoretical maturation windows

Maturation window	Temperature (°C)	Depth (m below seabed)
Immature	<80	<2083
Early oil	80-100	2083-2639
Peak oil	100-120	2639-3194
Late Oil	120-150	3194-4028
Wet Gas	>150	>4028

3.2.3 Net exhumation estimation

A scheme for estimating net exhumation in the Norwegian Sea was created as part of this authors specialization project. This scheme is applied to well `6507/12-1` within the study area to investigate whether the area has been net exhumed. Since net exhumation estimates are not the main focus of this thesis, the workflow will only be briefly outlined here. The reader is advised to consult Blilie (2018) for further elaboration on method, uncertainties and results of this work. MATLAB sciprts for this net exhumation scheme are attached in appendix B.

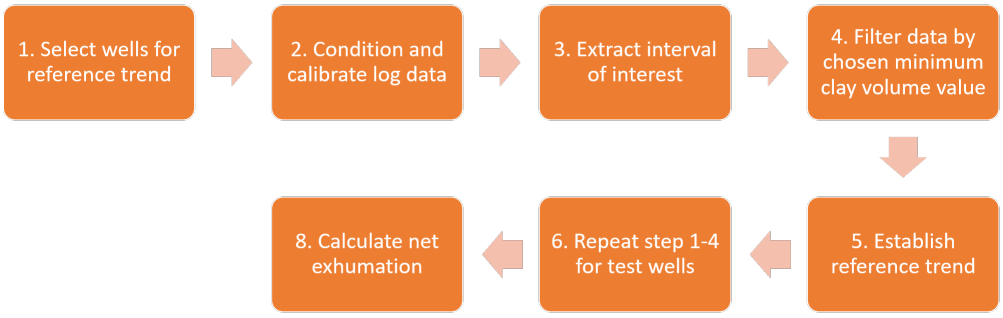

Figure 3.8: The general workflow for establishing a reference trend and comparing it to test wells in order to estimate net exhumation. Figure from (Blilie 2018)

There are some key assumptions that have to hold in order for the suggested scheme to be reasonable. First, compaction has to be considered an irreversible process. Second, it is assumed that velocity-depth trends can be linearly approximated. The shales in the interval are assumed homogeneous within the area used to create the reference trend. Lastly, the undercompaction effect of overpressure is assumed equal througout this study area.

1. **Select wells for reference trend**

   Hansen (1996) proposed a roughly coast-parallel zero net exhumation line in his work. The wells used to create a reference, zero net exhumation trend are taken from parts of the shallow water Norwegian Sea region situated well behind this proposed zero-line, where one should be confident that the net exhumation is zero.

2. **Condition and calibrate log data**

   The logs used for net exhumation estimates in this project are the gamma ray and the sonic log, which are imported into MATLAB and quality checked. The gamma ray log is calibrated and the sonic log is converted to P-wave velocity.

3. **Extract interval of interest**

   The estimates are based on intervals of Cretaceous shale. Therefore, the depth interval of log data corresponding to Cretaceous strata is extracted for each of the reference wells.

4. **Filter data by chosen minimum clay volume value**

   Since this reference trend is to be based on shale lithology, it is important to exclude intervals consisting of less shale than a chosen minimum clay volume ($V_{clay,min}$), here set to 0.5. Clay volume is calculated using the Gamma Ray (GR) log:

$$V_{clay} = \frac{GR_{log} - GR_{min}}{GR_{max} - GR_{min}}$$
$$V_{clay} = \frac{GR_{log} - GR_{min}}{GR_{max} - GR_{min}} \geqslant V_{clay,min}$$
$$GR_{log} \geqslant V_{clay,min}(GR_{max} - GR_{min}) + GR_{min}$$

   The GR_{max} value represents the shale line, meaning 100% shale and the GR_{min} value represents the sand line, meaning 100% sand. Using the equation above one can create a gamma ray cut-off based on desired $V_{clay,min}$ requirement.

5. **Establish reference trend**

   The reference trend is established by plotting the resulting velocity or density values against depth for all the well together and make a linear least squares best fit. The result of this is seen for velocity values in figure 3.9. It is decided to also plot the velocity-depth trends from the work of Storvoll et al. (2005), and Johansen (2016), though these are not established using mainly data from the shallow water Norwegian Sea region.

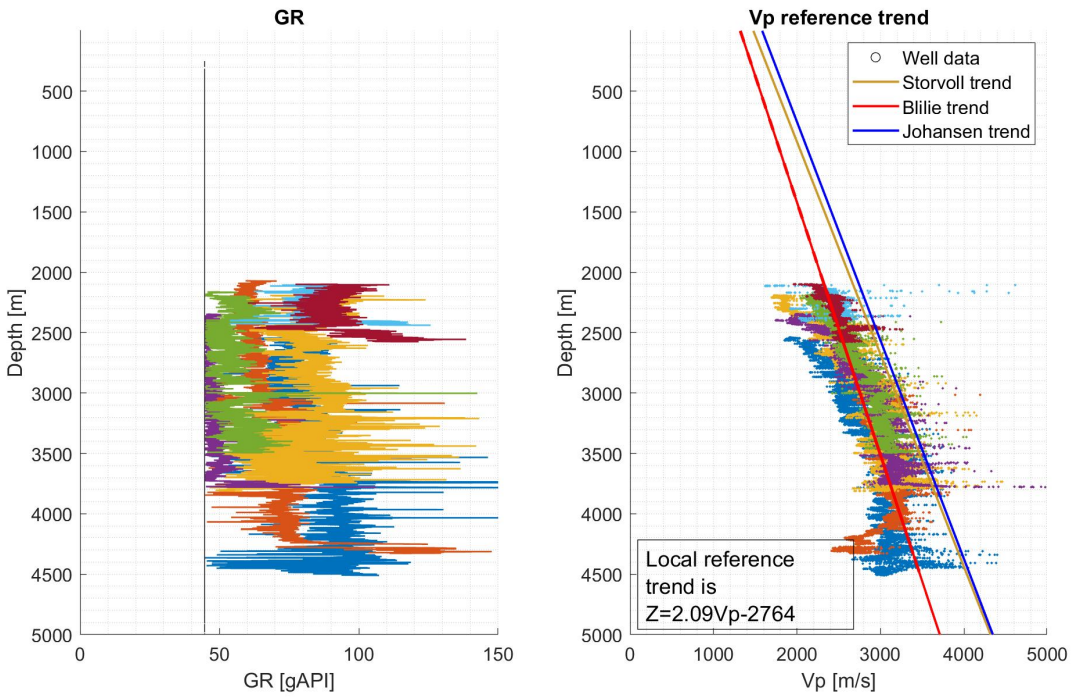

Figure 3.9: Reference trend for assumed zero net exhumed Cretaceous intervals in the Norwegian Sea as established in this authors Specialization project (Blilie 2018)

6. **Repeat step 1-4 for test wells**

   The previous steps need to be repeated only this time for test wells with a goal to estimate the net exhumation for that well.

7. **Calculate net exhumation**

   The filtered velocity data is plotted and a best fit line with the slope forced to be equal to that of the reference trend is created. The depth difference between these two lines represents a base case for the net exhumation. To represent the usually significant amount of uncertainty in these estimates, the standard deviation in the data is calculated by looking at deviation of the plotted data points from the best fit line. The standard deviation lines are plotted along with the test well best fit line, giving a minimum, base and maximum net exhumation estimate.

3.2.4 PetroMod 1D modelling

PetroMod 2014 is used for 1D modelling of burial history in well `6507/12-1`, with a goal to gain insight into source rock maturity in the study area. Depth, thickness and time of deposition of the intervals penetrated by the well are extracted from chronostratigraphic data (Paleoservices LTD. 1980; Saga Petroleum AS 1983b). The different layers are assigned appropriate lithologies and their status in terms of petroleum system elements are also decided. The kinetic model from Pepper and Corvi (1995) is used for the Spekk Formation and the coal-rich part of the Åre Formation, with type II and III kerogen as indicated by source rock analyses from the well (Continental Shelf Institute 1981). These reports also indicate a hydrogen index of 350 and an average TOC of 8.5% in the Spekk interval along with a hydrogen index of 150 and mean TOC of 8% in the coal-rich part of the Åre Formation for the study area. These numbers are therefore used as input to the model. Some source rock potential of the Melke Formation is also possible, however this is exluded in the modelling due to expected insignificant contribution and unknown hydrogen index. The main input table for this modelling is seen in figure 3.13.

The boundary conditions (tables seen in figures 3.10 to 3.12) are also a crucial factor when creating a 1D model in PetroMod. It should be noted that there are significant uncertainties related to these, as is discussed in section 6.5. The paleo water depth is extracted from biostratigraphical data, but is poorly constrained and should only be considered a rough estimate (Laboratoire de Geologie de Boussens 1981a). Surface-water interface temperatures through time are automatically generated based on the input values of the other boundary conditions and the geographical position of the study area today. The boundary condition with the greatest impact on resulting maturity is the paleo heat flow. The heat flow of today is based on the regional heat flow maps of Pascal (2015) and yields a very good fit with the measured bottom hole temperatures in the `6507/12-1` well. However, the heat flow through history is more uncertain. Conceptually, following the model of McKenzie (1978), the heat flow should increase at the onset of rifting and decrease exponentially during the post-rift thermal subsidence stage. This is taken into account when constructing the heat flow table. Though the general shape of the heat flow curve may be reasonable, the absolute values of the rifting episode in the Late Jurassic to earliest Cretaceous should be considered

uncertain. These are based on the work of Hermans et al. (1992) and since the goal is to make a maximum maturity case for the given burial history, the maximum paleo heat flow values are somewhat exaggerated. For uncertainties regarding the PetroMod 1D modelling, see section 6.5.

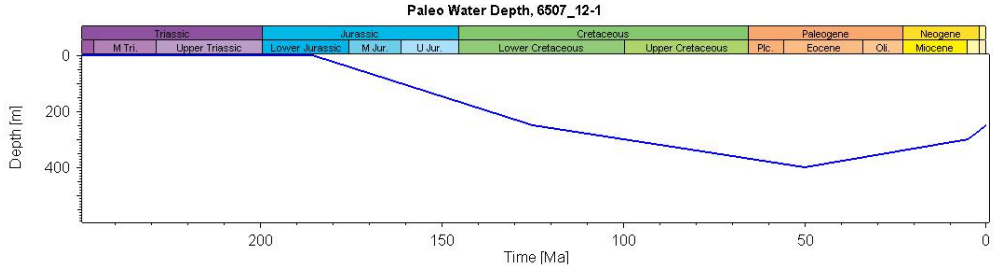

Figure 3.10: Paleo water depth for well `6507/12-1` roughly estimated through biostratigraphic reports (Laboratoire de Geologie de Boussens 1981a)

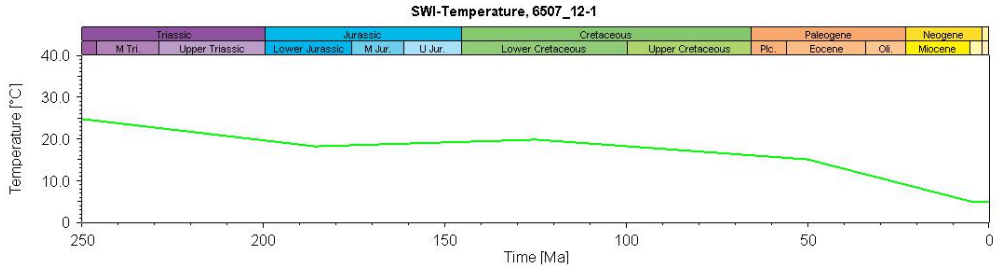

Figure 3.11: Surface-water interface values automatically generated from geographical position and the input of the other boundary conditions.

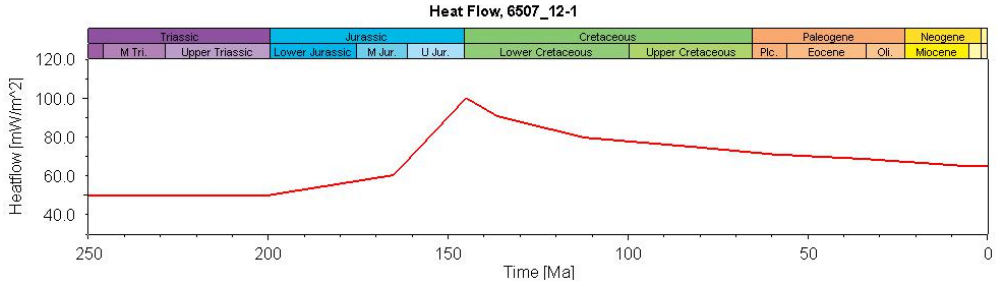

Figure 3.12: Paleo heat flow through time. Estimated from Hermans et al. (1992). Heat flow of today chosen based on the regional maps of Pascal (2015), giving a good match of the temperature gradient observed in the well (see figure 5.16).

Layer	Top [m]	Base [m]	Thickness [m]	Eroded [m]	Depo. Start [Ma]	Depo. End [Ma]	Erosion Start [Ma]	Erosion End [Ma]	Lithology	PSE	TOC [%]	Kinetic	HI [mgHC/gTOC]
Naust	250	1342	1092		2.60	0.00			Conglomerate (typical)				
Kai	1342	1495	153		14.00	4.00			Shale (typical)	Overburden Rock			
Brygge	1495	1826	331		50.00	23.00			Shale (typical)	Overburden Rock			
Tare	1826	1884	58		60.00	50.00			Shale (typical)	Overburden Rock			
Tang	1884	1929	45		66.00	60.00			Shale (typical)	Overburden Rock			
Springar	1929	2012	83		85.00	80.00			Shale (typical)	Overburden Rock			
Lyr	2012	2032	20		140.00	110.00			Shale (typical)	Seal Rock			
Spekk	2032	2052	20		150.00	145.00			Shale (organic rich, 8% TOC)	Source Rock	8.50	Pepper&Corvi(1995)_TII-S(A)	350.00
Melke	2052	2094	42		166.00	157.00			Shale (organic rich, 3% TOC)	Source Rock			
Garn	2094	2128	34		170.00	166.00			Sandstone (typical)	Reservoir Rock			
Not	2128	2143	15		171.00	170.00			Shale (typical)	Seal Rock			
Ile	2143	2213	70		176.00	171.00			Sandstone (typical)	Reservoir Rock			
Ror	2213	2303	90		190.00	176.00			Shale (typical)	Seal Rock			
Tilje	2303	2412	109		195.00	190.00			Sandstone (clay rich)	Reservoir Rock			
Åre	2412	2500	88		199.00	195.00			Sandstone (typical)	Reservoir Rock			
Åre Coal	2500	2920	420		202.00	199.00			Coal (with impurities)	Source Rock	8.00	Pepper&Corvi(1995)_TIIIH(DE)	150.00
grey beds	2920	3060	140		205.00	202.00			Sandstone (typical)				
red beds	3060	3712	652		215.00	205.00			Sandstone (typical)				

Figure 3.13: Main input table for the PetroMod 1D modelling

Chapter 4

Tectonostratigraphic development of Ellingråsa Graben

Through seismic interpretation, well data and with the aid of published conceptual models, a proposed tectonostratigraphic development of the Ellingråsa Graben will be outlined in this chapter. A closer look is taken at the tectonic activity occurring from Triassic until today and how this has affected erosion and sedimentation. Focus will be on strata and tectonic activity of Triassic and younger age, as these events to a large degree have governed the configuration of the graben as it appears today and also hold the highest petroleum geological significance.

4.1 Tectonic development

The Ellingråsa Graben is located far east on the Halten Terrace. Situated between 65°00'N - 65°45'N, it is a highly N-S elongated graben structure bound to the east by the northern part of the BFC and to the west by antithetic faults against the Høgbraken Horst. This antithetic fault zone is hereby termed the Ellingråsa West Fault Zone (EWFZ). To the north, the southern tip of the Nordland Ridge is found, and the horst structure that is home to the Midgard field delineates the graben in its southern tip. Figure 4.1 shows a structure map of the BCU illustrating the graben position relative to other main structural elements in the area, along with the location of all seismic lines presented in this thesis. This section will give an overview of the graben-bounding faults, structures and the influence of Triassic evaporites, before taking a closer look at the BFC. A model for formation of the closure where `6507/12-1` is located is created and presented before lastly, pre-, syn- and post-rift sedimentary sequences (relative to the late Middle Jurassic to earliest Cretaceous rift event) are proposed based on observations and implications from the seismic and well data.

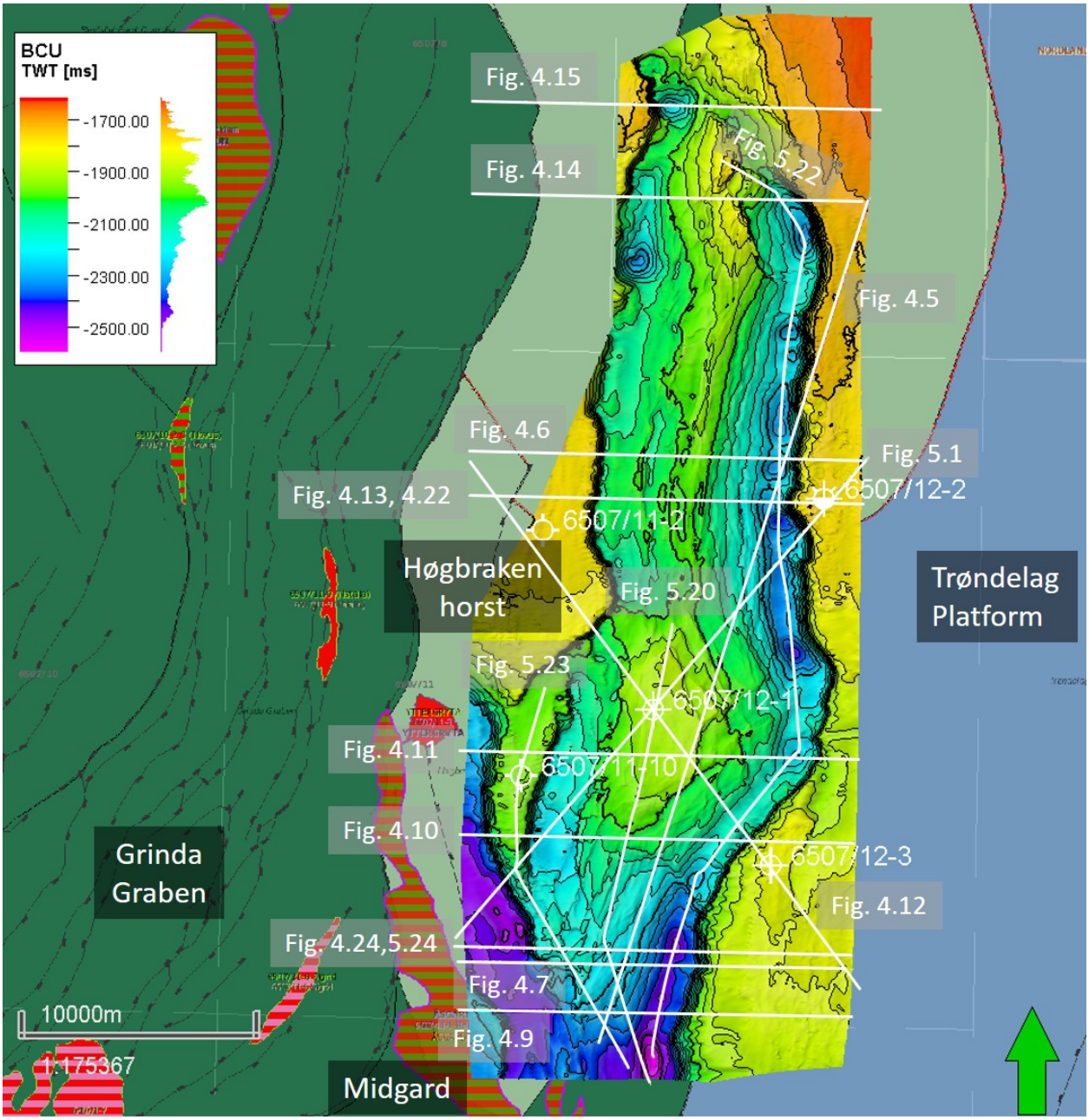

Figure 4.1: BCU structure map showing the main structural features of the Ellingråsa Graben at BCU level, along with the location of all seismic lines shown in this thesis. For all lines without interpretation, see Appendix A

4.1.1 Graben-bounding faults and main structural features

Figure 4.1 shows the structural features of the Ellingråsa Graben as they appear on the BCU level (depth in TWT). In figure 4.2, the main bounding lineaments of the graben are marked along with some of the larger normal faults inside the graben. As seen in the figure, the BFC confines the graben towards the Trøndelag Platform to the east, while antithetic major faults (EWFZ) delimit the graben towards west. Another significant feature of the graben which is apparent from this map is the structural closure on which the `6507/12-1` well was drilled. A closer look at the mechanisms involved in creating this closure is given later in this chapter. The BCU surface also displays several distinct depocenters formed by earliest Cretaceous rifting. This is observed in the hanging wall of the BFC and locally along the EWFZ. Notice also the significantly deeper depth in the southernmost part of the area.

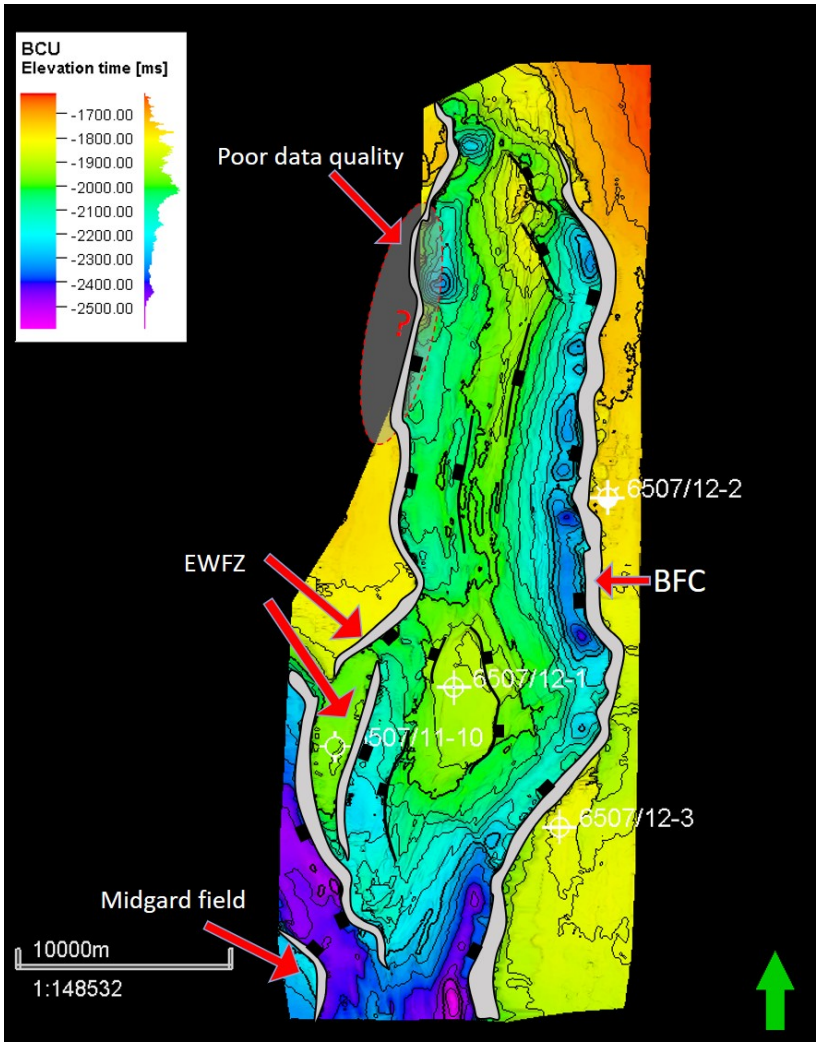

Figure 4.2: BCU structure map with the main bounding lineaments marked. As mentioned, EWFZ denotes the antithetic bounding faults, Ellingråsa West Fault Zone.

4.1.2 Evaporites and their influence

Salt is very ductile, weak and will undergo viscous flow under low shear stresses. Therefore, the presence of evaporites in the pre- or syn-rift strata introduces a significant rheological boundary which may create regionally extensive detachment surfaces in basins, with listric faulting and abundant hanging wall deformation, thus governing structural style and geometry (Marsh et al. 2010; Wilson et al. 2015).

The evaporite in well 12-2

As mentioned in chapter 2, evaporites of Triassic age related to Ladinian rifting and marine incursion are found in the area and are fully penetrated in well 6507/12-2. Here, two evaporite intervals of around 400 meters each were found, separated by 500 meters of Triassic mudstone. As figure 4.3 shows, the top of the halite units are associated with a decrease in acoustic impedance, low density and very low gamma ray values. From both seismic (see for instance figure 4.6) and from logs in well 6507/12-2 (figure 4.3) it is seen that the lower salt package appears to be more heterogeneous, with abundant internal reflections and varying gamma ray values, than the upper unit. Both evaporite intervals are halite dominated, while the mudstone dividing them consists of anhydrite, calcareous and dolomitic claystone along with thin sand beds (Wilson et al. 2015). Regionally, there are large lateral variations in facies and composition of this salt unit, from halite dominated relatively thick packages in 6507/12-2 to mudstone dominated with only thin intervals of carbonate and anhydrite in well 6507/6-1 north of the study area (Wilson et al. 2015). The salt packages also thin and/or shale out east toward 6510/2-1. Further description of the lithology and depositional environment of the salt unit in the Ellingråsa Graben is found in section 4.2.

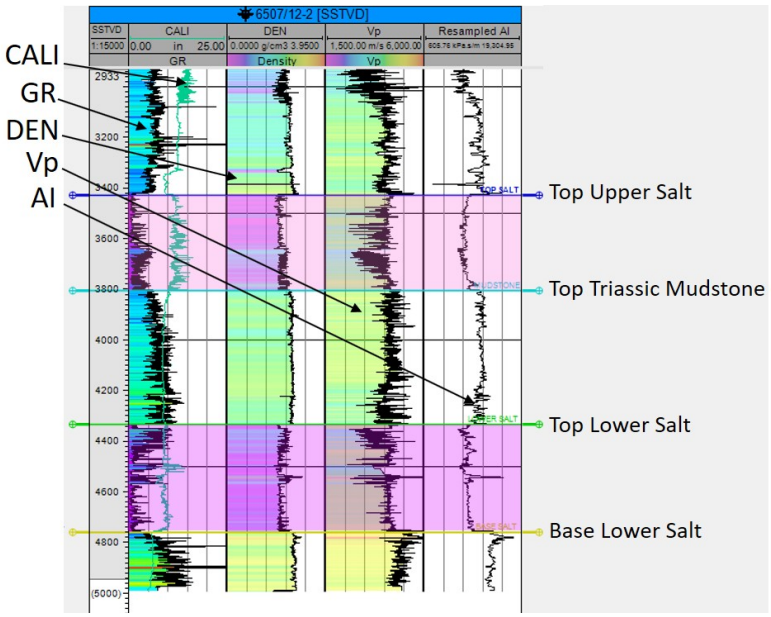

Figure 4.3: Log characteristics of the salt units in well 6507/12-2 show that the salt layers are associated with a decrease in AI and very low gamma ray values.

A closer look at the lower salt Interval

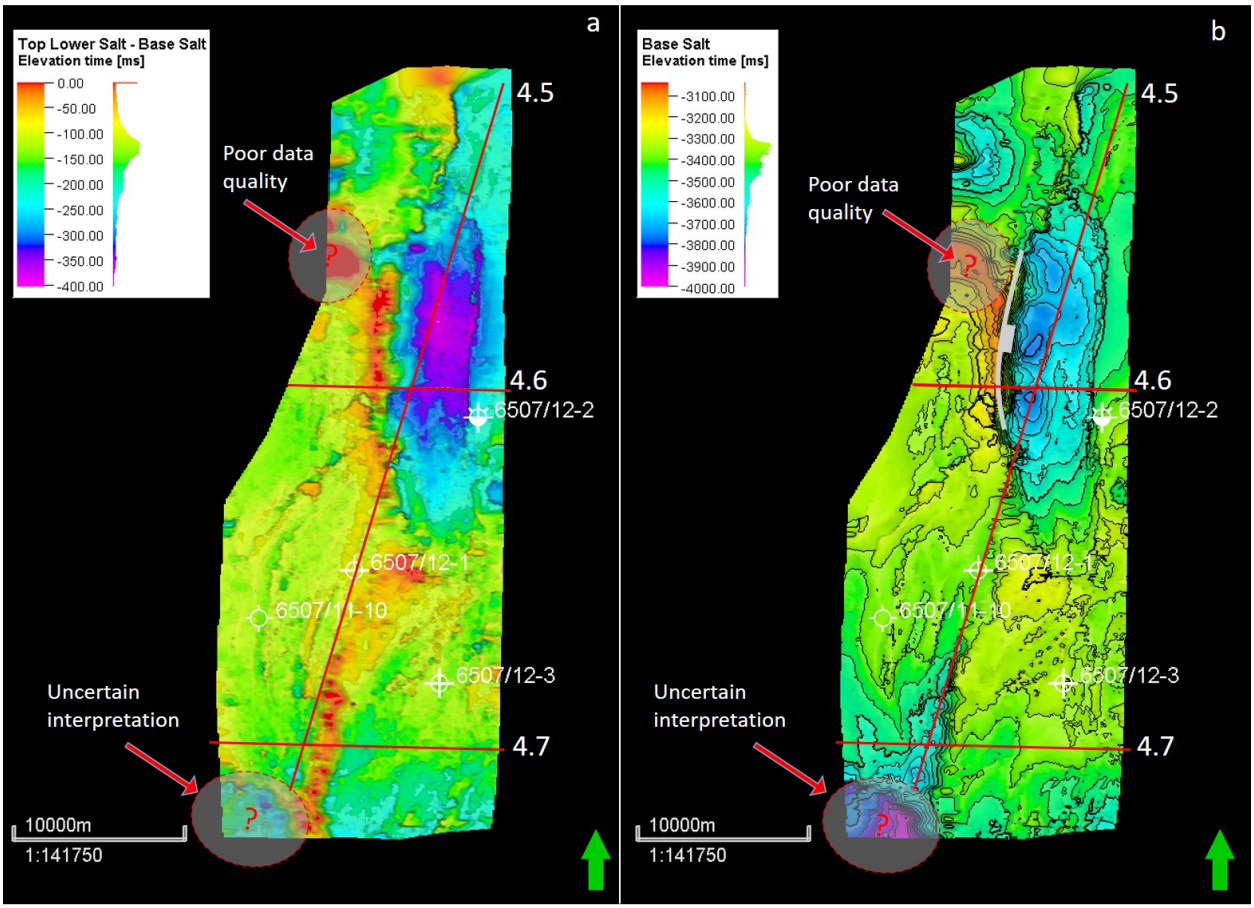

Figure 4.4: Maps in TWT. (a) Isochron map from top to base of the lower salt unit. (b) Elevation of base evaporites. Large thickness variations of the lower salt unit are seen across the graben, with thicknesses up to 400 ms TWT in the thickest parts. Base salt unit illustrates the possible topography of an old half-graben basin in which the salt unit was deposited.

Top and base of the lower salt package represent relatively continuous high amplitude reflectors well suited for mapping, and so these horizons were gridded to get a better idea of the thickness variations and configuration of this unit. The resulting elevation and isochrone maps seen in figure 4.4 reveals significant thickness changes within this strata. Immediately standing out is the deep elevation of the base salt horizon and large lower salt thickness in the east part of the graben, close to well `6507/12-2`, revealing what is interpreted to be a local Triassic (assumed Ladinian, see chapter 2) half-graben salt basin. The adjacent footwall has very thin deposits of the lower evaporite unit, due to a lack of accommodation space at the time of deposition.

The sub-salt fault bounding this half-graben has an approximately N-S strike and is dipping relatively steeply towards east, giving the basin itself a N-S elongation with a thickening of infilling evaporite strata towards west, as can clearly be observed in figure 4.4. The dimensions of the basin are approximately 19,6 km (N-S) by 6,2 km (E-W) and the package is around 380 ms TWT at its thickest.

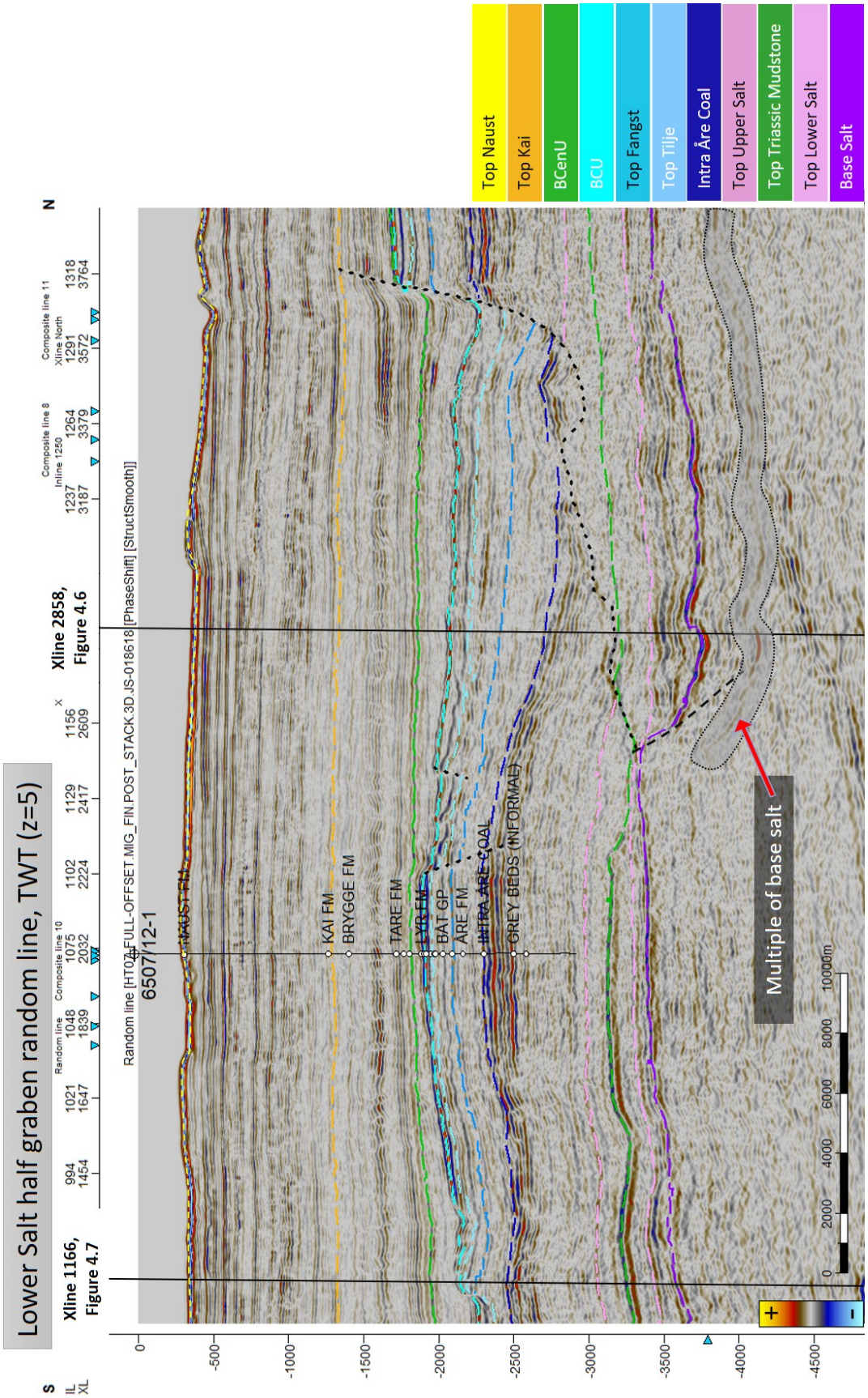

Figure 4.5: Z=5. Recall the reversed SEG polarity (see chapter 3). Random line cross section through the study area, showing the local Ladinian evaporite half-graben. The lower evaporite unit shows large thickness variations related to infilling of the graben structure and variable available accommodation space. The package is thinnest across the footwall of the east-dipping fault delimiting the half-graben, and becomes gradually thicker further south, away from the basin. Notice also the much more even thickness of the mudstone dividing the two salt intervals and the upper salt interval, indicating that the topography was evened out by the time of deposition of these units. For location of line, see figure 4.4.

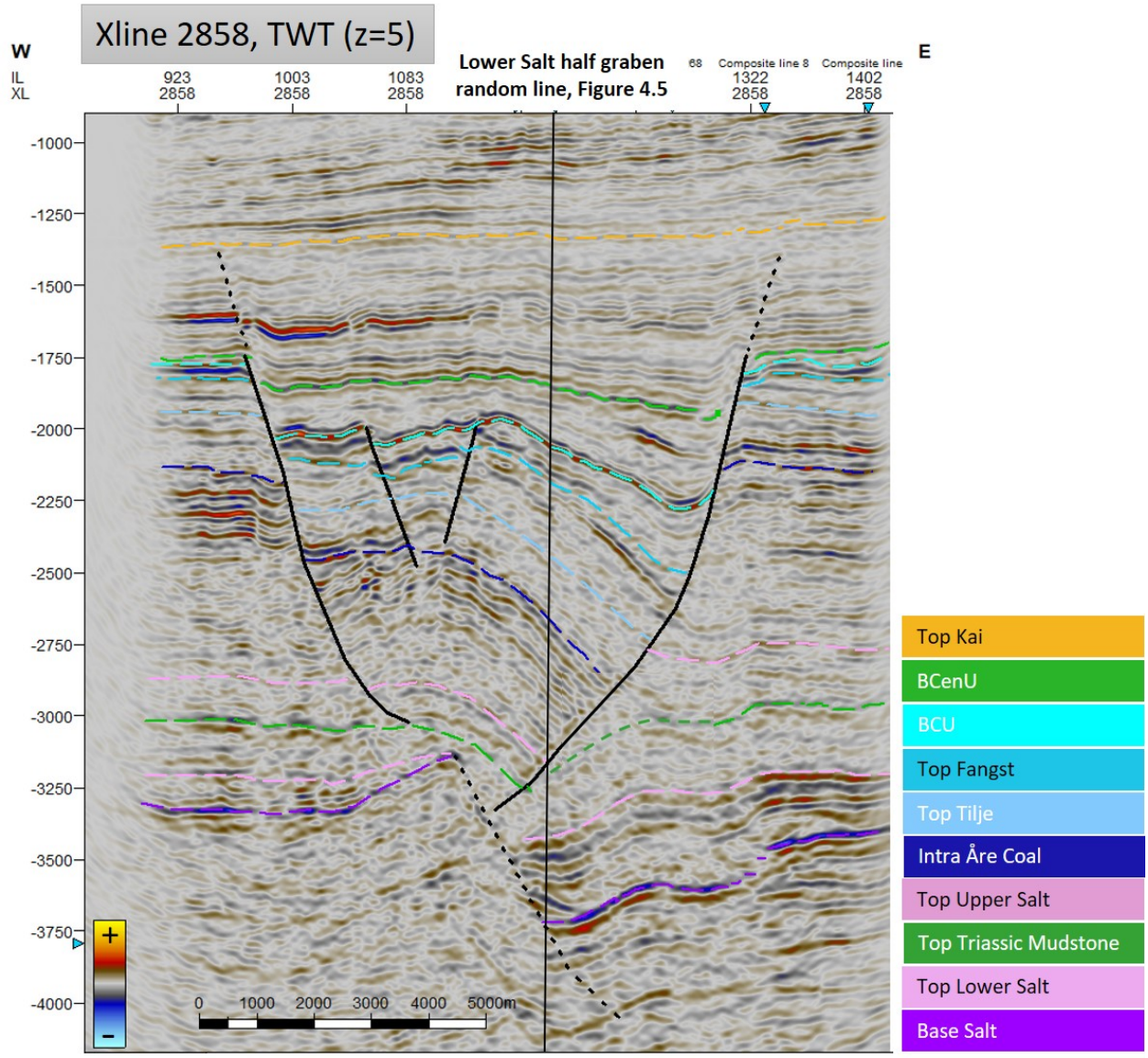

Figure 4.6: Xline 2858 showing the thickness variation of the lower salt interval E-W across the study area and the Triassic half-graben in which it is infilling. A clear trend of thickening strata in the hanging wall towards the east-dipping bounding fault is observed, along with immediate thinning over the footwall. The wavy seismic under the fault plane is a velocity effect related to the fault. See figure 4.4 for location of line.

Figure 4.5 illustrates the thickness changes occurring in the lower salt interval in the study area. See figure 4.4 for location of line. The half-graben is seen as a distinct thickening of the lower salt package, before suddenly thinning to almost zero thickness over the footwall of the graben bounding fault. The layer thickens gradually again further south, possibly due to rotation of the fault block providing more accommodation space further south. The topography appears to have been evened out by the onset of deposition of the mudstone separating the two salt intervals, since the thickness of this unit is more or less uniform throughout the area.

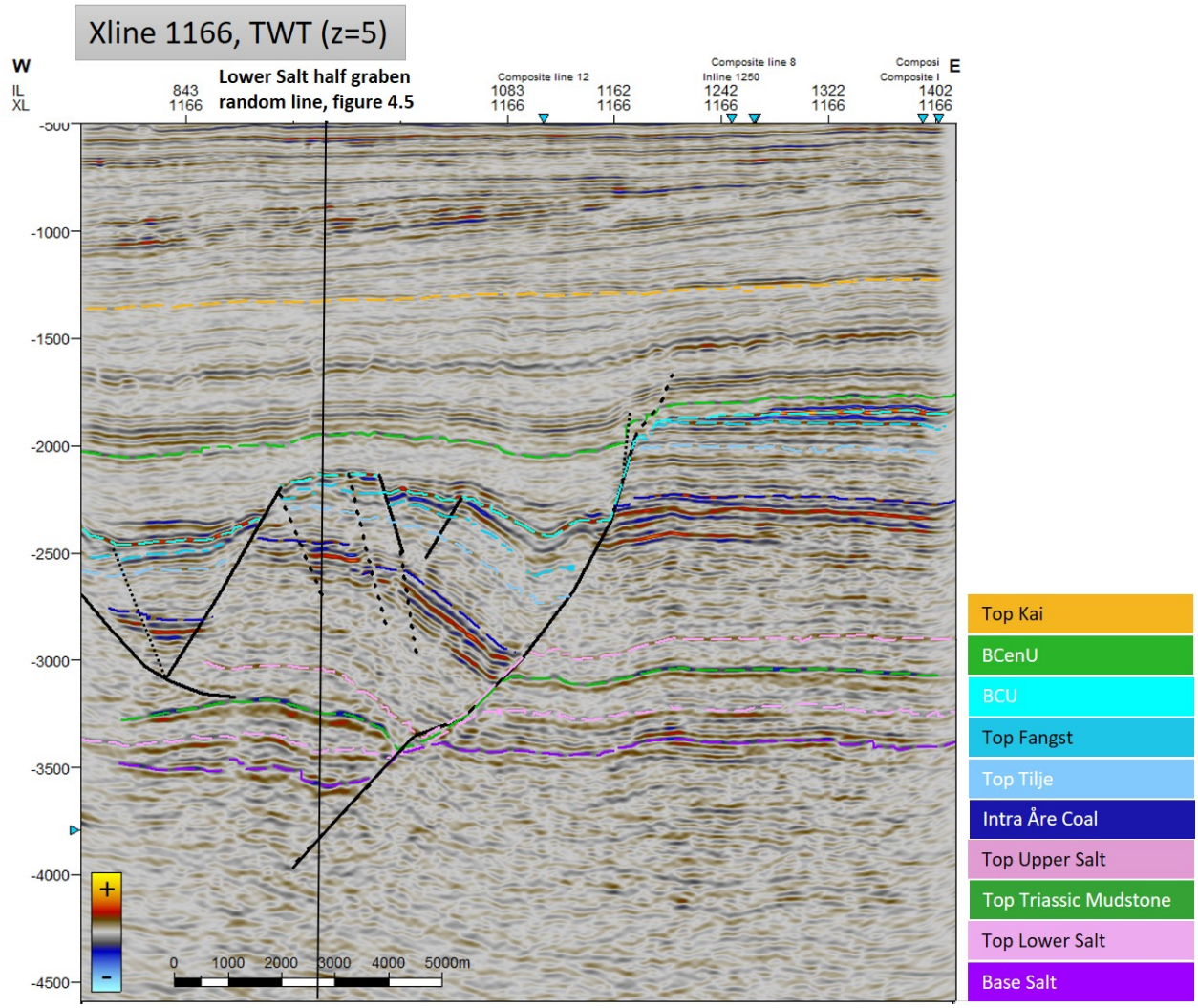

Figure 4.7: E-W cross section through southern part of the graben. Here, the BFC is hard-linked through the evaporite unit and shows a slight ramp-flat-ramp geometry causing hanging-wall deformation. Both the lower salt, mudstone and upper salt units appear to be of relatively uniform thickness from E-W in this area. See figure 4.4 for location of line.

Figure 4.6 is an E-W cross section through the study area, also showing the east-dipping Triassic half-graben structure and the hanging-wall thickening of the lower salt package. The increasing thickness and divergent nature of the internal reflectors in the lower salt interval indicate deposition occurring syn-rift. The immediate thinning of the lower salt over the footwall is also seen, thickening slightly again towards west, away from the half-graben. The more or less uniform thickness of the mudstone separating the evaporite intervals again speaks to more or less leveled out topography at this stage. A cross-section south of the half-graben structure (figure 4.7) shows that the BFC is hard linked through the evaporite unit in this area and a slight ramp-flat-ramp geometry with associated hanging wall deformation is observed (see upcoming paragraph). The whole salt unit from top to base salt seems to have a relatively uniform thickness in this area, with the exception of some pillowing in the graben associated with differential load of the overlying sediment package. The lack of

thickness variation in the strata across the west-dipping sub-salt fault segment indicates that this faulting is younger than the evaporites, that is, post-Early Norian (see section 4.2 for dating of salt intervals).

Upper Salt interval

The upper salt interval has not been gridded across the study area due to its reflection pattern being quite discontinuous and low amplitude, making mapping challenging and time consuming. Instead, it has been interpreted on relevant cross sections, and generally found to have less lateral thickness variations and a more homogeneous seismic character than the lower salt interval. Some pillowing is observed in the middle of the graben, as seen in figure 4.7, but other than this the salt appears to be quite immobile, as expected in the area (Jackson and Lewis 2016). Though the Ellingråsa Graben is lacking dramatic salt related features like large diapirs and domes, there are many observations indicating that this upper salt layer has still had a significant, though perhaps subtle, influence on the style of deformation and faulting within the graben.

The interplay between salt and Jurassic deformation

As mentioned, the weak mechanical properties of halite makes the unit of Triassic evaporites a regional detachment surface where faults tend to sole out, leading to different styles of deformation sub- and supra-salt (Jackson and Hudec 2017). That the upper salt acts as this ductile boundary being able to accommodate large amounts of deformation in the Ellingråsa Graben is indicated by the observation that the lower salt half-graben is still relatively intact and undisturbed. Only small amounts of deformation associated with the tectonic activity in the Jurassic and Cretaceous is observed here, which along with the lack of any consistent relationship between style of faulting along the BFC and thickness variation of the lower salt unit yields the conclusion that the salt associated deformation in the graben is caused by the upper evaporite interval.

Below follows a series of cross-sections across the seismic, from south to north, included to show how the salt related deformation features change along-strike of the BFC. Location of all lines described in the upcoming paragraph are found in figure 4.8.

Farthest south in the study area, the BFC offset on the BCU level is very large, as can be observed from figure 4.1, indicating significant throw (see also upcoming section 4.1.3). In this area, the BFC appears to be hard-linked with a west-dipping fault offsetting the evaporites. A significant dip change is seen, from quite steep in the supra-evaporite package, to a much more gentle dip coming into the evaporites. It is easy to quickly relate the hard-linking of faults here to the large displacement in the area, however linking of faults in a salt setting is also influenced by other factors such as the local salt facies (see Wilson et al. (2015)) strain rates and salt interval thickness. Some hanging wall deformation with rollover folding and rotation of interval strata is seen in the immediate hanging wall of the BFC. The EWFZ here appears to be soling out on the upper salt level, but the hanging wall strata of this fault zone shows less deformation. A cross-section showing these observations is found in figure 4.9.

Figure 4.7 is located a little further north, and illustrates a beginning decoupling of sub-

and supra-salt fault in the BFC. The east-dipping EWFZ appears to be detaching in the evaporite layer at this location as well, possibly with a larger degree of listricity here, but there are still not many signs of hanging wall deformation related to this. Rollover of strata towards the BFC is easily observable, and there appears to be a quite substantial amount of deformation in the hanging-wall with a short-wavelength syncline-anticline pair and heavily rotated internal strata. Some pillowing of the upper salt interval is seen in the middle of the graben. This is interpreted to be extensional pillowing set up by the listric faulting. As the hanging wall slides down a listric normal fault, the strata will bend toward the fault and a fan of syn-kinematic wedges will accumulate during this bending. As this rollover sags it expels underlying salt, which then flows away from the fault (Jackson and Hudec 2017). The rollover thus forms one flank of the salt pillow, as is seen on the east-dipping salt pillow flank in figure 4.7.

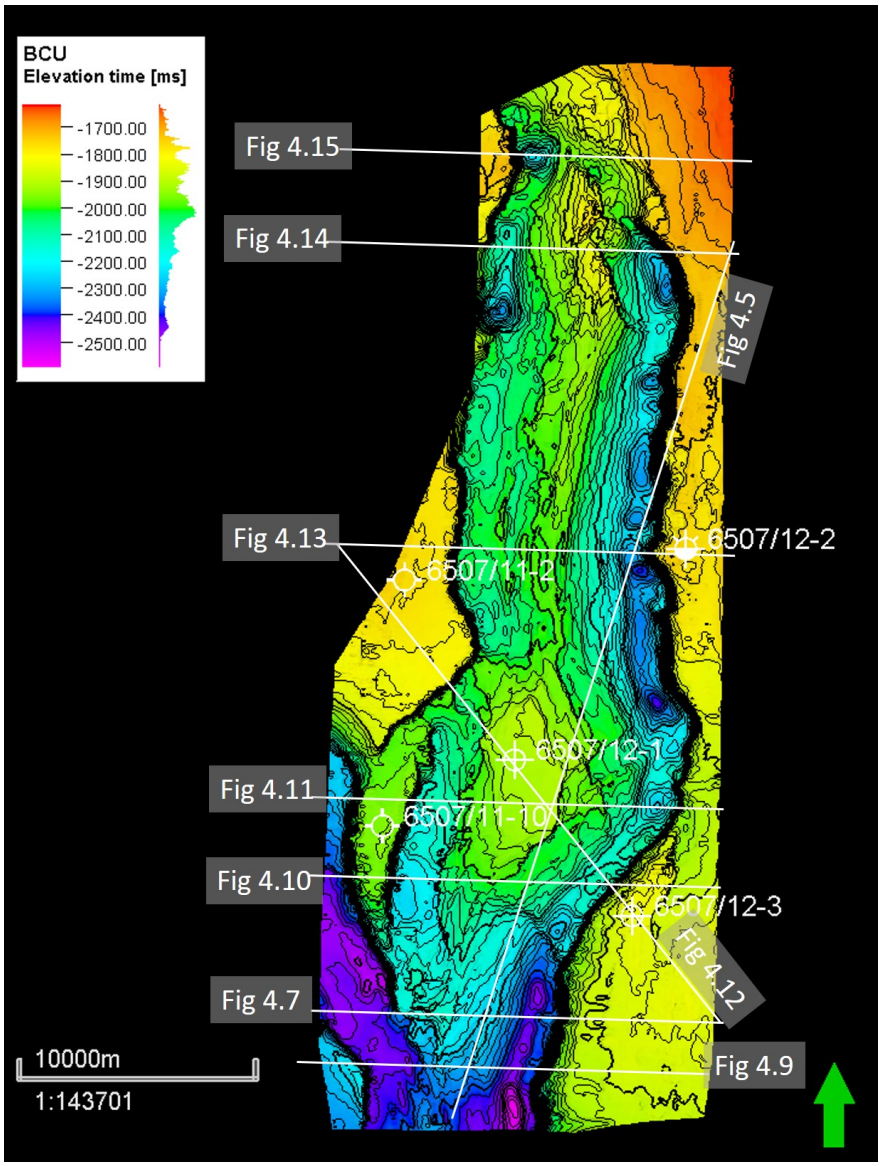

Figure 4.8: BCU structure map (depth in TWT) with location of cross sections.

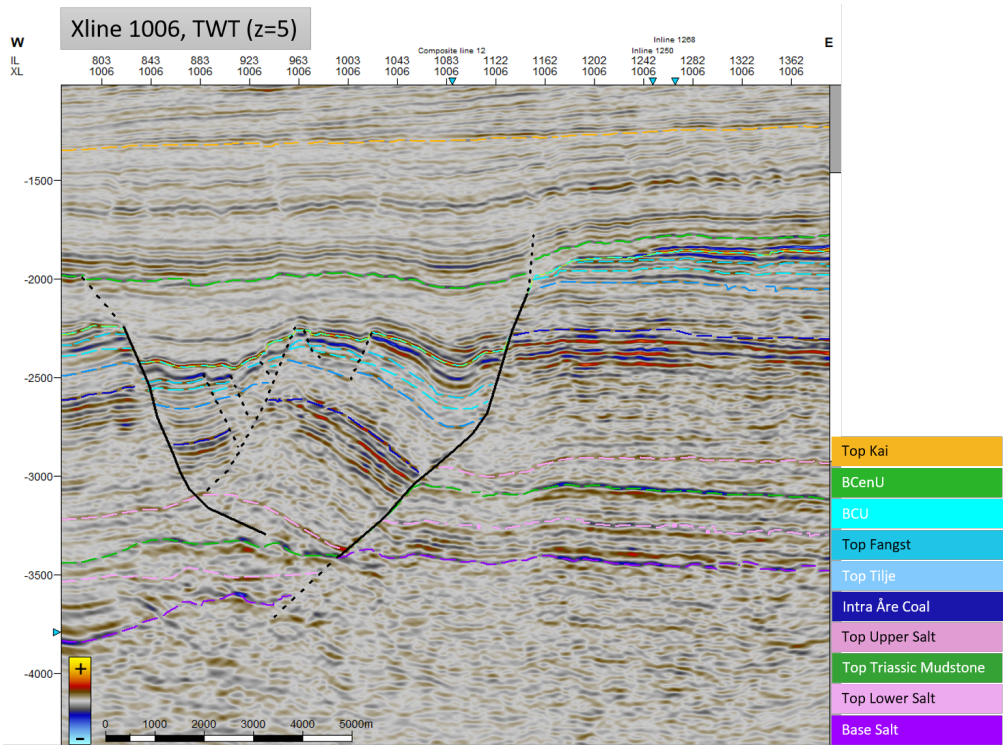

Figure 4.9: Large BFC offset and significant dip change coming into the evaporite strata. BFC significanly offsetting the evaporite unit in this location.

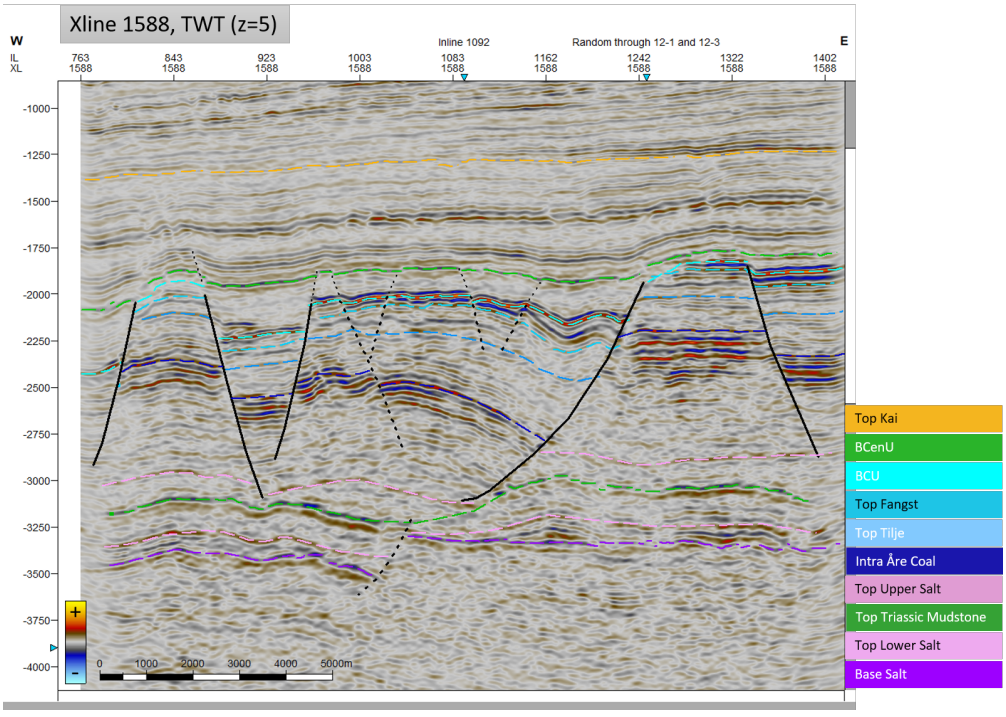

Figure 4.10: Ramp-flat-ramp geometry created as the BFC is effectively decoupled from the deeper fault offsetting the evaporites.

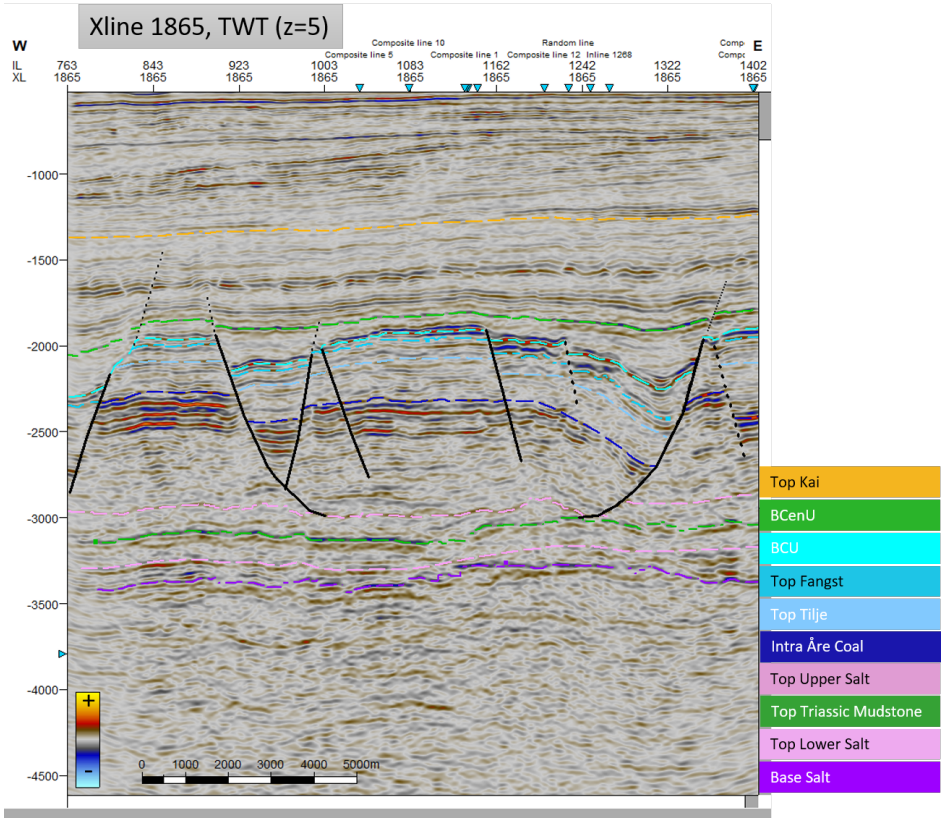

Figure 4.11: Unfaulted salt package of uniform thickness. Both bounding faults are listric in nature in this E-W cross section.

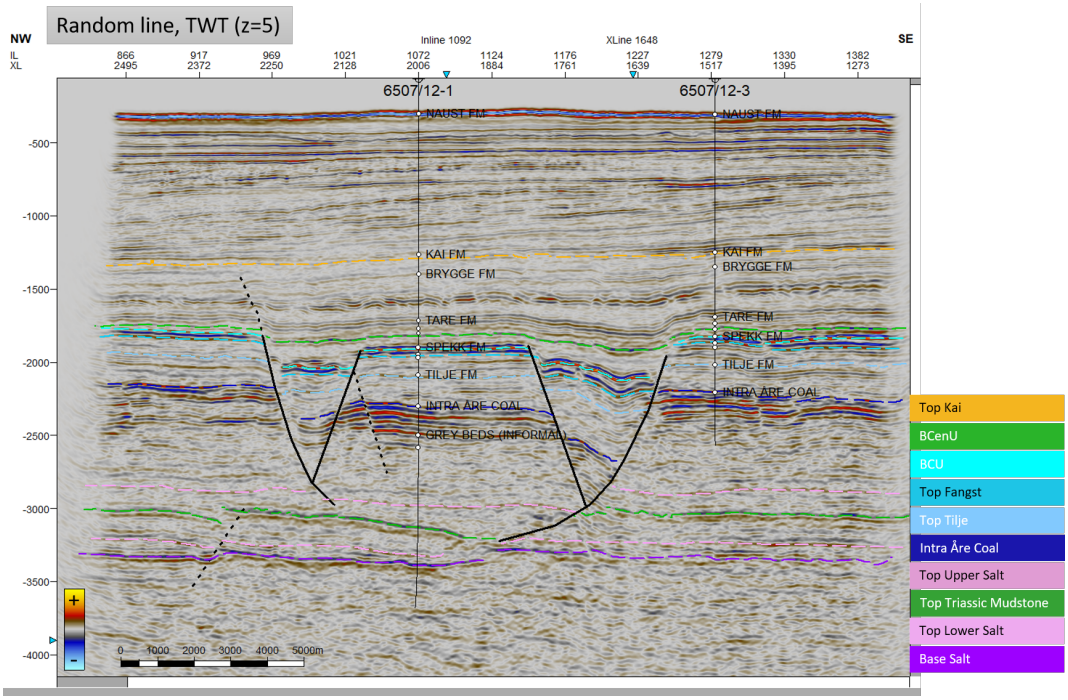

Figure 4.12: Largely similar features as for figure 4.11, but here seen in the NW-SE direction.

In xline 1588 (figure 4.10), again located further north, a form of ramp-flat-ramp geometry is created in the BFC as the supra-salt fault detaches in the upper salt layer and is effectively decoupled from the deeper fault offsetting the evaporites. Significant rollover towards the fault is also observed here, and the short-wavelength syncline-anticline pair is still clearly visible in the syn-rift strata of the Viking Group. On the west side, the style of deformation is much more characterized by brittle, non-listric faulting, however the EWFZ fault also appears to be stopping in the upper salt interval. Some gentle pillowing of the upper salt layer is also seen here, thought to arise from the listric faulting in the BFC.

Figure 4.11 shows a cross-section at xline 1865, where the salt unit is more or less unfaulted and of uniform thickness. At this location in the graben, both graben-bounding faults appear listric in nature, however the hanging wall to the east seems to be more characterized by ductile rollover features and rotation of strata than the hanging wall to the EWFZ. A minor possible salt pillowing feature can be observed close to where the BFC soles out into the upper salt horizon.

A random line is taken through the graben crossing well `6507/12-1` and `6507/12-3` (figure 4.12). Here, the horst feature on which well `6507/12-1` is drilled is clearly seen. The graben is in this area bound by listric faults at each side, both detaching in the upper salt. Everything below the upper evaporite horizon appears relatively undisturbed by post-Triassic tectonic activity in this area. As before, more significant hanging wall deformation related to the listric nature of the faults is present in the BFC hanging wall, while deformation is more characterized by brittle faulting in the antithetic hanging wall. A closer look at the formation of the closure on which well `6507/12-1` is drilled is given in section 4.1.4.

Xline 2713 in figure 4.13 goes through the `6507/12-2` well, penetrating both evaporite intervals. Here, the increased thickness of the lower salt interval is clearly seen compared to figures 4.9-4.12, and it is seen that the well is situated within the Triassic salt half-graben. The thinning of the layer across the footwall of the EWFZ is also obvious here. Significant rollover related to the listric style of the BFC is seen at this cross section as well, while the hanging wall to the antithetic EWFZ is again much less influenced by rollover deformation. Pillowing of the upper salt horizon is also observable.

Drastic changes occur from xline 2713 in figure 4.13 to xline 3717 in figure 4.14 further north. Here, the EWFZ is related to significant amounts of throw, listricity and rollover of hanging wall strata. The BFC still shows hanging wall deformation, however more gently than the observations made further south. From figure 4.8 it is seen that xline 3717 is located close to where the displacement across the BFC dies out. The salt horizons are here interpreted with less confidence due to degrading data quality in the area.

The northernmost cross section included is xline 4025 (figure 4.15). This cross section illustrates that the Ellingråsa Graben transitions into a half-graben bound by an east-dipping master fault, here soling out in the upper evaporites, decoupled from a fault slightly offsetting the evaporite package.

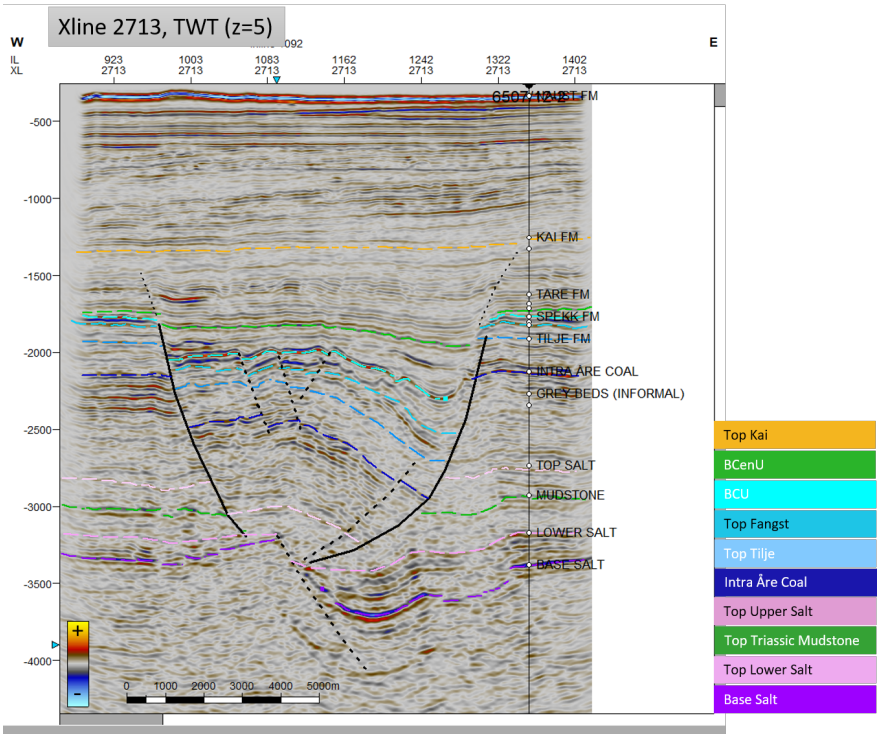

Figure 4.13: Well 6507/12-2 is situated in the Triassic lower salt interval half graben.

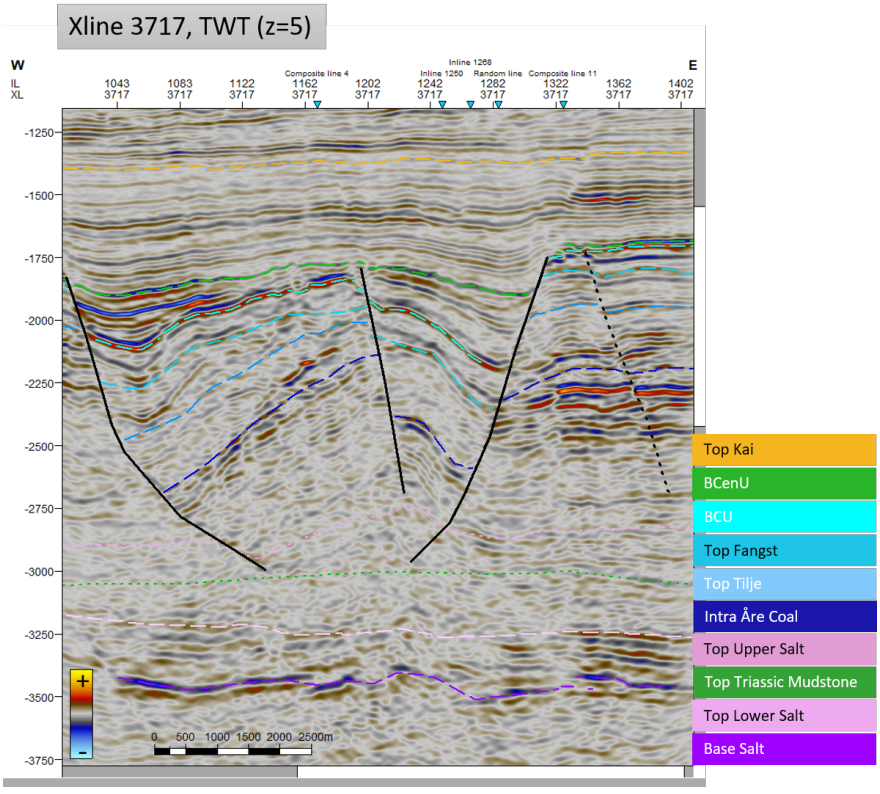

Figure 4.14: Significant amounts of throw on the EWFZ observed as well as reduced displacement across the BFC far north in the study area.

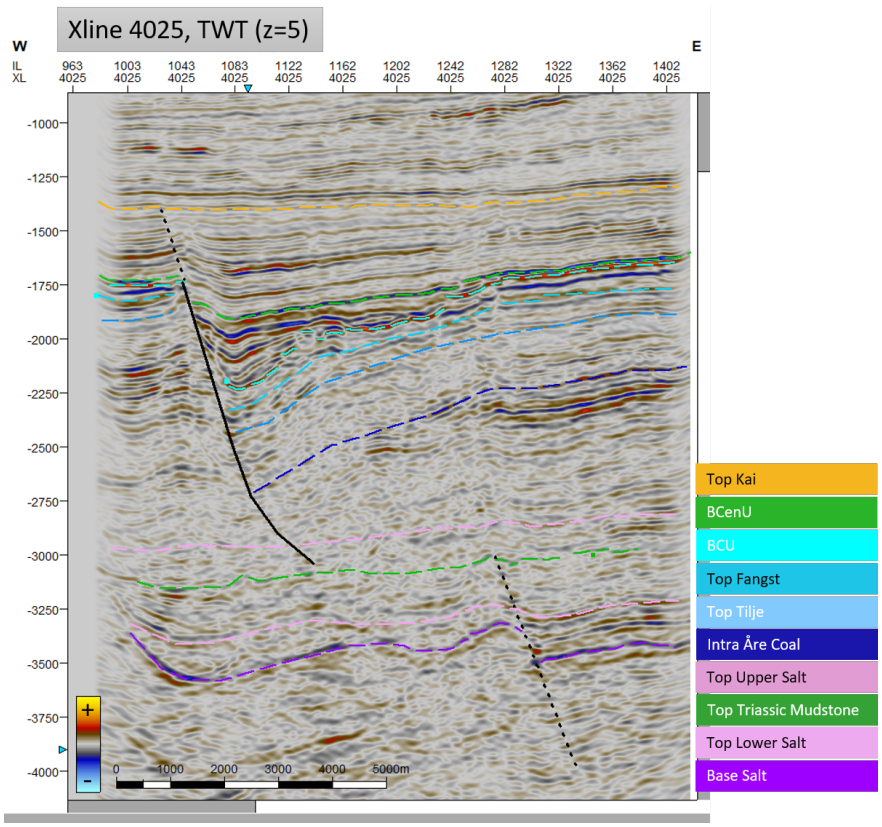

Figure 4.15: Ellingråsa Graben transitions into half-graben bound by east-dipping master fault furtherst north where displacement across the BFC dies out completely.

Summarizing the observations of salt and tectonic interplay from S-N along the graben, it is farthest south seen that the BFC is hardlinked to a fault offsetting the salt unit involving significant dip-change, becoming more listric and decoupled a little further north. Significant rollover and hanging wall deformation such as small-wavelength syncline-anticline pairs are seen in the BFC hanging wall, while the hanging wall to the EWFZ generally appears more characterized by brittle faulting. Still, the EWFZ also detaches in the evaporite level, becoming increasingly listric towards north. Pillowing of the upper salt horizon is also common, the degree of which may be related to the amount of syn-kinematic sedimentation. Relatively far to the north in the graben, around where the throw of the BFC starts drastically reducing, the antithetic EWFZ shows large amounts of throw, high listricity and associated hanging wall rollover. Farthest north, the BFC disappears and the graben transitions into a half-graben bounded by an east-dipping fault. Here, the displacement on the BFC has died out. The earlier faulted strata are monoclinally folded towards the antithetic fault.

4.1.3 Characteristics and activity of the BFC

Previous work done on the BFC has primarily been conducted further south (Elliot et al. 2011; Wilson et al. 2013; Bell et al. 2014; Wilson et al. 2015), while the study area in this thesis comprises the very northern end of the fault complex. Where Elliot et al. (2011) describes the BFC as a complex consisting of numerous faults, the complex appears to consist of one laterally hard-linked major graben bounding fault in the study area of this thesis.

The previous chapter has already described the BFC as being very listric and for the most part detaching in the salt layer, however becoming more throughgoing towards the southern end of the study area. The footwall of the BFC is characterized by sub-horizontal, parallel reflectors, indicating that activity on the fault was accommodated primarily by hanging wall subsidence rather than footwall rotation and uplift. A closer look was taken at the BCU surface in order to estimate a line of BCU-erosion along strike on the BFC footwall. The result of this is seen in figure 4.16.

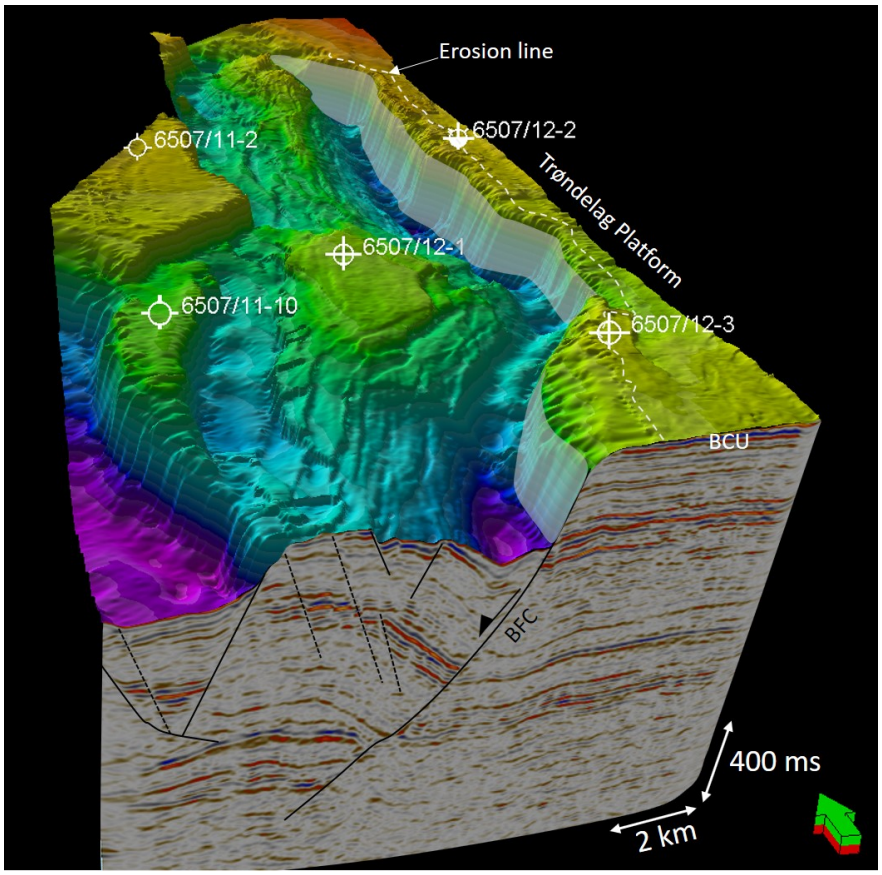

Figure 4.16: Figure illustrating the estimated erosion line on the BCU surface along-strike of the BFC. Cross section shown is xline1166 (figure 4.7

Figure 4.16 shows that the area over which the BCU appears to be erosive on the BFC footwall scarp increases significantly towards south. Here, the unconformity erodes deep into the Middle Jurassic at the edge of the footwall. It is important to note that this erosion line only considers erosion by the Base Cretaceous unconformity. Erosion by the intra-Melke

unconformity, presumably in Callovian time, is expected to also be a significant contributor to erosion of Middle Jurassic sand and deposition of syn-rift sands in the hanging walls during Late Jurassic, however this erosional surface is extremely challenging to locate on seismic. This erosional period may not show the same pattern as the BCU, depending on local variations in fault activity and catchment.

The southern area is where the throw on the fault is the highest, as figure 4.17 showing the result of throw measurements taken on the Åre Coal horizon illustrates. The BFC is here suggested split into 4 different segments based on differences in throw. Observe that the largest area of erosion on the BCU surface corresponds to the location of largest throw on the BFC. As figure 4.17 shows, there are two segments (S1, S3) of large throw, corresponding to N-S striking parts of the BFC with large visible offsets and what looks like deep local depocenters in the hanging wall on the BCU level as well. Segment 2 (S2, figure 4.17) has more of a NE-SW strike direction, smaller throw measured and the BCU level offset seems to be less here than in its N-S striking neighboring segments to the south and north. The fourth segment, S4, represents the tipping out of the whole fault complex and shows a rapid decrease in throw measurements.

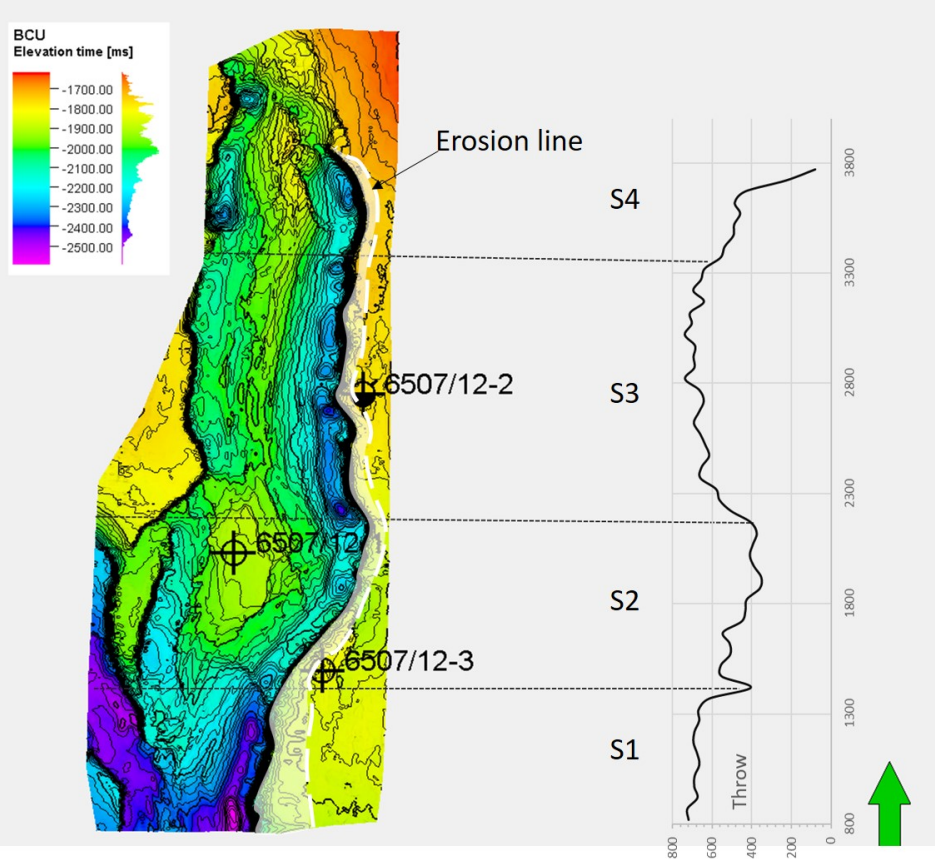

Figure 4.17: Throw measurements on the Åre Coal Horizon and suggested segments S1-S4 of the BFC fault complex in the study area, based on seemingly consistent differences in throw along strike.

The relatively consistent difference in throw along-strike could be an indication that these segments formed at different stages of tectonic activity, specifically that S1 and S3 are previously soft-linked segments of the BFC and that S2 represents a former relay ramp area that is now completely breached and hard-linked to the north and south. S4 probably also evolved and migrated further north as rifting occurred through time, as fault segment development is conceptually described by authors such as Gawthorpe and Leeder (2000).

This is supported by taking a look at the interpreted thicknesses of the Late Jurassic Viking Group and the thickness of the Cretaceous strata, seen in figures 4.18 and 4.19. Figure 4.18 indicates that the hanging wall in the area of the NE-SW striking fault segment S2 is characterized by significantly less syn-rift sedimentation of the Viking Group and less increase of strata thickness is observed towards the footwall. Less thickness of the Viking Group in this segment can be an indication of less available accommodation space at this location at the time of deposition, especially since the BCU is not expected to be erosive in this deep hanging wall area. This supports major tectonic activity along this segment occurring at a later stage than for segments S1 and S3. The Cretaceous strata seen in figure 4.19 is also less thick here, again an indication of less accommodation space in the area during the Cretaceous. It is important to note that the smaller thicknesses seen here could also be attributed to other factors such as local sediment starvation rather than less tectonic activity and thus accommodation space, or a combination of these factors.

Based on this argumentation, it is in this thesis proposed that major faulting of the S2 segment occurred at a late stage relative to faulting of segments S1 and S3, creating hard linkage of the BFC in the area when it did form.

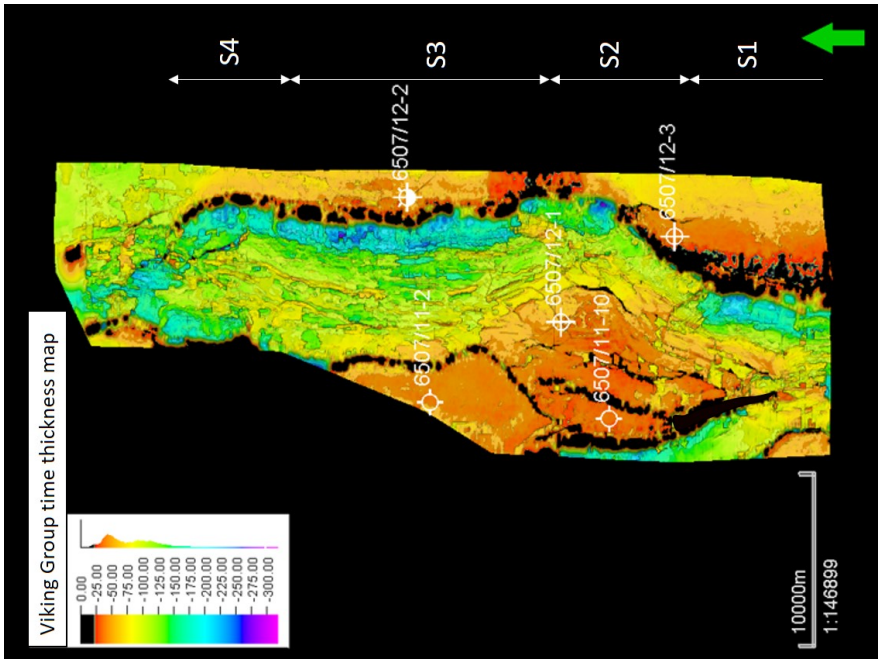

Figure 4.18: Thickness of Late Jurassic Viking Group strata (in TWT). It is important to note that significant erosion of this strata has taken place related to tectonic acitivty in the earliest Cretaceous, especially visible in black where thickness of the Viking Group is interpreted to be 0 ms TWT over fault footwalls.

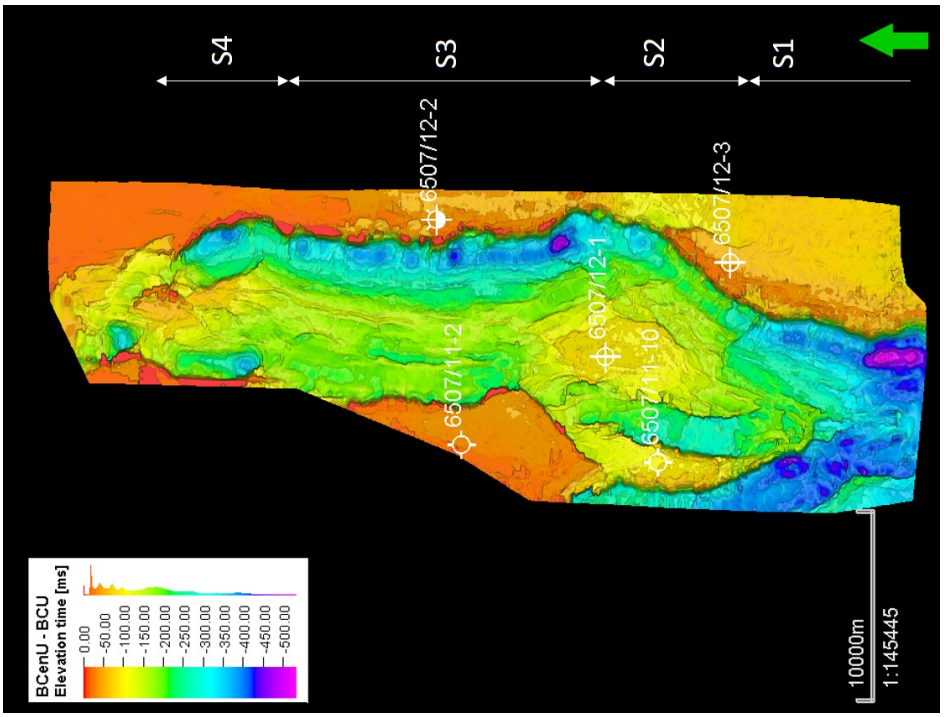

Figure 4.19: Thickness of Cretaceous strata. Significant thickness varations from bounding fault footwalls to the middle of the graben structure is observed, with the thickest Cretaceous deposits found in the immediate hanging wall of the BFC

Figure 4.20 shows the BCU surface with RMS-amplitude extraction on a variance cube, highlighting structural features. Here the erosional style of the Spekk Formation appears to be characterized by gliding out of segments of organic rich strata, possibly with small faults soling out near the base of the organic rich strata as described by Løseth et al. (2011).

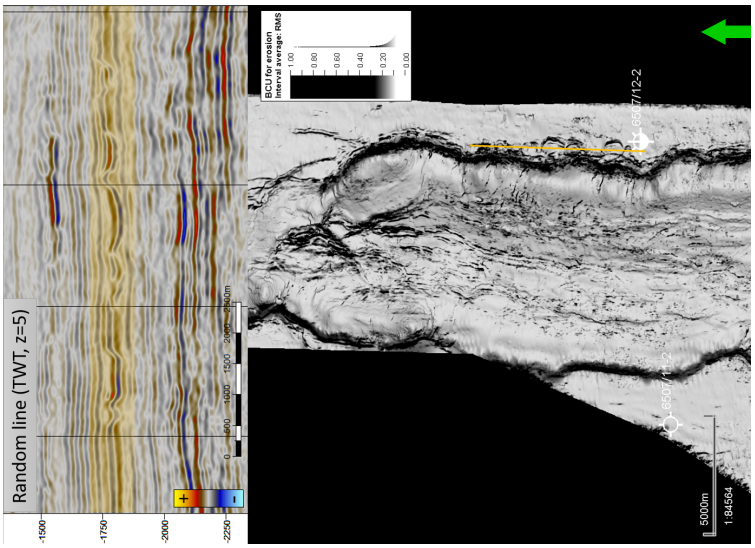

Figure 4.20: Erosional style of the organic rich Spekk Formation characterized by gliding out of segments as seen here in both map view and in a cross section.

4.1.4 Formation of closure X

This section is concerned with attempting to create a model to explain the formation of the horst structure or anticline closure on which well 6507/12−1 is located, termed the X closure by Saga Petroleum AS (1980). It should be noted that the model proposed in this thesis is highly conceptual and based on implications from seismic and wells, and relatively poorly constrained, especially regarding the western flank of the graben. Further discussion of key uncertainties is found in chapter 6.

Figure 4.21a shows a conceptual sketch of the Triassic evaporite unit in pink, the Early Jurassic strata in blue and finally the pre-rift Middle Jurassic deposits in yellow. The figure describes the situation in the Middle Jurassic, immediately prior to major increase in tectonic activity. Drawing the layers as having totally uniform thickness and being deposited in an environment completely without topography and variation in accommodation space is clearly a simplification, as both the outlined tectonic history in chapter 2 and well information in the upcoming section 4.2 shows. Some increasing thickness of the Early to Middle Jurassic is also observed (see section 4.1.5). These simplifications are not however thought to significantly alter the model presented, and can therefore be justified. The position of the N-S striking segments S1 and S3 of the BFC are stippled in figure 4.21a.

Faulting of the N-S striking segments has initiated in figure 4.21b, which could represent a late Middle Jurassic, Bathonian to early Callovian stage, based on chronostratigraphy from the wells combined with thickness maps. The west-dipping faults detach at the evaporite level, and associated gentle rollover of faulted strata is observed in the hanging wall. Syn-kinematic sedimentation of the Melke Formation is illustrated in brown, sediments suggested to be derived from erosion of the BFC footwall. Initiation of gentle pillowing as salt moves away from the heavily loaded syn-rift wedge towards the centre of the graben is also proposed.

Figure 4.21c shows a growing syn-rift wedge, increasing rollover and salt pillowing along with significant erosion of the Melke Formation on the BFC footwall. This figure is thought to represent approximately Callovian time, immediately prior to antithetic faulting of the EWFZ. The significant erosion illustrated in the figure is associated with the IMU. The significant erosion of the BFC footwall in the model is supported by the dating of the Melke Formation to post-Callovian and the reports of a major unconformity separating the Melke Formation from the underlying Garn Formation in well 6507/12−2 located on this footwall (see upcoming section 4.2). Note that the BFC faulting in the N-S direction initiating prior to the EWFZ is based on a clear lack of increase in sediment thickness of the Late Jurassic Viking Group, typical of syn- and post-rift deposits, along the hanging wall of the antithetic faults (in the area surrounding the closure), see figure 4.18. However, these conclusions are clearly uncertain due to a lack of well data in this area.

In figure 4.21d, both faulting along the EWFZ and hard-linking of the BFC segments S1 and S3 through NE-SW striking segment S2 has initiated. These events are grouped together solemnly because there is no evidence to support one occurring before the other. The antithetic faults are also observed on seismic as listric in nature, however the hanging wall deformation seems to be more characterized by brittle faulting than rollover of strata. This is included in the conceptual model, and it is proposed that this brittle style of deformation is caused by rapid strain rates along the antithetic faults. This could also explain the lack of syn-rift wedges as the area could easily become starved of sediment. Some erosion of the

EWFZ footwall is included, but the amount is extremely poorly constrained due to a lack of trustworthy well data in the area.

At this point, the closure is beginning to form, constrained by rollover and/or faulting towards listric faults in both the NE-SW and NW-SE direction, such that the combined anticline/horst structure illustrated in figure 4.21d exist in different versions in all directions across the closure. Figure 4.2 shows that there is a faulted anticline ridge trending approximately N-S along the whole graben structure, set up by rollover (and faulting) towards listric bounding faults in both the east and west direction. The difference between this feature and the closure on which well `6507/12-1` is located is simply that the bounding fault changes strike direction multiple times and quite drastically in this area, confining the hanging wall deformation and rollover to create a closure. This is also illustrated by figures 4.11 and 4.12.

Figure 4.21e finally illustrates the situation after deposition of the post-IMU Melke Formation, with the IMU marked in red. Finally, draping of the topography by the Spekk Formation (in black) and some erosion over the footwalls (BCU), exposing strata down to the Middle Jurassic sands at certain locations (as discussed in section 4.1.3) is seen in figure 4.21f. Thus, according to this model the closure was formed at the earliest Cretaceous (Berriasian), however some evidence of post-Jurassic faulting is seen (see section 4.1.5), so further structuring of the closure is suggested to have continued further into the Cretaceous.

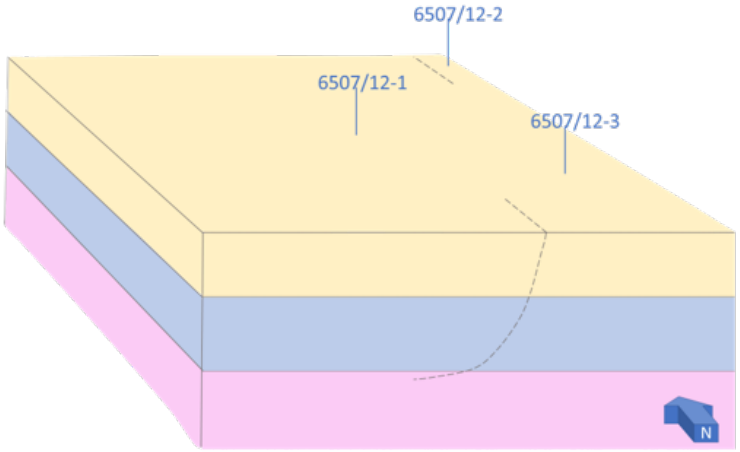

(a) Middle Jurassic just before onset of BFC faulting. Note that flat, uniform layers without any topography is a simplication. Future location of the BFC N-S striking segments S1 and S3 is stippled.

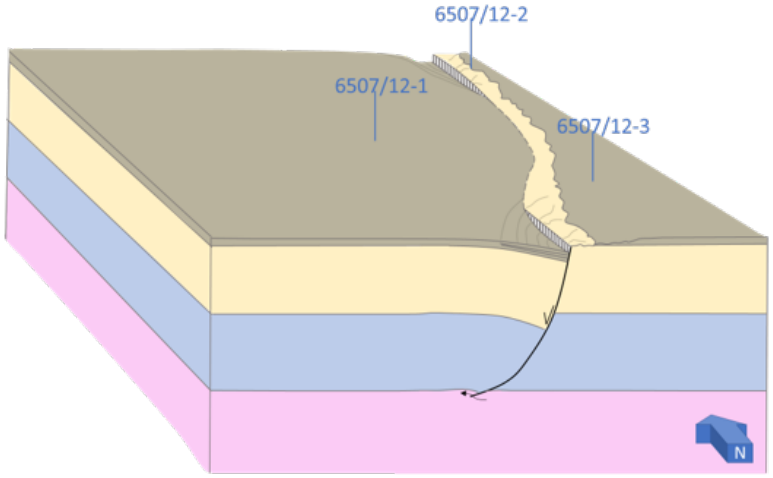

(b) Late Bathonian to Early Callovian. Listric faulting, associated rollover and syn-rift sedimentation of the Melke Formation derived from erosion at the BFC footwall is suggested. Gentle pillowing of the salt unit is also illustrated.

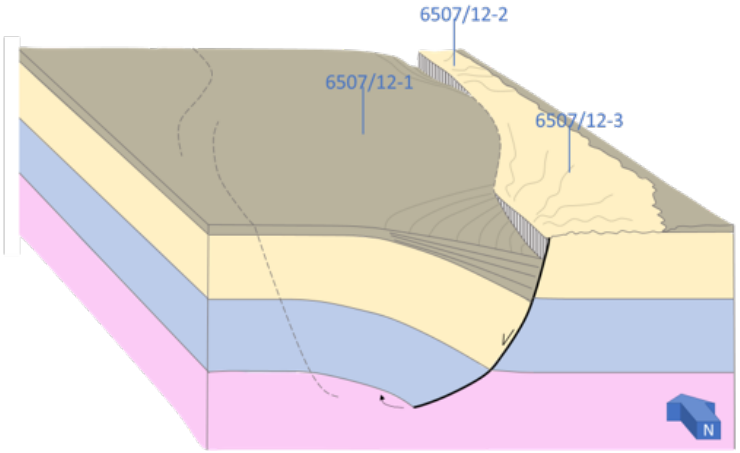

(c) Callovian time, extensive erosion of the BFC footwall and associated syn-rift sedimentation in the hanging wall. Increasing rollover of pre-rift strata and continued salt pillowing is proposed. Location of antithetic faults and NE-SW striking BFC segment S2 is stippled.

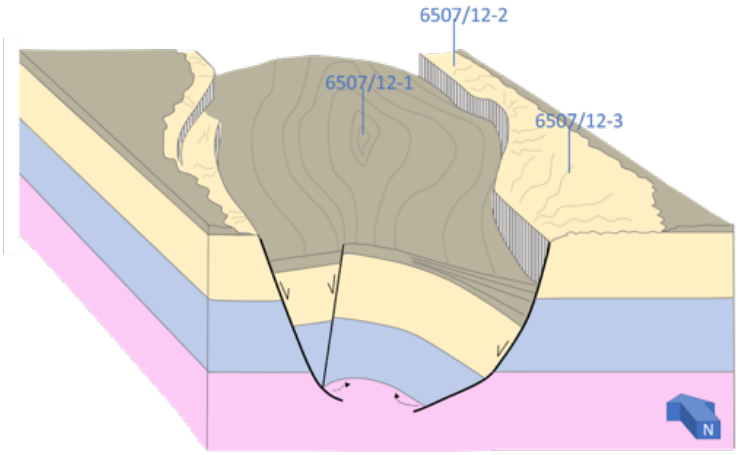

(d) Antithetic faulting and hard-linking of the BFC segments initiated, creating a closure bound in every direction by listric faults with associated rollover or brittle faulting.

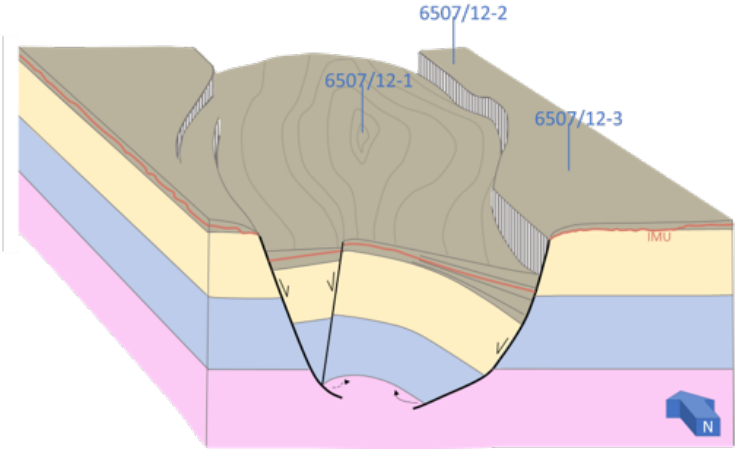

(e) Oxfordian time, deposition of post-IMU Melke Formation. IMU marked in red.

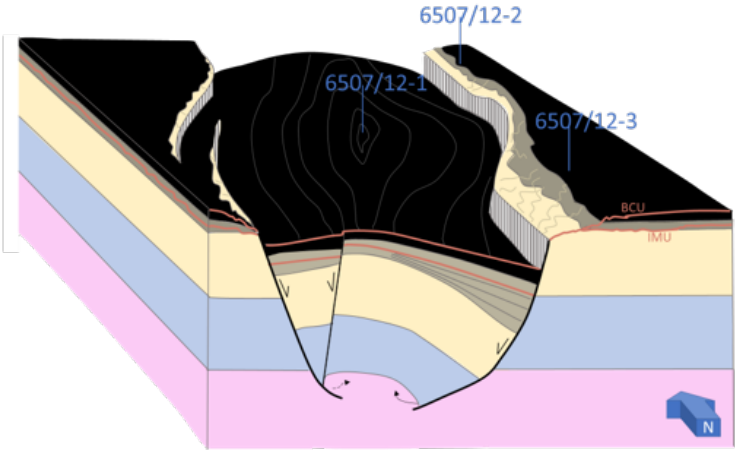

(f) Finally Spekk depositionand BCU erosion is suggested as the scenario by the earliest Cretaceous

Figure 4.21: Conceptual sketch illustrating stages of formation of the closure that well `6507/12-1` is placed on. Evaporites in pink, Early Jurassic in blue, Middle Jurassic in yellow, Melke Formation in brown and Spekk Formation seen in black.

4.1.5 Sedimentary rift sequences

This section summarizes observations from thickness maps, well data and seismic cross sections to suggest a division of the Triassic to Quaternary strata in the Ellingråsa Graben into pre-, syn- and post-rift sequences, relative to the major regional rifting event taking place in the Late Jurassic to earliest Cretaceous (see chapter 2). The division into rift sequences is aided by descriptions from published literature. Differences between findings of previous publications and local observations in the study area are discussed where relevant. The division of strata is vizualised in figure 4.22.

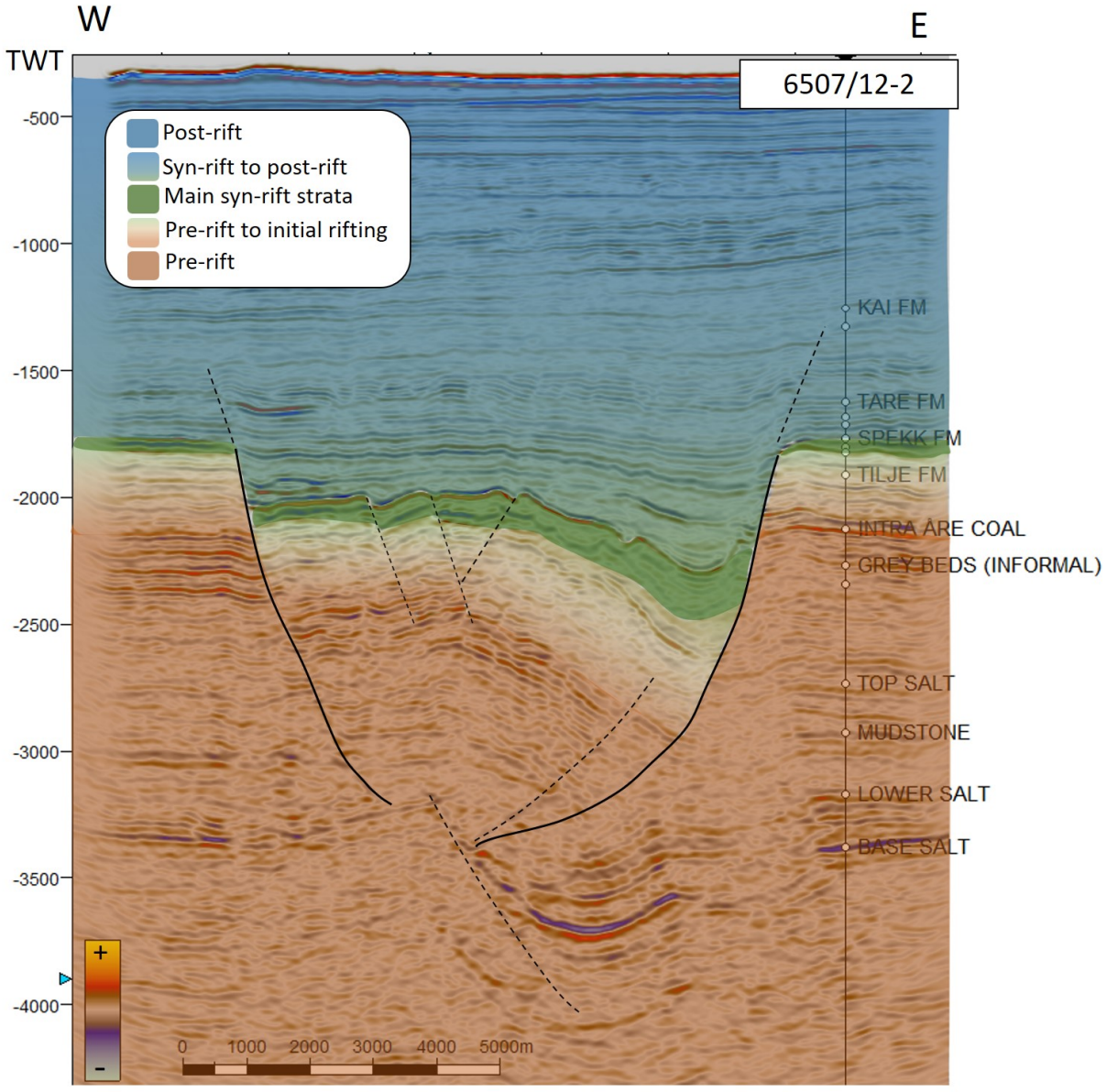

Figure 4.22: Stratigraphy of the Ellingråsa graben from Triassic to Quaternary, here divided into rift sequences relative to the Late Jurassic to Early Createceous major rift event. Gradual transitions from pre-rift to syn-rift and from syn-rift to post-rift strata is marked. Figure is Xline 2713 (see also figure 4.13)

Pre-rift strata

The Triassic salt unit has already been discussed in detail in section 4.1.2 and will therefore only be mentioned briefly here. These were deposited as evaporites in a sabkha environment in response to Triassic rifting and subsequent flooding (Wilson et al. 2015), obviously predating the rifting of the Late Jurassic to Early Cretaceous. Overlying the salt unit are the Triassic grey and red beds, deposited in an extensive fluvio-lacustrine flood basin with climate gradually changing from very arid in the red beds to more humid leading up to deposition of the coals of the Early Jurassic Åre Formation (Müller et al. 2005). On seismic, the pre-rift classification of this Triassic to Eary Jurassic strata is observed by its heavily faulted nature, however commonly detaching at the evarpoite level, as described in section 4.1.2. In addition, no syn-rift wedges are observed, and the strata is quite heavily deformed with significant hanging-wall rollover in response to faulting. The time thickness map showing elevation time from the faulted Intra Åre coal horizon to the top of the intra-evaporite mudstone unit is seen in figure 4.23. The intra-evaporite mudstone unit is a relatively flat surface, largely unaffected by tectonic events of the Jurassic. From the figure one can observe that the thickness of this sequence is equal on each of the graben flanks, where the strata is more or less horizontal. The apparent smaller thickness in the hanging wall of the BFC to the east and in the northern part of the hanging wall to the antithetic fault are due to significant amounts of rollover and do not represent depositional thickness differences. The elevated structure on which well `6507/12-1` is drilled also clearly stands out on this map.

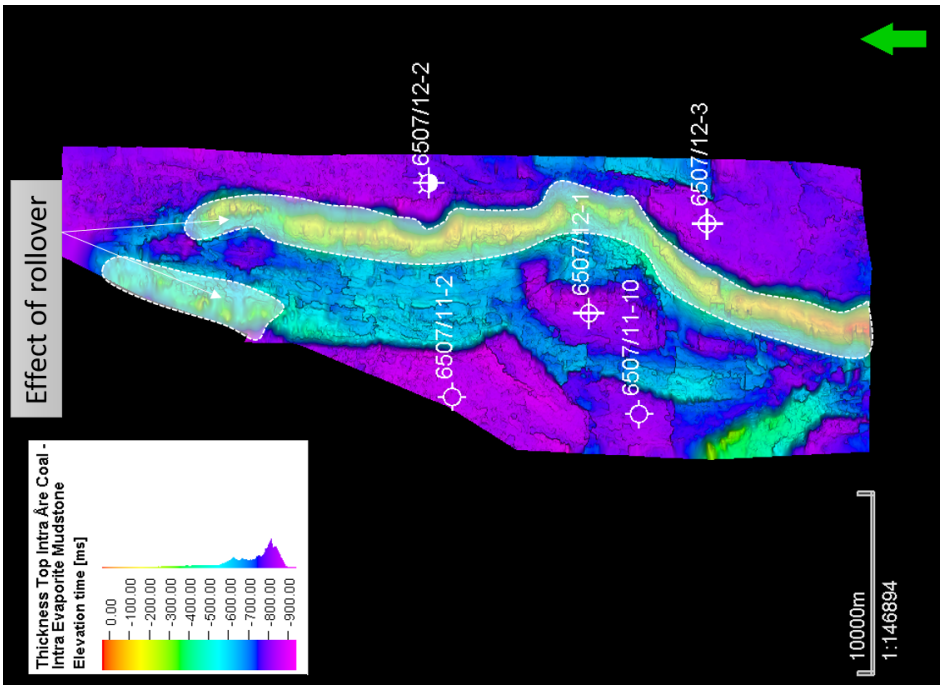

Figure 4.23: Thicknes in TWT from intra Åre Formation coal horizon to intra Triassic evaporite mudstone unit. Observe equal thicknesses on both graben flanks.

Pre-rift to intial rifting transition

In chapter 2, the Early to Middle Jurassic period is described as less tectonically active than both the Triassic rifting and the late Middle Jurassic to earliest Cretaceous rift event to come. Above the coals of the Åre Formation a transition from a lower delta plain setting to open marine conditions is described in literature (Thrana et al. 2014). A report for block 6507/12 by Saga Petroleum AS (1985a) reports this Early Jurassic sequence above the coal as having increasing sand content reflecting transgression and establishment of a marginal marine to marine depositional system continuing into the Tilje Formation. This transgression is thought to have been induced by gradual tectonic activity forming a marine seaway between seas to the north and south (Ravnås et al. (2014) and Thrana et al. (2014), see also section 2.3). Marsh et al. (2010) describes the Early Jurassic from top of the coal unit as the start of the rift initiation stage, an initial period of slow subsidence where sedimentation is able to keep pace with the subsidence. This is based on sediment thickening towards faults observed on seismic in the Smørbukk area. Conceptually, small, isolated segments of active faulting with local hanging wall basins would be expected in the initial rifting phase (Gawthorpe and Leeder 2000). Such thickening in the Early Jurassic strata is difficult to observe in the Ellingråsa Graben. This is partly because thickness maps will show a significant thickness increase in the hanging wall towards the BFC due to rotation of the strata, overprinting actual depositional thickness changes, and partly due to the discontinuous reflection pattern of the strata at this level. Interpretation of several more horizons in the Early to Middle Jurassic interval would also be needed to determine the exact onset of initial rifting. Some possible syn-rift tendencies can be seen in the southern part of the study area (figure on the Åre Formation level 4.24), indicating that the N-S striking fault segment S1 of the BFC was active in this period. It should however be noted that this gently diverging reflection pattern is only a local, relatively low confidence observation. The same diverging pattern is not observed in the remaining Early to Middle Jurassic strata (pre-Viking group), indicating less tectonic activity in the area during this time period. This is line with the reports from Blystad et al. (1995) regarding time of main activity along the BFC. Note also that, in line with the timing of faulting suggested in sections 4.1.3 and 4.1.4, syn-rift wedges of pre-late Middle Jurassic age are not observed in the hanging wall of the antithetic faults bounding the Ellingråsa Graben.

Either way, reports from wells (Paleoservices LTD. 1980; Paleoservices LTD. 1986; Saga Petroleum AS 1983a) indicate several cycles of transgression and regression in the Early to Middle Jurassic deposits, with an overall transgressive trend, as is also thoroughly described by Ravnås et al. (2014) in literature. This is linked to tectonic activity in the area on a regional scale, all leading up to the main rift event taking place in late Middle Jurassic to earliest Cretaceous.

Syn-rift strata

Late Middle Jurassic, Bathonian to Callovian, represents a major unconformity recognized in all 3 wells on the 6507/12 block (Saga Petroleum AS 1983a; Paleoservices LTD. 1986). This is the IMU, a regional unconformity seen in most wells on the Halten Terrace (see also chapter 2). It is associated with uplift of rift shoulders, hanging wall subsidence and large

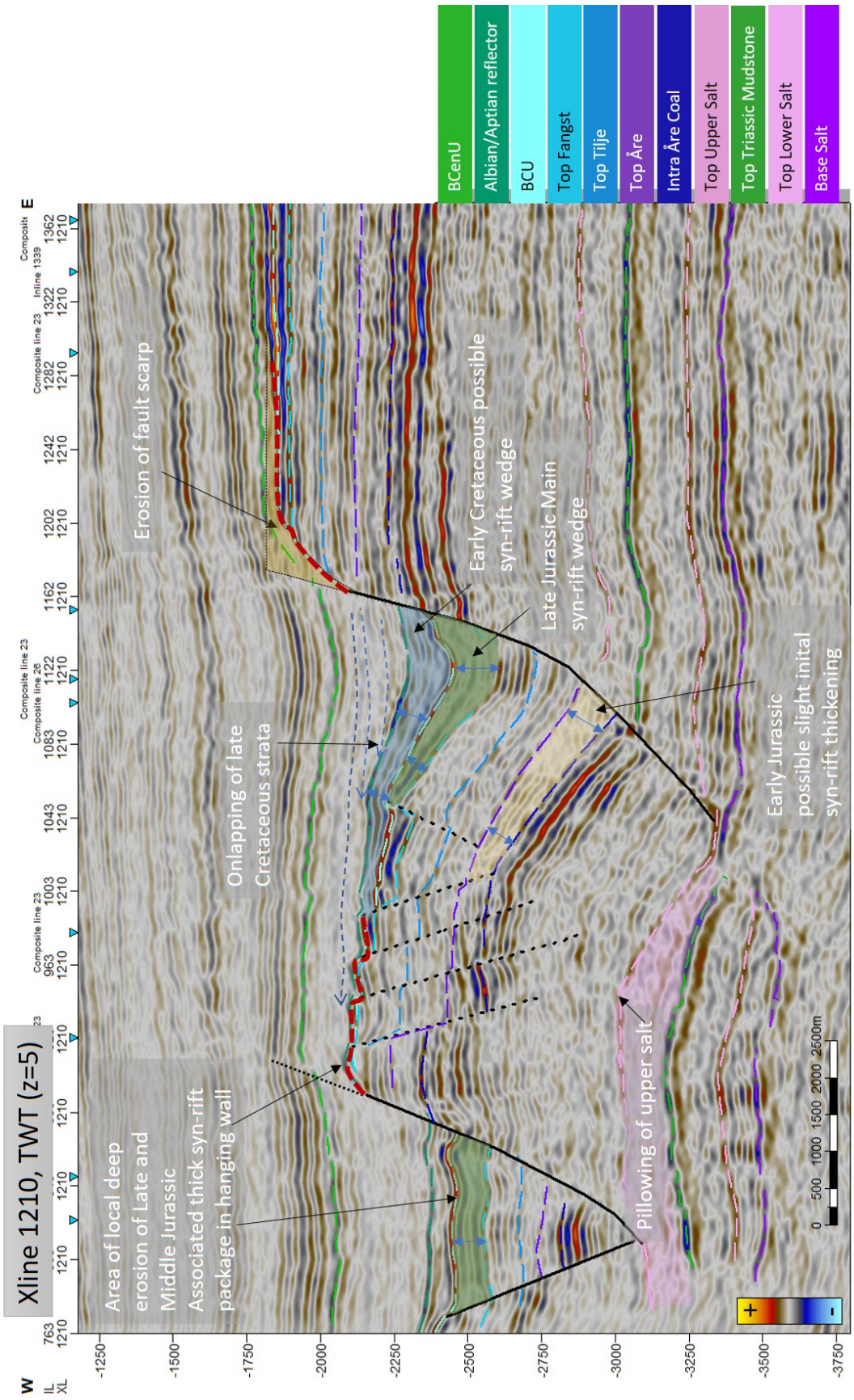

Figure 4.24: Possible syn-rift tendencies in the Early Jurassic marked, indicating some active tectonism at this time. Large syn-rift wedge of Late Jurassic age marked, recognizable throughout the study area, and indicating the main tectonic event occurring from Late Jurassic to earliest Cretaceous. Some evidence of syn-deposition also seen in the Early Cretaceous strata which the Late Cretaceous strata laps onto. The BCenU reflector is also faulted, indicating tectonic activity post-dating the Cretaceous. Local deep erosion over an intra-graben synthetic fault and erosion over the BFC footwall with previous fault scarp surface are indicated.

syn-rift deposits, occurring in the middle of deposition of the Melke Formation mudstones. In the 6507/12-2 well, the whole of the Melke Formation is dated to late Oxfordian, post-dating the Callovian unconformity with an unconformable base (Stratlab AS 1990), while the 6507/12-1 well is determined to contain Melke deposits of both pre- and post- Callovian age, suggesting that the unconformity has not eroded into the Middle Jurassic sandstones at this location. Sadly, the IMU is hard to pin-point on seismic in the study area due to a lack of angular discordance or change in reflectivity. However it should be expected to follow the Top Fangst horizon for parts of the BFC footwall in the study area, and be constrained within the Melke Formation for the most of the graben, based on the argumentation and well information above. An important exception is local intra-graben footwalls, as is seen in figure 4.24, where significant erosion appears to have taken place. Note also that the distance from Top Fangst to Top Tilje is slightly greater within the graben than on the BFC footwall, also suggesting significant erosion of the Middle Jurassic sands over the footwall at this time.

With erosion follows deposition of new sediments, and an easily recognizable feature in the whole study area is the major late Middle Jurassic to Late Jurassic syn-rift wedge with divergent strata thickening significantly towards the faults. This is especially visible in the hanging wall of the BFC and is observed to a varying degree in all cross sections in this thesis and in the thickness map seen in figure 4.18. These syn-rift wedges are expected to contain intra-Melke sandstones, re-deposited from eroded Jurassic sand, probably in a deep-marine environment based on conceptual models for rift basin development such as Gawthorpe and Leeder (2000). In figure 4.24, a clear syn-rift wedge is seen in the BFC hanging wall, related to significant erosion of the fault scarp, indicated on the figure. Another thick syn-rift package is marked in a local hanging wall to the west in the figure. This is related to the local deep erosion of an intra-graben fault footwall. The same wedge shape is not seen here however, probably due to the confined accommodation space available in this small graben structure lacking significant asymmetry.

Following the major erosion and deposition of syn-rift strata in Callovian came deposition of the post-Callovian part of the Melke Formation and eventually the organic rich Spekk Formation at the culmination of the rifting. The Spekk formation is of Early Kimmeridgian age in 6507/12-2 and Kimmeridgian to Berriasian age in well 6507/12-1 (Stratlab AS 1990) and is a thin layer of black shale, draping the rift topography created during the previous rift event. Because its thickness is below the vertical resolution of the seismic in most places, its base is not interpreted in this thesis and the formation is included in the syn-rift strata between the BCU horizon and top of the Fangst Group. It should be noted that while most of the wedge thickness observed in the hanging walls is expected to belong to the Melke Formation or intra-Melke sandstones, the Spekk Formation is also expected to thicken at these locations. Its top boundary is unconformable in both wells due to erosion or sediment starvation at earliest Cretaceous times. This erosive event resulted in the famous BCU surface. On figure 4.24, the Spekk formation is eroded and is completely missing over the BFC footwall scarp and at the crest of the intra-graben synthetic fault, so the BCU is clearly locally erosive in the study area. See section 4.1.3 for elaboration on BCU erosion on the BFC footwall. What amount of erosion in figure 4.24, and in general, should be attributed to events of the Callovian or earliest Cretaceous is not known, however conceptually the Callovian erosive period is thought to be more extensive than that of the

earliest Cretaceous. Possibilities of intra-Spekk syn-rift sands should also be considered in the hanging wall of faults with major erosion at the BCU level.

Syn-rift to post-rift transition

After the major rifting event, the newly formed graben structure is expected to be in a deep water, sediment starved environment. In literature, the Cretaceous in the Norwegian Sea is largely described as a period of tectonic quiescence (Færseth and Lien 2002). Looking at the cross sections (figures 4.9-4.15 and figure 4.24) from the study area, it is quite clear that this does not exactly hold for the Ellingråsa Graben. Faulting of the Cretaceous strata and visible offset of the BCenU surface is commonly observed, often associated with a change in dip of the faults. These observations are made from south to north in the study area, and are as common in the antithetic bounding faults as for the BFC, indicating that the fault zones on both sides of the graben have been tectonically active long after the rifting of the Jurassic.

An Albian/Aptian reflector, based on biostratigraphy from well `6507/12-1` (Paleoservices LTD. 1980), is mapped over the study area. This gives an indication of the thickness of the Early Cretaceous strata, which is highly variable due to differential accommodation space available (see time thickness map, figure 4.25). There is no Early Cretaceous strata found in either well `6507/12-2` or `6507/12-3` on the eastern flank, and only 20 meters of the Early Cretaceous Lyr Formation was penetrated in well `6507/12-1`. In the hanging walls, however, the Early Cretaceous strata grows quite thick, with the exception of fault segment S2, where there clearly has not been space to accommodate deposition of Early Cretaceous strata of significant thickness (see previous section 4.1.3).

In figure 4.24, a syn-rift wedge in this early Cretaceous strata is also suggested, based on increasing thickness and somewhat diverging reflectors towards the BFC. The Late Cretaceous strata is onlapping the Albian/Aptian reflector and there is a clear angular discordance between the Early and Late Cretaceous. The Late Cretaceous appears to have been a period of infilling previously created rift topography, naturally resulting in large thickness variations of the total Cretaceous package in the study area (figure 4.19). The observation of faulting of the Cretaceous strata along with possible syn-rift signs in the Early Cretaceous strata differ from the description of the Cretaceous on the Halten Terrace as a period of little tectonic activity, and indicates that the Ellingråsa Graben may have experienced more post-Jurassic tectonic activity than other parts of the region. The Cretaceous strata in the study area is therefore considered to represent a transition from syn-rift to post-rift rather than purely post-rift.

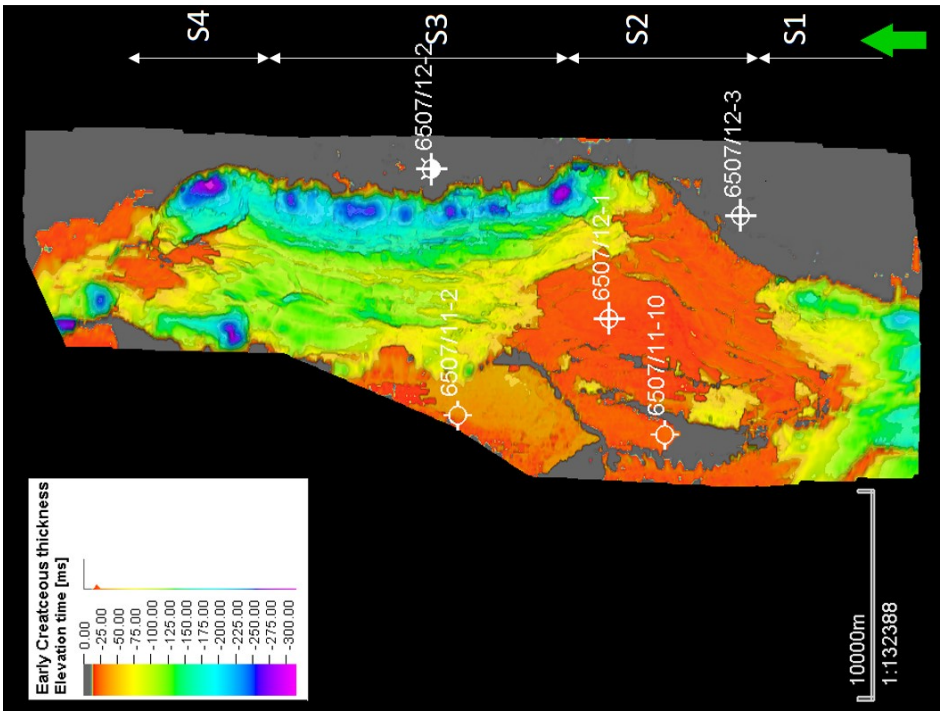

Figure 4.25: Time thickness map showing approximate Early Cretaceous thickness over the study area.

Post-rift strata

The bounding lineaments are clearly recognized on the BCenU elevation map (figure 4.26), with the greatest throw along the BFC to the south (segment S1) in the study area. The Paleocene to Oligocene Rogaland and Hordaland groups are observed as gradually evening out this topography. There is some evidence of faulting of this strata as well (see figures 4.9-4.15). Note also the abundant polygonal faulting, typical for the Brygge Formation. Thickness variations of the Paleocene to Oligocene strata is seen in figure 4.27. Some of the thickness variation may also be due to differential thermal subsidence in the area, in which case with a southward increasing gradient. By the time of erosion and deposition of the Naust Formation, the topography appears to have been more or less evened out, as no dramatic truncation features are observed related to this erosive event.

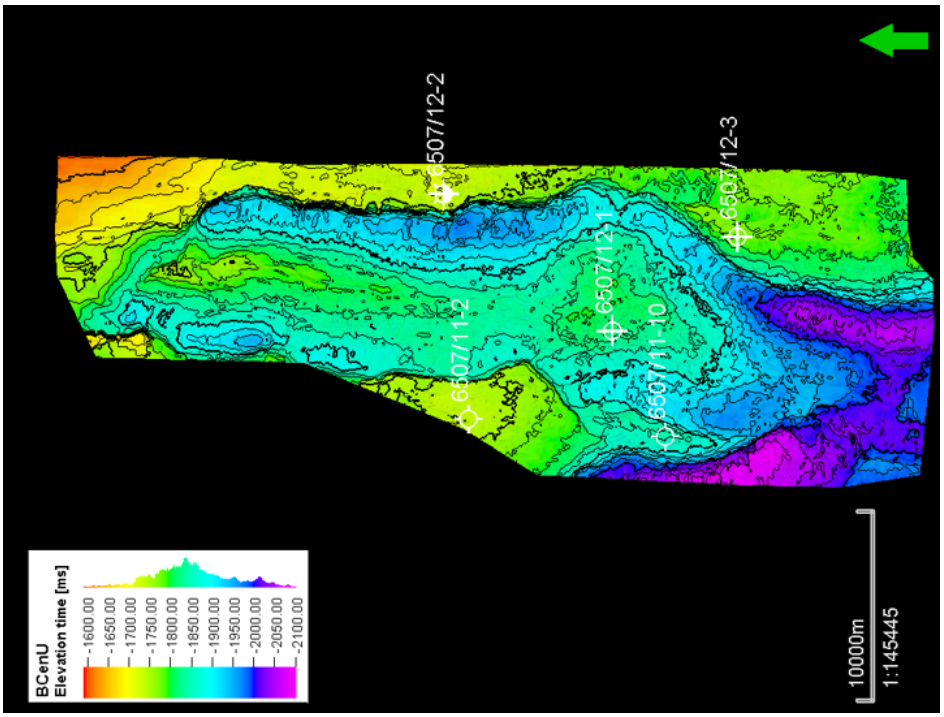

Figure 4.26: Elevation map of the BCenU surface across the study area

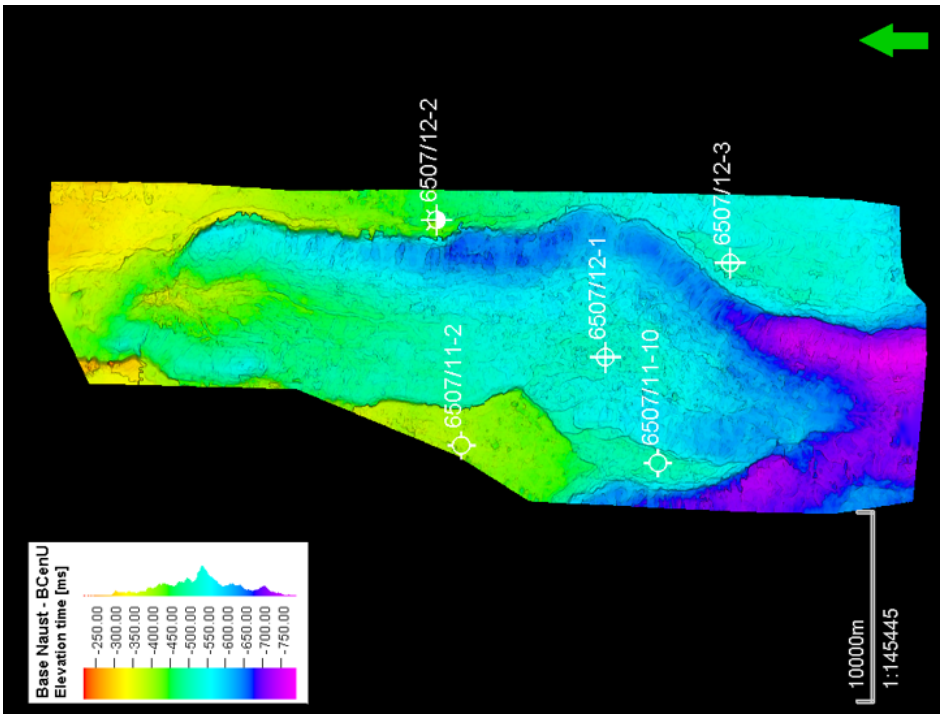

Figure 4.27: Time thickness map showing thickness of the Paleocene to Oligocene strata in the study area

4.2 Lithostratigraphy and depositional environment

This section will cover the lithostratigraphy and depositional environments of the strata found in the Ellingråsa Graben starting from Triassic, with emphasis on the petroleum geologically significant Jurassic interval. The basis of these considerations is the information from the 6507/12-1, 6507/12-2 and 6507/12-3 wells along with any implications available from seismic. Some of the information presented herein is summarized in the stratigraphic chart created for the Ellingråsa Graben in figure 4.28.

4.2.1 Triassic

The Triassic is only penetrated by the 6507/12-1 and 6507/12-2 wells. The correlation between these wells for the Triassic interval is seen in figure 4.29. 960 meters MD of Triassic strata was drilled through in 6507/12-1 and over 2400 meters MD in 6507/12-2, however neither well penetrated the entire Triassic interval (Paleoservices LTD. 1980) and only the 6507/12-2 well penetrated the evaporite unit.

This thesis starts its consideration of stratigraphy in the Ellingråsa Graben with the evaporite unit, in well 6507/12-2 consisting of two distinct evaporite layers of approximately 380 meters each, separated by a mudstone interval of around 500 meters. From figure 4.29 it is seen that the top of both evaporite units are actually associated with a *decrease* in acoustic impedance, set up by the decreasing density values rather than by a change in velocity. This is likely because of the great depth, causing above-lying strata to be highly compacted and cemented thus yielding high velocities and densities. Both evaporite intervals are considered deposited in a playa lake salt pan environment (Robertson Research International Limited 1982), related to the rifting and marine incursion as mentioned in section 2.2.2, though the lower unit shows much greater thickness variation than the upper unit (see also section 4.1.2). Both salt intervals are dominated by halite, with small intervals of sheet-flood silts and sand. The lower of the two salt intervals appears slightly more heterogeneous, especially towards the top, than the younger salt interval. This may be related to several distinct layers of anhydrite present in the lower salt interval, creating large variations in density values (see for instance the log response at 4565 meters) (Robertson Research International Limited 1982). This is also represented by more varying acoustic impedance values on the log and by internal reflections on seismic (figure 4.5). The mudstone separating the two salt intervals consists of playa mud-flat deposits, typically dolomitic or anhydritic at the base of the interval and light grey to red-ish brown continental calcareous sediements. Thin beds and nodules of anhydrite are common in this mudstone, possibly deposited as gypsum on the mud-flats. The age of the evaporite unit, from top upper salt to base lower salt is considered mostly Late Triassic, Ladinian to Norian (Robertson Research International Limited 1982). From literature (Müller et al. 2005), the salt interval is suggested to be of Ladinian to Early Carnian age. The dating from the stratigraphical report for well 6507/12-2 could be wrong, or it could indicate prolonged salt deposition in the study area compared to the rest of the region. Above the evaporite unit the depositional environment slowly changes from a marginal sabkha setting to fluvial continental deposits, reflecting an overall regression from precipitation of evaporites in an ephemeral lake setting to deposition of the continental red beds (Robertson Research International Limited 1982).

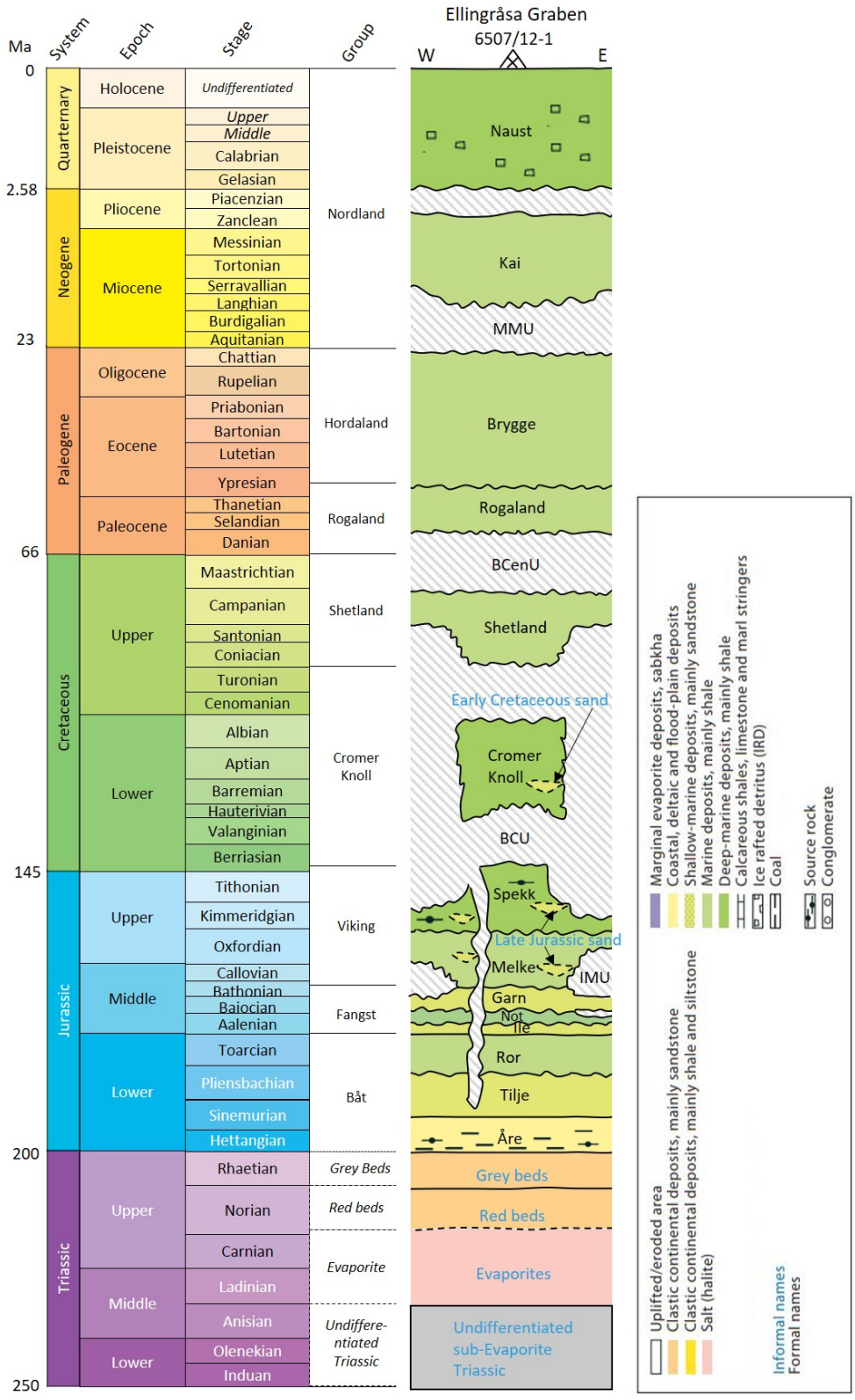

Figure 4.28: Generalized lithostratigraphic chart created for the Ellingråsa Graben, based on biostratigraphical and sedimentary reports from the wells on block 6507/12.

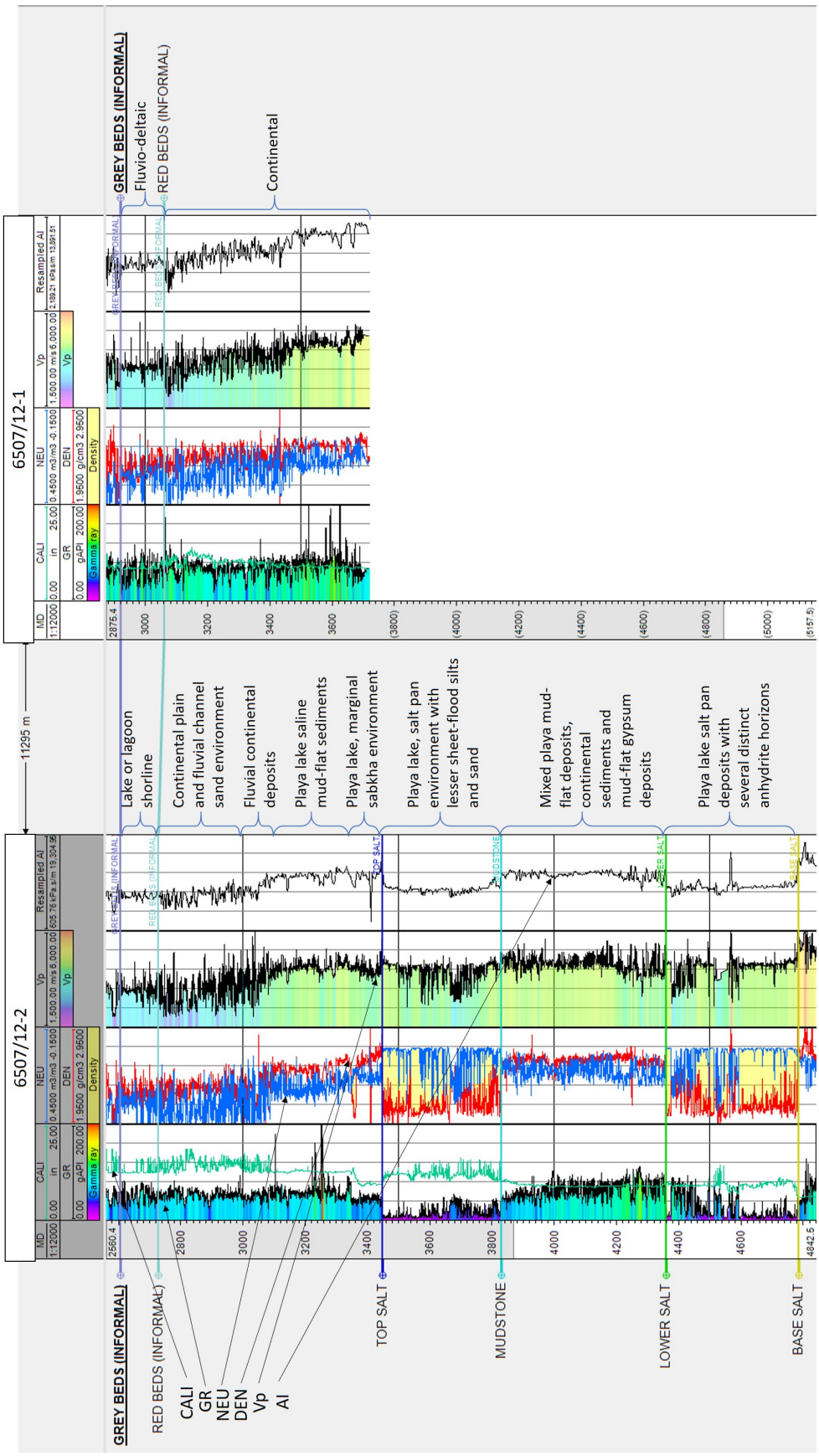

Figure 4.29: Triassic stratigraphy and well correlation, flattened on top Grey beds (informal). Grey and Red beds formation tops from NPD and top and base of salt layers and mudstone picked by this author. Description of depositional environment from Paleoservices LTD. (1980), Robertson Research International Limited (1982)

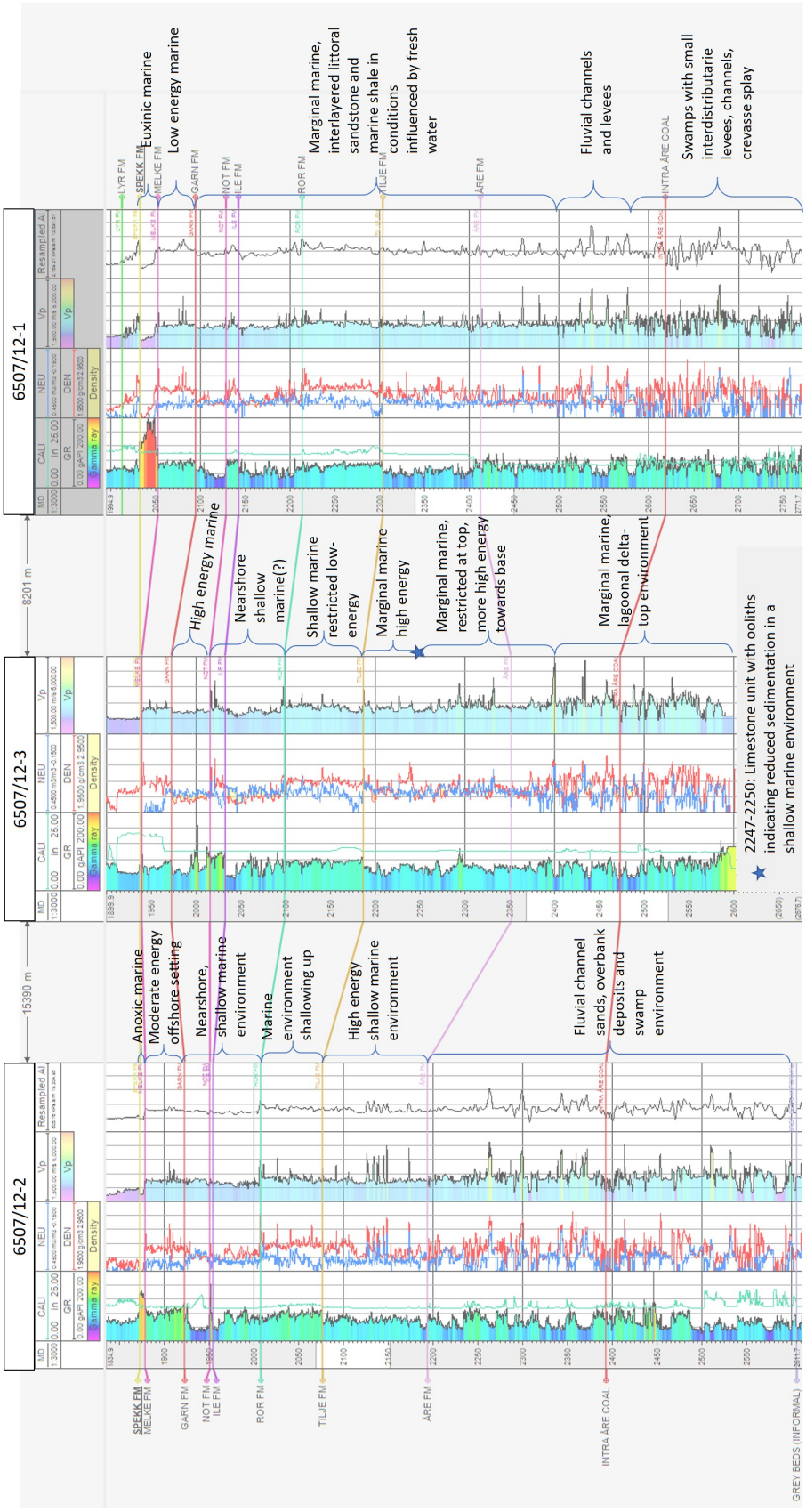

Figure 4.30: Jurassic stratigraphy and well correlation, flattened on top Spekk. Description of depositional environment from Paleoservices LTD. (1980), Robertson Research International Limited (1982) and Laboratoire de Geologie de Boussens (1981b)

The latest Triassic grey beds, with approximately constant thickness from the well correlation in figure 4.29, were deposited in a fluvio-deltaic to lake and lagoonal environment with periods of coal swamp development, reflecting a change in climate from arid to more humid conditions (Robertson Research International Limited 1982). This transition is also well-documented in literature as seen in section 2.3.

4.2.2 Jurassic

The environment of the Jurassic deposits in the Ellingråsa Graben range from a lower delta plain setting with distributary channels and swamps to open marine conditions in an overall transgressive sequence (see figure 4.30 for summarized depositional environment conclusions from well studies). This is also the general trend reported by authors like Ravnås et al. (2014) (see section 2.3). Both the most prominent reservoir and source rock intervals are found within this succession.

The earliest Jurassic sediments rests conformably on the Triassic, and the transition from the relatively arid continental deposits in the red and grey beds to the humid, swamp influenced marginal marine delta plain and channel deposits of the Åre Formation is gradual (Saga Petroleum AS 1983b). This gradual transition is also reported by Thrana et al. (2014), as described in section 2.3. Abundant coals are found in the Åre Formation, as seen in figure 4.31, and most of the formation is termed the "Coal Unit" in the sedimentological studies conducted for the wells in the area (pre-dating Dalland et al. (1988) formal lithostratigraphic scheme). These coals are observed on petrophysical logs as small intervals with extremely low density and low gamma ray readings. Top Intra Åre Coal is picked on the youngest of these intervals and corresponds to a decrease in AI and a bright soft reflector on seismic (see figure 4.7).

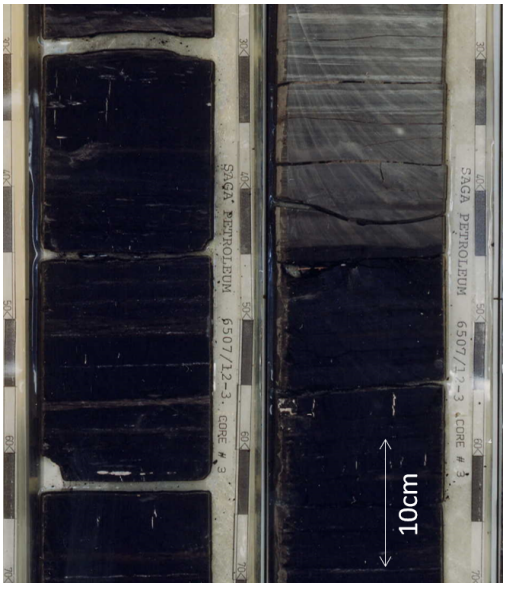

Figure 4.31: Core from lower part (at 2504 m) of the Åre Formation, well 6507/12-3.

The Åre Formation is reported as texturally immature, indicating provenance not far from the site of deposition (Robertson Research International Limited 1982). In well 6507/12-2 the thickness of the Åre Formation is 412 meters, with an age from Hettanganian to Sinemurian, consistent with reports from literature (Thrana et al. 2014).

The Tilje formation of Sinemurian to Pliensbachian age in well 6507/12-2 (Robertson Research International Limited 1982) overlies the Åre Formation and is described as thinly interbedded, bioturbated fine sand and silt with minor amounts of medium and coarse sand, deposited in a high energy, tidal-influenced marginal marine to shallow marine environment (Robertson Research International Limited 1982; Paleoservices LTD. 1986). This means that an overall transgressive trend occurs from deposition of the Åre Formation to the Tilje Formation, which can be related to the opening of the marine strait between the Thethys and Boreal Sea, as described in section 2.3. Figure 4.32 shows a core from the Tilje Formation taken from the Midgard discovery well (6507/11-1) just southeast of the study area, illustrating the small-scale interbedding of silt and fine sand. In the 6507/12-3 well, a 3 meter layer of limestone with Oolites is reported intra-Tilje Formation, between 2247-2250 meters. This is thought to a indicate a period of reduced sedimentation in a shallow marine environment (Paleoservices LTD. 1986). This layer has not been reported in the other wells in the study area nor is it mappable on seismic. It may therefore be only a local phenomena, and could indicate differences in sediment supply between the three closely located wells. The heterogeneity of the formation can be observed in terms of varying log responses throughout the interval. In well 6507/12-1 and 6507/12-2 the formation is a little over 100 meters thick, thickening significantly towards well 6507/12-3. However, the biostratigraphic study from Paleoservices LTD. (1986) reports no good samples in the interval surrounding the boundary between the Tilje and Åre formations, so the Top Åre pick from NPD Fact Pages may be erroneous. The formation has a Sinemurian to Late Pliensbachian age in the wells (Laboratoire de Geologie de Boussens 1981a; Saga Petroleum AS 1983a; Stratlab AS 1990), in line with the age suggested by Ichaso and Dalrymple (2014).

Figure 4.32: Core from the Tilje formation (at 2507 m), well 6507/11-1.

Overlying the Tilje Fm are the mudstones of the Ror Formation, showing an overall coarsening upwards trend into silts and fine sands registered in all wells in the study area (Saga Petroleum AS 1983b), though this coarsening up is not obvious from the log responses. The coarsening up trend is also described in literature (Dalland et al. 1988), as mentioned in section 2.3. The base of this interval is described as unconformable with an abrupt change from the Tilje Formation sands to anaerobic mudstones (Robertson Research International Limited 1982) reflecting the rift induced transgression in the Early Toarcian (see section 2.3). The Ror Formation is around 70-90 meters thick in the wells, the thickest interval found in the `6507/12-1` well situated in the middle of the graben.

From figures 4.28 and 4.30 it is seen that the Tofte Formation described in section 2.3 is not present in the study area. Overlying the mudstones of the Ror Formation is the Ile Formation, reported as having a Late Toarcian to Aalenian age (Robertson Research International Limited 1982). However, more recent stratigraphical studies reports the Ile Formation as being of Aalenian age in the study area, which is more in line with the regional understanding (see section 2.3). Over the Ile Formation, the Aalenian to Bajocian Not Formation and the Bajocian to Bathonian Garn Formation are found. From studies of well data and sidewall cores, these three formations (at the time of these studies termed "Middle Jurassic Sandstones") are described as having been deposited in a near-shore shallow marine environment (Laboratoire de Geologie de Boussens 1981b; Robertson Research International Limited 1982; Paleoservices LTD. 1986).

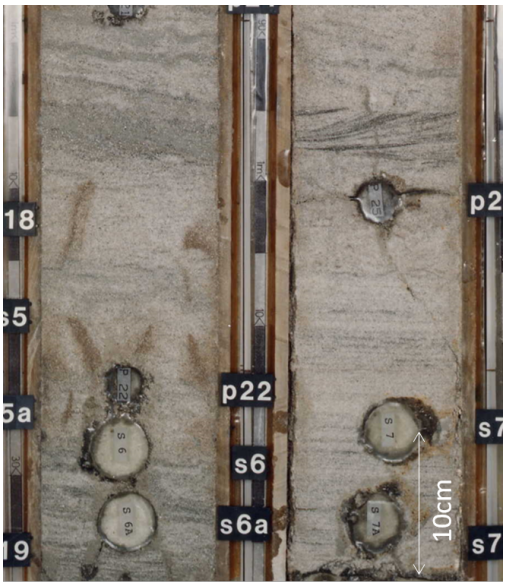

Figure 4.33: Core from the Garn formation (at 1987 m), well 6507/12-3.

While these early studies generally do not differentiate between the Ile, Not and Garn formations, it is clear from the log data seen in figure 4.30 that the Not Formation is a high Gamma Ray, high density interval associated with higher AI, separating the homogeneous Garn Formation from the underlying Ile Formation with a more heterogeneous log signature. Deposition of the Not formation is associated with a trangressive period starting from the upper Ile Formation, caused by a mixture of tectonic activity and rising eustatic sea level (see section 2.3). A core interval from the Garn Formation in well 6507/12-3 is seen in figure 4.33, showing laminated and bioturbated medium grained sand.

In well 6507/12-2, NPD Fact Pages have not defined a formation top for the Not or Ile formations, indicating that they are not present in the well. This thesis provides a new suggestion for top Not Formation and top Ile Formation, based on log response and biostratigraphical data from a sidewall core taken at 1985 meters indicating Toarcian age at this depth (Robertson Research International Limited 1982). Further explanation of these new suggested formation tops is found in section 6.3. A zoomed-in well correlation panel illustrating this is seen in figure 4.34. Using these formation top picks, the Ile Formation is around 55 meters thick in the 6507/12-2 well, thickening slightly to around 70 meters in wells 6507/12-3 and 6507/12-1. Figure 4.34 also illustrates that the Not Formation is suggested to be only a couple of meters thick in the 6507/12-2 well, either related to erosion at base Garn Formation or non-deposition. An erosive bare Garn is described by Corfield et al. (2001). The Garn Formation is only 28 meters thick in the 6507/12-2 well, versus 42 and 34 meters in the 6507/12-3 and 6507/12-1 wells, respectively.

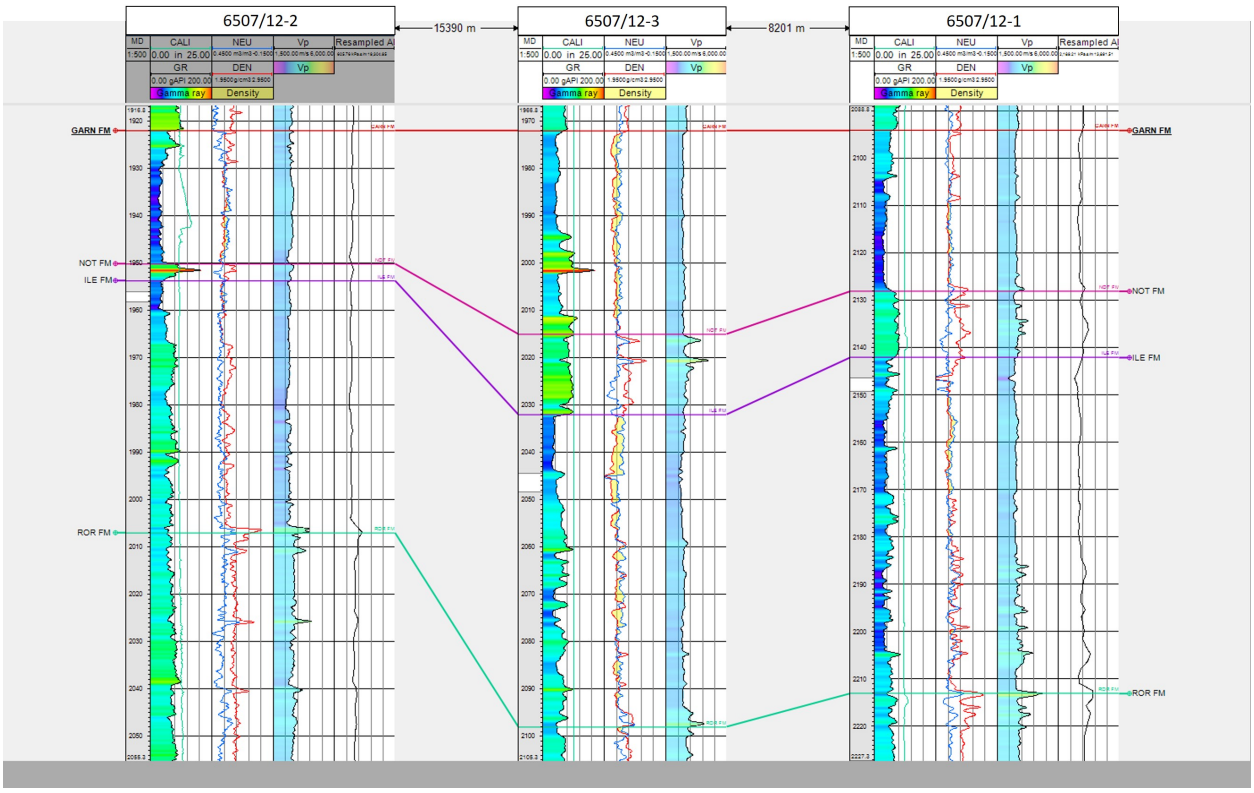

Figure 4.34: Well correlation window zoomed in on the suggested formation top picks for the Ile and Not formations, flattened on top Garn Formation.

As previously explained, tectonic activity increased significantly in the Late Jurassic, causing thick syn-rift packages to be deposited in the hanging walls of major faults and erosion in elevated areas. The significantly smaller thickness of the Melke Formation observed in 6507/12-3 compared to 6507/12-2 may indicate a greater time gap related to the IMU in 6507/12-3 than in 6507/12-2. Biostratigraphic data from well 6507/12-3 is sadly quite poor in this time interval (see Paleoservices LTD. (1986)), and cannot be used to support this argumentation. The Melke Formation is dated as Late Oxfordian in well 6507/12-2 (Stratlab AS 1990), with a hiatus from the Late Oxfordian to Bajocian in the Garn Formation under. In well 6507/12-1 this time gap is significantly smaller and the associated IMU is found within the Melke Formation rather than at the base of the formation as in well 6507/12-2. However, it should be noted that the biostratigraphical reports are conficting and contradicting in this interval, as is discussed in section 6.3.

In the wells, the lithology of the Late Jurassic Viking Group is described as open marine mudstone in the Melke Formation, and shales with very high organic content in the overlying Spekk Formation. The high TOC in the Spekk formation is clearly reflected by very high gamma ray readings and low density and velocity in the interval. While the depositional environment following the rift induced transgression in the Melke Formation is low energy open marine, it is described as anoxic and sulfidic in the overlying Spekk Formation, facilitating preservation of organic material and thus causing the high TOC in the formation (Robertson Research International Limited 1982; Laboratoire de Geologie de Boussens 1981b). Figure 4.30 clearly illustrates the difference in erosion and accommodation space at BCU time through Spekk thickness variation, from only 2 meters in 6507/12-3 to around 20 meters in 6507/12-1. Although these formations are described as having shale lithologies in the well positions, local sandstones should be expected, especially intra-Melke, in the thick syn-rift wedges close to the BFC where erosion on the adjacent footwalls is considered to be deep.

4.2.3 Cretaceous

The Cretaceous strata in the area is of highly variable thickness due to topography created after the latest rifting episode 4.19. Lack of accommodation space during the Early Cretaceous in the elevated footwalls of the study area has resulted in no deposits of Early Cretaceous age here, as clearly seen from wells 6507/12-2 and 6507/12-3 in figures 4.25 and 4.35. Well 6507/12-1 however, has a thin layer of Early Cretaceous (Hauterivian to Albian) deposits of the Cromer Knoll Group (Lyr Formation). This shows that more accommodation was available in the Early Cretaceous here, in the middle of the graben, as should be expected. It is also expected to find Early Cretaceous deposits in the immediate hanging wall of major faults (see section 4.1). In well 6507/12-1 the Early Cretaceous strata is described as red and grey claystones, marl and occasional limestone deposited in a marine shelf environment (Paleoservices LTD. 1980). The vaying Cretaceous thickness is in line with the description from (Færseth and Lien 2002), see section 2.2.2. The Late Cretaceous (mainly Campanian) is described as red and brown to greyish claystone with a deep marine depositional environment, probably with reduced oxygen conditions (Saga Petroleum AS 1983a). The log response in this interval is fairly homogeneous with relatively low velocities and gamma ray values around 50-60 gAPI.

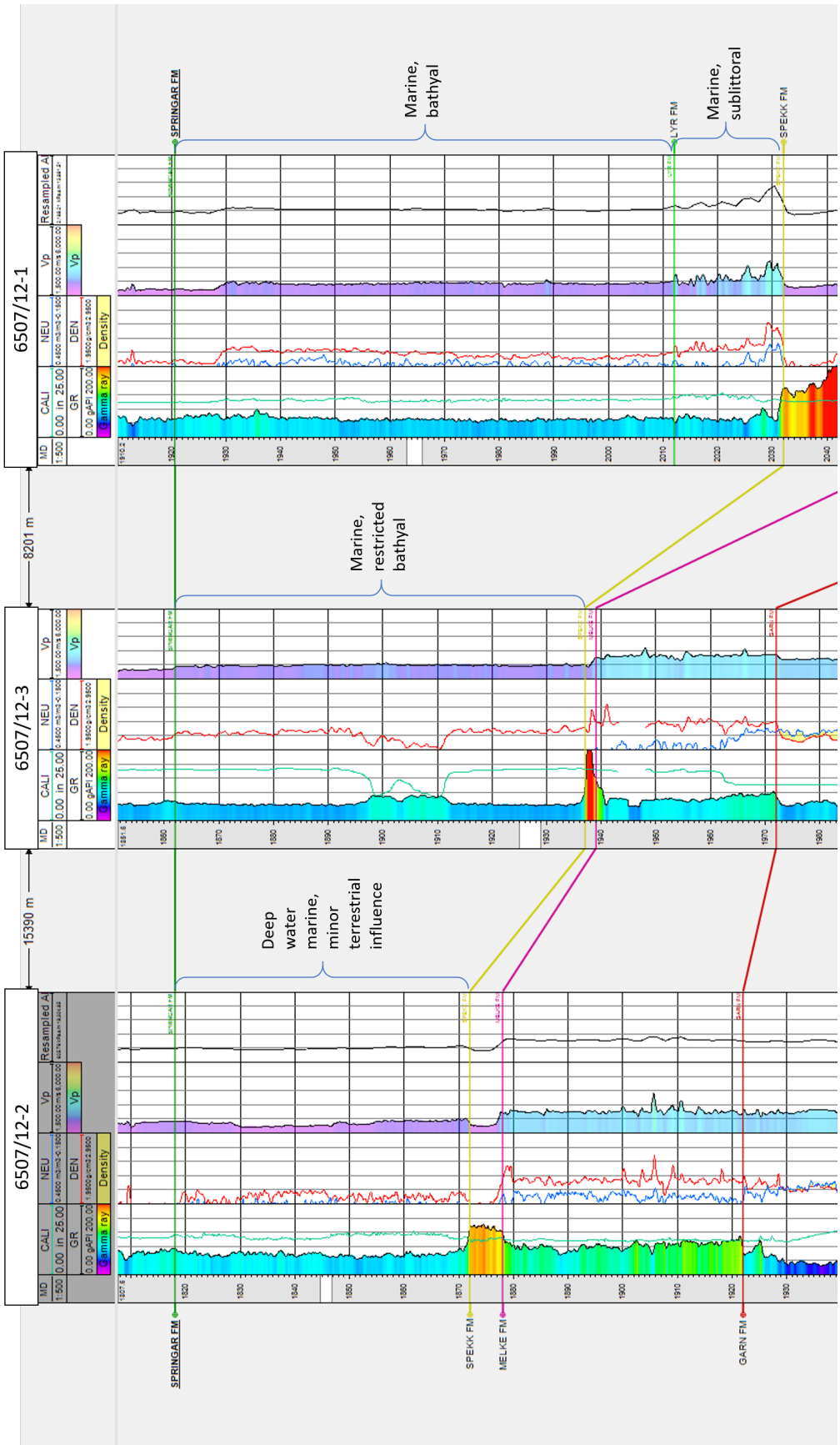

Figure 4.35: Cretaceous stratigraphy and well correlation, flattened on top Springar (BCenU). Description of depositional environment from Paleoservices LTD. (1980), Robertson Research International Limited (1982) and Paleoservices LTD. (1986)

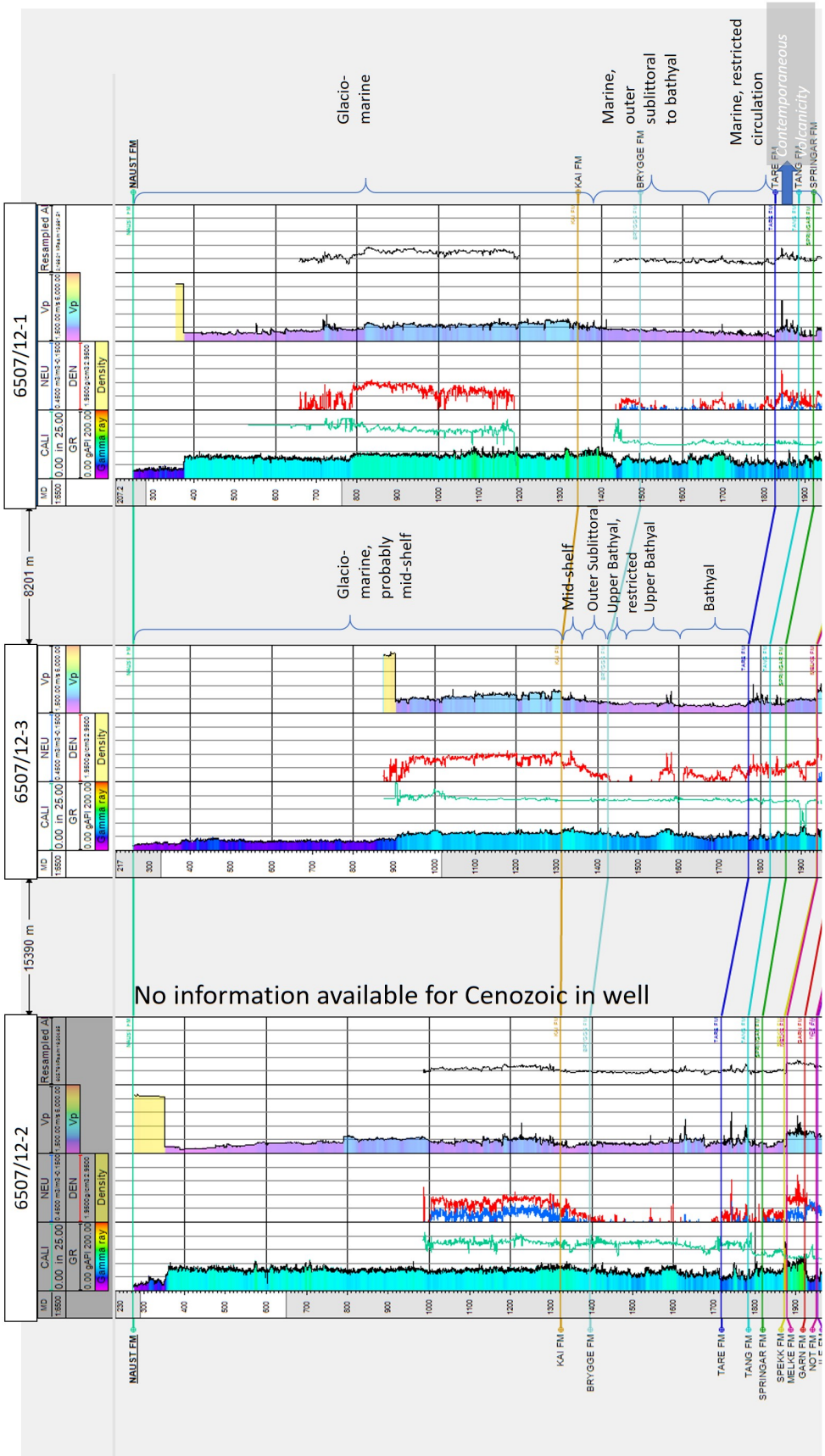

Figure 4.36: Cenozoic stratigraphy and well correlation, flattened on top Naust (BCenU). Description of depositional environment from Paleoservices LTD. (1980) and Paleoservices LTD. (1986)

4.2.4 Cenozoic

Base Cenozoic is expected to rest unconformably on the Cretaceous sediments (BCenU). Neither the latest Cretaceous Maastrichtian interval nor sediments of earliest Paleocene age are observed in wells 6507/12-1 and 6507/12-2, thus documenting this hiatus (Saga Petroleum AS 1983a). This is in line with observations from most of the wells in the Norwegian Sea (Bunkholt et al. (submitted), see section 2.2.2). As figure 4.36 shows, the depositional environment in which the Cenozoic sediments are deposited is largely marine, from bathyal at the base of the interval towards a mid-shelf environment in a regressive trend as the basin was slowly filling up with sediments. Note also the recorded volcanic influence in the Paleocene Tare Formation. A hiatus associated with the MMU is reported from earliest Miocene to deposition of the Kai formation starting from Middle Miocene (Stratlab AS N/A). Uplift during this time period is suggested (Henriksen and Vorren 1996), as explained in section 2.3, this is not confirmed in the study area, but cannot be ruled out.

Finally, the thick Pliocene to recent Naust package of glacio-marine sediments was deposited after the proposed uplift and erosion event during the Middle Miocene. The affect of the late, rapid deposition of this formation on source rock maturation is discussed in section 5.1.3.

Chapter 5

Hydrocarbon potential of the Ellingråsa Graben

The offshore petroleum adventure in the Norwegian Sea began in the Ellingråsa Graben, and 5 wells have been drilled within the study area, though only one located *in* the graben itself. The exploration effort in the area has yielded disappointing results with dry wells and few shows. This chapter will take a closer look at the petroleum system elements, namely reservoir, seal, trap and source rock, in the Ellingråsa Graben, in an attempt to explain why the previous wells have been found dry. Finally, an effort is made to gain insight into whether there is any hydrocarbon potential in the graben despite the dry wells. This thesis *does not* however consider or evaluate specific potential closures or prospects seen in the Ellingråsa Graben.

5.1 Evaluating petroleum system elements

A petroleum system comprises a mature source rock and its migration paths, along with the reservoir rocks, caprocks and traps that can be charged by that source rock (Allen and Allen 2013). These elements and the correct timing of their formation are all necessary for a petroleum system to be working and yield significant accumulations of hydrocarbons. This section will evaluate both the existence and quality of these elements in the Ellingråsa Graben.

5.1.1 Reservoir

The parameters of primary importance for the reservoir unit are porosity (ϕ) and permeability (k), meaning the proportion of the gross volume of rock consisting of pore space and the ease of flow through this system of pores. Good reservoir quality rock is highly porous, constituting a container for large volumes of hydrocarbons to be trapped within, and with a high interconnectivity of pores in the rock giving large permeability allowing easy flow of hydrocarbons from the reservoir into the wellbore. The fraction of the body of rock consisting of reservoir quality lithology, the Net-to-Gross, is also, naturally, very important and should be as high as possible.

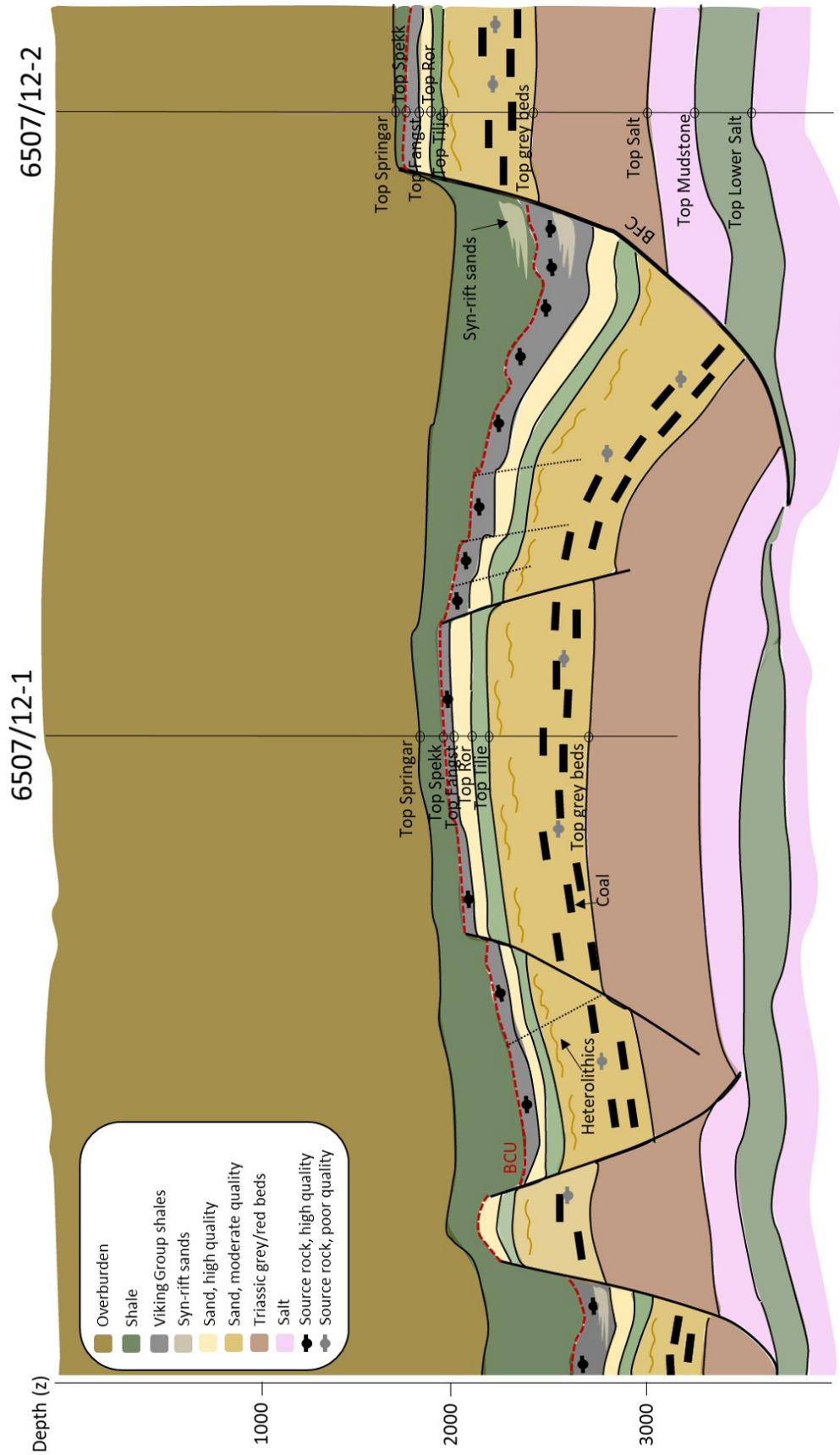

Figure 5.1: Petroleum system elements in the Ellingråsa Graben.

Any type of rock with sufficient porosity and permeability can function as a reservoir for hydrocarbons, from sandstone to carbonates to fractured and weathered basement (Allen and Allen 2013). The reservoir quality is governed by many different factors such as depositional nature, lithology, sediment provenance, diagenesis, tectonic activity and reservoir architecture.

Potential reservoir units in the Ellingråsa Graben and their quality

The Jurassic sandstones are generally considered the most important reservoir intervals on the NCS, so these intervals are evaluated more thoroughly than the possible reservoir units in the remaining strata, which are only briefly reviewed in this thesis. Altogether, a total of 5 possible reservoir complexes are presented and evaluated:

- Triassic Grey and Red beds
- Early Jurassic Åre and Tilje Formations
- Middle Jurassic Ile and Garn Formations
- Possible Intra Viking Group sandstones
- Possible Cretaceous sandstones

Figure 5.2: Core photo from well 6507/12-1 taken at 3708 m depth showing a brown to reddish, laminated, fine grained and compacted sandstone

The Triassic red beds were deposited in a continental arid fluvial environment transitioning to fluvio-deltaic to lake and lagoonal setting with more humid conditions in the grey beds. The base of the package is only seen in the 6507/12-2 well, where the grey and red beds have a total thickness of approximately 800 meters, from 2600 meters to 3450 meters at the top of the salt unit. This represents a temperature of approximately 90-120 °C. The great depth and high temperatures of this interval gives a large probability of the strata being highly compacted and cemented, as the temperatures lie well within the quartz cementation window (Walderhaug 1996; Bjørlykke and Egeberg 1993). Significant fluid overpressure possibly retarding the cementation process is not registered in the strata on this level in the study area. A core photo from well 6507/12-2 taken in the red bed interval (3708 m) shows a brown to red, compacted sandstone with some lamination of lighter material, seen in figure 5.2. The depth of the Triassic possible reservoir units is even greater within the graben than on the flank where well 6507/12-2 is located. Therefore, despite the massive thickness and good lateral continuity, the reservoir properties are not expected to be very good. Their stratigraphic position and approximate depth is illustrated in the conceptual sketch in figure 5.1.

The Early Jurassic Tilje and Åre formations are in this thesis considered to be one reservoir unit, due to the lack of a sealing unit dividing them. These formations have a thickness of 620 m and 530 m in wells 6507/12-1 and 6507/12-2, respectively. This reservoir unit is expected to be present and relatively thick throughout the study area, largely unaffected by erosion in during the Jurassic rifting except locally at footwall scarps. The lower 200-300 meters of this interval consists of coal-rich deposits, previously referred to as the coal unit (Saga Petroleum AS 1985a). This lower part is characterized by peat swamps, fluvial channel systems with crevasse splay and lacustrine deposits in the Heidrun field, a little north of the study area (figure 5.3) (Thrana et al. 2014). As mentioned, the Åre Formation has an overall transgressive trend, going from the non-marine coastal plain deposits passing into marginal marine lower delta plain and interdistributary bay deposits followed by tide-influenced to open marine deposits in the upper part (see also figure 4.30). Figure 5.4 illustrates the proposed tidal influenced transgressive shoreface setting observed in the upper part of the formation. Figure 5.5 shows a core photo from the middle part of the Åre Formation, with fine-grained grey sand thinly interlaminated with mud, typical for a tidal-influenced environment.

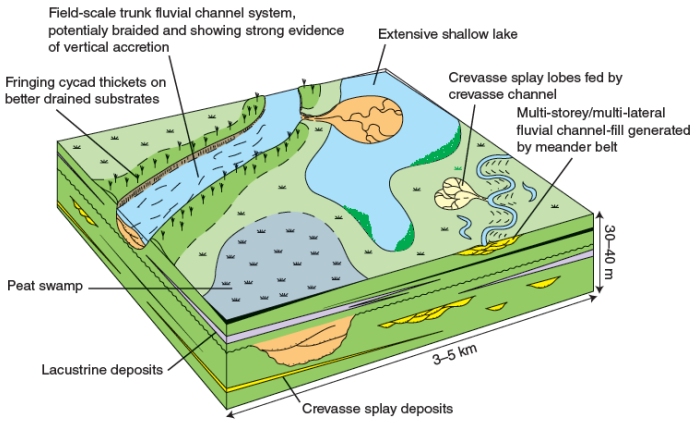

Figure 5.3: Conceptual model for the lower, coal-rich part of the Åre Formation. From Thrana et al. (2014)

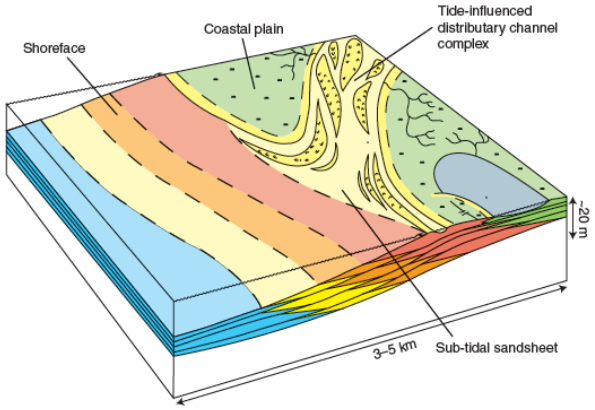

Figure 5.4: Conceptual model for the uppermost part of the Åre Formation. From Thrana et al. (2014)

The Tilje Formation overlying the Åre Formation is described as being deposited in a marginal marine to shallow marine environment with a high tidal influence yielding heterolithic strata (see section 4.2). The main part of the formation is interpreted as a variety of facies in a beach complex setting (Saga Petroleum AS 1985a). Towards the top of the formation, heavily bioturbated tidal flat to shallow marine strata with storm sands are observed in wells `6507/12-1` and `6507/12-2`, fitting with the descriptions from (Ichaso and Dalrymple 2014). A core photo from the Tilje formation illustrating the typical heterolithic nature of the formation is seen in figure 4.32.

Considering the change in facies occurring from deposition of the lower Åre Formation to the top of the Tilje Formation, the reservoir properties are expected to increase towards the top of the formation. Heterogeneous strata with low Net-to-Gross values likely leading to tortuous fluid flow paths and poor permeability are expected at the base of the formation, transitioning into better Net-to-Gross values and better permeabilities as the depositional environment becomes increasingly marine. Due to the tidal influence, significant heterogeneities are expected throughout the interval. This can significantly reduce both lateral

and vertical permeability, thus lowering reservoir quality (Martinius et al. 2005).

The Tilje-Åre reservoir unit is buried at depths between approximately 2300-3000 meters in the graben. Bjørlykke and Egeberg (1993) states that quartz cementation is not usually a significant factor in sandstones buried at depths shallower than 2500 meters in the Norwegian Sea, meaning that the porosity destruction by quartz cementation should not be too significant, especially in the most sandy, upper part of the unit. Pore-filling Kaolinite is reported along with local growth of dolomite cement (Saga Petroleum AS 1985a), having a reducing impact on porosity. Average reservoir parameters have been estimated this Early Jurassic interval. The Net-to-Gross average is 0.45 in well 6507/12-1, 0.22 in well 6507/12-2 and the porosity averages at 0.25 in both wells. The lower Net-to-Gross values observed in the well situated on the Trøndelag Platform is thought to represent deposition in a generally lower energy environment.

Despite the heterolithic nature of the strata and the associated low Net-to-Gross values, this Early Jurassic unit is considered a viable reservoir option, and is an important hydrocarbon bearing interval in many producing fields in the Norwegian Sea today (NPD Fact Pages).

Figure 5.5: Core photo from well 6507/12-1 taken in the Åre Formation at 2520 m depth showing a light grey sandstone with abundant thin laminations of finer, darker material typical of a tidal-influenced environment (Nichols 2009)

The Middle Jurassic sandstones, namely the Ile and Garn formations constitute the most promising reservoir interval in the study area, as well as regionally on the mid-Norwegian shelf (Rønnevik 2000). These formations are separated by a layer of open marine mudstones of the Not formation, however the thickness of this formation is variable in the study area, possibly related to an erosive base Garn Formation (see section 4.2). The reservoir complex is 132 and

83 meters thick in the 6507/12-1 and 6507/12-2 wells. The Ile formation is described as a sand-rich, but heterogeneous formation, probably deposited in a tidal influenced delta setting (Martinius et al. 2005). It is described as micaeous and predominantly medium grained within the study area (Saga Petroleum AS 1985a). A core photo from the Ile formation (well 6507/11-2) is seen in figure 5.6.

The Not formation is described in the area as a highly micaeous and shaly siltstone with occasional thin layers of fine sand deposited in a sheltered low energy bay or lagoon (Saga Petroleum AS 1985a). It is 15 and 17 meters in wells 6507/12-1 and 6507/12-3, respectively, thinning to only a couple of meters thick in well 6507/12-2. Despite its modest thickness it may still constitute a pressure barrier and thus effectively separate the Garn and Ile reservoir zones. Side wall core in well 6507/12-2 however indicates a somewhat increasing sand or silt content towards the top of the formation (Saga Petroleum AS 1981).

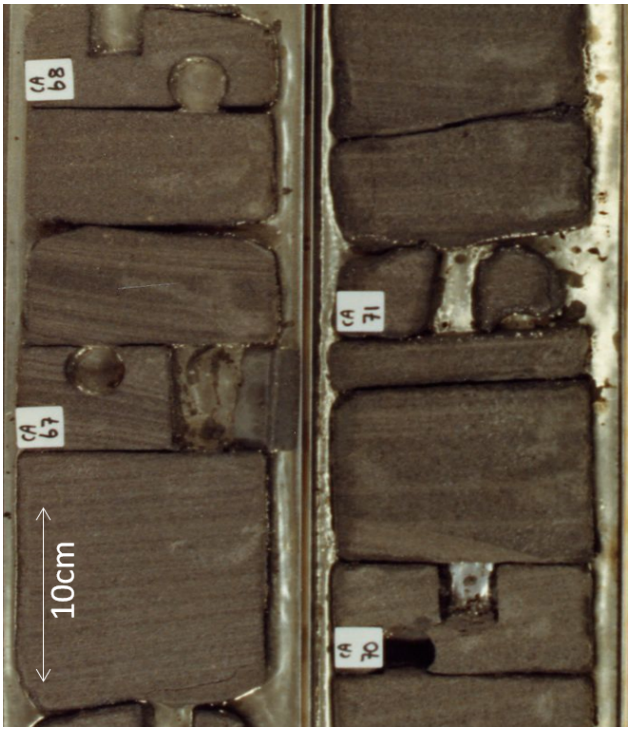

Figure 5.6: Core photo from the Ile Formation, well 6507/11-2 taken at 2010 m depth showing a grey, medium grained sandstone with thin laminations of finer, darker material.

The Garn formation is described as clean, fine to medium, occasionally coarse grained sand representing a regressive pattern of coarsening up from the mudstones of the Not formation to a high energy shoreface environment (see also section 2.3). A core from the Garn formation taken from well 6507/12-3 is seen in figure 4.33, showing a medium grained, laminated and bioturbated sand with relatively poor consolidation.

The Middle Jurassic reservoir complex is buried at depths varying from approximately 1900 to 2700 meters as seen in figure 5.7. This indicates that the depositional style of the formations will be the primary control on reservoir quality, since the effect of diagenesis is generally quite modest at such shallow burial depths. Figure 5.8 shows a model for evolution

of the Garn Formation pore system with increasing burial depth, proposed by Ehrenberg (1990). This model suggests that the Garn Formation in the study area is expected to have total porosity values between a little over 20% to almost 30%. In the wells, the average porosity values are estimated to 26-29% (Saga Petroleum AS 1985a). This is a good fit with the proposed porosity model, since the depth of the Top Garn formation is 2095 and 1992 meters TVD in wells `6507/12-1` and `6507/12-2`, respectively.

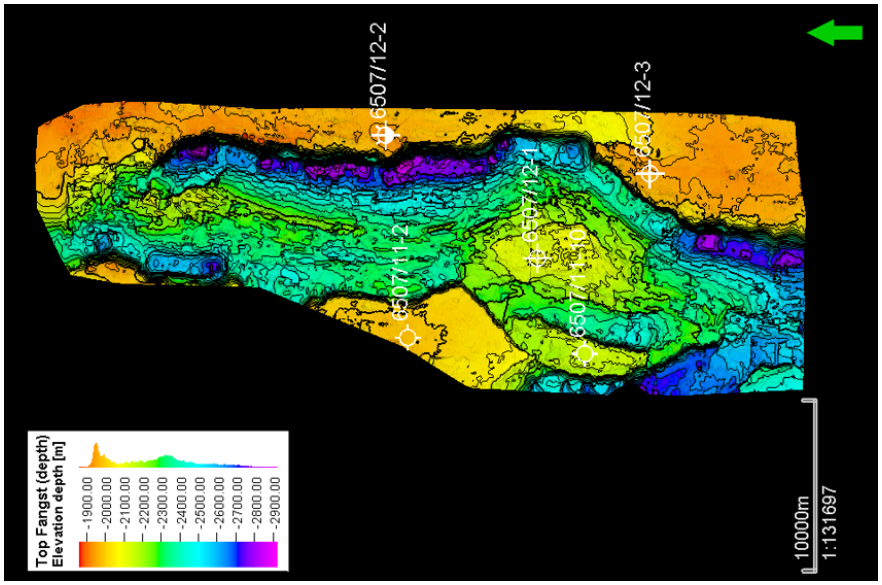

Figure 5.7: Elevation map (depth in meters) of the Top Fangst horizon.

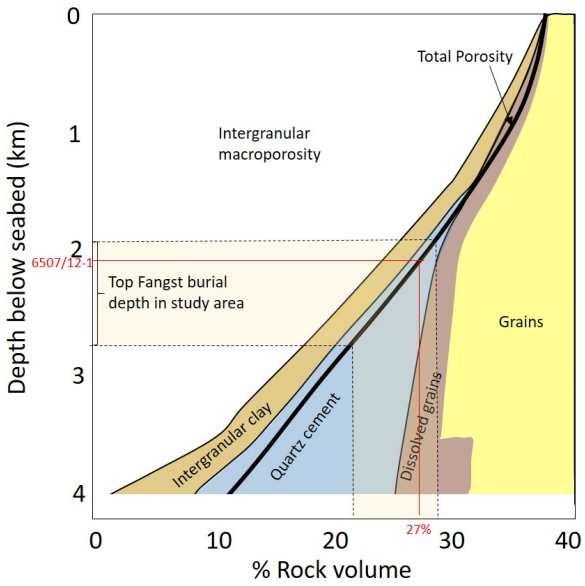

Figure 5.8: Evolution of the Garn Formation pore system with increasing burial depth. Top Fangst Group burial depth and associated expected porosities marked. Modified from Ehrenberg (1990)

The high mica content in the Ile Formation may enhance formation of clay mineral cement, reducing porosity. Abundant mica can also have a negative effect on the degree of sorting, due to the expected shape differences of mica and quartz grains. This could be a reducing factor in both permeability and porosity. This, along with the more heterogeneous strata reducing Net-to-Gross values and expected permeability, makes the estimated reservoir quality of the Ile Formation more moderate than the expectations for the Garn Formation. The average Net-to-Gross values of the Ile formation is measured to 0.7 and 0.5 in wells 6507/12−1 and 6507/12−2, while the Garn formation averages at 0.73.

In summary, the Middle Jurassic reservoir complex is of very good to good quality, the Ile formation in the lower part having somewhat lower reservoir quality than the upper Garn formation. The Not formation dividing these sandstones consists mainly of silt and mudstone and is considered non-reservoir.

Reservoir lithology within the Viking Group has not been penetrated by wells in the study area, but is expected to be locally present in the hanging wall syn-rift wedges, near deeply eroded footwall scarps (see figure 5.1). Though there is no hard evidence for the existance of such sandy syn-rift facies in the study area, intra-Melke or intra-Spekk sandstones are encountered in a number of wells on the NCS (examples are 6407/10−1 and 6407/12−3). In addition, the seismic clearly shows internal reflectors in the syn-rift wedge and erosion of sand at the adjacent footwalls. In the study area, the Callovian erosion period forming the IMU is considered to be more deeply erosive than the later formation of the BCU, and the probability of extensive syn-rift sandstones occurring in the Melke Formation is therefore considered higher than sandstone strata being present intra Spekk Formation. Shallow marine Rogn deposits (see section 2.3) are generally not expected to be found in the Ellingråsa Graben, due to a lack of gentle dip-slope topographies facilitating shallow marine environment during the Late Jurassic to earliest Cretaceous rifting period. Very locally, however, intra graben faulting and associated deep erosion may create conditions favorable for deposition of such facies. Such an area is seen in figures 4.24 and 5.24 where erosion on the intra-graben synthetic fault could give way to deposition of shallow marine stratigraphy on the rollover dip-slope, in addition to deep-water sandy facies in the graben to the west. This could be encountered both as ROgn Formation sand and as intra-Melke Formation sand. The outline of the local area within the graben where this may occur is seen in figure 5.21. The same principle applies to the Cretaceous strata, where local erosion over footwall scarps could provide sand deposition of reservoir quality sand in the adjacent hanging walls within the Early or Late Cretaceous strata.

Generally, the reservoirs of the Viking Group and in the Cretaceous, if present, are expected to be deposited in a deep-water environment. The reservoir quality of such deep water facies are only expected to be moderate. This is due to their lack of lateral extensiveness and the possibly poor connectivity between individual fans or lobes. Their provenance area is probably very close to site of deposition, enhancing the probability of texturally and mineralogically immature deposits, depending of course on the lithology of the source.

The reservoir quality of the Cretaceous and Early Paleocene deep-water systems found in the Norwegian Sea are highly variable and difficult to predict, but deposits of turbidity currents are found to have the coarsest and least clay-rich sediments, yielding higher porosity, permeability and thus reservoir quality (Lien et al. 2006). Section 5.3 takes a closer look at possible sand lithologies in the Early Cretaceous and Late Jurassic.

5.1.2 Trap and seal

Hydrocarbons generated in a source rock are more buoyant than the water occupying the pore space of the subsurface rocks, and will therefore flow upward through porous and permeable rocks (see also section about migration 5.3) (Allen and Allen 2013). For hydrocarbon to accumulate at a certain place, a non-porous, non-permeable unit is needed to hinder further flow, and a geometry creating a trap for the hydrcarbons to accumulate within must be in place. A regional sealing unit is a laterally extensive rock interval of low permeability, commonly shales and evaporites. These constitute good caprocks, effectively retarding further flow of hydrocarbons. Faults can also form important local seals, restraining the hydrocarbons from flowing in the lateral direction. A caprock is effective in terms of sealing if its capillary pressure is greater than the buoyancy pressure acting upward, exerted by the hydrocarbon column below. The seal capacity is defined both in terms of the rock's membrane seal and hydraulic seal abilities (Allen and Allen 2013). The membrane seal capacity is determined by capillary entry pressure and is largely a function of pore throat radius and interfacial tension, meaning that finer-grained caprocks having smaller permeabilities, pore throats and thus larger capillary entry pressures, will have a greater membrane seal capacity than more permeable rocks. The hydraulic seal capacity is determined by the fracture pressure of the caprock, the key question being what amount of pore pressure the sealing unit can handle before tensile fractures are generated. Brittle rocks have smaller tensile strengths and fracture more easily than ductile rocks. Therefore, the ideal sealing unit is ductile and highly impermeable, as is the case for halite. The two most common trap types are structural and stratigraphic traps, and combinations of these also, of course, exist. Structural traps are formed by tectonic activtiy and gravitational processes like salt doming, where faults and folding create geometries permitting retention of hydrocarbons (Allen and Allen 2013). Stratigraphic traps on the other hand, arise from changes in rock character, such as pinch-out of sand bodies within a sealing shale or carbonate reefs overlain by deep-water facies.

Trap types in the Ellingråsa Graben area

As the seismic sections in this thesis show, there are abundant faults in the Ellingråsa Graben area, setting up structural traps in the fault blocks, like the footwall traps the `6507/12-2`, `6507/12-3`, `6507/11-2` and `6507/11-10` wells are located on. There is also the large closure X located within the graben, formation of which is described in section 4.1.4, where well `6507/12-1` was drilled and found dry in 1980. Figures 5.9a to 5.9c illustrate approximate trap area for this combined anticline-horst 4-way closure structure, with suggested spill point indicated with red arrows, on both the Top Fangst and Top Tilje Level.

Potential stratigraphic traps may also exist. If submarine fans or shallow marine deposits of reservoir quality exist in the hanging walls, these could be partially or completely enclosed within impermeable shale lithology and thus effectively retain any hydrocarbons finding its way into the trap. This trap concept has not been tested in the Ellingråsa Graben.

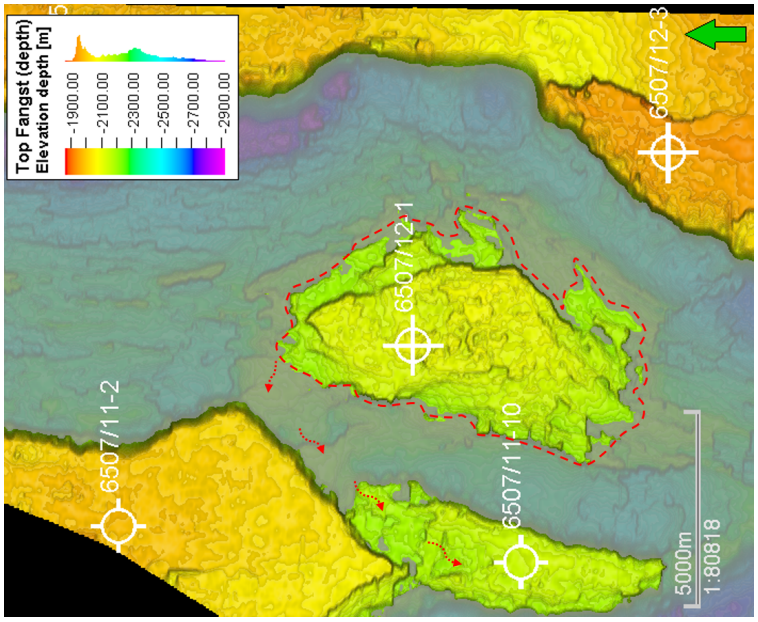

(a) Approximate trap area of the closure on which 6507/12-1 was drilled. Suggested spill point and spill path is marked with red arrows.

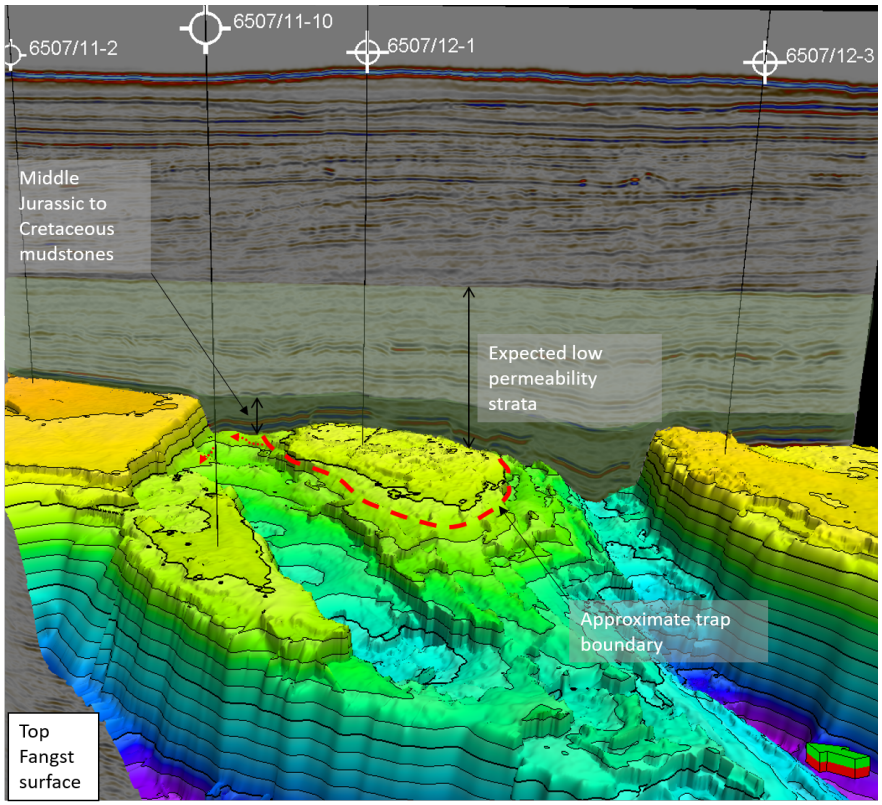

(b) Closure in 3D view with trap area marked in red and Caprock interval(s) marked. Suggested spill point and spill path is marked with red arrows.

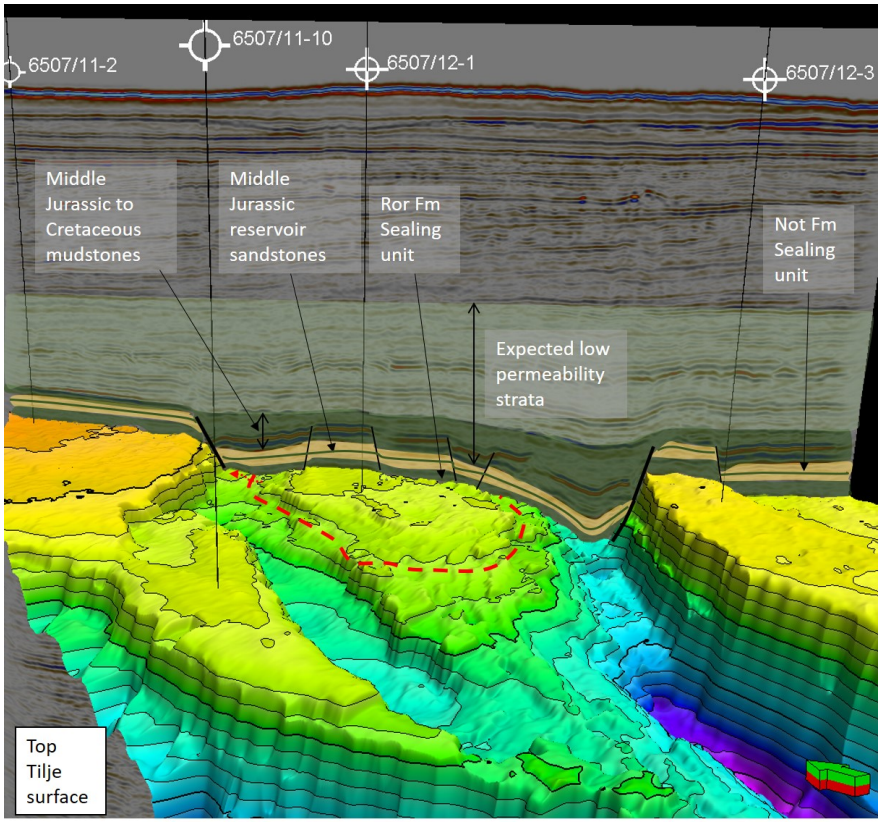

(c) Closure in 3D view at Tilje level with trap area marked in red and Caprock interval(s) marked. Suggested spill point and spill path is marked with red arrows.

Figure 5.9: Trap, suggested spill point and caprock at the location of well `6507/12-1`. Red color does not indicate fluid type.

Sealing units in the Ellingråsa Graben

The primary seal capping the entire Jurassic interval full of promising reservoir units are the shales of the Viking Group and the Cretaceous deep-water shale deposits. This interval is marked in figure 5.9b showing the Top Fangst surface. However, as explained in sections 2.3 and 4.2, the Cenozoic strata also consist of non-permeable lithologies, so in reality the sealing caprock is several hundred meters thick even in locations where the Cretaceous interval is thin. Figure 5.9c illustrates the anticline trap at the top of the Tilje Formation, and shows that the second regionally present, relatively thick sealing unit is the shale of the Ror Formation. Lastly, the Not Formation separating the Garn Formation from the Ile Formation, is considered a non-permeable zone in the study area, as indicated in figure 5.9c. An overview of the reservoir and sealing units as they appear in the wells on block 6507/12 is seen in figure 5.10. It should be noted that the salt unit obviously also has sealing properties, with its ductile rheology and very low permeability. However, functioning reservoirs below this level is very unlikely, and thus this unit is not considered further in this work.

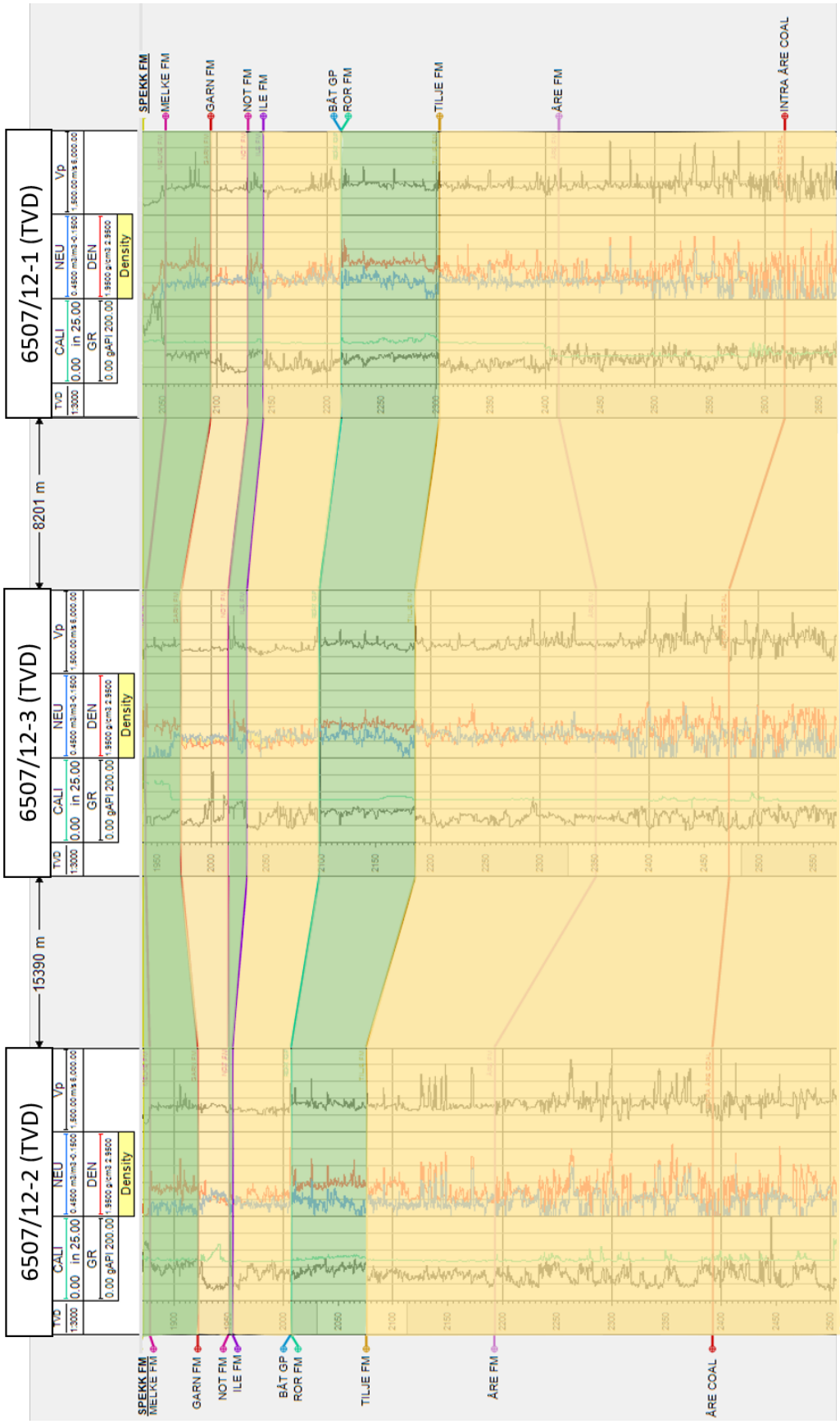

Figure 5.10: Sealing (green) and reservoir units (yellow) marked in a well correlation panel in the study area

5.1.3 Source rock

Oil and gas form from organic material such as algae and plants when exposed to high temperatures. Source rocks are therefore rocks with a high fraction of organic content (TOC). Deposition of rocks with high amounts of organic matter preserved is facilitated by high productivity along with restricted circulation and anoxic bottom water conditions. This combined with a balanced sedimentation rate low enough to prevent significant dilution of organic content but not so low that significant degrading of organic matter occurs on the seafloor, may yield source rocks with very high TOC (Gluyas and Swarbrick 2004). A source rock can be evaluated by its richness (fraction of organic matter) and quality of the hydrocarbons generated from the rock. Of course, the presence of a good quality source rock with high TOC within the migration envelope is not sufficient, as the rock also needs to be *mature* to produce hydrocarbons from kerogen. Maturity depends on temperature but also the duration of burial at different temperatures, as the this section will later illustrate.

The source rocks present in the Ellingråsa graben

The main organich-rich source rocks found within the study are are the Spekk Formation, the Melke Formation and the coal-rich part of the Åre Formation (see conceptual sketch, figure 5.1). The most important source rock on the mid-Norwegian shelf is the Late Jurassic Spekk Formation, characterized by high hydrogen indices and mainly type II kerogen in the study area, making it a good source for oil (GeoChem Laboratories (U.K) Limited 1982). The TOC of the Spekk Formation averages at between 8-9 %wt in the `6507/12-1` and `6507/12-1` wells, with a hydrogen index at around 350 in well `6507/12-1` (Saga Petroleum AS 1985a). The formation is very thin in the wells of the study area, ranging from only 2 meters in well `6507/12-3` to 20 meters in well `6507/12-1`, however it is expected to show some thickening towards the hanging walls of major faults. Though the Spekk Formation is thin it is capable of producing large amounts of hydrocarbons, and its high richness should theoretically facilitate good expulsion efficiency due to massive overpressure generation during cracking of kerogen to petroleum. The Melke Formation below is generally considered to have an insignificant oil potential compared to the Spekk Formation due to it being deposited in an open marine environment (Karlsen et al. 1995). In addition, heavy dilution effects harming both TOC and expulsion efficiency are considered to be present in the thick syn-rift wedges due to higher sedimentation rates here. The early source rock maturation studies from wells on block `6507/12` do not differentiate between the Spekk and Melke formations, probably due to the small thickness of the Spekk Formation (Continental Shelf Institute 1981; GeoChem Laboratories (U.K) Limited 1982).

The Early Jurassic coal unit of the Åre Formation is a massive, thick unit present throughout the study area, easily recognizable on seismic. The kerogen of this unit is expected to be of very heterogeneous composition as the formation includes rooted coals, drifted coals, mudstones and shales, but is considered to consist of mainly terrigenous organic matter, that is, type III kerogen (Hollander 1984; Karlsen et al. 1995). Thus, the unit is mainly a source for gas and some condensate (Hollander 1984), though some claystones of the Åre Formation are found to have locally high hydrogen indices giving some potential for oil generation as well (Karlsen et al. 1995). In the Ellingråsa Graben, the Åre Formation is shown to be a

source rock (kerogen type III) with good potential for gas. Very high TOC values (43-54%) are recorded in samples from the coal unit in well 6507/12-2, however predominantly consisting of intertinite without much potential for hydrocarbon (GeoChem Laboratories (U.K) Limited 1982). Deeper, leaner coals are found in the same well below 2520 meters with a woody to amorphous kerogen assemblage, positive for generation of hydrocarbons. The amorphous component is however of very poor quality, so oil proneness is not likely (GeoChem Laboratories (U.K) Limited 1982). In well 6507/12-1 some samples contained a high proportion of the organic material cuticula, capable of producing heavy oil (Continental Shelf Institute 1981). The coal-rich Åre Formation is estimated to have an average hydrogen index of 150 in the study area. Though the Spekk Formation is considered the most important source rock on the Halten Terrace, the Åre Formation could be a significant contribution in shallowly buried areas where the Spekk Formation may be immature.

It should be noted that well 6507/12-2 encountered some Triassic shales with potential hydrocarbon generation properties as well (GeoChem Laboratories (U.K) Limited 1982) and that, conceptually, there could be source rock potential in the Permian strata (Bugge et al. 2002). These possibilities are however not evaluated further in this thesis.

Maturity in the Ellingråsa Graben

In order to investigate the level of maturity at the source rock intervals, simple temperature based maturity maps are created using depth converted surfaces and the geothermal gradient, 36°C/km based on well data (Saga Petroleum AS 1980), in the study area as a temperature-depth relation (see chapter 3). This was done for the BCU level, representing maturity of the Spekk Formation source rock, and for the Top Åre coal surface illustrating the maturity of the coal-rich Åre Formation source rock. The results of this simple temperature modelling are found in figures 5.11a-5.11b. Based solemnly on temperature and theoretical maturity intervals from literature, the Spekk Formation should be immature over most of the area and marginally mature in the deepest parts. Note that the most of the BCU level is situated close to 80°C (here taken as the lower temperature bound of the early oil window), so the accuracy of the depth conversion is crucial for the appearance of this temperature map. This is further discussed in chapter 6. The top of the coaly part of the Åre Formation is within the hydrocarbon generation window temperature-wise, with temperatures from 100-120°C in the deepest parts. An algorithm for calculating net exhumation from sonic logs in Cretaceous shales is constructed and applied to well 6507/12-1 to investigate whether today's burial depth is in fact the maximum burial depth the study area has experienced, as this has an impact on source rock maturation (see section 3.2.3). Based on porosity of the reservoir intervals and the lack of significant quartz cement growth (section 5.1.1) the area is however not expected to be uplifted significantly. The results of this net exhumation estimation confirm this (figure 5.12). This is also in line with the study area being located west of the zero net exhumation line proposed by Hansen (1996). Based on this it is concluded that today's burial depth is the deepest the source rock intervals have experienced, and thus the highest temperatures, unless extremely high heat flows have occurred in the past.

Based on these simple temperature maps and estimates of net exhumation, significant hydrocarbon generation from the Åre Formation with some possible minor contribution from the Spekk Formation in its deepest parts is indicated. However, the wells have been found

dry, without shows (except very weak shows in well 6507/12-3) and maturity studies have concluded that all source rocks evaluated are immature (Continental Shelf Institute 1981; GeoChem Laboratories (U.K) Limited 1982; Robertson Reasearch International Ltd. 1984). As stated in the beginning of this section, source rock maturity is dependant on temperature, but not temperature alone. To investigate why these intervals are found to be immature despite their at least partially mature temperatures, a closer look is taken at the effect of *time* on maturation as well as an interesting interplay between rapid sedimentation and heat flow possibly retarding maturation in the study area.

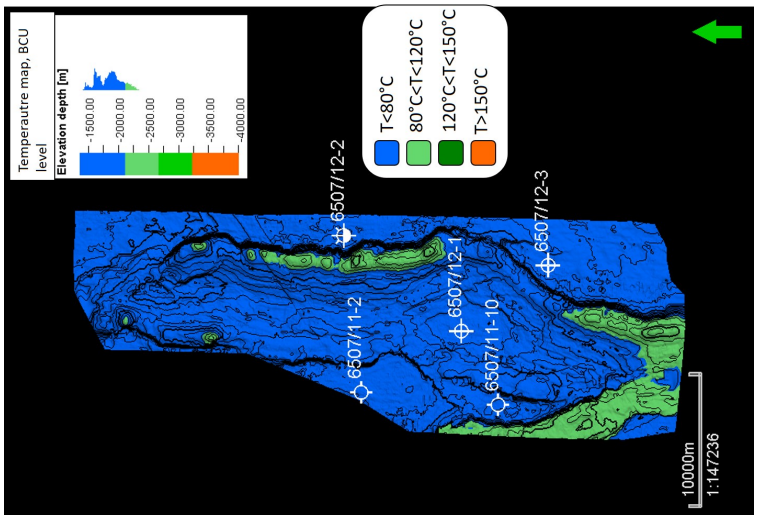

(a) Temperature based maturity of BCU level

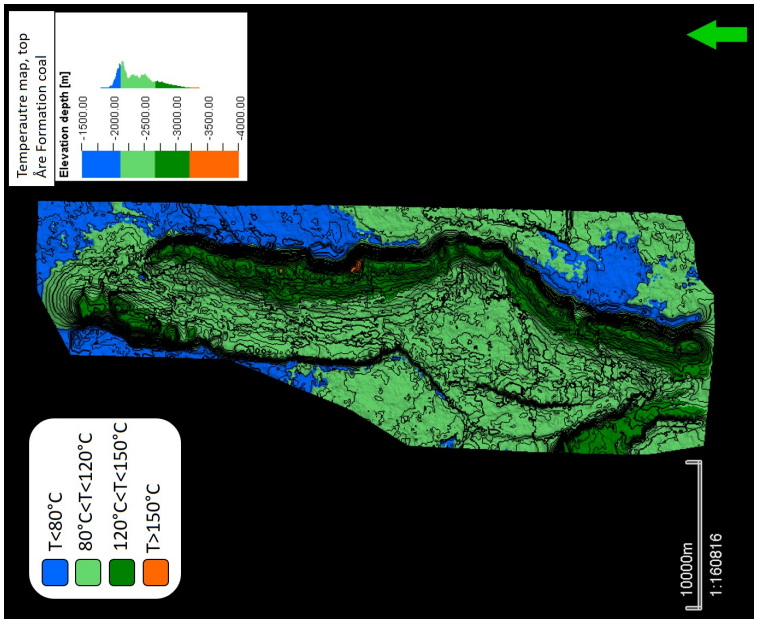

(b) Temperature based maturity of Top Åre coal level

Figure 5.11: Simple temperature-based maturity maps for the BCU level and top Åre Coal level

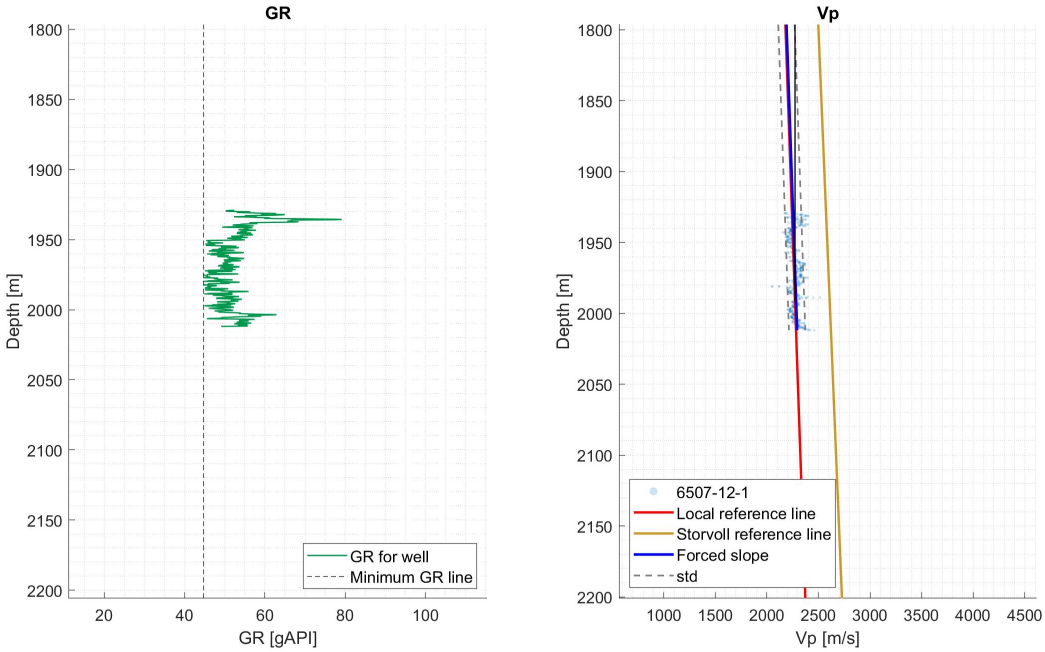

Figure 5.12: Net exhumation estimation from Cretaceous shales in the 6507/12-1 well. Right figure shows interval used for estimation delimited by gamma ray values. Figure to the left shows P-wave velocity in the interval compared to established veloctiy trend by Storvoll et al. (2005) and locally established reference trend (see section 3.2.3 for description of method)

While extensive 3D basin modelling is outside the scope of this thesis, some simple 1D modelling for well 6507/12-1 in PetroMod was conducted to take into account the burial history and thus the time aspect of maturation. Modelling in PetroMod also allows for experimentation with the effects of different kinetic models as well as different heat flows and burial histories. The reader is advised to review section 3.2.4 covering the process of 1D PetroMod modelling with an explanation of input values and boundary conditions. The results of the PetroMod modelling can be seen in figures 5.13-5.14. These burial graphs illustrate that time is an important factor, as it is seen that deep burial of the intervals with source potential did not occur until deposition of the thick Naust package starting from around 2.6 Ma. Figure 5.13 also shows that while the Spekk Formation in the well position has never seen temperatures high enough for kerogen maturation, the coal-rich part of the Åre Formation has experienced such temperatures (though in the lower end of the theoretical temperature maturation window) since the Cretaceous due to the elevated heat flow in this time. It should be noted that paleo heat flow values are considered uncertain and that high paleo heat flow values related to the late Middle Jurassic to earliest Cretaceous rifting based on the work of Hermans et al. (1992) are used herein (figure 3.12). Even in this case, which could be considered a maximum maturity case for the well location, the transformation ratio is only at 5% in the coal-rich source rock interval of the Åre Formation, while the Spekk Formation is completely immature. Note that this modelling is done for the location of well 6507/12-1 which is somewhat elevated compared to the very deepest parts of the study area. However, the same principle holds for the deeper locations, explaining the discrepancies

between the maturity calculations based on simple temperature maps and those measured on data from the wells.

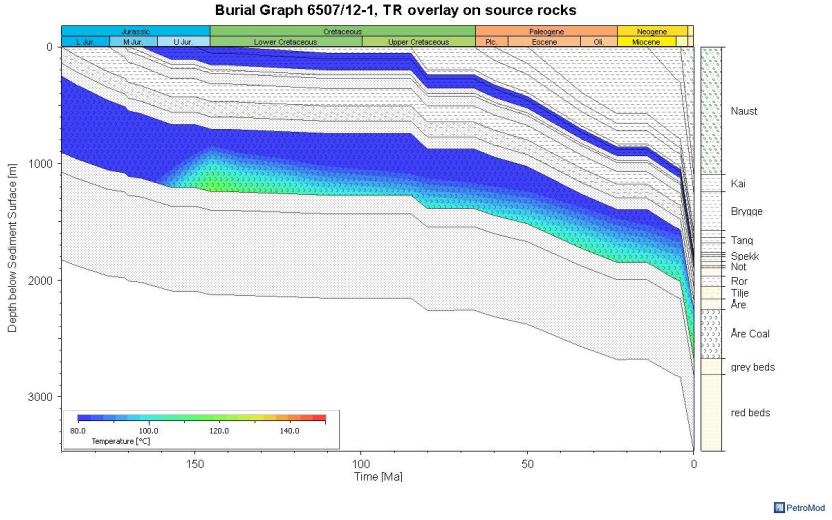

Figure 5.13: Burial graph for well `6507/12-1` in the study area with a temperature overlay. Note that the temperature color range is set to 80-150 °C, so that all temperatures under 80°C will have the same blue color.

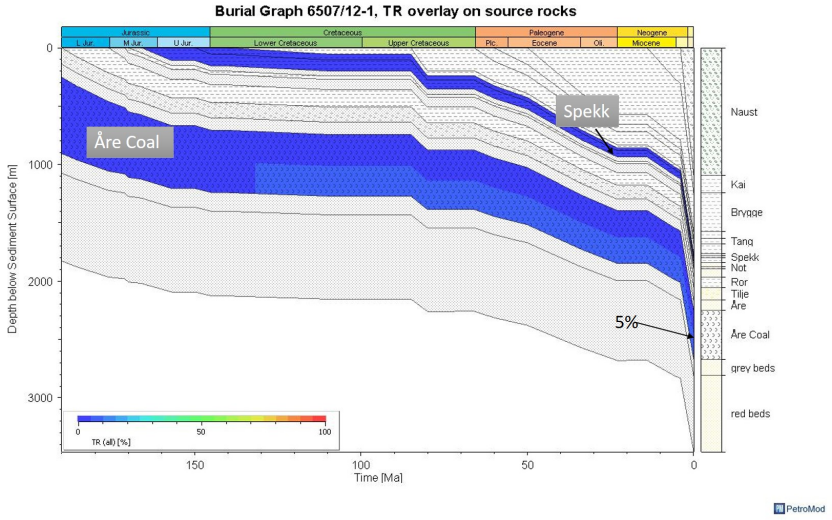

Figure 5.14: Burial graph for well `6507/12-1` in the study area with a transformation ratio overlain, indicating that though the temperature is high enough to produce hydrocarbons, the maturity as measured by the transformation ratio (kinetic model by Pepper and Corvi (1995)) is very immature in both the Spekk and Åre Coal source rock intervals in the well position.

The goal of this simple modelling is to to illustrate a concept and values resulting from the modelling should not be considered exact. The large difference between the real vitrinite reflectance data from well 6507/12-1 and the predicted vitrinite reflectance by Sweeney and Burnham (1990) shows that the model is in need of further calibration (figure 5.15). The real data clearly indicates less maturity. This may be linked to heat flow and heat flow history but also other factors possibly retarding vitrinite maturation, like for instance overpressure. Different types of vitrinite could also be a source of error, and since vitrinite reflectance is measured optically, the well data should not be considered certain either. According to Karlsen et al. (1995), expulsion of hydrocarbons from the Spekk Formation in the Norwegian Sea generally occurs aruond vitrinite reflectance values of 0.7%, while expulsion from deeper coal intervals like the coal-rich part of the Åre Formation tend to happen at vitrinite reflectance values between 0.7%-0.85%. Following this, data from the well also indicates immature source rocks.

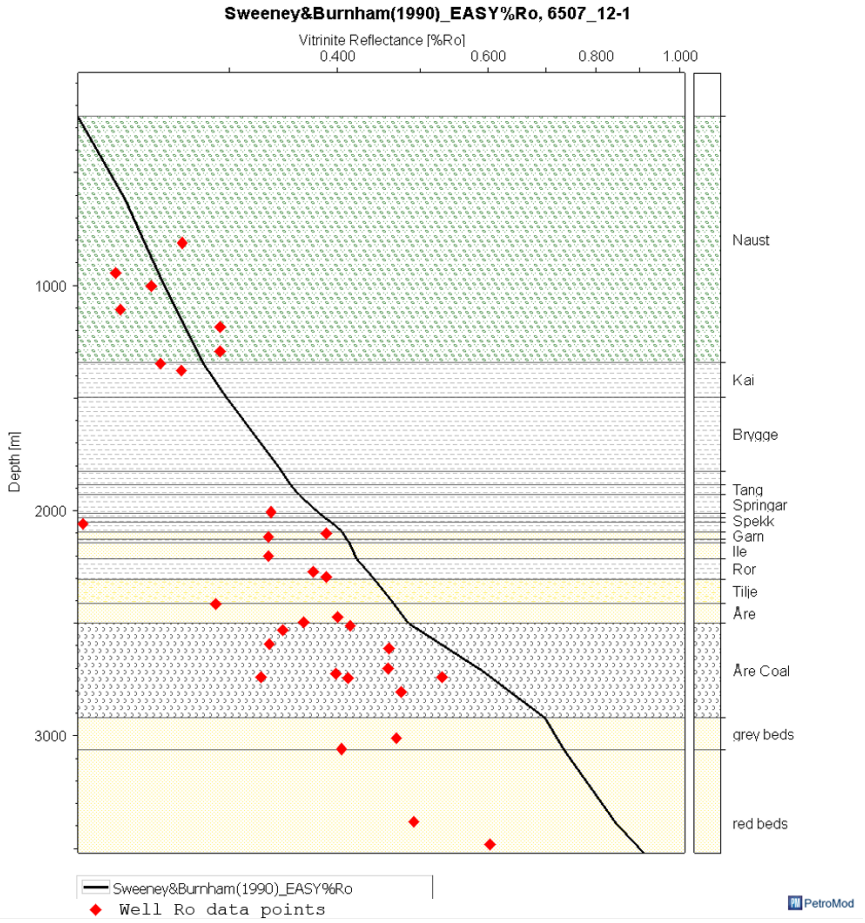

Figure 5.15: Sweeney and Burnham (1990) predicted vitrinite reflectance with depth compared to real measured vitrinite reflectance from the 6507/12-1 well (Saga petroleum 1981).

Figure 5.16 shows measured bottom hole temperatures for well 6507/12-1 along with the the thermal conductivity of the different lithologies in the well and the modelled thermal

gradient. Notice how the low thermal conductivity of the coal-rich part of the Åre Formation causes an increase in thermal gradient in this interval. This increasing gradient is also observed in the real temperature measurements seen in red. The good fit of the temperature data indicates that the used present-day heat flow value of 65 mW/m^2 and the chosen lithologies governing thermal conductivity are appropriate.

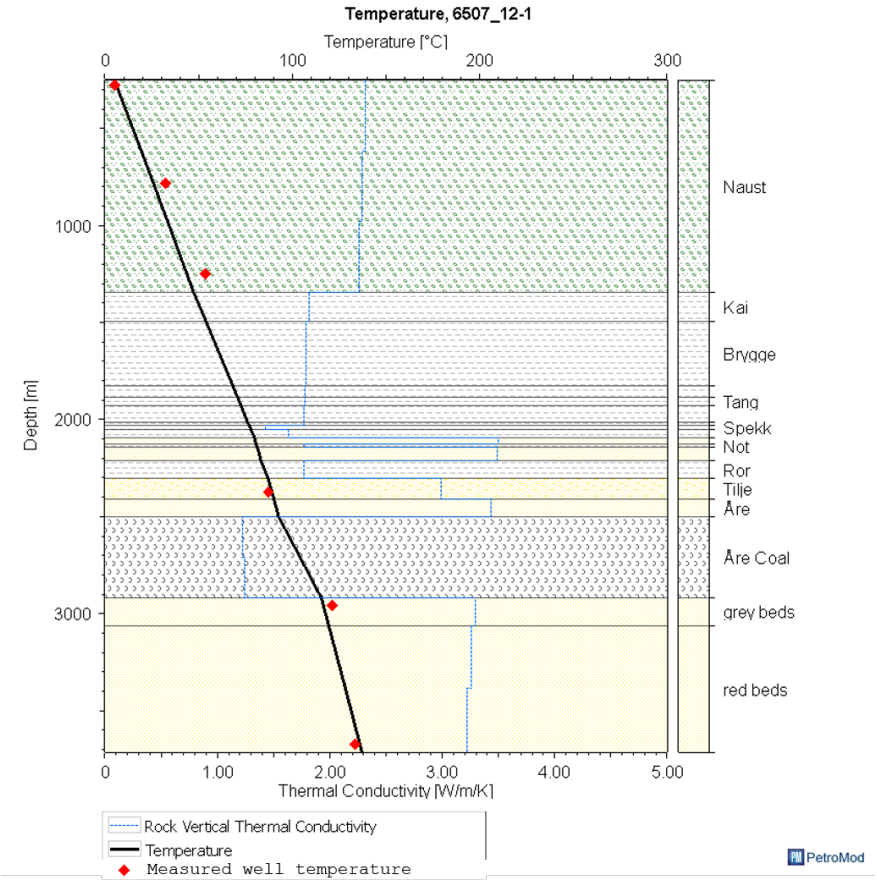

Figure 5.16: Temperature and thermal conductivity (based on choice of lithology in the model) plotted against depth for the 6507/12-1. Real (corrected) borehole temperature datapoints plotted in red.

In order to illustrate one of the effects of rapid, late sedimentation of the Naust package on maturity, an alternative case was constructed where the overburden is deposited steadily over the last 100 Ma. This is of course not a realistic case in the study area, but is included to show the resulting difference in transformation ratio keeping all other parameters equal in both cases. This shows the effect of prolonged burial time at temperatures of hydrocarbon maturation in the Åre Formation coal interval, as the transformation ratio in this case is much higher (figure 5.17).

It should be noted that both the kinetic models of Pepper and Corvi (1995) and Burnham (1989) were tested, yielding similar results.

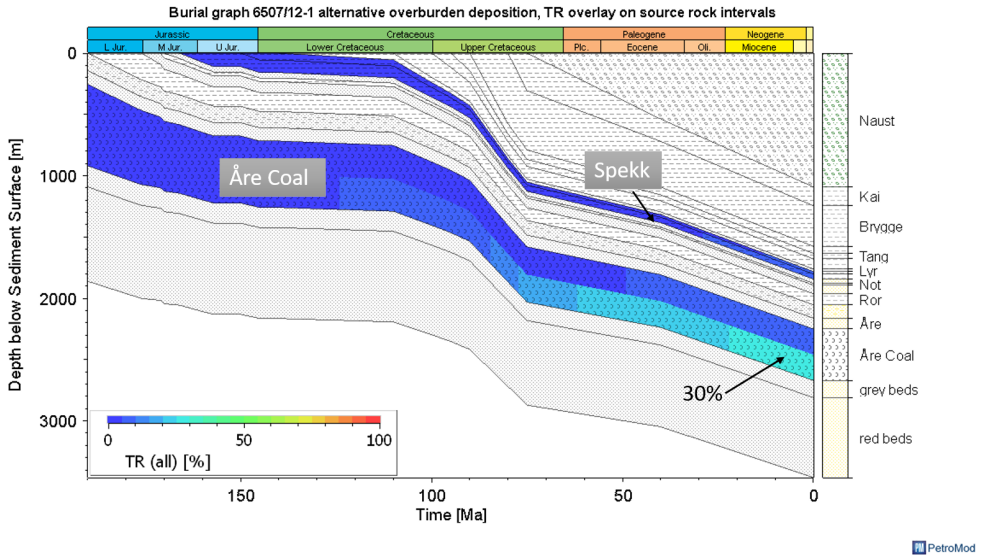

Figure 5.17: Constructed alternative burial graph for well 6507/12-1 with the overburden deposited slowly and steadily over the last 100 Ma. The maturity as measured by the transformation ratio (kinetic model by Pepper and Corvi (1995)) is more mature in the Åre Coal source rock interval compared to figure 5.14 due to prolonged exposure to sufficiently high temperatures.

The previous paragraph has illustrated that the thick glacio-marine Naust package being deposited very late and very rapidly, meaning that the source rock intervals have been exposed to mature temperatures for a short amount of time, contributes significantly to their immaturity. For this modelling, the paleo heat flow curve, change in heat flow through time, is given as input to the model (figure 3.12). In the model it assumed that the heat flow in the study area is in a steady state today and has been for at least the past 10 Ma. However, this may not be the case.

A system is in thermal steady state when the heat flow is constant everywhere (Hantschel and Kauerauf 2009). Changing thermal boundary conditions, geometry, properties or temperatures gives a non-steady or transient state where the system will gradually return to equilibrium when the conditions are no longer changing. This can occur during sudden deposition or erosion (Hantschel and Kauerauf 2009; Pascal 2015), and may therefore be a significant effect in the study area considering the late and rapid deposition of the very thick Naust package. Deposition results in deeper burial and higher temperatures of underlying sediments where the actual sediment temperatures are lower than for the steady state solution. Heat is therefore absorbed, heating the suddenly deeply buried layers, making heat flow values decrease towards the surface. That is, rapid deposition can push the shallow heat flow out of its steady state, temporarily lowering it and creating lower temperature gradients. This effect can be very small when sedimentation rates are relatively low, but may be large where sedimentation rates are rapid compared to the rate of heat transport and re-equilibration in the system (Palumbo et al. 1999). Pascal (2015) modelled this effect for 1000 meters of deposition occurring at different time points between 2.7 Ma and 20 ka, and calculated subsequent heat flow pertubation with respect to a reference steady state (figure

5.18). The results of this illustrates the principle of reduced heat flow due to sedimentation, though 1000 m of sediments deposited during the Quaternary, let alone over the last 100 or 20 ka, is somewhat unrealistic. Though the pertubation effect may be overestimated in this case, the rapid emplacement of the thick Naust package has probably had a temporary cooling effect in the graben. Pascal (2015) finds no correlation between the thickness distribution of the Quaternary sediments and heat flow values. Such a correlation would indicate transient effects being present today, but the absence of such a correlation does not exclude heat flow transients. Even if the heat flow has reached a steady state today, the sudden deposition of the Naust package should be considered when modelling heat flow history for the study area. Such an altering of the relatively recent heat flow history could have a significant impact on the level of maturity of the source rock intervals, and could also aid in explaining the discrepancies between the modelled vitrnite reflectance and the measured well data. An interesting idea for further work would be to model this effect in the study area. However, such modelling should also take into account the counter-acting effect of overpressure generation during the same rapid burial causing porosity preservation and thus lower the thermal conductivity of the overpressured sediment.

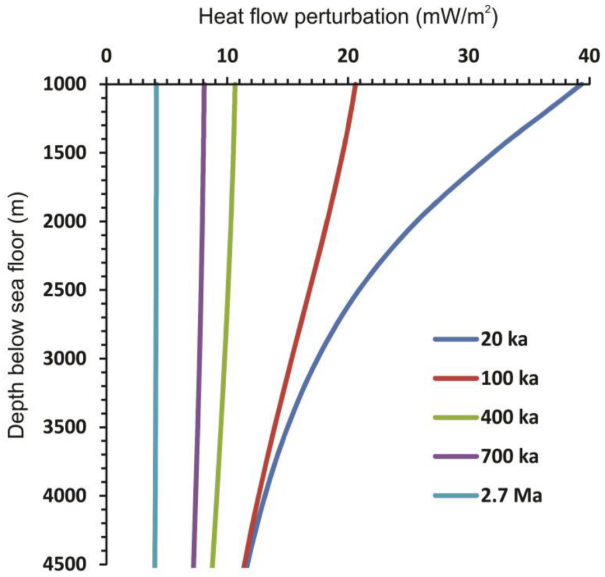

Figure 5.18: Modelled heat flow pertubation versus depth caused by sudden deposition of a column of 1000 meters of sediments at variable time point during the Quarternary. From Pascal (2015)

5.2 The dry wells

The previous section has evaluated whether the essential petroleum system elements needed to accumulate significant amounts of hydrocarbons are present in the Ellingråsa Graben. The conclusion is that there clearly are good reservoir intervals in the Jurassic capped by low permeability regional sealing units. Multiple geometries capable of trapping migrating hydrocarbons exist within mainly structural closures along with some potential stratigraphic traps in syn-rift sands. The Spekk Formation is shown to be a source rock interval of excellent quality, along with some potential for mainly gas in the coal-rich part of the Åre Formation and small possible contributions from the Melke Formation underlying the Spekk Formation. The problem, and the hypothesised reason for the lack of discoveries in the study area, is maturity. The source rocks are immature in the wells, and are expected to be so throughout the study area, possibly with some marginal maturity in the deepest parts. That this is the most important reason for the wells being dry is supported by the lack of reported shows. If a well had failed due to for instance an insufficient seal allowing hydrocarbons to escape the trap there should be detectable residue of hydrocarbons in the reservoir intervals. The lack of such data indicates that hydrocarbons never entered the traps and thus supports that the main problem is maturity and migration, or lack there-off.

Proper dry well analyses evaluating each well individually to investigate if other crucial elements have failed in addition to the maturity problem could have been conducted, but is considered to be unnecessary since all wells appear to share this common issue.

Not having mature source rock in the study area does not necessarily mean that hydrocarbons cannot *accumulate* within the study area. It simply means that for hydrocarbon accumulations to occur, the area has to be charged from another location with deeper burial of source rocks. If this is the case for the Ellingråsa Graben - if the graben has been fed with hydrocarbons from a deeper source - the wells being dry and without shows must mean that this charge takes migration routes avoiding the drilled structural traps. The next section will briefly look into whether such alternative migration routes are possible, and if so, where these would be located.

5.3 A closer look at migration

Secondary migration takes petroleum from the source location to the traps via permeable carrier beds. The driving mechanism for secondary migration is the density difference between the petroleum and water expressed through the buoyancy force. In a hydrostatic situation this is the only driving force in need of considering, while in hydrodynamic conditions, flow of water may retard or enhance petroleum migration (Gluyas and Swarbrick 2004). As mentioned in section 5.1.2, the capillary entry pressure is working against the buoyancy force. Petroleum will migrate through a pore throat once the buoyancy pressure exceeds the capillary pressure.

Hydrocarbons will have a tendency to rise within a sediment column due to the buoyancy effect. At the same time, the capillary force will make hydrocarbons prefer to migrate from small to larger pores. Thus, petroleum will tend to migrate upward along the coarsest pathways with the highest permeability, or jump up in the stratigraphy through open fracture

systems (Gluyas and Swarbrick 2004). Migration tends to take place along the same specific, high permeability routes within the carrier beds, because the interfacial pressure becomes significantly lower once a pore has been saturated with hydrocarbons, making the capillary entry pressure smaller as well.

Assuming that the implications of immature source rock intervals from section 5.1.3 are correct so that no significant amount of hydrocarbons have been generated within the study area, the area is dependant on long-distance migration from deeply buried source rocks to charge the traps. Though migration over fairly long distances is reported in the Norwegian Sea, it is found to be relatively uncommon by Karlsen et al. (1995) in the discovered fields thus far. In order to consider migration into the study area, seismic covering the surrounding area towards the main hydrocarbon generation locations to the south-west of the Ellingråsa Graben should be included and interpreted, which is clearly outside the scope of this thesis. However, assuming that petroleum enters from the south (see figure 5.19), orthocontours are used to make a migration map for the top Fangst surface. Petroleum entering the system at this level will migrate along the top of the permeable zone, against the non-permeable Viking Group. As expected, the map clearly shows that any hydrocarbons should end up in the trap where the dry `6507/12-1` well is drilled. The case is the same for any petroleum with the same entry point at the Tilje Formation level, migrating upwards against the base of the non-permeable Ror Formation. The expected migration path is also illustrated in figure 5.20 showing an arbitrary cross section from the assumed charge entry point up to the structural closure where `6507/12-1` is found.

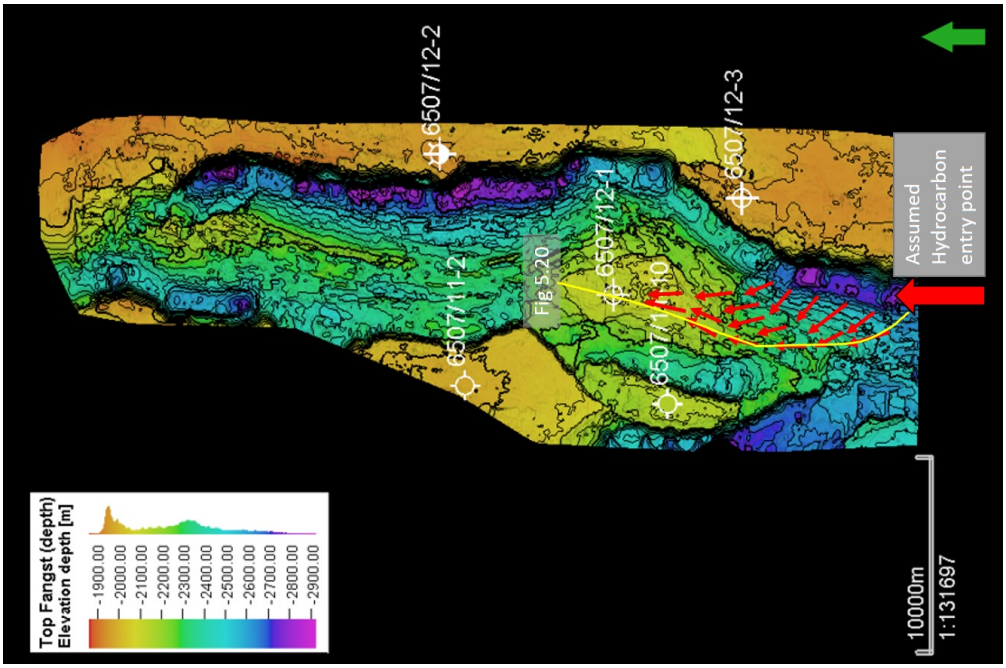

Figure 5.19: Map showing orthocontours at the top Fangst level, indicating where any hydrocarbons entering the study area from the deepest part in the south at the Fangst Group level would migrate. See figure 5.20 for cross section.

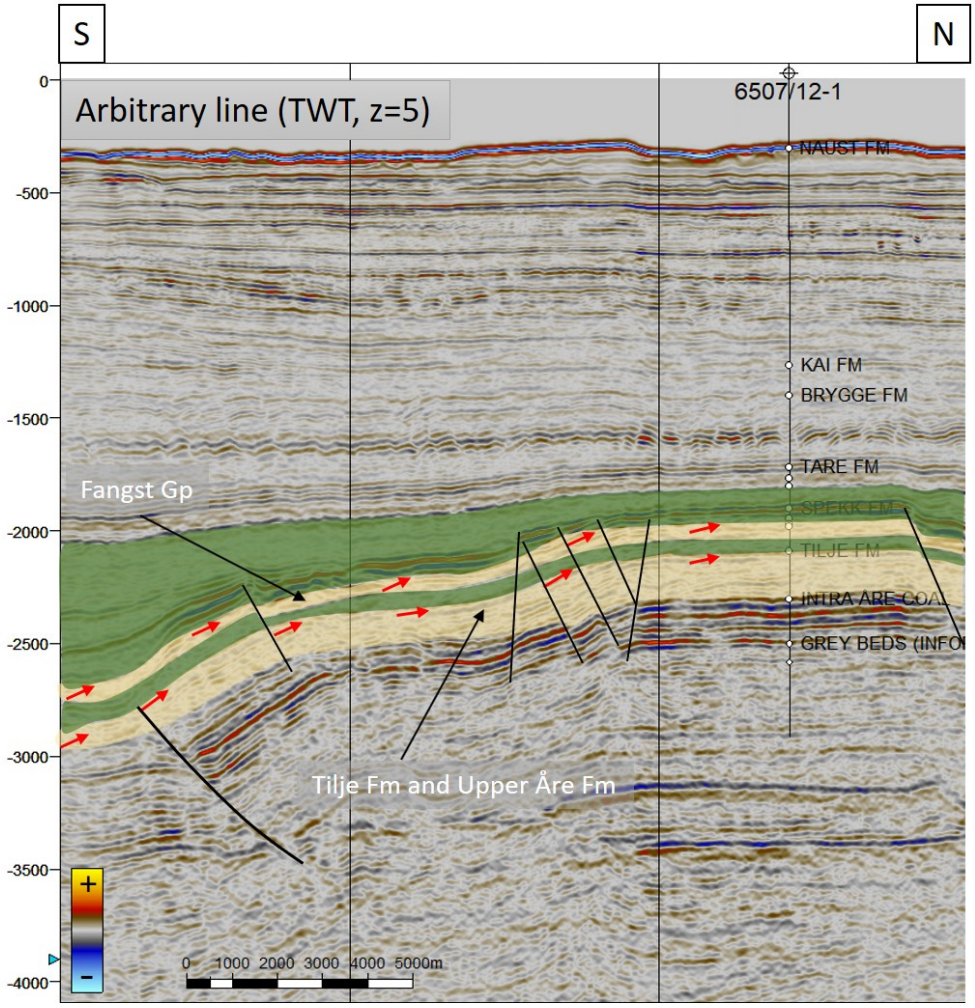

Figure 5.20: Cross section illustrating most likely migration route for hydrocarbons entering the Ellingråsa Graben from the south, migrating upward along the base of the Viking Group and Ror Formations seals in the Fangst Group and Tilje-Åre Formations carrier beds, respectively. See figure 5.19 for location of line.

Figure 5.19 and 5.20 indicate that hydrocarbons have not entered the graben at the Fangst Group or Tilje Formation level, since these should migrate directly to the closure where `6507/12-1` is found dry without shows. This is of course assuming that the small-offset faults crossing the carrier beds are non-sealing, which is considered to be a reasonable assumption due to small offsets and generally low clay content in the faulted formations.

However, what if charge did *not* enter at the level of these carrier beds, but instead migrates within the proposed syn-rift sands of the Viking Group or in the post-rift sands of the Cretaceous strata? In order to investigate such a possibility, a map with probable extent of these sands is created. This map is highly generalized and is based on thickness of the syn-rift wedge, observed internal reflectors within the Viking Group and Early Cretaceous at these locations and on observations of erosion along the BFC. For further elaboration on this, see chapter 4. It should be noted that interpretation of individual internal reflectors within the Viking Group is not conducted in this thesis and is an idea for further work.

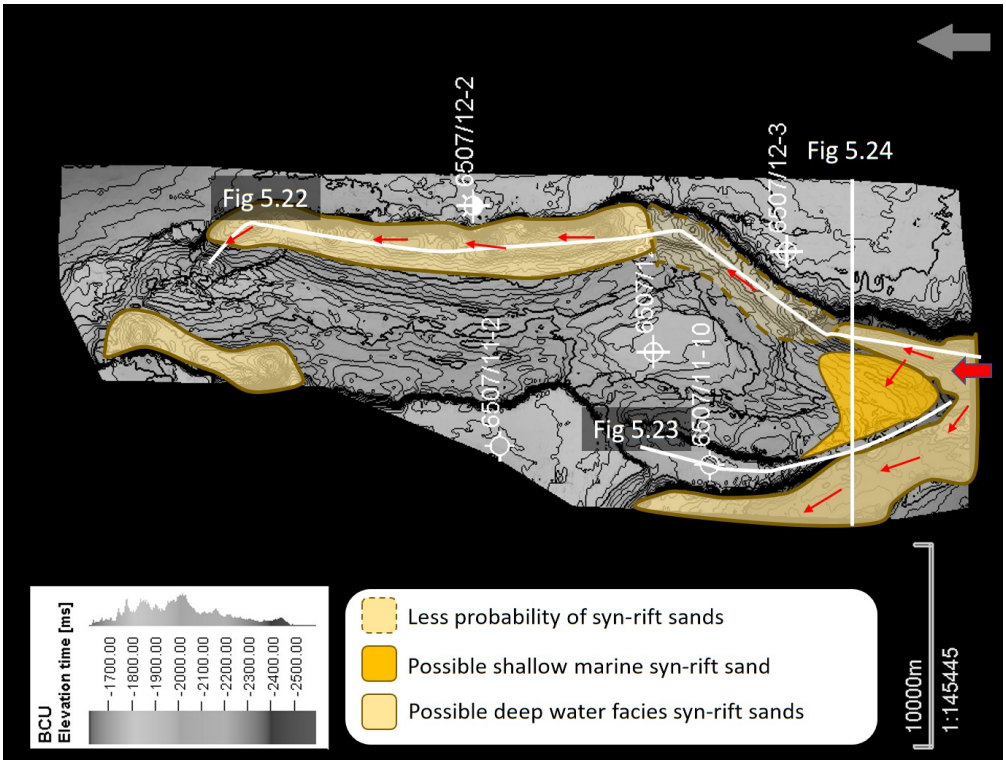

Figure 5.21: BCU map with areas of higher probability of syn-rift sand lithologies being present indicated. Assuming charge entering at this level from the deepest part of the study area to the south, possible migration paths are marked with red arrows (not indicating fluid type).

The syn-rift sands of the Viking Group and sands in the Early Cretaceous are mainly expected to be deposited as submarine fans in deep water (see also section 5.1.1). The heavily rotated strata in the hanging wall creates a relatively steep slope. This indicates that the aerial extent of eroded sand from the footwall re-deposited as syn-rift sands is quite small resulting in submarine fans restricted to the immediate hanging wall of the BFC or locally the EWFZ. A suggested aerial extent of the deep water sand facies is seen in figure 5.21. Note that the areas marked are not likely to represent continuous sand bodies, but rather a perimeter outlining the area where syn-rift sands could be expected. Figure 5.22 shows an arbitrary line through the syn-rift wedge of the BFC hanging wall. The Fangst Group, Viking Group, Early Cretaceous and Late Cretaceous are indicated on the seismic, and conceptual sand bodies are sketched within the Viking Group and in the Early Cretaceous strata. For this to be a working migration route assuming charge enters at this level, there are four main requirements that need to be fulfilled:

- The individual sand bodies have to be well connected. This is needed for a functioning, continuous high-permeability pathway to exist. This is a big issue, depending heavily on the abundance and lateral extent of sand bodies. Figures 5.21 and 5.22 indicate that syn-rift sands are less likely to occur within the Viking Group in the area of fault segment S2 (but also within the Early Cretaceous which is completely missing here). If there are no syn-rift sands for hydrocarbons to migrate along in this area, the migration route is clearly compromised and relies on migration through low permeability shale.

- Generally, the base seal needs to be intact. Deposited submarine fans may have an erosive base and may therefore locally be in direct connection with the excellent permeability Garn Formation. In this case, the Garn Formation will likely steal the charge, possibly steering the hydrocarbons in a different direction. This will most likely be toward the closure where 6507/12−1 is located, but this is of course dependant on where the breached base seal occurs. Note that figure 5.22 shows where stolen charge would end up in a two-dimensional world.

- Charge must not escape across the BFC. This means that either the BFC needs to be sealing, that the sand bodies are separated from the BFC by shale or that the juxtaposed footwall stratigraphy has poor carrier-bed properties so that the charge will continue to move along the syn-rift fans in the hanging wall. The large throw along the BFC increases the probability that the fault itself is sealing, however this is not in any way certain. Checking the pressure data from the wells on block 6507/12 gives no indication of different pressure regimens across the BFC indicating sealing properties across the fault (Saga Petroleum AS 1980; Saga Petroleum AS 1981; Saga Petroleum AS 1985b). Any possible syn-rift sands of the Viking Group are generally juxtaposed against the coal-rich part of the Åre Formation (see figure 5.24) which is likely to be relatively heterogeneous, clay rich and may therefore have low permeabilities and tortuous flow paths. Thus, it seems reasonable that any charge could follow the syn-rift sands even in the case that the BFC is non-sealing. The possible Early Cretaceous sandstones, however, are generally juxtaposed against the upper part of the Åre Formation or the Tilje Formation. Though these formations are also described as relatively hetereogeneous (sections 4.2 and 5.1.1), it is considered more likely that charge could be diverted across the BFC at this level. Any charge escaping across the fault is likely to be trapped within the closures of 6507/12−2 or 6507/12−3. These wells being dry indicate that this has not occurred.

- If present, the sand bodies have to be sufficiently permeable to act as carrier beds for hydrocarbons. The porosity and permeability of submarine fans are often questionable and variable. The grains are commonly angular and immature due to short transport distances and can be poorly sorted and micaeous, possibly yielding low-permeability sand.

As mentioned in section 4.1.5, there is an area of local deep erosion to the south in the graben (recall figure 4.24). A fault within the graben, synthetic to the BFC, has here experienced significant erosion of the rollover anticline footwall. A cross section through the crest of this eroded area is seen in figure 5.23, clearly illustrating the local area of very deep erosion. The erosion products may here be deposited either in the hanging wall to the west or possibly as shallow marine sand along the rollover anticline dipslope. The assumed outer perimeter of this local area with possible shallow marine syn-rift deposits within the Viking Group is marked in figure 5.21. Xline 1210 (figure 4.24) is presented again in figure 5.24, this time with conceptual location of both the deep-water sand facies and the possible shallow marine sand facies marked. It should again be emphasised that the presence of such sand bodies is highly conceptual.

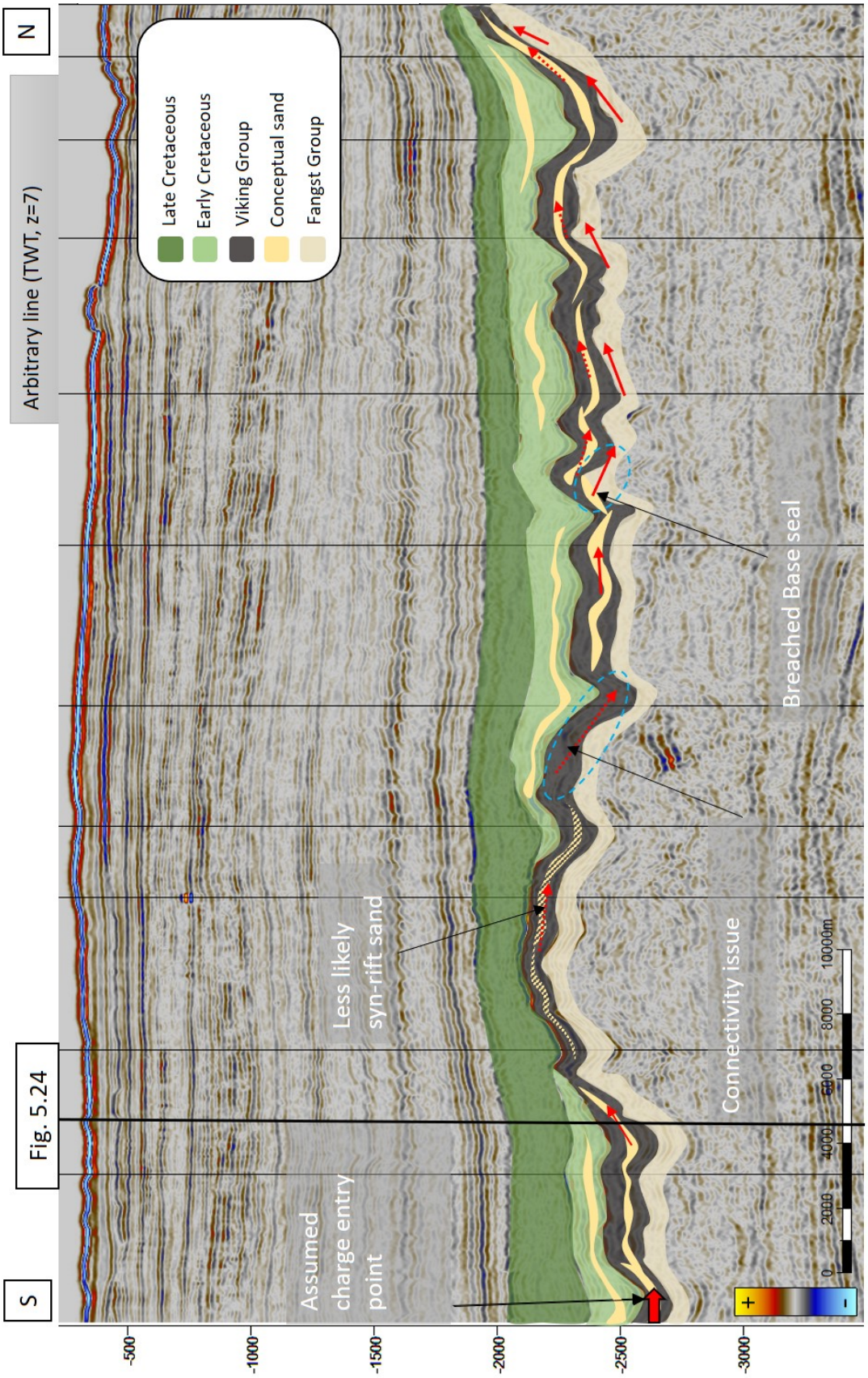

Figure 5.22: Seismic line along-strike of the syn-rift hanging wall wedge, with conceptual sand bodies sketched. Main issues for migration along this path to be viable are connectivity of the sand bodies and the risk of a breached base seal as illustrated in the sketch. Location of line seen in figure 5.21.

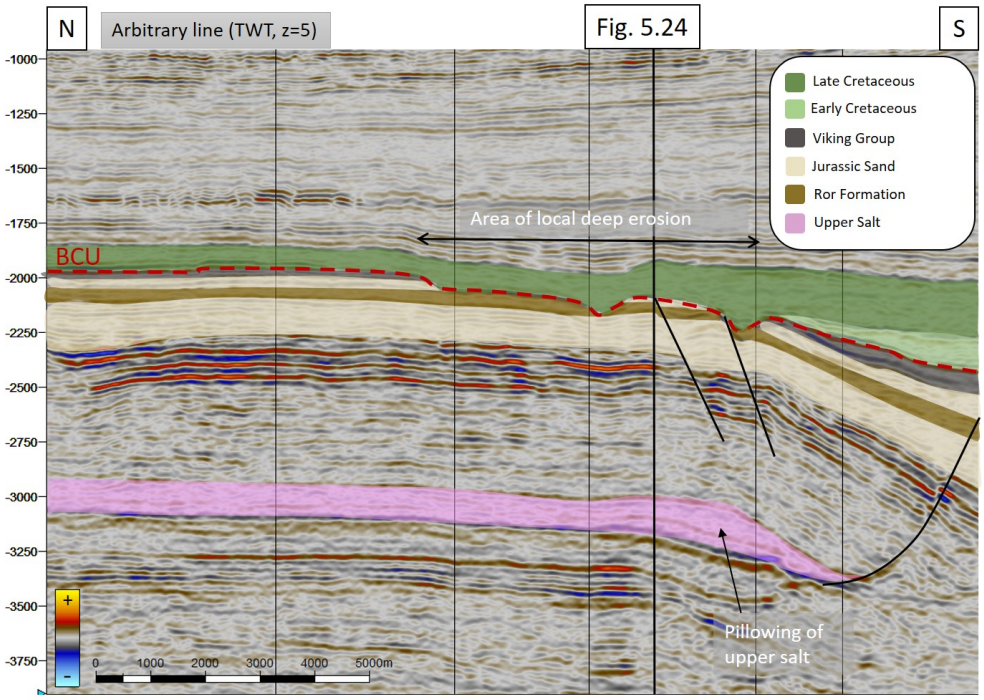

Figure 5.23: Arbitrary line showing the local area of deep erosion at the BCU level. Notice also the very visible gentle pillowing of the upper salt interval marked in pink. See figure 5.21 for location of line.

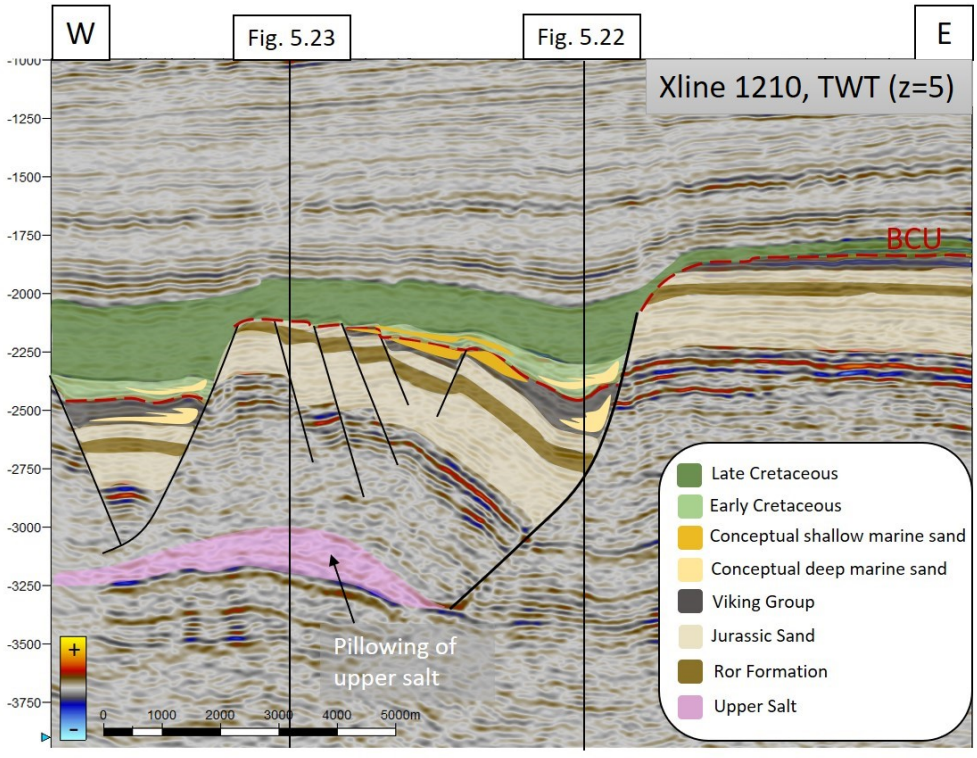

Figure 5.24: Arbitrary line showing the local area of deep erosion at the BCU level.

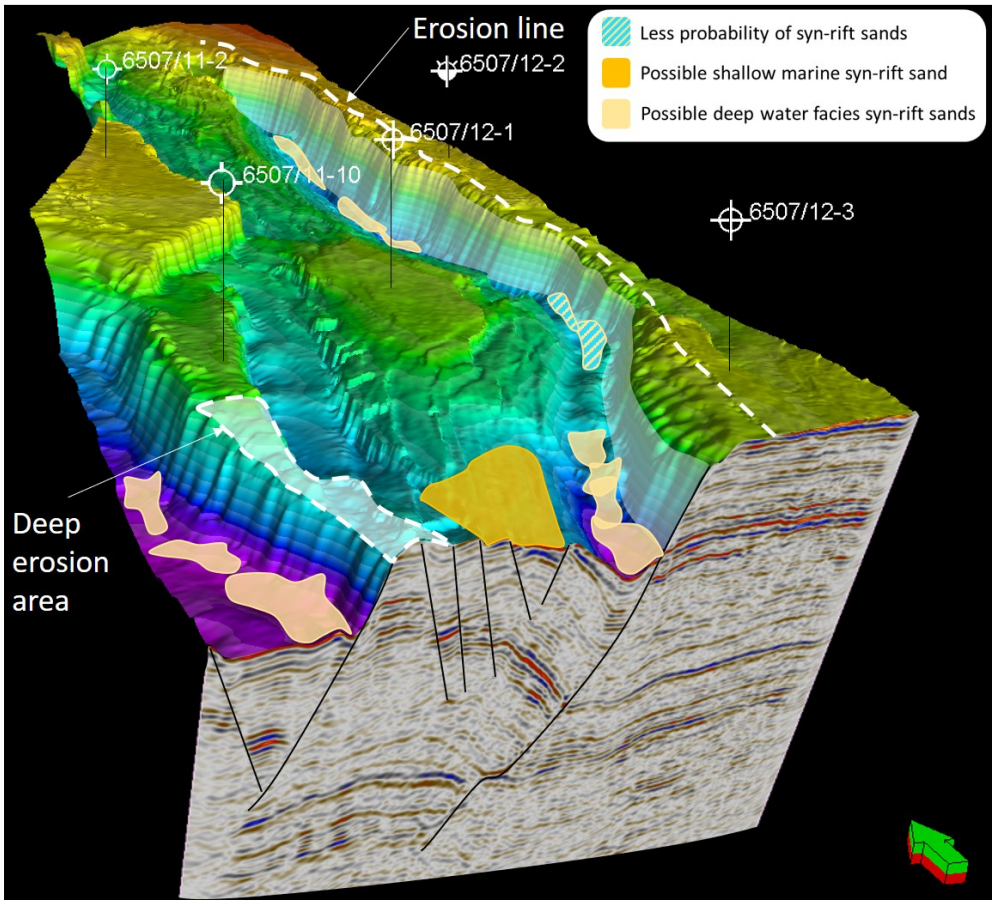

Figure 5.25: 3D sketch showing erosion and possible locations of sandy facies within the Late Jurassic or Early Cretaceous on the BCU level.

Figure 5.25 shows a the BCU surface with these possible sand bodies sketched in 3D, created to illustrate how the sand bodies might be distributed in the study area. The BFC erosion line from section 4.1.3 is also sketched as areas of more erosion are expected to yield more sand deposits in the hanging wall. The approximate extent of the area of deep, local erosion across the synthetic footwall is also marked on this figure. Figure 5.21 shows red arrows indicating the path hydrocarbons migrating along these conceptual sand bodies would follow, and illustrates that this would provide a migration path bypassing the drilled closures. If the migration route is cut off due to connectivity issues, these syn- or post-rift sands enclosed in shale could in theory provide stratigraphic traps and thus be filled with hydrocarbons (see section 5.1.1).

All seals are expected to have some leakage, so a functioning petroleum system will often show signs of hydrocarbons in the form of pockmarks, gas chimneys or shallow soft spots. There is however a general lack of such indications within the study area, with no observed pockmarks and very little soft bright spots. The few shallow soft bright spots that do exist could very well come from biogenic gas. Therefore it is concluded that though the possible sand bodies within the Late Jurassic and Early Cretaceous strata could provide both migration routes and reservoirs for hydrocarbon, it is highly unlikely. The hydrocarbon potential of the Ellingråsa Graben is considered to be low and significant accumulations

unlikely in this thesis. The charge issue makes further exploration in the graben structure come with a high risk. Further work constraining migration paths and looking at data covering the area between the graben and the main hydrocarbon producing locations should be conducted before making any final conclusions.

Chapter 6

A discussion of uncertainty and confidence

This thesis has proposed models and drawn conclusions based on well data, studies and seismic interpretation. However, geological evaluations always come with a substantial portion of uncertainty, which is both frustrating at times but also part of the beauty of earth science. This chapter will provide an overview and briefly discuss the key uncertainties within this thesis.

6.1 Summary of the main findings

In the previous chapters, the tectonostratigraphy and future hydrocarbon potential of the Ellingråsa Graben has been investigated. A subtle, but significant, interplay between the Triassic salt unit and style of faulting along the main lineaments is described, with listric faulting detaching at the upper salt level, hanging-wall rollover and gentle salt pillowing being the main features. Based on throw measurements along the BFC, observations of footwall erosion and thickness maps revealing syn-rift thickening in the hanging walls, the BFC is divided into four segments. The two segments showing the largest amount of throw, namely S1 and S3 (see figure 4.17), have an approximately N-S strike and are hard-linked through a NE-SW striking fault with significantly less throw and less syn-rift development observed in the rift climax strata. Syn-rift development along the EWFZ is also sparse, however increasing toward north where displacement along the BFC dies out and the Ellingråsa Graben transforms into a half-graben bound by the east-dipping EWFZ. Because of this, it is suggested that the EWFZ and segment S2 of the BFC formed at a later stage than segments S1 and S3. Although the EWFZ also appears to be detaching in the upper salt level, associated ductile style hanging wall rollover is much less common. Deformation here instead appears to have been accommodated through brittle planar faulting of the hanging wall, which is suggested to be due to higher strain rates than along the BFC. In wells `6507/12-2` and `6507/12-3`, base Melke Formation represents a major unconformity, proposed herein to correlate with the IMU. In well `6507/12-1`, this unconformity is situated within the Melke Formation, indicating that erosion during the Callovian did not penetrate into the Garn Formation at this location. Due to a lack of well data, the amount of Callovian erosion

on the western flank of the graben structure is poorly constrained, however the significantly smaller syn-rift thicknesses in the hanging-wall indicates less erosion here. A model for formation of closure X where well 6507/12-1 is situated is presented. The model (see figure 4.21) summarizes the observations and arguments mentioned above and suggests that the trap formed due to varying strike directions of the graben-bounding listric faults causing hanging wall rollover in multiple directions in combination with brittle intra-graben faulting creating a combined anticline-horst structure. Biostratigraphic and sedimentological reports from block 6507/12 is largely in line with the regional understanding of the Halten Terrace based on key literature, presented in chapter 2.

An evaluation of the petroleum system elements in the graben is also conducted. All wells have penetrated multiple reservoir units of good quality in the Jurassic interval. The Garn Formation appears to have the best Net-to-Gross, porosity and permeability, closely followed by the more heterogeneous Ile Formation. The Tilje and Åre formations are also important reservoir units in the area though of only moderate quality due to heterogeneities and high fraction of fine-grained material. The relatively shallow burial depth in the area suggests that depositional factors constitute the primary control on reservoir quality, rather than diagenetic factors such as cement growth. This is further confirmed by few observations of cement in the Jurassic sediments (Saga Petroleum AS 1985a). In addition, syn-rift sands of possible reservoir quality are expected to be present in the immediate hanging wall of the BFC in the Viking Group sandstones. These are expected to be deposited in a deep-water environment. Very locally though, a gentle dip-slope may exist, facilitating deposition of shallow-marine syn-rift sands (Melke sand or Rogn Formation). Both trap geometries and multiple high quality sealing units are expected to be present in the study area, with the Cretaceous strata as the top seal. The major risk factor is the source rock. The Spekk Formation is considered the main source rock interval in the area, as well as on the rest of the Halten Terrace, but there are reports of high TOC and gas potential in the coal unit of the Åre Formation as well (Robertson Reasearch International Ltd. 1984). However, both these units are estimated to be immature to marginally mature in the deepest parts, througout the study area. Due to the lack of a mature source rock in the graben itself, the system has to be charged with hydrocarbons through long-distance migration from a mature area. The dry wells drilled on block 6507/12 is concluded to result from immature source rocks, and lack of the required long-distance migration routes into the traps. A closer look is taken at possible migration routes with an aim to explain why - if hydrocarbons have entered the graben from the south - the drilled prospects have been found dry. This concluded that the syn-rift sands expected in the Viking Group in the immediate BFC hanging wall could possibly represent higher permeability strata, steering charge away from the drilled traps. The likelihood of this depends on the connectivity of the individual syn-rift sand bodies as well as their porosity and permeability. In addition, an unbreached base seal separating these carrier beds from the Middle Jurassic strata should be present. A general lack of signs of hydrocarbons in the study area in the form of shallow soft bright spots or pockmarks however reduces the likelihood of significant mature hydrocarbons in the study area and leads to the conclusion that the graben is likely to be situated in a migration shadow.

6.2 Confidence and mapping

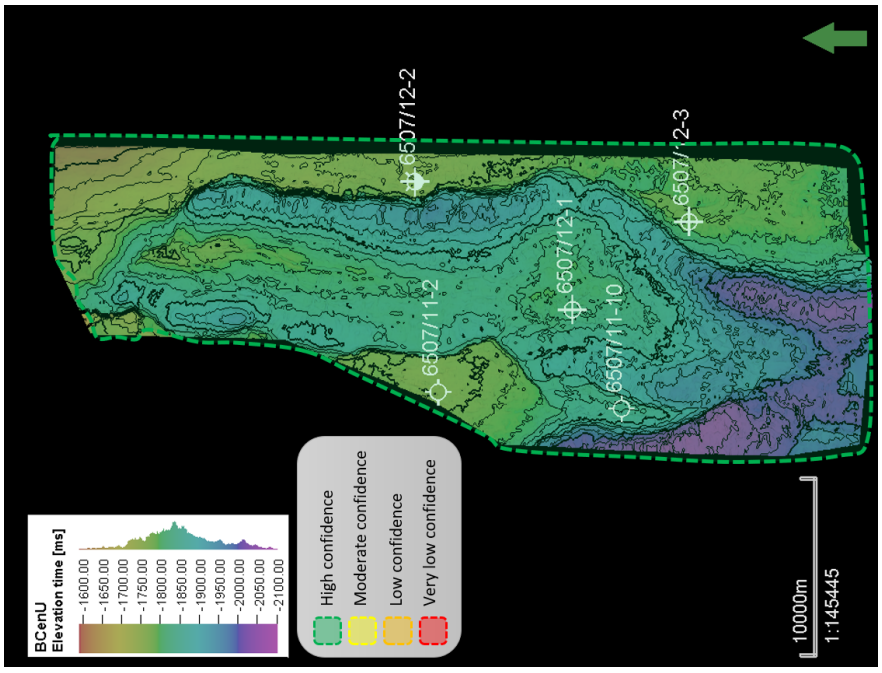

(a) Confidence map for the BCenU surface, illustrating that this interpretation is confident throughout the study area.

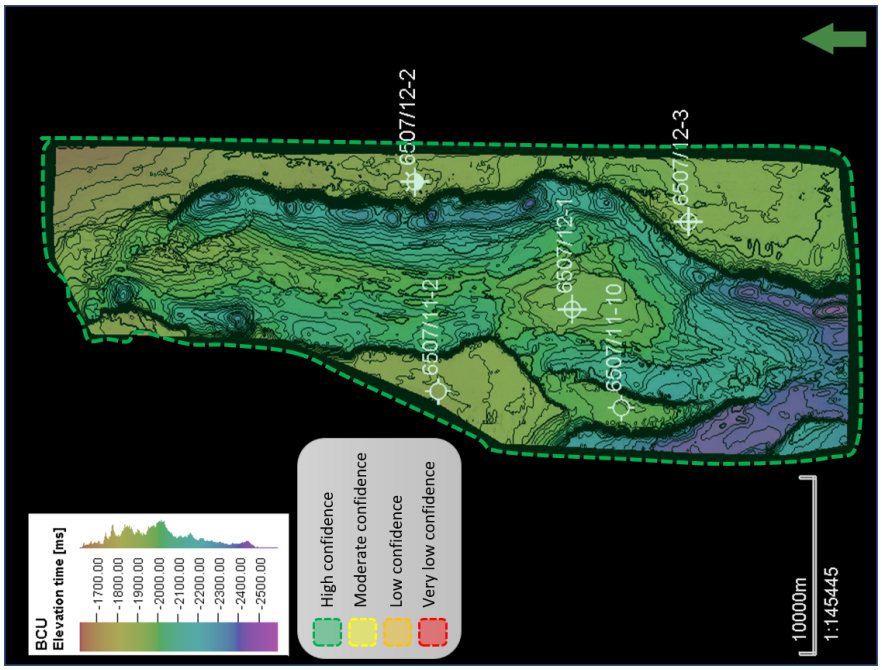

(b) Confidence map for the BCU surface, illustrating that this interpretation is confident throughout the study area.

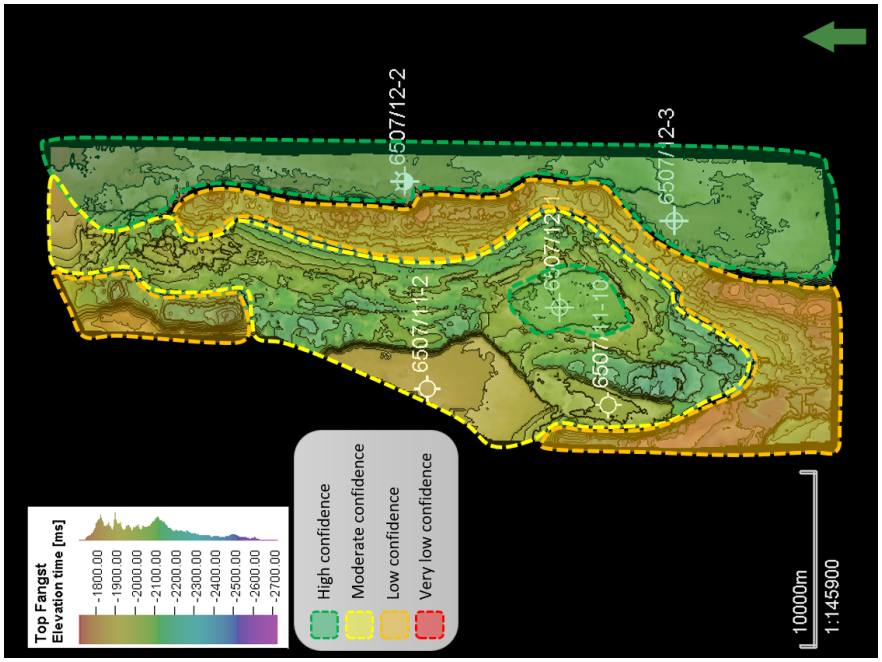

(c) Confidence polygons for the Top Fangst surface. Low confidence mostly due to erratic, distcontinuous reflectors rather than poor data quality.

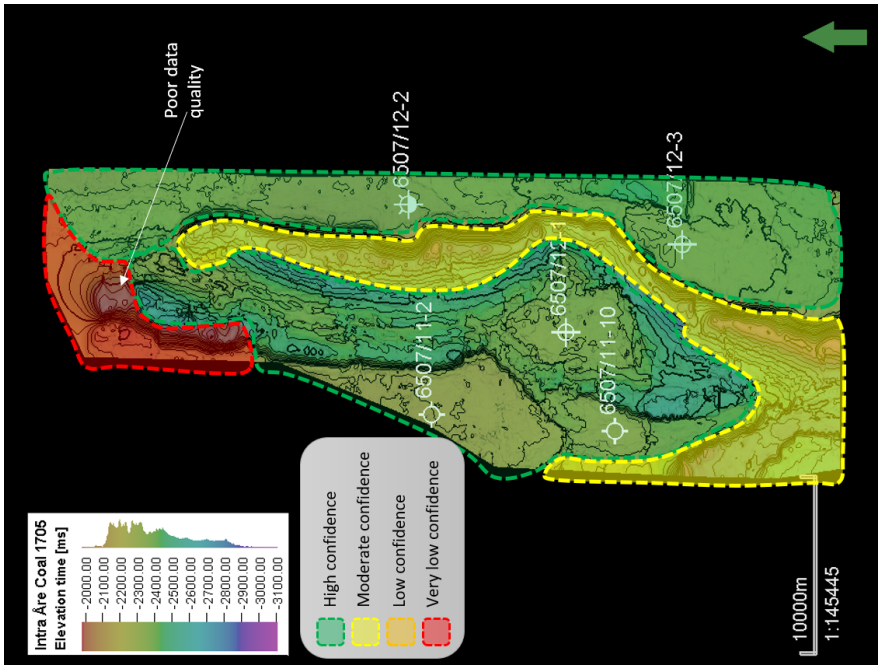

(d) Confidence polygons for the Top Åre Coal horizon. Very low confidence due to degrading data quality at the Åre level in the north-western part of the study area is marked.

Figure 6.1: Examples of confidence polygons created for mapped horizons.

There are significant variations in confidence regarding the mapping of different horizons on seismic. The basis for choice of horizons to map is given in section 3.2.1. Some horizons, like the seabed or the (mostly) high ampltiude soft BCU are easier to follow than others. Problems arise both due to poor data quality and geological related issues giving erratic, chaotic reflectivity patterns in certain areas. This is dealt with through creating simple confidence polygons for each of the mapped surfaces, indicating the degree of confidence in that the interpretation is correct over the study area. Figures 6.1b-6.1d show examples of these for selected surfaces. Generally, the confidence is very high in the shallow strata, for example seabed, Top Kai and the BCenU surface. For the most of the surfaces, any potential lack of confidence arises primarily from geological conditions rather than problems with data quality. However in the deep parts of the stratigraphy, for instance at the evaporite levels, lack of confidence is to a larger degree linked to poor data quality. Possibly the least confident of the horizons mapped is top Fangst (figure 6.1c). The uncertainty regarding this horizon is especially large in the immediate hanging wall of the BFC. The choices of Top Fangst in this area governs the thickness of the syn-rift wedge of the Viking Group, and is thus an important factor in determining the expected amount of erosion over the adjacent footwall, as well as timing and amount of activity on the fault segments. Though the thickness of the Viking Group syn-rift wedge is relatively uncertain, the thickness of the Cretaceous strata in the immediate hanging wall is much more confident, as is seen from the confidence polygons in figure 6.1a and 6.1b. Figure 6.2 shows an arbitrary line through part of the uncertain hanging wall area with fault segments S1, S2 and S3 marked, illustrating that the vayring Cretaceous thickness across the fault segments is confident though the Viking Group Thickness is more uncertain. This variation along with the less throw measured along segment S2 constitute valid arguments for the division into segments and the later formation of segment S2, despite the uncertainty regarding the top Fangst horizon. The later initiation of fault segment S2 would also conceptually support less syn-rift accumulation along this segment, making the Top Fangst interpretation reasonable, though still uncertain.

6.3 The headache of uncertain chronostratigraphic data

The wells on block 6507/12 are some of the first wells drilled in the Norwegian Sea. Several studies exist for biostratigraphy, lithostratigraphy and sedimentology of wells `6507/12-1` and `6507/12-2`, as well as multiple well-correlation studies where these wells are included. Examples included and used in this thesis are Paleoservices LTD. (1980), Laboratoire de Geologie de Boussens (1981b), Robertson Research International Limited (1982), Saga Petroleum AS (1983a), Saga Petroleum AS (1983b), Saga Petroleum AS (1985a), and Stratlab AS (1990). The data available for well `6507/12-3` is more sparse. Though an abundance of data can be helpful when generating and constraining models, it can also cause a real headache when the results and conclusions of these reports are conflicting and contradicting. The amount of confidence in biostratigraphic data is highly dependant on sample quality and which interpretation scheme is used along with the experience of the biostratigrapher analyzing the samples. Cavings in the well and reworked sediments in cores and cuttings are also common sources of error. Combined, this can lead to widely different conclusions when analyzing the same data, as it has in the case of wells `6507/12-1` and

6507/12-2.

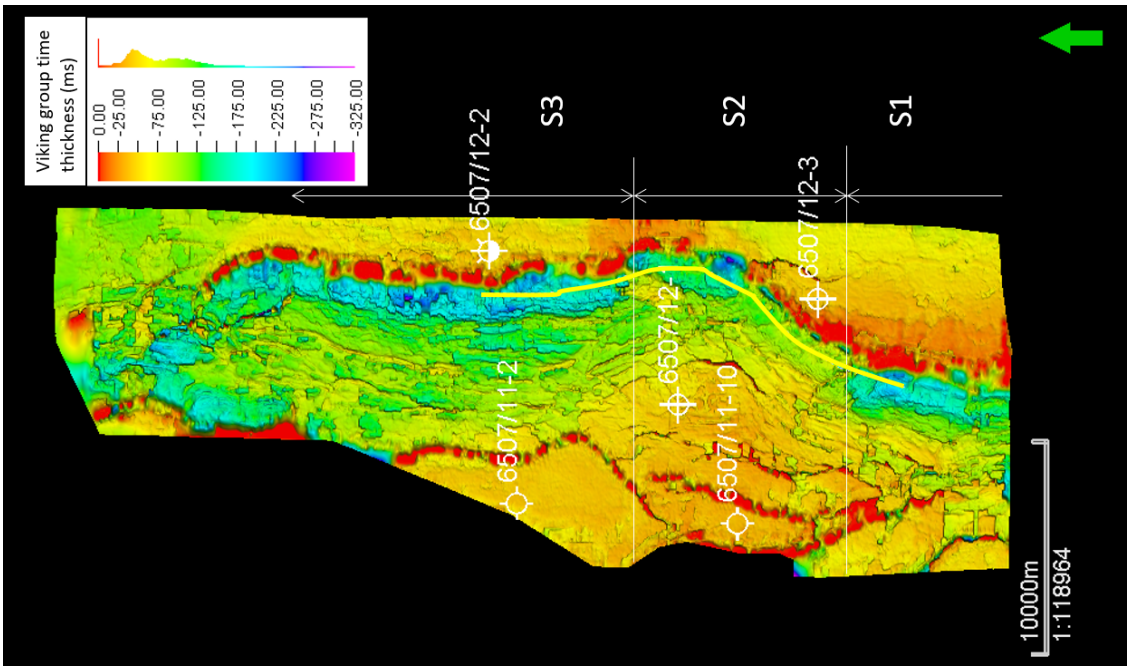

(a) Thickness map in TWT for the Viking group. Fault segments as proposed from section 4.1.3 and location of arbitrary line is marked.

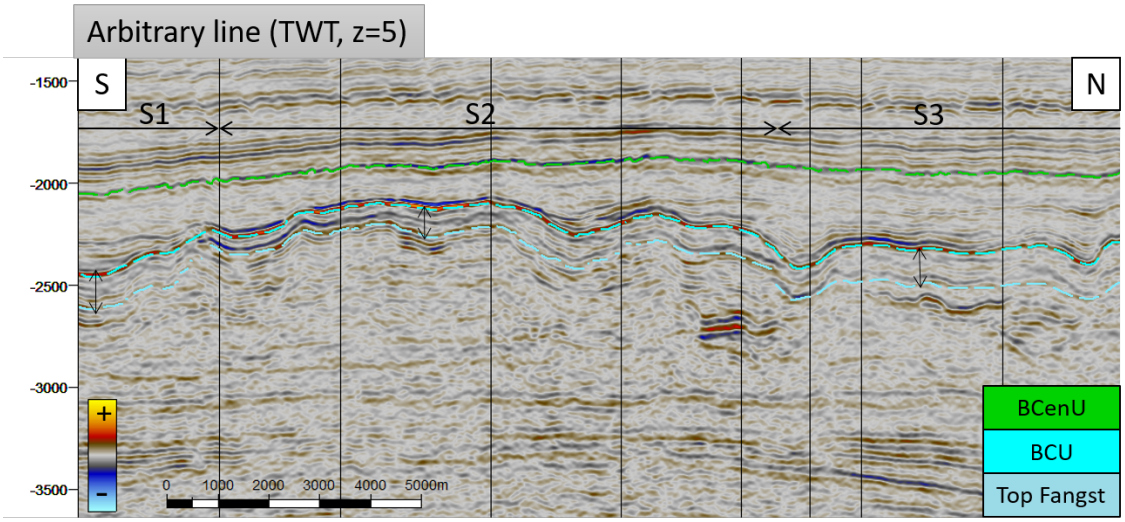

(b) The substantial amount of uncertainty in the Top Fangst surface in this area makes the syn-rift Viking thickness uncertain. The BCU and BCenU interpretations are however confident, making the thickness of the Cretaceous strata confident in the same area.

Figure 6.2: Arbitraty line along-strike of the immediate BFC hanging wall showing thickness variations of the Late Jurassic and Cretaceous strata, however with significant uncertainty related to the Top Fangst horizon.

The most conflicting conclusions are regarding the chronostratigraphy and lithostratigraphy in the Middle and Late Jurassic strata, crucial for dating of the IMU and placement

of the Jurassic formation tops, which again to a large degree impacts the conceptual model in terms of amount of erosion and formation thicknesses seen in the wells. An example is the discrepancy in the dating of the Melke Formation in the interval between 1880 m and 1920 m in well 6507/12-2. Saga Petroleum AS (1983a) dates this interval to Bathonian to Oxfordian with a basal unconformable boundary to a Bajocian sandstone below. Stratlab AS (1990) however dates the same interval between 1880 m and 1920 m to Late Oxfordian with an unconformable boundary to an Early Bajocian sandstone below. Assuming this unconformity represents the IMU, the age of the IMU must be Bajocian or Bathonian according to Saga Petroleum AS (1983a). Following Stratlab AS (1990) the hiatus associated with the IMU spans from Early Bajocian to Late Oxfordian, placing the erosion associated with IMU somewhere within this time interval. For the 6507/12-1 well, the hiatus has a much smaller timespan in Stratlab AS (1990), constraining the age of the IMU much better, giving it an approximate Callovian age. Thus according to one report, the IMU is associated with Bajocian to Bathonian erosion, whilst in another the same unconformity has a Callovian age. It was chosen to trust the report supporting a Callovian age of the IMU. Arguments for this was a better fit with literature (Bell et al. 2014; Bunkholt et al. submitted) and the more recent date of the Stratlab AS (1990) report, meaning that at this time the authors may have had a better understanding of the regional geology through more well data and possibly higher quality seismic data.

Another area where there are significant differences is the placement of formation tops of the Middle Jurassic sandstones in well 6507/12-2. An overview and comparison of the formation top placements from NPD and two different biostratigraphic reports is seen in figure 6.3. This figure is included to give some insight into the very conflicting results provided by different reports. It is chosen to ignore the Stratlab AS (N/A) report due to several questionably picked formation tops both compared to the petrophysical logs and considering the conceptual and regional understanding of the stratigraphy of the Halten Terrace (Dalland et al. 1988). The formation tops from this report are included to illustrate the large range in conclusions coming from these reports. Ignoring the Stratlab AS (N/A) report, it is observed that an essential difference between the information from NPD Fact Pages and (Stratlab AS 1990) is whether the sandstone coming in at 1922 mMD is the Ile Formation or the Garn Formation. That the whole Garn and Not intervals are missing would indicate very deep erosion during the Callovian, removing the whole Garn and Not interval. This seems relatively unlikely as the Garn Formation is encountered (and cored!) in well 6507/12-3 and this seismic horizon is correlatable to the top of the sand body in well 6507/12-2. Adding to arguments for the sand at 1922 mMD being of the Garn Formation is the fact that most biostratigraphic studies report a Bajocian age at this level, including the report from Stratlab AS (1990). NPD reports of 87 meters of Garn Formation sand in the 6507/12-2 well, going directly to the Ror Formation at its base, meaning that the Ile and Not formations are completely missing. This indicates substantial amounts of erosion at the base of the Garn Formation. However, no such erosional cuts are observable on seismic nor are there any signs of associated thickening due to deposition in the hanging-wall (see figure 4.13) at this level. The Garn Formation *thickening* from 34 meters in the 6507/12-1 well situated in the center of the graben to 87 meters in well 6507/12-2 on the footwall of the BFC is not in line with neither the conceptual understanding of the study area nor observations from the 6507/12-3 well situated further south on the same footwall.

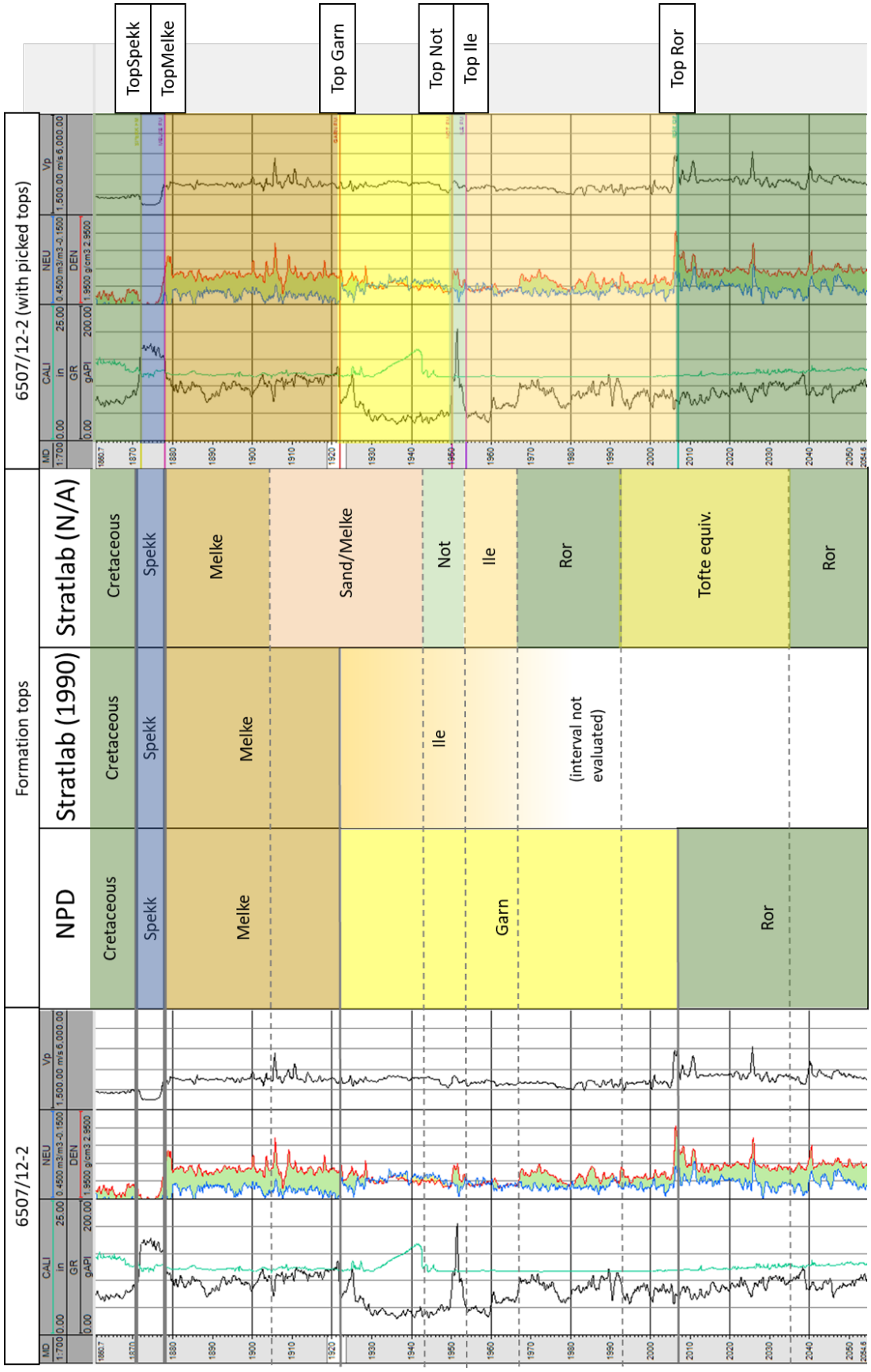

Figure 6.3: An overview of lithostratigraphy as described by NPD, Stratlab AS (1990) and Stratlab AS (N/A). Formations tops as picked in this thesis seen to the right.

Thus, new formation picks are made for Top Not and Top Ile in this thesis for well 6507/12-2, as mentioned in section 4.2. Top Not Formation was picked at the gamma ray-spike seen at 1950 mMD. According to Saga Petroleum AS (1985a) this peak is due to heavy minerals (side wall core sample at 1952 mMD), a signature often recognized near the base of the Not Formation (Bunkholt, *pers.comm.*) The top Ile Formation is picked at a gamma ray and density decrease at 1954 mMD, meaning that only the basal 4 meters of the Not Formation are present in the well. A sidewall core at 1985 meters indicate a late Toarcian age, consistent with the known age of the Ile Formation (Robertson Research International Limited 1982; Dalland et al. 1988). With these formation tops both the Garn, Not and Ile formations are present in well 6507/12-2, however all formations are thinning from the 6507/12-1 well, fitting with the conceptual model proposed in section 4.1.4.

6.4 Depth conversion and maturity maps

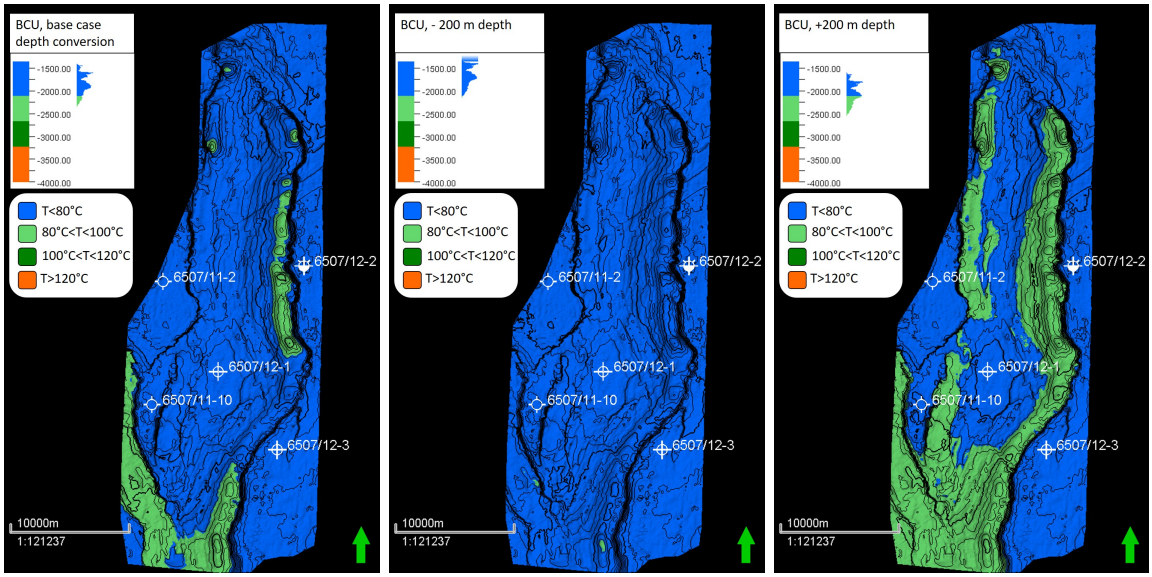

(a) The base case depth (b) Shifted up 200 meters (c) Shifted down 200 meters

Figure 6.4: Temperature maturity maps for the depth converted BCU surface, showing the differences in apparent maturity with a 200 meter downward or upward shift of depth.

The constructed temperature maturity maps are uncertain, with uncertainty inherited from both seismic interpretation and possible errors in the depth conversion. However, the validity of the temperature maturity maps are only briefly only discussed herein, because the immaturity of the source rock intervals is largely confirmed through source rock analysis on actual samples.

Because the BCU surface used to illustrate temperature for the Spekk Formation is found at depths extremely close to the theoretical start of the early oil window at 80°C, the appearance of the resulting temperature maturity map is highly sensitive to relatively small errors in the depth conversion. This is illustrated by figure 6.4, showing the base case depth converted surface along with the maps if the surface is shifted up or down by

only 200 meters. The data used to create the velocity model (section 3.2.1) is of good quality, but the confidence in the depth conversion is still questionable due to the choice of intervals for velocity and uncertainty in the interpretations defining those intervals. Thus, one must consider the possibility that this temperature map could appear both far more mature or immature. Though this is definitively a substantial uncertainty in the project, the consequences of these estimates being erroneous are relatively small: The conclusion that the main source rock intervals in the study area are immature remains the same due to the evidence provided by modelling and hard data.

6.5 Uncertainty in PetroMod 1D modelling

As previously discussed (section 5.1.3), the results of the PetroMod 1D modelling for well `6507/12-1` are uncertain and highly dependant on the boundary conditions and main input. As discussed in section 6.3, the chronostratigraphy governing the main input to the model should not be considered hard, certain data. In addition, any erosional periods with significant uplift are exluded in this modelling due to the lack of such information from the well reports (Saga Petroleum AS 1980; Laboratoire de Geologie de Boussens 1981a; Saga Petroleum AS 1983a). Still, significant uplift and erosion may have occurred where large hiatuses are recorded (see lithostratigraphic chart for the Ellingråsa Graben, figure 4.28). In the modelling, these are considered to be periods of non-deposition rather than uplift and erosion, and is clearly a possible source of error.

The boundary conditions are of relativey low confidence (figure 3.10 to 3.12). Present day heat flow is estimated from Pascal (2015) and is considered reasonable, however paleo heat flow is much more uncertain. The paleo water depth is based on biostratigraphical reports (Laboratoire de Geologie de Boussens 1981a), but these come with a large amount of uncertainty and do not give exact numbers. The chosen paleo water depths effects both sediment compaction and the temperature at the sediment-water or sediment-air interface. In order to investigate how large an effect the chosen paleo water depth curve has on temperature and maturity, a case where water depth was set to zero through geological time from the Triassic until Pliocene before increasing rapidly to the 250 meters water depth in the well location today. This is of course not realistic, but is meant to provide an upper bound on the effect of paleo water depth on maturation. The resulting burial graph with transformation ratio overlain is seen in figure 6.5 and shows that even in this extreme, completely unrealistic case, the transformation ratio for the coal-rich part of the Åre Formation is only at 11%. Therefore, though the paleo water depth is very uncertain, its values are not considered to significantly affect the result of the model in terms of maturity.

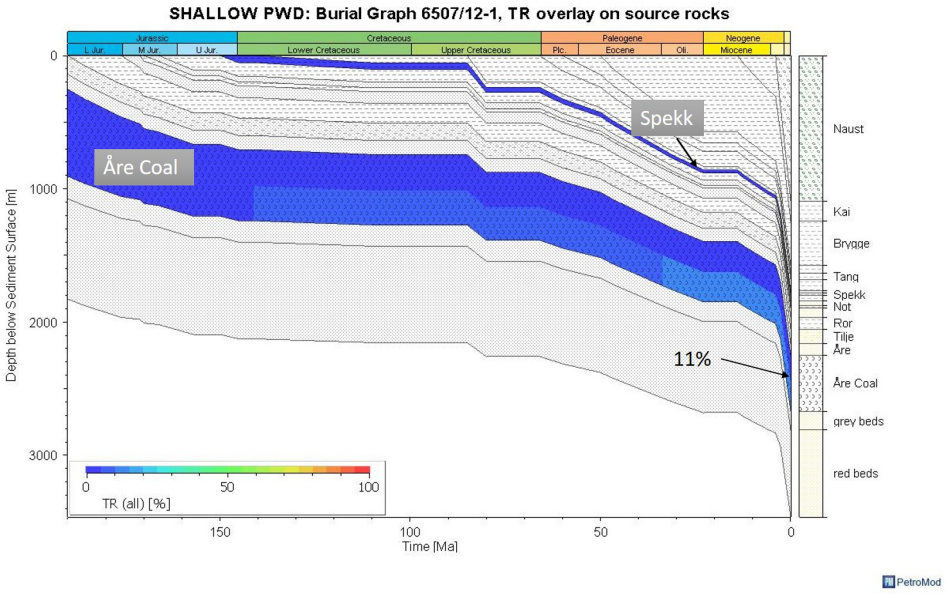

Figure 6.5: Transformation ratio for a theoretical case with zero seawater depth until Pliocene.

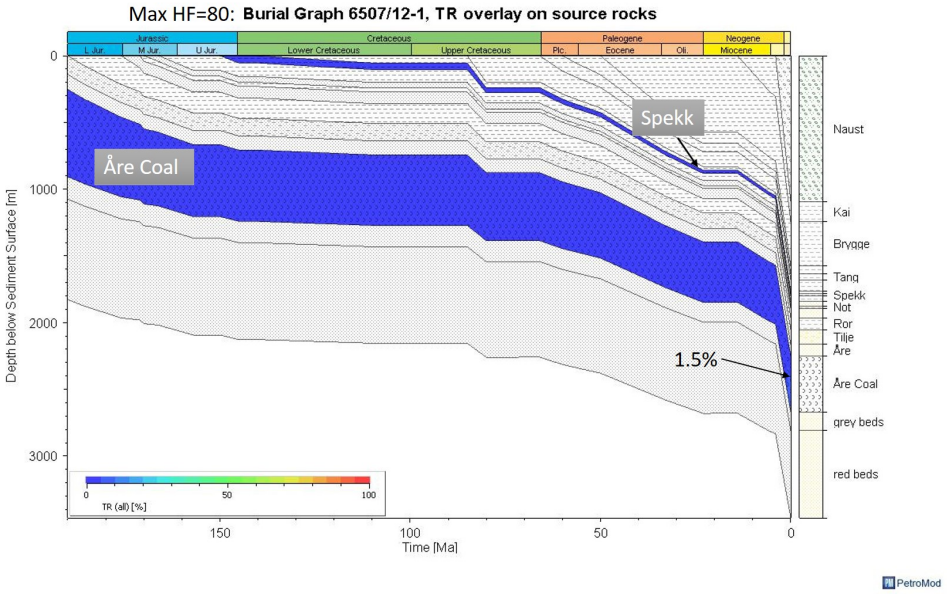

Figure 6.6: Transformation ratio if lowering the max heat flow during rifting to 80 mW/m^2

The maximum paleo heat flow during the rifting is in the modelling set to 100 mW/m^2, which is overestimated compared to the calculations of Hermans et al. (1992) and Fu and Unnithan (2009), where maximum paleo heat flow is estimated to around 80 mW/m^2. Figure 6.6 shows the resulting burial curve with transformation ratio overlain for a case with

maximum paleo heat flow of 80 mW/m^2. Here, the transformation ratio is only at 1.5% for the present-day burial of the coal-rich part of the Åre Formation. The likely overestimated paleo heat flow of 100mW/m^2 was allowed because the goal was to construct what could be considered a maximum maturity case for the source rock intervals in the study area. Even in this case, the source rocks are largely immature (figure 5.14). The lower paleo heat flow case also results in a better vitrinite reflectance fit with the measurements from the well, however modelled vitrinite reflectance is still significantly overestimated. As discussed in section 5.1.3, there are also uncertainties regarding the recent heat flow history and whether the heat flow of today is in a steady-state.

The uncertainties in the modelling do not however change the result that the source rock intervals encountered in well 6507/12-1 are immature, despite their partially mature temperatures, even in cases with presumably overestimated heat flow and zero water depth through geological history. This is of course also further confirmed by source rock analyses on samples from the well (Continental Shelf Institute 1981). Though the 6507/12-1 well is somewhat elevated compared to the deepest parts of the study area, the very immature results here indicate that maturation is low even in the deepest parts.

Main uncertainties summarized

- There are significant uncertainties regarding low confidence interpretations. The Top Fangst horizon is a locally low-confidence horizon with high importance because it governs thickness of the overlying syn-rift Viking Group.

- The chronostratigraphic reports are commonly conflicting and contradicting, especially in the Middle to Late Jurassic time interval. This brings significant uncertainty regarding the timing of rifting, erosion and syn-rift deposition. It is chosen to trust in the younger reports where a better regional understanding and higher quality data probably existed.

- Welltops from both NPD Fact Pages and other stratigraphic reports can be conflicting, as figure 6.3 illustrates. Here, new formation tops were picked based on log response, information from sidewall cores in the well and the conceptual understanding of the area.

- There are significant uncertainties regarding the temperature maturity maps, inherited from uncertainties in the depth conversion and seismic interpretation. While this has a large effect on the appearance of the maturity map, it does not alter the conclusion that the source rocks are immature which is largely confirmed by analysing samples from wellls (Continental Shelf Institute 1981; GeoChem Laboratories (U.K) Limited 1982).

- Both input data and the boundary conditions of the PetroMod 1D modelling comes with significant uncertainty. However, even cases constructed to yield overestimated maturity gives immature source rocks in the 6507/12-1 well.

Chapter 7

Conclusion and further work

7.1 Conclusion

The aim of this thesis is to investigate the tectonostratigraphy and hydrocarbon potential of the Ellingråsa Graben, so far sparely described by publicly available literature. The thesis has drawn conclusions and suggested models and concepts based on 3D seismic data and well data from the study area.

The Triassic evaporite unit is proposed to govern the structural style of the Ellingråsa Graben through listric faulting of the BFC, associated hanging-wall rollover and gentle salt-pillowing. Throw measurements along the BFC, erosion estimates on the BCU surface and thickness of the associated hanging wall syn-rift wedge are combined to suggest a division of the BFC into 4 segments (S1-S4) in the study area. Segments S1 and S3 striking N-S represent areas of large throw, deep erosion and thick associated syn-rift wedges, while segment S2 striking mainly NW-SE is suggested to represent a former relay-ramp area between S1 and S2, today hardlinking the BFC in the study area. Segment S4 in the northernmost part of the Ellingråsa Graben shows rapid decrease in throw and erosion along with thinning of the syn-rift strata as the displacement across the BFC becomes smaller. Here, the Ellingråsa Graben transitions into a half-graben bound by an east-dipping master fault. The fault zone deliminting the graben to the west, EWFZ, generally has less syn-rift thicknesses in the hanging-wall and though also listric in nature, shows a more brittle style of deformation in the hanging wall with planar faulting accommodating strain. A model for formation of the closure where well `6507/12-1` is drilled is presented, proposing that the closure formed due to varying strike directions of the graben-bounding listric faults causing hanging wall rollover in multiple directions combined with brittle planar faulting, creating a combined anticline-horst structure. Well data suggests that the IMU is of approximately Callovian age in the study area. Significant erosion is suggested to have occurred along the eastern flank at this time due to large hiatuses and small thicknesses of underlying Jurassic sandstone in the wells at this location. Due to a lack of well data, the western flank is more poorly constrained. Generally, the strata up to this time is suggested to represent a pre-rift to initial rifting stage, while the Callovian to earliest Cretaceous represents rift climax. In the study area, there is also evidence of rifting through diverging hanging-wall reflectors and continued faulting into the Early Cretaceous. Late Cretaceous until today is considered post-rift,

though there is clearly some faulting of the post-rift strata as well, through re-activation of major faults.

Though there are good quality reservoirs, traps and seals in the study area, the source rocks are found to be immature. This means that the study area is dependant of long-distance migration from a deeper, mature source area to be charged with hydrocarbons The lack of this is suggested to constitute the main reason for the dry wells in the study area. A closer look at erosion and syn-rift strata in the study area reveals possible syn-rift sandstones in the immediate hanging wall of the BFC. These sandstones are suggested to be deposited in a deep-water environment and could be present in both the Melke Formation, Spekk Formation and in the Early Cretaceous strata. A local area of deep erosion within the graben may also facilitate deposition of shallow-marine sandstones on the footwall rollover dip-slope. If hydrocarbons have entered the study area at this level, these syn-rift sandstones could constitute migration pathways that would effectively bypass the drilled, dry prospects. This is dependant on the porosity and permeability of these syn-rift sands, their connectivtiy, the sealing properties of the adjacent BFC and the existance of an unbreached base seal stopping the highly porous and permeable Garn Formation from stealing the charge. These syn-rift sands could also represent reservoirs in stratigraphic traps where partially or completely enclosed in the surrounding shale. A general lack of signs of hydrocarbons in the form of shallow soft bright spots or seabed pockmarks reduces the likelihood of significant hydrocarbons having entered the study area and leads to the conclusion that the graben is likely to be situated in a migration shadow.

As always with geology, there are significant uncertainties in this study. The uncertainties having the greatest impact on the conclusion and implications from this thesis are confidence issues in the seismic interpretation, especially regarding the Top Fangst horizon, and uncertainty in the chronostratigraphic data and reports which are commonly conflicting and contradicting.

7.2 Suggestions for further work

This thesis represents some of the first published work on the Ellingråsa Graben, offshore mid-Norway. It has taken a relatively broad look at tectonostratigraphy and hydrocarbon potential of the structure, hopefully providing a useful basis for possible further work within this study area. Because of the little amount of published literature on this graben, there is an extremely wide range of possibilities regarding future work. Under follows a list of some findings and ideas presented in this thesis which would be interesting to explore further:

- No partial stacks of the `HT07` seismic data was available in this project. Should this data become available, performing AvO analysis would be an interesting idea for the future
- This thesis was focused on the strata from the Triassic salt unit and younger. It would be interesting to give more attention to the sub-salt strata and faults to investigate any consistent changes in structural style between the sub- and supra-salt faults, and ultimately compare this to the work of Wilson et al. (2015) further south on the BFC.

- Data from wells on the western flank of the Ellingråsa Graben has not been available during this project, and so the western flank is quite poorly constrained and significant uncertainties exist. Further work should include these wells to gain confidence regarding this western flank.
- The Ellingråsa Graben should be compared to the regional area to a larger degree, comparing the graben to nearby locations and wells
- A closer look could be taken at the older, possibly mature source rock intervals in the Permian or Triassic strata, as mentioned in section 5.1.3
- As mentioned, modelling the heat flow pertubation effect of the rapid deposition of the Naust package along with the heat flow increasing effect of overpressure and undercompaction yielding low thermal conductivities for the study area would be interesting. This to further explain why the source rock intervals are found immature despite their (partially) mature temperatures.
- Considering the future hydrocarbon potential of the Ellingråsa Graben, there are several possibilities that could be investigated. One of which is where the spill point from the Midgard field is located, and whether this could provide charge to the Ellingråsa Graben. Another suggestion is to focus on the heterogeneities observed in the hanging wall syn-rift wedge of the major faults, and interpret individual, possible sand bodies. AvO analysis could here be helpful in distinguishing sand and shale lithology.

Bibliography

Allen and Allen (2013). *Basin Analysis*. 3rd. Wiley-Blackwell.

Bell, R.E et al. (2014). "Iinsights into the development of major rift-related unconformities from geologically constrained subsidence modelling: Halten Terrace, offshore Mid-Norway". In: *Basin Research* 26, pp. 203–224.

Bjørlykke, Knut et al. (2010). *Petroleum Geoscience*. 2nd. Springer.

Bjørlykke, Knut and P. K. Egeberg (1993). "Quartz cementation in sedimentary basins". In: *AAPG Bulletin* 77, pp. 1538–1548.

Blilie, K. (2018). "A review of the shallow water Norwegian Sea region geology combining literature, seismic interpretation and net exhumation estimation". In: *Unpublished*.

Blystad, Per et al. (1995). "Structural elements of the Norwegian continental shelf, Part II: The Norwegian sea region". In: *NPD Bulletin* 8.

Brekke, Harald (2000). "The tectonic evolution of the Norwegian Sea Continental Margin with emphasis on the Vøring and Møre basins". In: *Dynamics of the Norwegian Margin, Geological Society* 167, pp. 327–378.

Bugge, T. et al. (2002). "Upper Permian as a new play model on the mid-Norwegian continental shelf: Investigated by shallow stratigraphic drilling". In: *AAPG Bulletin* 86.1, pp. 107–127.

Bunkholt, Halvor et al. (submitted). "The Halten and Dønna terraces and the Trøndelag Platform Tectono-Sedimentary Element". In: *Submitted to: In: Drachev, S. et al. (eds) Arctic Sedimentary Basins. Geological Society, London, Memoirs*.

Burnham, Alan K. (1989). "A simple kinetic model of petroleum formation and cracking". In: *Lawrence Livermore National Laboratory*.

Continental Shelf Institute (1981). *Source Rock Analysis of Well 6507/12-1*. Tech. rep.

Corfield, S. et al. (2001). "An integrated study of the Garn and Melke formations (Middle to Upper Jurassic) of the Smørbukk area, Halten Terrace, mid-Norway". In: *Sedimentary Environments Offshore Norway - Paleozoic to Recent, NPF Special Publications* 10, pp. 199–210.

Dalland, A. et al. (1988). "A lithostratigraphic scheme for the Mesozoic and Cenozoic offshore mid- and northern Norway". In: *NPD Bulletin* 4.

Doré, A. G. et al. (1999). "Principal tectonic events in the evolution of the northwest European Atlantic margin". In: *Petroleum Geology of Nortwest Europe - Proceedings of the 5th Petroleum Geology Conference*, pp. 41–61.

Ehrenberg, S. N (1990). "Relationship Between Diagenesis and Reservoir Quality in Sandstones of the Garn Formation, Haltenbanken, Mid-Norwegian Continental Shelf'. In: *AAPG Bulletin* 74.10, pp. 1538–1558.

Eidvin, Tom et al. (2007). "The Molo Formation, deposited by coastal progradation on the inner Mid-Norwegian continental shelf, coeval with the Kai Formation to the west and the Utsira Formation in the North Sea". In: *Norwegian Journal of Geology* 87, pp. 75–102.

Elliot, G.M et al. (2011). "The linkage between throw and footwall scarp erosion patterns: an example from the Bremstein Fault Complex, offshore mid-Norway". In: *Basin Research* 23, pp. 1–18.

Færseth, Roald B and Lien (2002). "Cretaceous evolution in the Norwegian Sea - a period characterized by tectonic quiescence". In: *Marine and Petroleum Geology* 19, pp. 1005–1027.

Fossen, Haakon (2010). "Extensional tectonics in the North Atlantic Caledonides: a regional review". In: *Geological Societly, London, Special Publications* 335, pp. 767–793.

Fu, Yanzhe and Vikram Unnithan (2009). "Forward modeling of paleo heat flow: a case study of Kristin Field, Mid-Norwegian continental shelf". In: *IEEE Explore*.

Gawthorpe and Leeder (2000). "Tectono-sedimentary evolution of active extensional basin". In: *Basin Research* 12, pp. 195–218.

GeoChem Laboratories (U.K) Limited (1982). *Geochemical Evaluation of Saga's 6507/12-2 well, Halten Bank, Offshore Norway*. Tech. rep.

Gluyas, Jon and Richard Swarbrick (2004). *Petroleum Geoscience*. 1st. Wiley-Blackwell.

Hansen, Sven (1996). "Quantification of net uplift and erosion on the Norwegian Shelf south of 66 degrees N from sonic transit times of shale". In: *Norsk Geologisk Tidsskrift* 76, pp. 245–252.

Hantschel, Thomas and Armin I. Kauerauf (2009). *Fundamentals of Basin and Petroleum Systems Modeling*. 1st. Springer.

Henriksen, Sverre et al. (1996). "The Norwegian Sea during the Cenozoic". In: *Onshore-Offshore Relationships on the North Atlantic Margin, edited by B. Wandas et al. NPD Special Publication* 12.

Henriksen, Sverre and Tore O. Vorren (1996). "Late Cenozoic sedimentation and uplift history on the mid-Norwegian continental shelf". In: *Gloabal and Planetary Change 12* 12.

Hermans, L et al. (1992). "Modelling secondary hydrocarbon migration in Haltenbanken, Norway". In: *NPF Special Publications: Structural and Tectonic Modelling and its Application to Petroleum Geology* 1.

Hollander, N. B. (1984). "Geohistory and hydrocarbon evaluation of the Haltenbank area". In: *Petroleum Geology of the North European Magin, Norwegian Petroleum Society*, pp. 383–388.

Ichaso, Aitor A. et al. (2016). "Basin analysis and sequence stratigraphy of the synrift Tilje Formation (Lower Jurassic), Halten terrace giant oil and gas fields, offshore mid-Norway". In: *AAPG Bulletin* 100.8, pp. 1329–1375.

Ichaso, Aitor A. and Robert W. Dalrymple (2014). "Eustatic, tectonic and climatic controls on an early syn-rift mixed-energy delta, Tilje Formation (Early Jurassic, Smørbukk field, offshore mid-Norway)". In: *From depositional systems to sedimentary successions on the Norwegian continental margin: IAS Special Publication* 46, pp. 339–388.

Jackson, Christopher A.-L. and Matthew M. Lewis (2016). "Strutucal style and evolution of a salt-influenced rift basin margin; the impact of variations in salt composition and the role of polyphase extension". In: *Basin Research* 28, pp. 81–102.

Jackson and Michael R. Hudec (2017). *Salt Tectonics - Principles and practice*. 1st. Cambridge University Press.

Johansen, Nora J. (2016). "Regional net erosion estimations and implications for seismic AVO signatures in the Western Barents Sea". In: *Master Thesis, NTNU*.

Karlsen, D. A. et al. (1995). "Petroleum geochemistry of the Haltenbanken, Norwegian continental shelf". In: *The Geochemistry of Reservoirs, Geological Society Special Publication* 98, pp. 203–256.

Kjærefjord, J.M. (1991). "Bayfill successions in the Lower Jurassic Åre Formation, Offshore Norway: Sedimentology and heterogeneity based on subsurface data from the Heidrun field and analogue data from the Upper Cretaceous Neslen Formation, Eastern Book Cliffs, Utah". In: *GCSSEPM Foundation 19th Annual Reserarch Conference*, pp. 149–158.

Laboratoire de Geologie de Boussens (1981a). *Biostratigraphical report*. Tech. rep.

— (1981b). *Sedimentological study of Jurassic deposits in 6507/12-1 well (Norway)*. Tech. rep.

Lien, Trond et al. (2006). "Depositional facies and reservoir quality of deep-marine sandstones in the Norwegian Sea". In: *Norwegian Journal of Geology* 86, pp. 71–92.

Løseth, Helge et al. (2011). "Deformation structures in organic-rich shales". In: *AAPG Bulletin* 95, pp. 729–747.

— (2017). "500 m of rapid base level rise along an inner passive margin - Seismic observations from the Pliocene Molo Formation, mid Norway". In: *Marine and Petroleum Geology* 86, pp. 268–287.

Marsh, N. et al. (2010). "The structural evolution of the Halten Terrace, offshore Mid-Norway: extensional fault growth and strain localisation in a multi-layer brittle-ductile system". In: *Basin Research* 22, pp. 195–214.

Martinius, A. W et al. (2005). "Reservoir Challenges of heterolithic tidal sandstone reservoirs in the Halten Terrace, mid-Norway". In: *Petroleum Geoscience* 11, pp. 3–16.

Martinius, A.W et al. (2001). "Sedimentology of the heterolithic and tide-dominated Tilje Formation Early Jurassic, Halten Terrace, Offshore mid-Norway". In: *Sedimentary Environments Offshore Norway - Paleozoic to Recent* 10, pp. 103–144.

Martinsen, O. J. et al. (2005). "Cretaceous and Paleogene turbidite systems in the North Sea and Norwegian Sea Basins: source, staging area and basin physiography controls on reservoir development". In: *Petroleum Geology: North-West Europe and Global Perspectives - Proceedings of the 6th Petroleum Geology Conference*, pp. 1147–1164.

McKenzie, Dan (1978). "Some remarks on the development of sedimentary basins". In: *Earth and Planetary Science letters* 40, pp. 25–32.

Morton, Andrew et al. (2009). "Evolution of provenance in the NE Atlantic rift: The Early–Middle Jurassic succession in the Heidrun Field, Halten Terrace, offshore Mid-Norway". In: *Marine and Petroleum Geology* 26, pp. 1100–1117.

Müller, Reidar et al. (2005). "Late Permian to Triassic basin infill history and palaeogeography of the Mid-Norwegian shelf - East Greenland region". In: *Norwegian Petroleum Society Special Publications, Elsevier* 12, pp. 165–189.

Nichols, Gary (2009). *Sedimentology and Stratigraphy*. 2nd. Wiley-Blackwell.

NPD (2019). "Fact Pages". In:

Ottesen, Dag et al. (1999). "Geological evolution of the Norwegian Continental Shelf between 61°N and 68°N during the last 3 million years". In: *Norwegian Journal of Geology* 89, pp. 251–265.

Paleoservices LTD. (1980). *Stratigraphical Report for well 6507/12-1*. Tech. rep.

— (1986). *Well 6507/12-3 Stratigraphical/Paleontological Final Report*. Tech. rep.

Palumbo, Filippo et al. (1999). "The thermal evolution of sedimentary basins and its effect on the maturation of hydrocarbons". In: *Geophysics Journal International* 139, pp. 248–260.

Pascal, Christophe (2015). "Heat glow of Norway and its continental shelf'. In: *Marine and Petroleum Geology* 66.

Pepper, Andrew S. and Peter J. Corvi (1995). "Simple kinetic models of petroleum formation. Part I: oil and gas generation from kerogen". In: *Marine and Petroleum Geology* 12.3, pp. 291–319.

Ravnås, R. et al. (2014). "Halten Terrace Lower and Middle Jurassic inter-rift megasequence analysis; megasequence structure, sedimentary architecture and controlling parameters". In: *Int. Assoc. Sedimentol. Spec. Publ.* 46, pp. 215–252.

Rise, L et al. (2005). "Large-scale development of the Mid-Norwegian margin during the last 3 million years". In: *Marine and Petroleum Geology* 22, pp. 33–44.

Robertson Reasearch International Ltd. (1984). *Results of "Rock-Eval" Pyrolysis Analyses of cuttings and core samples from Haltenbanken well: 6507/12-1*. Tech. rep.

Robertson Research International Limited (1982). *Stratigraphy, lithofacies and petrography of the Jurassic - Triassic interval of the Saga 6507/12-2 well, Norway*. Tech. rep.

Rønnevik, H.C (2000). "The exploration experience from Midgard to Kristin". In: *NPF Special Publication* 9, pp. 113–129.

Saga petroleum (1981). *Maturation Study on Well-site picked lithologies using Vitrinite Reflectance, well 6507/12-1 - Offshore Norway*. Tech. rep.

Saga Petroleum AS (1980). *Final Well Report for well 6507/12-1*. Tech. rep.

— (1981). *Final Well Report for well 6507/12-2*. Tech. rep.

— (1983a). *Biostratigraphic subdivision and correlation of the 6507/12-1 and 6507/12-2 wells*. Tech. rep.

— (1983b). *Sedimentology and Diagenesis of Jurassic Sediments Offshore Mid-Norway*. Tech. rep.

— (1985a). *Block 6507/12 Evaluation Report*. Tech. rep.

— (1985b). *Final Well Report for well 6507/12-3*. Tech. rep.

Storvoll, Vidar et al. (2005). "Velovity-depth trends in Mesozoic and Cenoozoic sediments from the Norwegian Shelf'. In: *AAPG Bulletin* 89.3, pp. 359–381.

Stratlab AS (N/A). *Mid-Norway Offshore Biozonation*. Tech. rep.

— (1990). *Draugen Trend: Upper to Middle Jurassic Stratigraphy of 9 wells from the Trøndelag Area*. Tech. rep.

Surlyk, F. (1990). "Timing, style and sedimentary evolution of Late Palaeozoic-Mesozoic extensional basins of East Greenland". In: *Tectonic Events Responsible for Britain's Oil and Gas Reserves, Geological Society Special Publication* 55, pp. 107–125.

Sweeney, Jerry J. and Alan K. Burnham (1990). "Evaluation of a Simple Model of Vitrinite Reflectance Based on Chemical Kinetics". In: *AAPG Bulletin* 74, pp. 1559–1570.

Thrana, Camilla et al. (2014). "Updated depositional and stratigraphic model of the Lower Jurassic Åre Formation, Heidrun Norway". In: *Int. Assoc. Sedimentol. Spec. Publ.* 46, pp. 253–290.

Walderhaug, O. (1996). "Kinetic Modeling of Quartz Cementation and Porosity Loss in Deeply Buried Sandstone Reservoirs". In: *AAPG Bulletin* 80, pp. 731–745.

Wilson, Paul et al. (2013). "Geometry and segmentation of an evaporite-detached normal fault array: 3D seismic analysis of the southern Bremstein Fault Complex, offshore mid-Norway". In: *Journal of Structural Geology* 51, pp. 74–91.

— (2015). "Lateral variation in structural style along an evaporite-influenced rift fault system in the Halten Terrace, Norway: Influence of basement structure and evaporite facies". In: *Journal of Structural Geology* 79, pp. 110–123.

Appendix A

Seismic lines without interpretation

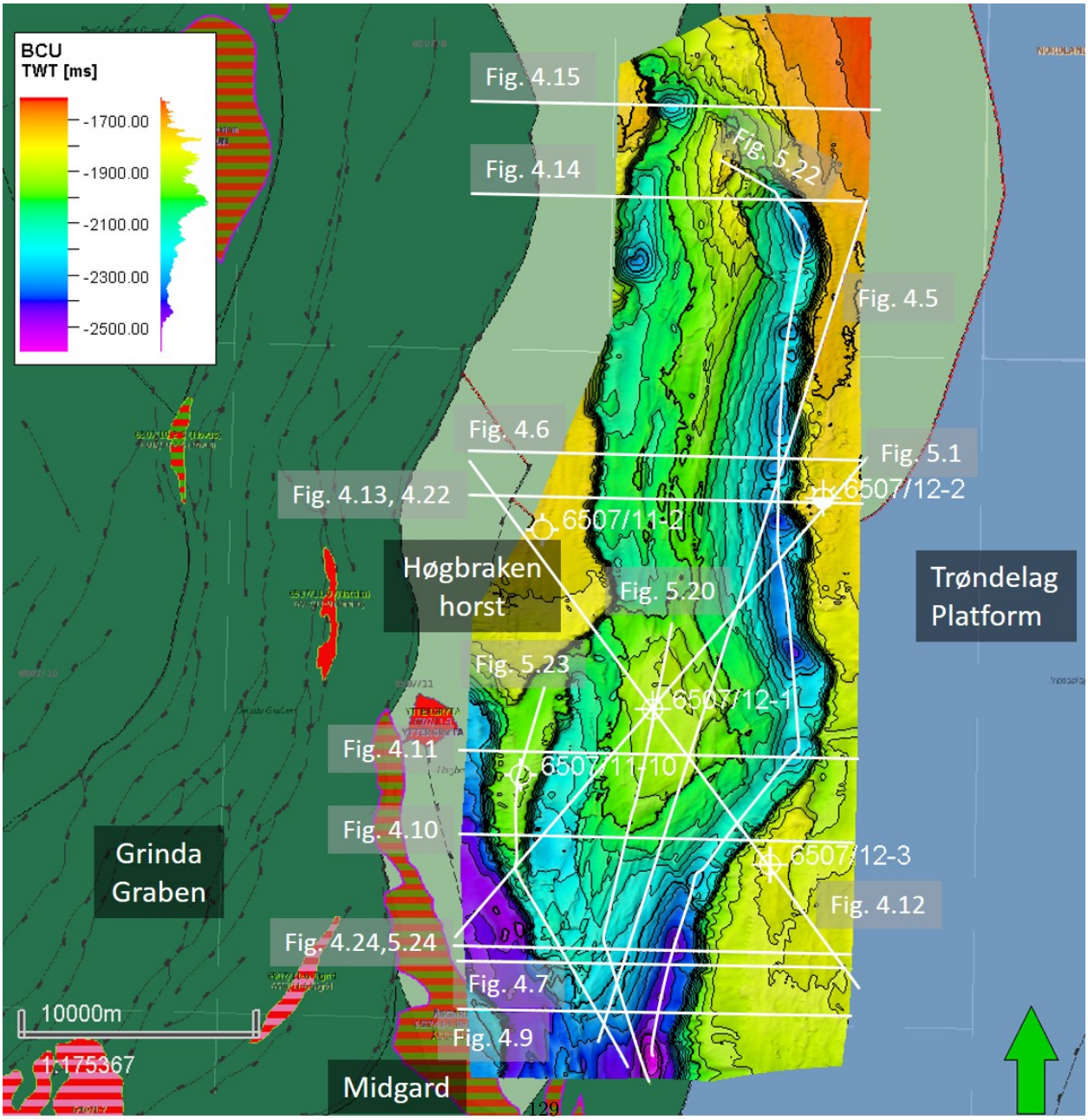

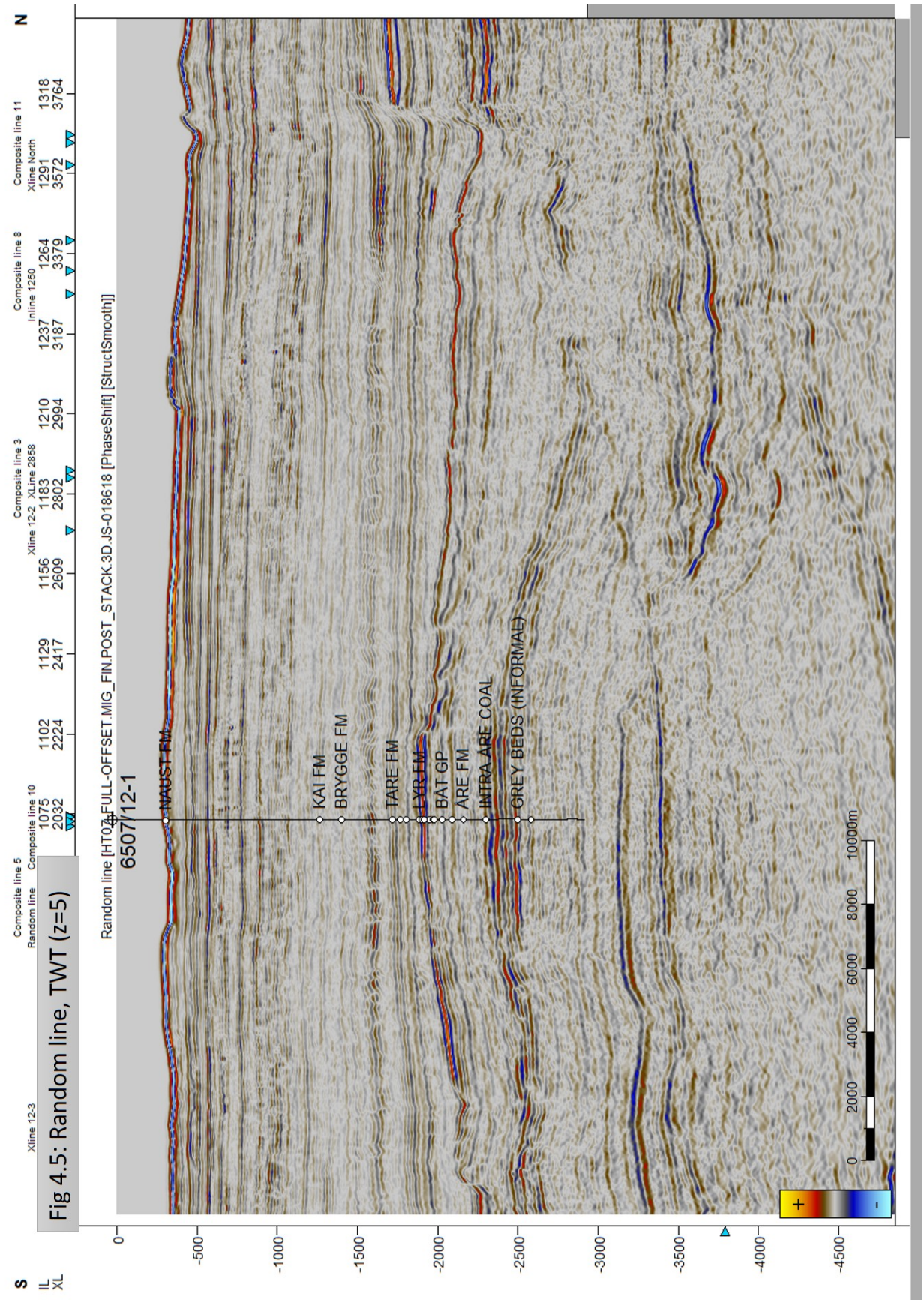
Random line [HT07_FULL-OFFSET.MIG_FIN.POST_STACK.3D.JS-018618 [PhaseShift] [StructSmooth]]
6507/12-1
NAUST FM
KAI FM
BRYGGE FM
TARE FM
LYR FM
BAT GP
ÅRE FM
INTRA ÅRE COAL
GREY BEDS (INFORMAL)
Fig 4.5: Random line, TWT (z=5)
S
N
IL
XL
0
-500
-1000
-1500
-2000
-2500
-3000
-3500
-4000
-4500
0
2000
4000
6000
8000
10000m
+
-

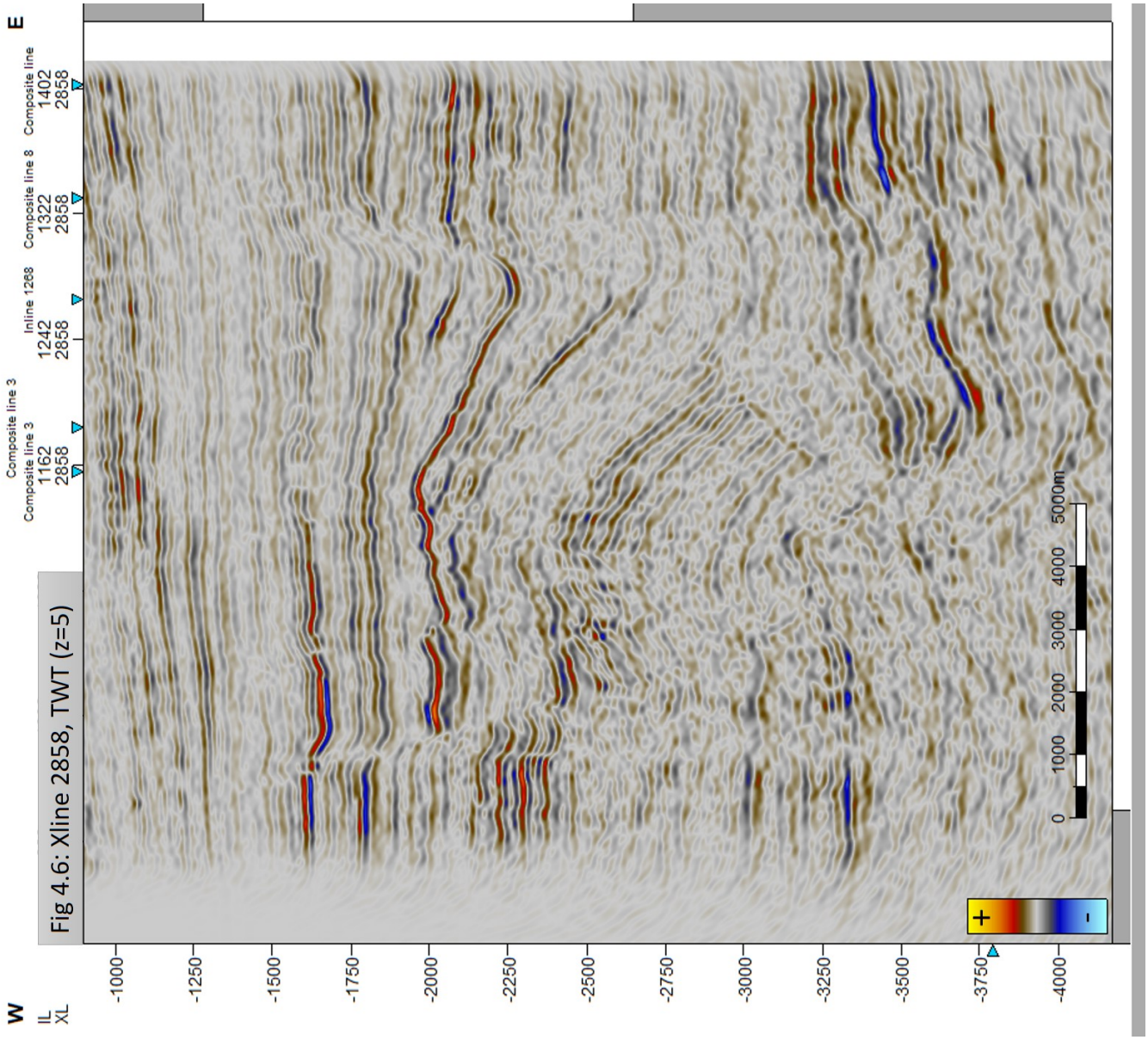
W
E
IL
XL
Composite line 3
1162
2858
Inline 1268
1242
2858
Composite line 8
1322
2858
Composite line
1402
2858
-1000
-1250
-1500
-1750
-2000
-2250
-2500
-2750
-3000
-3250
-3500
-3750
-4000
+
-
0
1000
2000
3000
4000
5000m
Fig 4.6: Xline 2858, TWT (z=5)

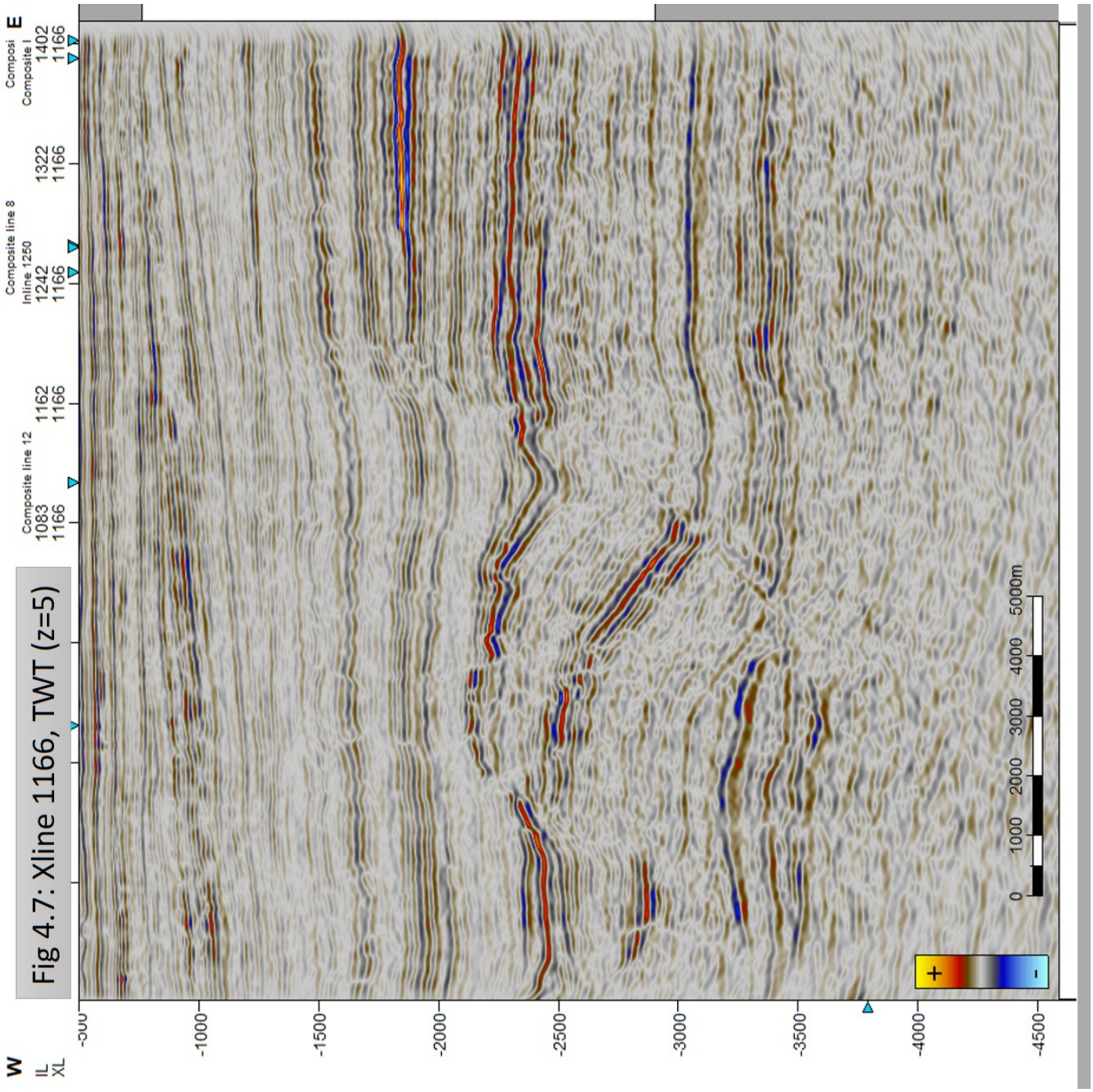
Fig 4.7: Xline 1166, TWT (z=5)
W
E
IL
XL
Composite line 12
1083
1166
1162
1166
Composite line 8
Inline 1250
1242
1166
1322
1166
Composi
Composite l
1402
1166
-500
-1000
-1500
-2000
-2500
-3000
-3500
-4000
-4500
0
1000
2000
3000
4000
5000m
+
-

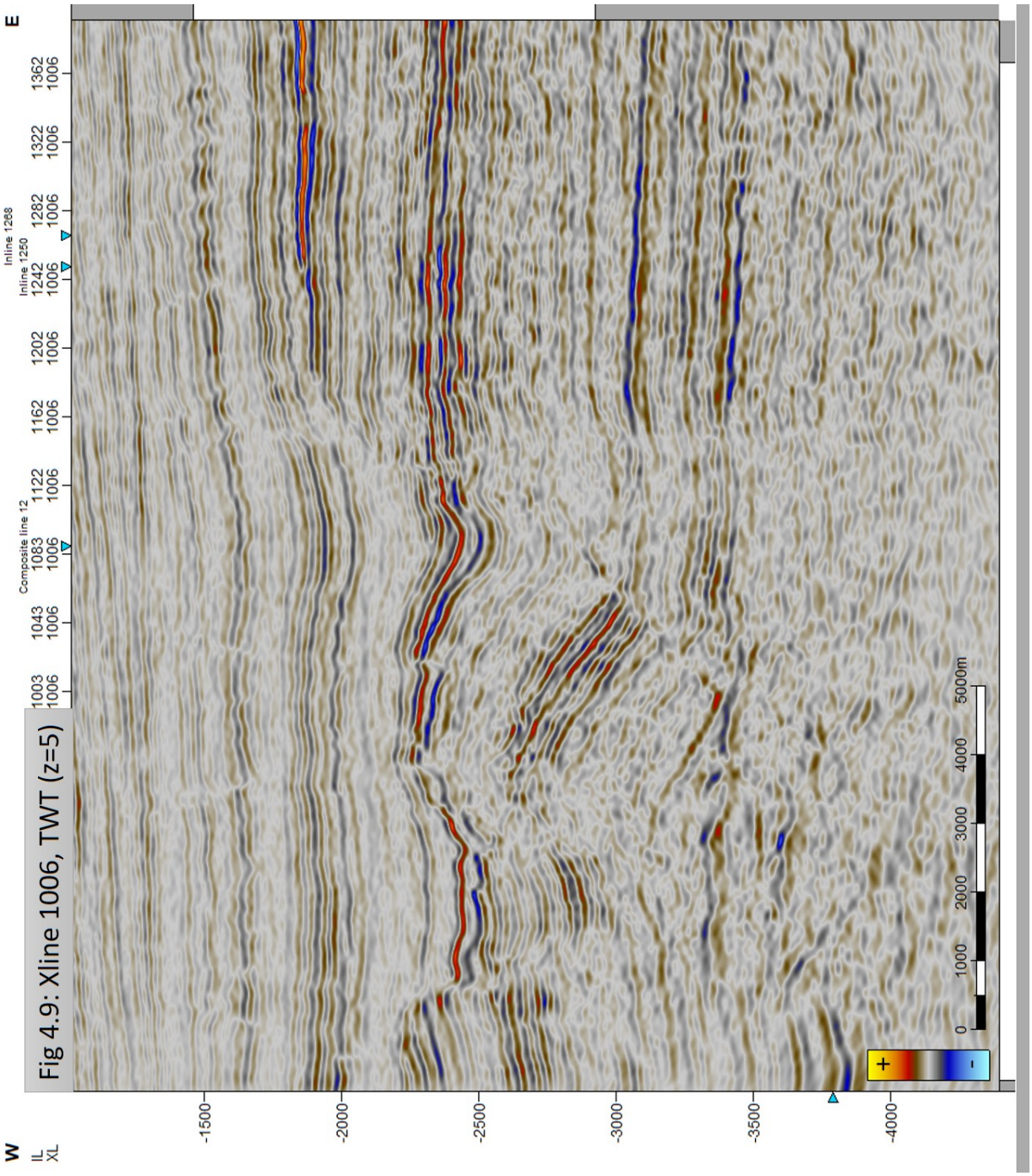
Fig 4.9: Xline 1006, TWT (z=5)
W
E
IL
XL
Composite line 12
Inline 1250
Inline 1268
1003 1006
1043 1006
1083 1006
1122 1006
1162 1006
1202 1006
1242 1006
1282 1006
1322 1006
1362 1006
-1500
-2000
-2500
-3000
-3500
-4000
0
1000
2000
3000
4000
5000m
+
-

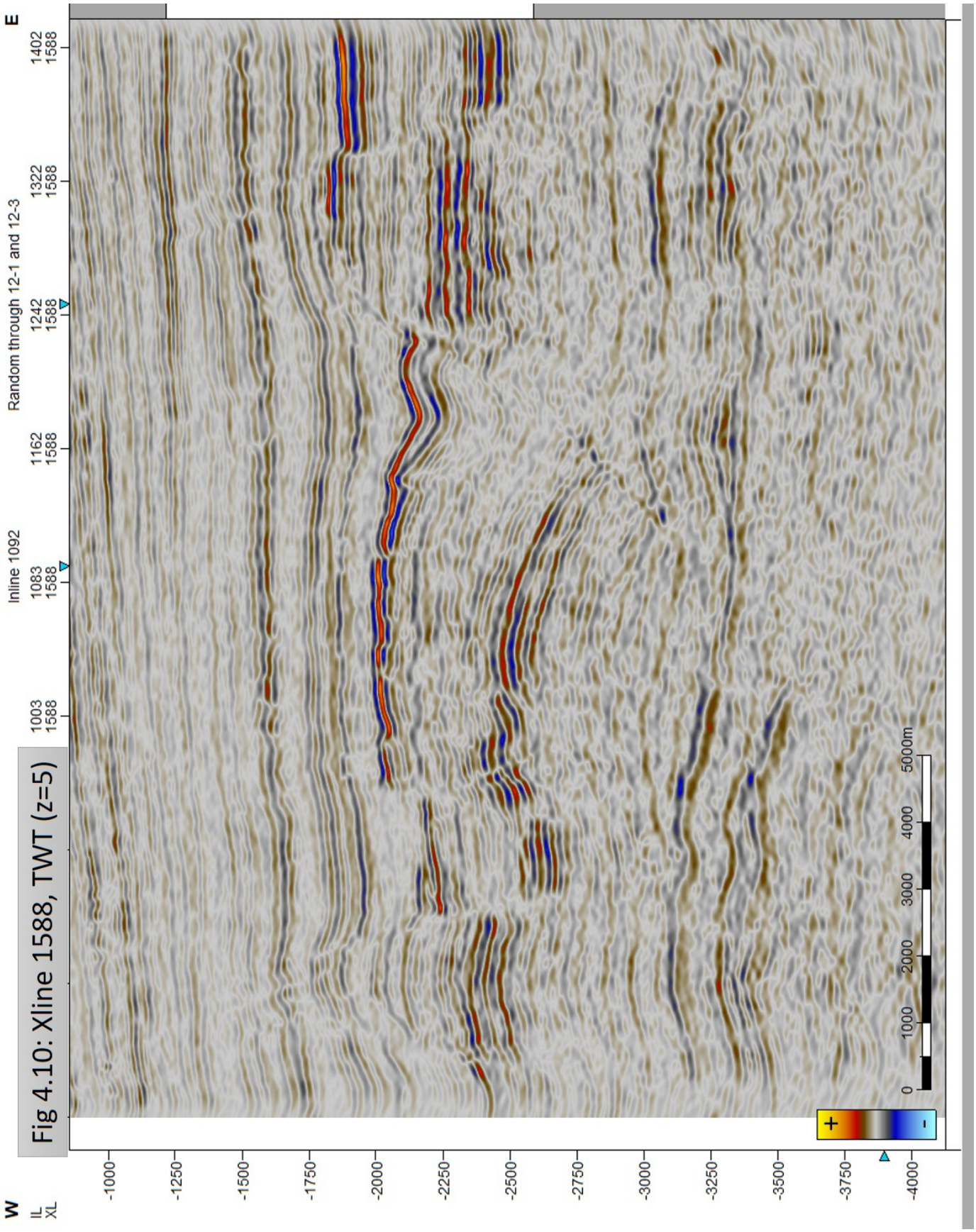
W
E
IL
XL
Inline 1092
Random through 12-1 and 12-3
1003 1588
1083 1588
1162 1588
1242 1588
1322 1588
1402 1588
-1000
-1250
-1500
-1750
-2000
-2250
-2500
-2750
-3000
-3250
-3500
-3750
-4000
0
1000
2000
3000
4000
5000m
+
-
Fig 4.10: Xline 1588, TWT (z=5)

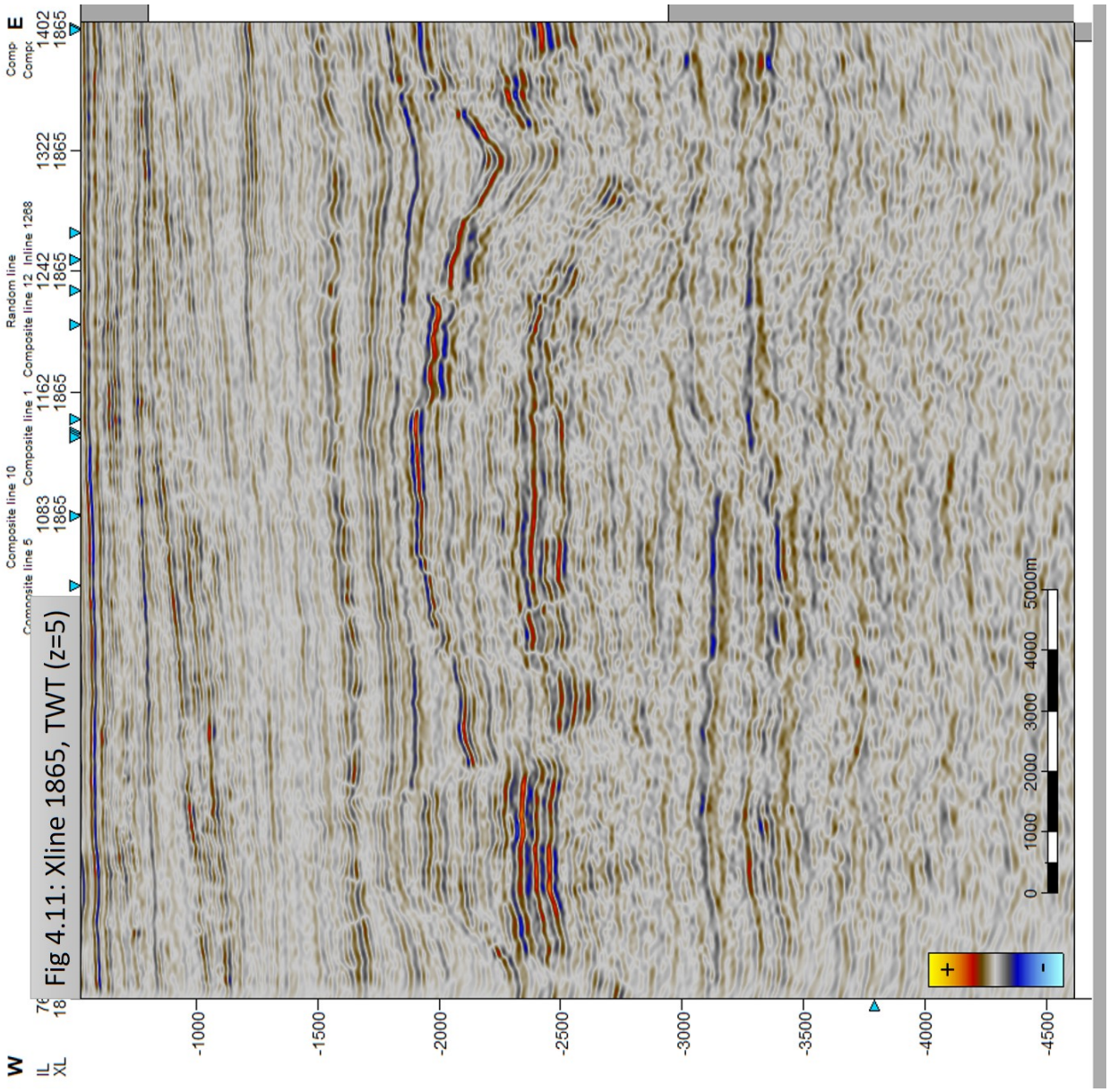

Fig 4.11: Xline 1865, TWT (z=5)

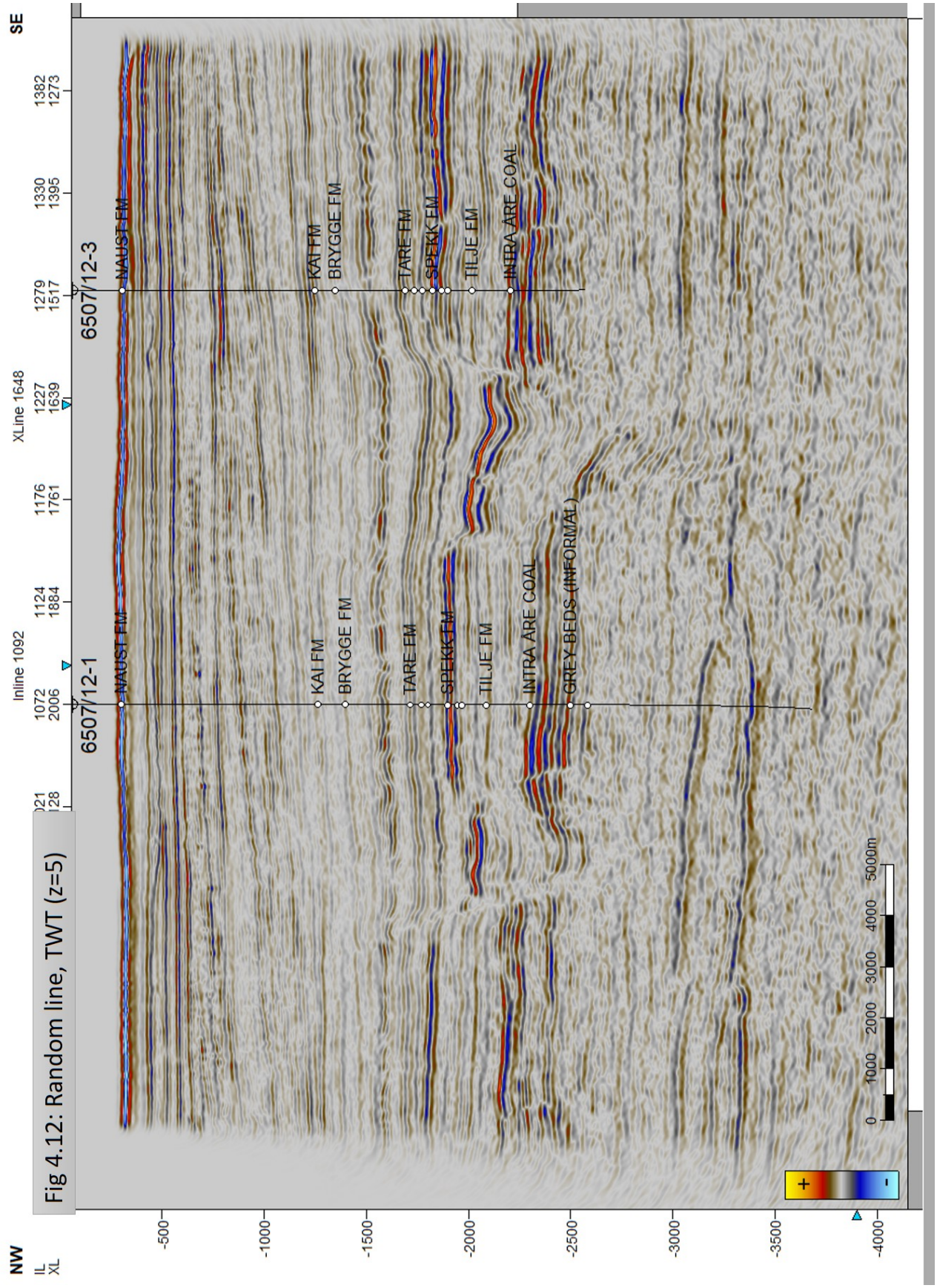

Fig 4.12: Random line, TWT (z=5)

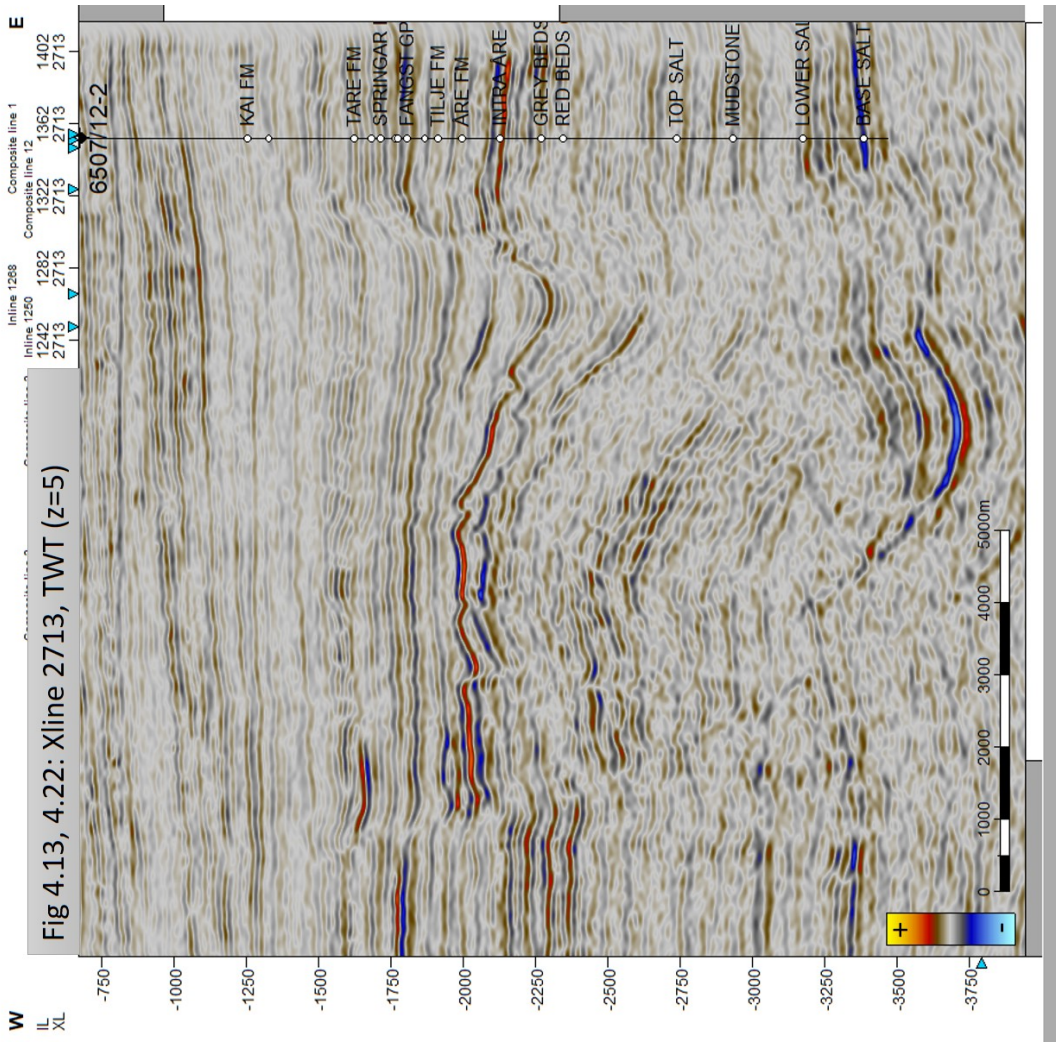
Fig 4.13, 4.22: Xline 2713, TWT (z=5)
W
E
IL
XL
Inline 1268
Inline 1250
Composite line 1
Composite line 12
1242
1282
1322
1362
1402
2713
6507/12-2
KAI FM
TARE FM
SPRINGAR
FANGST GP
TILJE FM
ARE FM
INTRA ARE
GREY BEDS
RED BEDS
TOP SALT
MUDSTONE
LOWER SAL
BASE SALT
-750
-1000
-1250
-1500
-1750
-2000
-2250
-2500
-2750
-3000
-3250
-3500
-3750
0
1000
2000
3000
4000
5000m
+
-

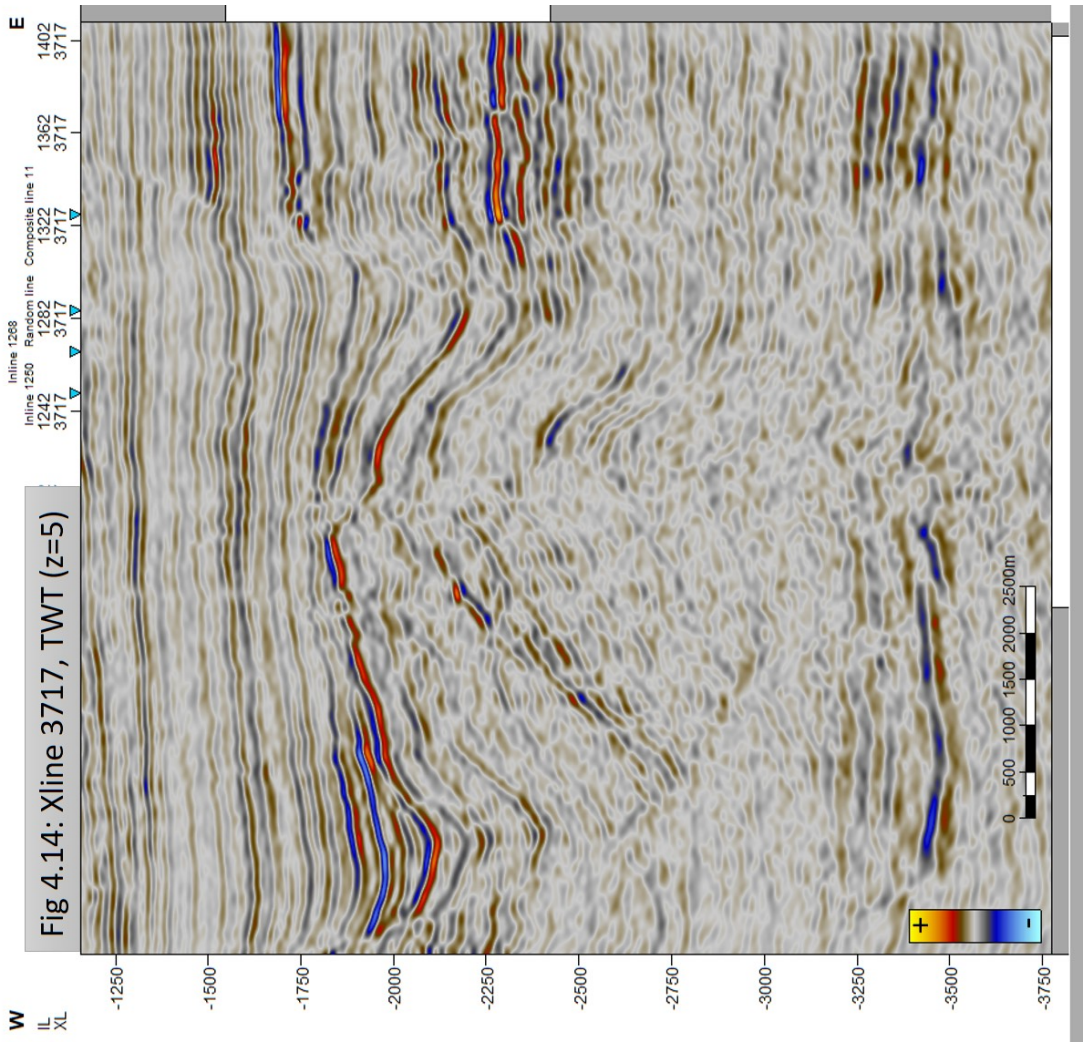
Fig 4.14: Xline 3717, TWT (z=5)
W
E
IL
XL
Inline 1268
Inline 1250
Random line
Composite line 11
1242
3717
1282
3717
1322
3717
1362
3717
1402
3717
-1250
-1500
-1750
-2000
-2250
-2500
-2750
-3000
-3250
-3500
-3750
0 500 1000 1500 2000 2500m
+
-

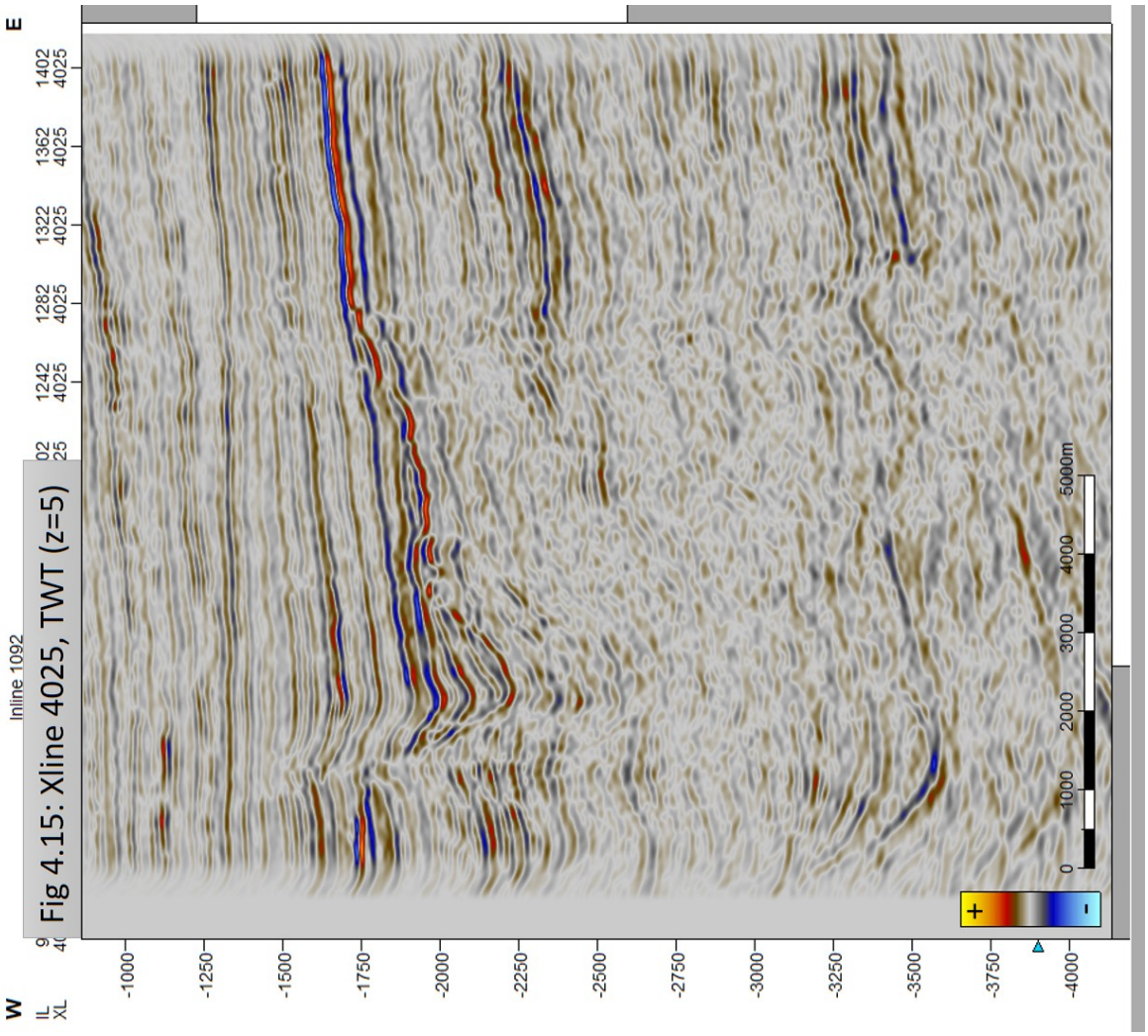
Fig 4.15: Xline 4025, TWT (z=5)
Inline 1092
W
E
IL
XL
1402 4025
1362 4025
1322 4025
1282 4025
1242 4025
-1000
-1250
-1500
-1750
-2000
-2250
-2500
-2750
-3000
-3250
-3500
-3750
-4000
0
1000
2000
3000
4000
5000m
+
-

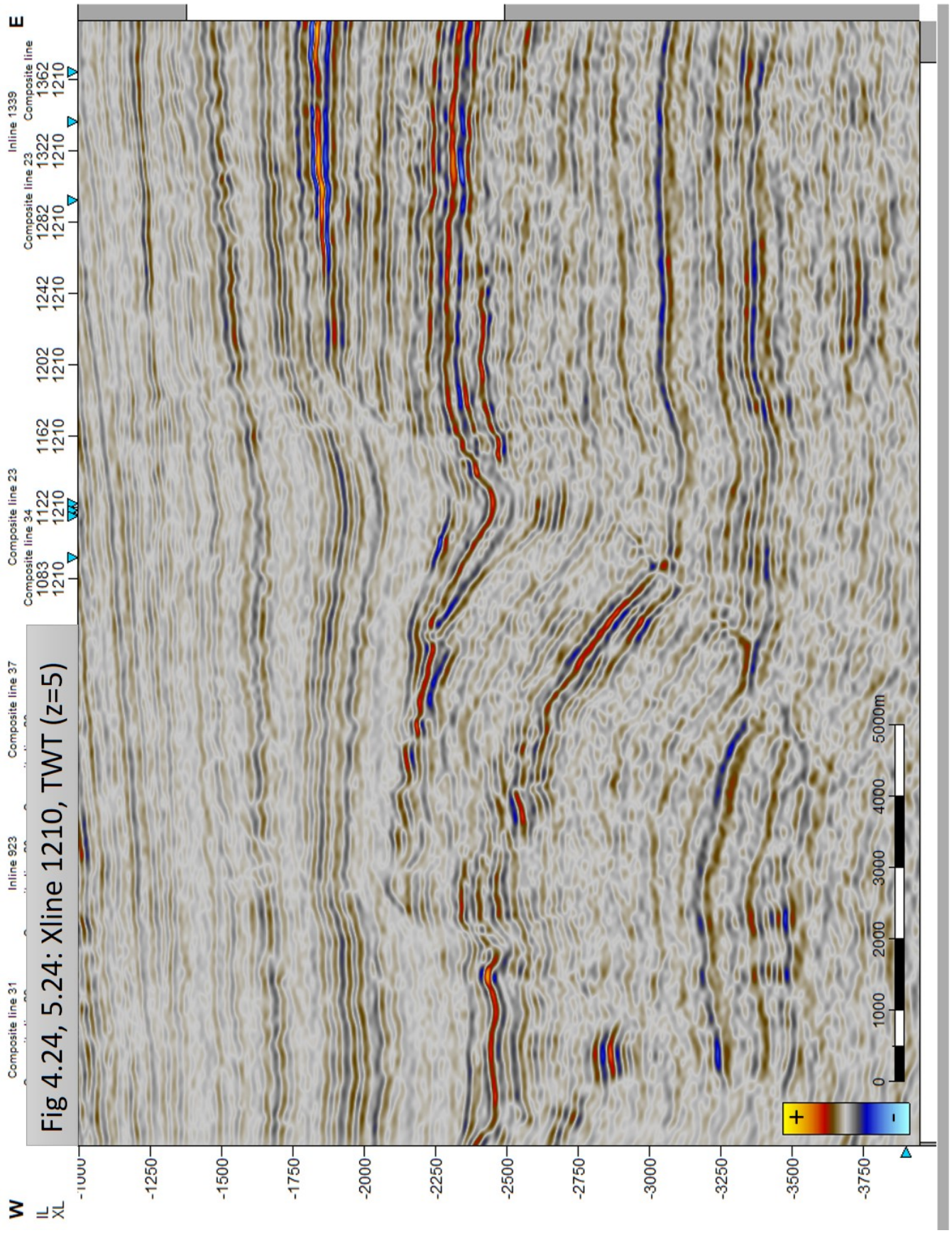
Fig 4.24, 5.24: Xline 1210, TWT (z=5)
W
E
IL
XL
Composite line 31
Inline 923
Composite line 37
Composite line 23
Composite line 34
1083
1210
1122
1210
1162
1210
1202
1210
1242
1210
Composite line 23
1282
1210
1322
1210
Inline 1339
Composite line
1362
1210
-1000
-1250
-1500
-1750
-2000
-2250
-2500
-2750
-3000
-3250
-3500
-3750
+
-
0
1000
2000
3000
4000
5000m

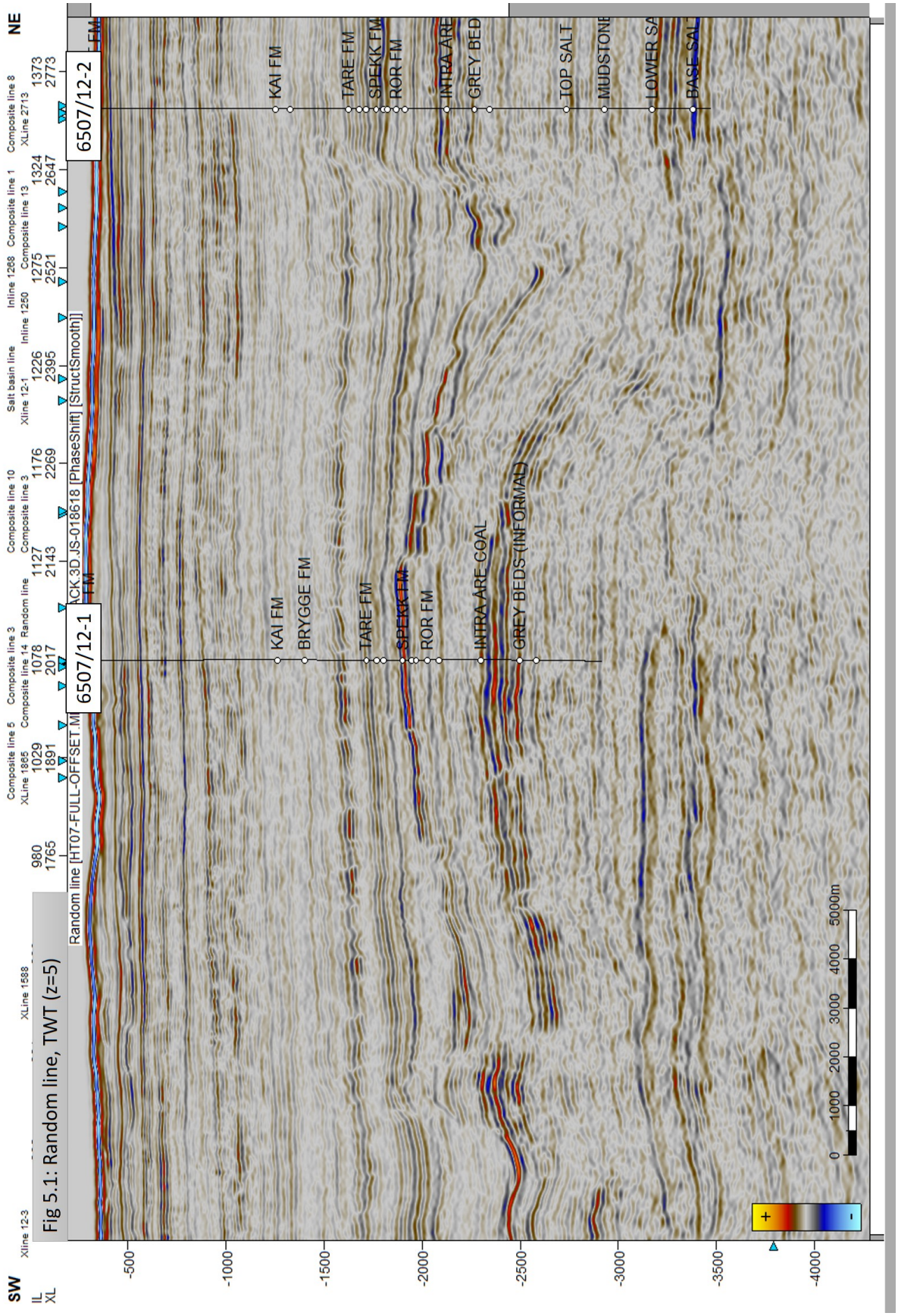

Fig 5.1: Random line, TWT (z=5)

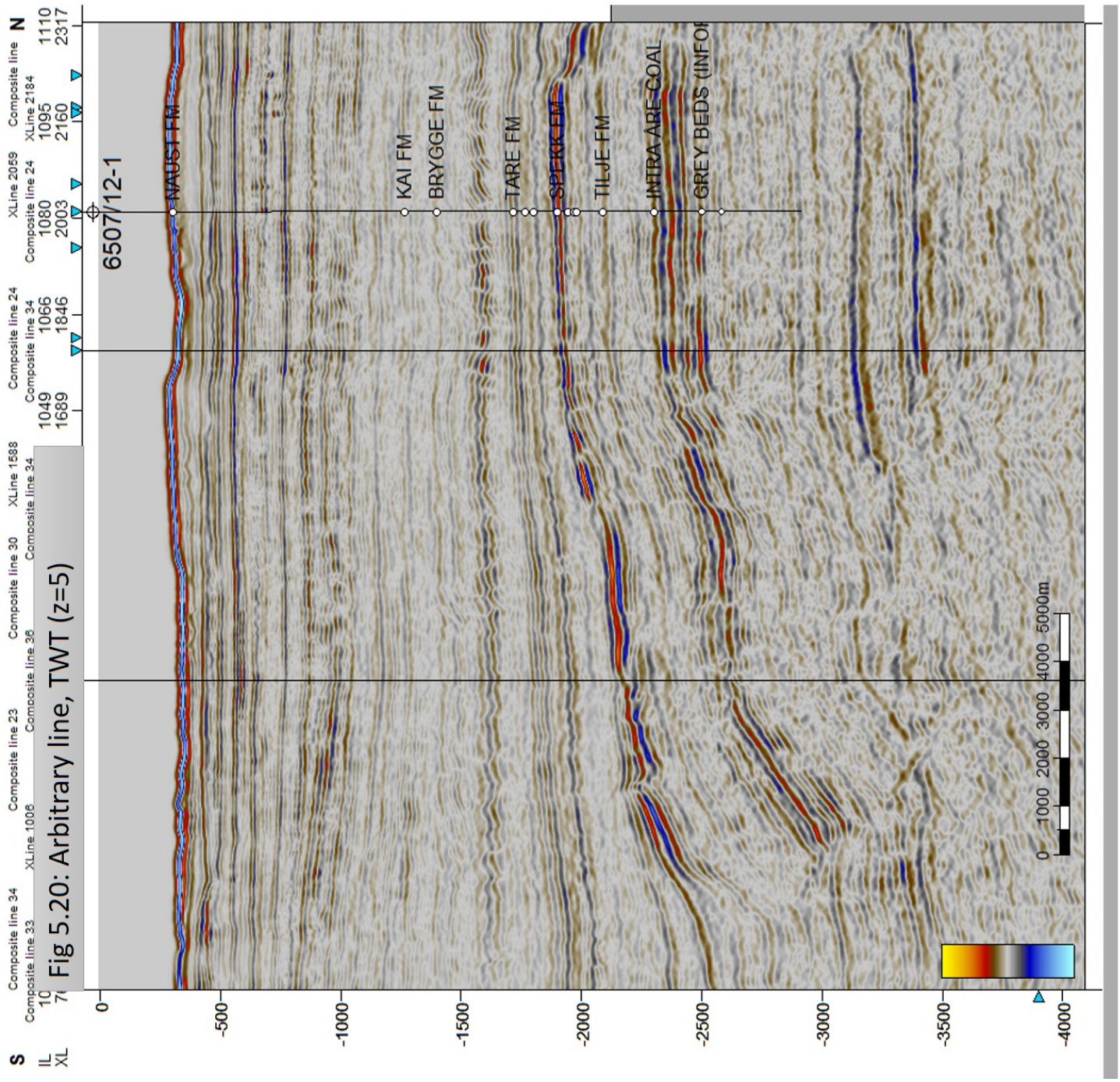

Fig 5.20: Arbitrary line, TWT (z=5)

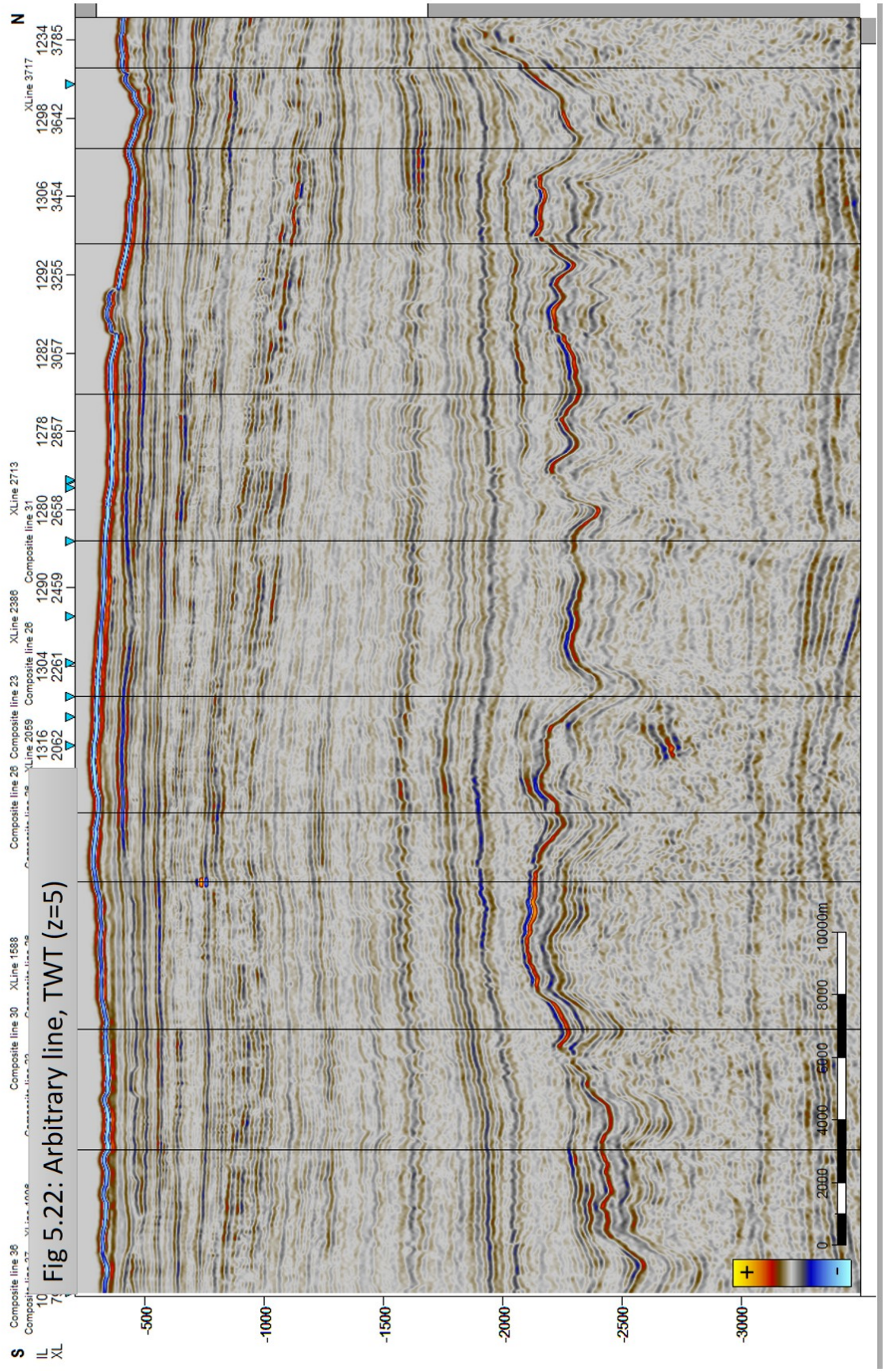
Fig 5.22: Arbitrary line, TWT (z=5)
S
N
-500
-1000
-1500
-2000
-2500
-3000
0
2000
4000
6000
8000
10000m
+
-

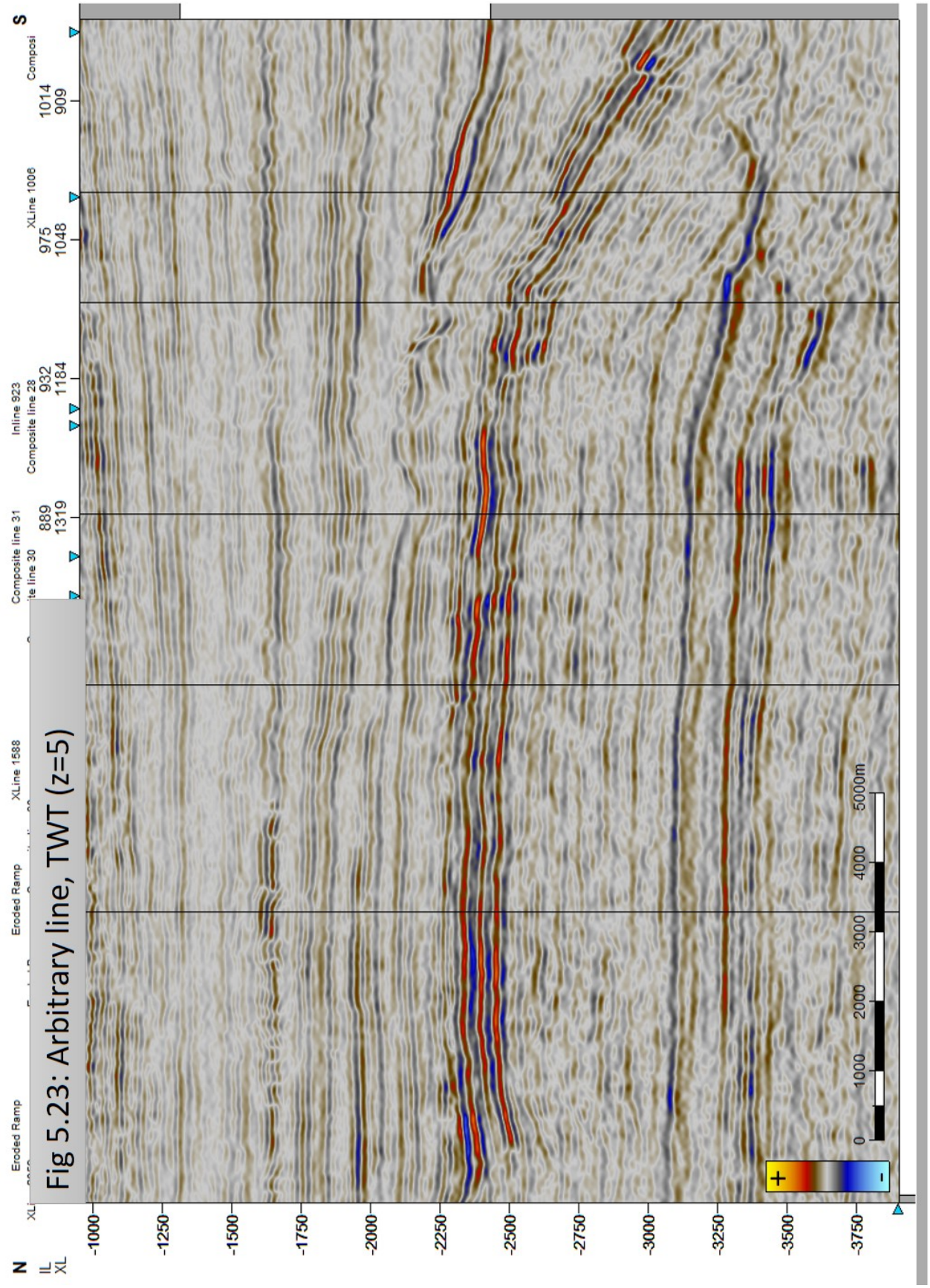
Fig 5.23: Arbitrary line, TWT (z=5)
N
S
IL
XL
Eroded Ramp
XLine 1588
Composite line 31
Inline 923
Composite line 28
XLine 1008
Composi
889
1319
932
1184
975
1048
1014
909
-1000
-1250
-1500
-1750
-2000
-2250
-2500
-2750
-3000
-3250
-3500
-3750
0
1000
2000
3000
4000
5000m
+
-

Appendix B

MATLAB Net Exhumation Scripts

Well information files

```
%Whole Cretaceous interval
%Handling matrices for reference wells
%Detph range is for cretaceous interval in each well (see excel
    sheet)

Ref1 = struct('filename', "6406-2-7", 'range', [2540 4510]);
Ref2 = struct('filename', "6506-6-1", 'range', [2071 4328]);
Ref3 = struct('filename', "6506-11-1", 'range', [2192 3813]);
Ref4 = struct('filename', "6506-12-5", 'range', [2346 3780]);
Ref5 = struct('filename', "6507-7-1", 'range', [2159 3495]);
Ref6 = struct('filename', "6507-7-10", 'range', [2106 2439]);
Ref7 = struct('filename', "6507-8-7", 'range', [2099 2575]);

refwells=[Ref1, Ref2, Ref3, Ref4, Ref5, Ref6, Ref7];

%Handling matrices for test wells
%Detph range is for cretaceous interval in each well (see excel
    sheet)

Test6306_10_1 = struct('filename',"6306-10-1",'range',[1200 2600])
    ;
Test6407_8_1 = struct('filename',"6407-8-1",'range',[2100 3600]);
Test6407_12_3 = struct('filename',"6407-12-3",'range',[1486 1570])
    ;
Test6408_4_1 = struct('filename',"6408-4-1",'range',[1350 1630]);
Test6507_11_6 = struct('filename',"6507-11-6",'range',[2150 2845])
    ;
Test6507_12_1 = struct('filename',"6507-12-1",'range',[1929 2012])
    ;
```

```
Test6510_2_1 = struct('filename',"6510-2-1",'range',[727 848]);
Test6607_5_2 = struct('filename',"6607-5-2",'range',[2560 3700]);
Test6609_10_1 = struct('filename',"6609-10-1",'range',[1480 1570])
    ;
Test6306_6_1 = struct('filename',"6306-6-1",'range',[800 1000]);
Test6306_5_1 = struct('filename',"6306-5-1",'range',[1762 2050]);
Test6406_12_2 = struct('filename',"6406-12-2",'range',[2177 3711])
    ;
Test6610_10_1 = struct('filename',"6610-10-1",'range',[1444 2030])
    ;
Test6305_9_1 = struct('filename',"6305-9-1",'range',[2523 2655]);
Test6305_9_2 = struct('filename',"6305-9-2",'range',[3016 3075]);
Test6305_8_1 = struct('filename',"6305-8-1",'range',[2976 3175]);
Test6404_11_1 = struct('filename',"6404-11-1",'range',[2748 3206])
    ;
Test6406_6_1 = struct('filename',"6406-6-1",'range',[2514 3324]);

Testwells=[Test6306_10_1 Test6407_8_1 Test6407_12_3 Test6408_4_1
    Test6507_11_6 Test6507_12_1 Test6510_2_1 Test6607_5_2
    Test6609_10_1 Test6306_6_1 Test6306_5_1 Test6406_12_2
    Test6610_10_1 Test6305_9_1 Test6305_9_2 Test6305_8_1
    Test6404_11_1 Test6406_6_1];


%plot_range, V_clay_min, GR_max, GR_min
plot_range=[1 5000];
V_clay_min=0.21;
GR_max=100;
GR_min=30;
```

Establishing reference trend

```

% Wells is an array [] of structs that have 'filename' (str) and '
    range' ([min max])
%
% Plot_range is used for plotting, wells(index).range is used for
    cutting out data
% to a speciifc depth
%
% Example:
% basic_plot([struct('filename', "6506-11-1", 'range', [3500
    3600]), struct('filename', "6506-6-1", 'range', [3300 3500])],
```

```
    [3130 3780], 0.6, 110, 30)
9
10 figure();
11 U = [0 0];
12
13 for file_index = 1:length(refwells)
14     M = dlmread(refwells(file_index).filename, '', 29, 0);
15
16     % Replace irrelevant data with NaN
17     GR_log = V_clay_min*(GR_max - GR_min) + GR_min;
18     for i = 1:length(M(:,1))
19         if M(i,2) < GR_log
20             M(i,2) = NaN;
21             M(i,3) = NaN;
22         elseif M(i,3) < 0
23             M(i,3)= NaN;
24         end
25     end
26
27     % Replace data outside the depth interval with NaN
28     for i = 1:length(M(:,1))
29         if M(i,1) < refwells(file_index).range(1) || M(i,1) >
               refwells(file_index).range(2)
30             M(i,2) = NaN;
31             M(i,3) = NaN;
32         end
33     end
34
35     for i = 1:length(M(:,1))
36         if ~isnan(M(i, 3))
37             U = [U; M(i,1) M(i,3)];
38         end
39     end
40
41
42
43     % Plot GR
44
45     subplot(1,2,1);
46     hold on
47     plot(M(:,2),M(:,1),'linewidth',1);
48     plot(GR_log*ones(length(M(:,1)), 1),M(:,1),'--k','linewidth'
           ,.5);
49     hold off
50     set(gca,'Ydir','reverse');
```

```
51      title('GR');
52      xlabel('GR [gAPI]');
53      ylabel('Depth [m]');
54      xlim([0 150]);
55      ylim(plot_range);
56      grid minor
57
58
59      %Plot Vp
60      subplot(1,2,2);
61      hold on
62      scatter(M(:,3),M(:,1),0.8,'linewidth',1);
63      %scatter(U(:,2),U(:,1),0.8,'linewidth',1);
64      %plot([0 5000],1.08 .* [0 5000] - 100,'--r','linewidth',2);
65      hold off
66      set(gca,'Ydir','reverse');
67      title('Vp reference trend');
68      xlabel('Vp [m/s]');
69      ylabel('Depth [m]');
70      xlim([0 5000]);
71      ylim(plot_range);
72      grid minor
73  end
74
75
76  P = polyfit(U(:,1), U(:,2), 1)
77  fit = P(1)*U(:,1)+P(2);
78  slope=1/P(1);
79  intersect=-P(2)*slope;
80  hansen=191*0.3048/10^(-6)
81
82  subplot(1,2,2);
83  hold on
84  plot(fit, U(:,1),'--r','linewidth',2);
85  h0=scatter(-1,-1,'k');
86  h1=plot([0 5000],1.76 .* [0 5000] - 2600,'color',[0.8 0.6 0.17],'
        linewidth',1.5);
87  h2=plot([0 5000],slope .* [0 5000] + intersect,'r','linewidth'
        ,1.5);
88  h3=plot([0 5000],1.81.* [0 5000] - 2865,'b','linewidth',1.5);
89  hold off
90  set(gca,'Ydir','reverse');
91  %set(gcf,'Position', get(0,'Screensize'));
92  xlim([0 5000]);
93  ylim(plot_range);
```

```
94 legend([h0 h1 h2 h3],'Well data','Storvoll trend','Blilie trend',
       'Johansen trend')
95 annotation('textbox', [0.6, 0.1, 0.1, 0.1], 'String', "Local
       reference trend is Z=2.09Vp-2764" )
96
97
98 %save figure as eps and jpg files
99 fpath='E:\Prosjektoppgave\Bilder\Exhumation_results'
100 saveas(gcf, fullfile(fpath,'reftrend_velocityv2'), 'epsc')
101 saveas(gcf, fullfile(fpath,'reftrend_velocityv2_jpg'), 'jpg')
102 fprintf("The trend line is: Vp= %d z  + %d\n", P(1), P(2));
103 fprintf("The trend line is: Z= %d Vp  + %d\n", slope, intersect);
```

Comparing test wells with reference trend

```
1  function Comparison_test_wells(wells, plot_range, V_clay_min,
       GR_max, GR_min, slope, intersect)
2  % Wells is an array [] of structs that have 'filename' (str) and '
       range' ([min max])
3  %
4  % Plot_range is used for plotting, wells(index).range is used for
       cutting out data
5  % to a speciifc depth
6
7  figure();
8  U = [0  0];
9
10 for file_index = 1:length(wells)
11     M = dlmread(wells(file_index).filename, '', 29, 0);
12
13     % Replace irrelevant data with NaN
14     GR_log = V_clay_min*(GR_max - GR_min) + GR_min;
15     for i = 1:length(M(:,1))
16         if M(i,2) < GR_log
17             M(i,2) = NaN;
18             M(i,3) = NaN;
19         elseif M(i,3)<0
20             M(i,3)=NaN;
21         end
22     end
23
24     % Replace data outside the depth interval with NaN
25     for i = 1:length(M(:,1))
```

```
26          if M(i,1) < wells(file_index).range(1) || M(i,1) > wells(
                file_index).range(2)
27              M(i,2) = NaN;
28              M(i,3) = NaN;
29          end
30      end
31
32      for i = 1:length(M(:,1))
33          if ~isnan(M(i, 3))
34              U = [U; M(i,1) M(i,3)];
35          end
36      end
37
38      % Plot GR
39
40      %Range to plot
41      range=[wells(file_index).range(1)-500 wells(file_index).range
            (2)+1500];
42
43      subplot(1,2,1);
44      hold on
45      g1=plot(M(:,2),M(:,1),'color',[0 0.6 0.3],'linewidth',1);
46      g2=plot(GR_log*ones(length(M(:,1)), 1),M(:,1),'--k','linewidth
            ',.5);
47      hold off
48      set(gca,'Ydir','reverse');
49      title('GR');
50      xlabel('GR [gAPI]');
51      ylabel('Depth [m]');
52      xlim([0 150]);
53      ylim(range);
54      grid minor
55      legend([g1 g2],'GR for well','Minimum GR line', 'location', '
            Southwest')
56
57
58      %Plot Vp
59      subplot(1,2,2);
60      hold on
61      GRpoints=scatter(M(:,3),M(:,1),0.8, 'filled','SizeData', 4);
62      plot([0 5000],slope .* [0 5000] + intersect,'r','linewidth'
            ,1.8);
63      plot([0 5000],1.76 .* [0 5000] - 2600,'color',[0.8 0.6 0.17],'
            linewidth',1.8);
64      hold off
```

```
65      alpha(GRpoints,0.2);
66      set(gca,'Ydir','reverse');
67      title('Vp');
68      xlabel('Vp [m/s]');
69      ylabel('Depth [m]');
70      xlim([0 5000]);
71      ylim(range);
72      grid minor
73  end
74
75
76  P = polyfit(U(:,1), U(:,2), 1);
77  fit = P(1)*U(:,1)+P(2);
78
79  %fitting intersect, forcing slope
80  b_fit=mean(U(:,1)-slope*U(:,2));
81  welltrend_vp=U(:,1)/slope - b_fit/slope;
82
83  %Standard deviation
84  std_vp=sqrt(sum((U(:,2)-welltrend_vp).^2)/(length(U(:,2)-1)));
85
86
87  %dZ for new intersects
88  dz_std=slope*std_vp;
89  dz_std_int=round(dz_std,0);
90
91  %std welltrends
92  welltrend_vp_stdplus=U(:,1)/slope - (b_fit+dz_std)/slope;
93  welltrend_vp_stdminus=U(:,1)/slope - (b_fit-dz_std)/slope;
94
95  %Vertical line Blilie
96  S=round(length(U(:,2))/2,0);
97  S_value=welltrend_vp(S);
98  plot_z=[0 0];
99  plot_z(1)=slope*S_value+intersect;
100 plot_z(2)=slope*S_value+b_fit;
101 S_vector=ones(length(range), 1)*S_value;
102
103 %Vertical line Storvoll
104 plot_zstorvoll=[0 0];
105 plot_zstorvoll(1)=1.76*S_value-2600
106 plot_zstorvoll(2)=slope*S_value+b_fit
107
108 %net erosion estimate Local
109 erosion_base=intersect-b_fit;
```

```
110 erosion_base_int=round(erosion_base,0);
111 erosion_stdplus=intersect-(b_fit+dz_std);
112 erosion_stdminus=intersect-(b_fit-dz_std);
113 %net erosion estimate Storvoll
114 erosion_base_storvoll=plot_zstorvoll(1)-plot_zstorvoll(2);
115 erosion_base_storvoll_int=round(erosion_base_storvoll,0);
116 %Add text to plot
117 text_exhumation = strcat(' Local trend, Net exhumation = ',
    sprintf('%d +/- %d m', erosion_base_int, dz_std_int));
118 text_exhumation_storvoll=strcat('Storvoll trend, Net exhumation =
    ', sprintf('%d +/- %d m',erosion_base_storvoll_int,dz_std_int))
    ;
119 %plotpoint_exhumation =min(plot_z)+(max(plot_z)-min(plot_z))/2;
120 plotpoint_z=range(2)*0.8
121
122 subplot(1,2,2);
123 hold on
124 plot(welltrend_vp, U(:,1),'b','linewidth',2);
125 plot(welltrend_vp_stdplus, U(:,1),'--','color',[0.5 0.5 0.5],'
    linewidth',1.3);
126 plot(welltrend_vp_stdminus, U(:,1),'--','color',[0.5 0.5 0.5],'
    linewidth',1.3);
127 plot(S_vector, [min(plot_z) max(plot_z)],'k','linewidth',1);
128 plot(S_vector, [min(plot_zstorvoll) max(plot_zstorvoll)],'k','
    linewidth',1);
129 %text(100,plotpoint_z,text_exhumation);
130 %text(100,plotpoint_z+100,text_exhumation_storvoll);
131 %text(S_value,plotpoint_exhumation,text_exhumation);
132
133 hold off
134 set(gca,'Ydir','reverse');
135 %set(gcf, 'Position', get(0, 'Screensize'));
136 xlim([0 5000]);
137 ylim(range);
138 legend(wells(file_index).filename,'Local reference line', '
    Storvoll reference line', 'Forced slope', 'std', 'Location','
    Southwest');
139
140 %save figure as eps and jpg files in specified folder
141 fpath='E:\Prosjektoppgave\Bilder\Exhumation_results';
142 %saveas(gcf, fullfile(fpath, wells(1).filename + '_velocity'), '
    epsc')
143 %saveas(gcf, fullfile(fpath, wells(1).filename+ '_velocity'), 'jpg
    ')
```

Kristin Blilie

Tectonostratigraphy and hydrocarbon potential of the Ellingråsa Graben

NTNU
Norwegian University of
Science and Technology